Advancement in the use of Optical Properties for Water Quality and Water Reuse in Public Water Treatment Cycles

by

Blair Hanson

B.A., State University of New York at Oneonta, 2012

A thesis submitted to the
Faculty of the Graduate School of the
University of Colorado in partial fulfillment
of the requirements for the degree of
Doctor of Philosophy
Department of Environmental Engineering
2023

Committee Members:

Fernando Rosario-Ortiz (chair)

Julie Korak

Juliana D'Andrilli

Diane McKnight

William Becker

Abstract

Hanson, Blair (Ph.D., Environmental Engineering)

Advancement in the use of Optical Properties for Water Quality and Water Reuse in Public Water Treatment Cycles

Thesis Directed by Professor Fernando Rosario-Ortiz

Dissolved organic matter (DOM) is a complex mixture of organic compounds resulting from the breakdown and transformational products of higher forms of organic matter (i.e., plants, animals and microbes). DOM is also a ubiquitous constituent of natural and treated waters and known to play key roles in many environmental and engineered and treated systems. Examples include the global carbon flux, fate and transport of contaminants, light absorption and photochemistry in water, and the production of disinfection byproducts in water treatment systems. Analysis of molecular size and optical properties have emerged as useful techniques to characterize DOM in terms of source and chemical composition of DOM. These relationships are useful to the water treatment industry and allow DOM to be used as surrogates for the removal of contaminants and differentiate between water sources such as natural surface water and treated wastewater effluent.

The main goal of my research is to advance the understanding of DOM molecular size and optical properties, their relationship to one another, and how they can be utilized in the water treatment industry, especially for potable water reuse treatment applications and the development of optical based sensors and probes. My research is primarily conducted using a size exclusion chromatography system (SEC) coupled with absorbance, fluorescence, and dissolved organic

carbon (DOC) detection. In the Chapter 1, I develop a method to calculate fluorescence quantum yield as a function of molecular size and demonstrate the ability of this method to provide compositional information regarding absorbing and fluorescing fractions of DOM. In Chapter 2, I apply mass balance principals to blends of DOM sources to demonstrate conservative mixing behavior with respect to the molecular size distributions and optical properties of DOM. Finally, in Chapter 6, I investigate the composition of "protein-like" fluorescence components in DOM for a paired surface water and wastewater effluent to advance the understanding of these metrics in the context of an urban water cycle and inform future development of optical sensors.

Acknowledgements

I would like to acknowledge the many individuals who have supported me, directly contributed to this research, and provided funding for me to complete my doctoral dissertation. First, I must thank my committee chair and graduate advisor, Fernando Rosario-Ortiz for providing me with the opportunity earn a Ph.D. After taking the "Environmental Organic Chemistry" course (instructed by Fernando) in my first year of graduate school, he offered me a position in his research group and introduced me to the world of "dissolved organic matter photophysical properties" (a topic I initially felt was intimidating but am now fascinated by). Fernando certainly pushed me to work hard but also gave me space and allowed me to work at my own pace when I needed it. His trust and confidence in me played a significant role in my decision to begin the doctoral dissertation journey. The other members of my graduate committee include Julie Korak, Julianna D'Andrilli, Bill Becker, and Diane McKnight, each of whom uniquely supported and helped me along the way.

Others that I would like to thank include the members of Rosario research group, Shelby Buckley, Kari Norris, Frank Leresche, Mackenzie Bowden, and Carley Brucker; the members Julie Korak's research group; Ayush Shahi, Annabell Mungan, Emma Wilder, Lauren Magliozzi, and Leah Flint; and the many other students that I have learned from (and at times commiserated with) throughout my graduate school career. Amanda Scott and Brett Clark, served as my supervisors while I worked at SUEZ Water Technologies & Solutions (currently Veolia Water Technologies & Solutions), where I began learning the process of method development. Collaborators Kate Murphy and Urban Wünsch played large roles in completing the research described in Chapter 4. Dorothy Noble and Stefan Peterson, were (and still are) excellent in their roles as managers of the environmental engineering lab (at the University of Colorado Boulder), ensuring that instrumentation functions properly and maintaining a safe and productive environment for graduate students to complete their research.

Finally, I would like to thank my many friends and family that helped and supported me outside of school and research. To my parents Barbara and Brian Hanson, my brother Reid Hanson, and my grandmother Marylin Hanson (as well as my aunts, uncles, and cousins), I look forward to having more time to spend with you all in the future and hope to return the support you have provided for me.

Table of Contents

List of Tables

List of Figures

Chapter 1

Introduction

1.1 Background

Dissolved organic matter (DOM) represents a diverse mixture of compounds originating from the molecular remnants of plants, animal materials, and microbial exudates (Perdue and Ritchie, 2003). DOM represents a major part of the global carbon cycle and is an important factor in numerous chemical and physical processes in natural and engineered systems (Bauer et al., 2013; Bianchi, 2011). For example, DOM serves as a substrate for microbial growth (Azam et al., 1983) and can complex with metals and organic pollutants, impacting their fate in natural waters (Ravichandran, 2004). Additionally, DOM impacts water treatment processes, including reactions with chlorine, resulting in the formation of disinfection byproducts, some of which are harmful to humans if consumed (Nikolaou and Lekkas, 2001; Singer, 1999). However, due to the complex chemical composition of DOM, determination of its characteristics relies on the development and application of numerous analytical methods (Perdue and Ritchie, 2003).

1.2 Size Exclusion Chromatography

One property that has received considerable attention in the study of DOM is average molecular weight and the overall size distribution of sub-components. Although molecular weight (MW) can be assessed using different techniques (e.g., vapor pressure osmometry, field flow fractionation and high resolution mass spectrometry (Aiken et al., 1987; Appiani et al., 2014; McAdams et al., 2018; Pavlik and Perdue, 2015; Remucal et al., 2012), many assessments are

based on the use of size exclusion chromatography (SEC) (Her et al., 2002; Huber et al., 2011). SEC can be used to determine the *apparent* MW (AMW) distribution of DOM. Determination of the AMW (in contrast to *absolute* molecular weight) is based on the fact that the separation is not strictly due to molecular weight, but instead based on hydrodynamic size, which is affected by solution chemistry and non-ideal interactions within the SEC-column (Hawkes et al., 2019; Swift and Posner, 1971). Therefore, the terms AMW and molecular size are use synonymously throughout the text. Applications of SEC for the study of DOM include systems where quantification is based on carbon, nitrogen, or optical properties, therefore offering different qualitative and quantitative information about the samples (Huber et al., 2011).

The type and amount of information obtained from SEC analysis is dependent upon the form of detection that is paired with an SEC system. Early SEC studies often relied on UV-Absorbance detectors that were constrained to detection at a single wavelength (typically at wavelength (λ) of 254 nm) per analysis and thus were limited in their analysis capabilities. For example, it is known that only a portion of DOM absorbs light (chromophoric DOM), and that within the chromophoric DOM pool, different fractions and components absorb in varying intensities at various wavelengths relating to structure and behavior within the environment.

In recent years there has been significant development to the forms of detection that can be coupled with SEC. For example, commercially available online absorbance detectors now have the ability to record scans of wavelength ranges and fluorescence detectors can scan either a range of excitation wavelengths at a set emission wavelength or a range of emission wavelengths at a set excitation wavelength. Additionally, TOC instruments that have traditionally been used for offline bulk water analysis can now be configured as online SEC detectors (Her et al., 2003, 2002).

Moreover, by coupling multiple forms of detection, it is now possible to capture several properties of DOM samples in a single SEC analysis.

1.3 Optical Properties

The application of DOM analysis with optical properties (i.e. absorbance and fluorescence) has gained significant attention over the past 30+ years (Coble et al., 1990; Coble, 1996; Helms et al., 2009; Henderson et al., 2009; Murphy et al., 2008; Summers et al., 1987; Weishaar et al., 2003). These forms of analysis offer high sensitivity, fast analysis times, and require little sample preparation or alteration (Korak et al., 2014). While TOC is generally used as a simple measure for DOM concentration, optical properties can provide information relating to the nature and contents of DOM, allowing optically derived metrics to be used as surrogates for DOM source and composition. For example, Weishaar et. al. demonstrated that the specific UV absorbance at λ = 254 nm ($SUVA_{254}$) is correlated to DOM aromaticity by comparison to ^{13}C NMR data, and McKnight et. al. demonstrated that the fluorescence index (ratio of fluorescence emission intensity at λ = 450 nm to λ = 500 at excitation λ = 370 nm) is correlated to both aromaticity and the microbially vs. terrestrially derived nature of DOM (McKnight et al., 2001).

While absorbance analysis records one data point at a given wavelength, fluorescence analysis requires an excitation and emission wavelength for each data point. These data points are then compiled into three-dimensional fluorescence excitation emission matrices (EEMs) and have been used to distinguish DOM sources, and in general as a surrogate for the physicochemical properties of DOM (D'Andrilli et al., 2013; Korak et al., 2014; Murphy et al., 2008). While fluorescence offers the possibility to collect signals with high sensitivity and relative simplicity (Coble et al., 2014; Korak et al., 2015; Leenheer, 2009; Rosario-Ortiz and Korak, 2017), the

specific chemical components responsible for DOM fluorescence have yet to be identified (Stedmon and Nelson, 2015). Understanding the chemical characteristics of the main types of fluorophores within DOM would help to address deficiencies in fluorescence analysis, such as spectral overlap between fluorophores and the impacts of local environments on fluorescence signals. Insights into fluorophores would highlight fluorescence methods and properties that are sensitive to differences in DOM source and composition and inform how they can be applied, such as the use of DOM fluorescence as a surrogate for wastewater impact (Ulliman et al., 2020).

Chapter 2

Thesis Organization

The main goal of this thesis is to advance the understanding of DOM molecular size and optical properties, their relationship to one another, and how they can be utilized in the water treatment industry, especially in potable water reuse treatment applications. The findings of this research fill knowledge gaps and are important to further the use of these properties in the water treatment industry, including the further development of optical based sensors and probes. The research was primarily conducted with a size exclusion chromatography system (SEC) coupled with absorbance, fluorescence, and dissolved organic carbon (DOC) detection but also involved the use of bulk water absorbance, fluorescence, and DOC instrumentation, a bench scale ozonation process, and a bench scale biofiltration system. This Chapter provides an overview of the content of the following chapters.

Chapter 3 provides a literature review focusing on the opportunities and challenges currently faced by the potable water reuse industry relating to (1) monitoring technologies for the detection of microbial and chemical contaminants (2) monitoring technologies for the detection of chemical contaminants; (3) monitoring considerations related to operational needs; and (4) data management and analytics. Section 3.4.2 highlights the potential for optical-based sensors but also discusses the need for further development of these technologies.

In Chapter 4, a method is developed for the calculation of online fluorescence quantum yield (Φ_f) using the SEC system. This system allows for the decoupling of absorbance and fluorescence signals as a function of apparent molecular size. Previous research has suggested that

bulk water Φ_f is promising with regards to DOM source differentiation and may be especially useful in de facto reuse scenarios. SEC-Φ_f results found that Φ_f increases from ~<1 to 2.5-3 % for the DOM isolates and riverine samples analyzed. Additionally, Pony Lake Fulvic Acid (PLFA) was dosed with ozone at levels similar to those used in treatment systems to demonstrate the ability of the method to track changes to optical properties and molecular size following a chemical process.

Chapter 5 is a demonstration of the conservative mixing behavior with respect to molecular size and optical properties when sources of DOM are blended. A pair of DOM sources derived from DOM isolates Suwannee River fulvic acid (SRFA) and Suwannee River humic acid (SRHA) were analyzed with the SEC system. Mass balance properties were then applied to predict molecular size and optical signals of blended samples using that of the individual sources in the blend pairs (i.e., end members). A fundamental understanding of the conservative mixing behavior of DOM optical properties and molecular size are critical if these properties are to be used for applications of DOM source differentiation.

Chapter 6 aims to further the understanding of Peak B and Peak T (i.e., "protein-like fluorescence") in the DOM of a paired surface water and wastewater. The SEC system was used to collect the large and medium-to-small molecular size fractions from the surface and wastewater pair for analysis with an offline benchtop fluorometer. The offline fluorescence data was used to investigate (1) The details of the occurrence of "protein-like" fluorescence in the collected fractions, and the impacts of spectral overlap from the Peak A region on the interpretations of Peak B/T like fluorescence in the medium-to-small fraction and (2) the potential for quenching of "protein-like" fluorescence by Peak A fluorescence between the collected fractions. SEC data was also used to compare the characterizations of source water DOM and wastewater derived EfOM.

Finally, a biofiltration experiment was performed to isolate microbially derived DOM for analysis and characterization. This data was used to investigate the link between "protein-like" fluorescence and microbial activity. This information will be important for the future development of fluorescence-based probes used in water treatment.

Chapter 7 provides a summary and conclusions of the findings in Chapters 3-6 and Chapter 8 discusses the recommendations and future work that would build off the research presented in Chapters 3-6.

Chapter 3

Review of Potable Reuse Monitoring Technologies

3.1 Introduction

Potable water reuse is at a critical juncture, as the need for reuse is growing significantly. Changes in climatic patterns, coupled with population growth in arid regions, will continue to drive the expanded use of reuse to supplement existing water resources (Haddeland et al., 2014). Researchers, consultants, and utilities are looking for more sustainable treatment approaches which can expand traditional water portfolios. However, because the quality of this *new resource* (*i.e.,* wastewater) may necessitate more extensive treatment, there is the possibility that aesthetic or health-based water quality issues may arise if proper care is not taken. Implementing appropriate water quality monitoring and interpreting data correctly are key to ensuring the delivery of safe water. While many technologies and approaches to monitoring potable water reuse are currently available, additional tools are needed to ensure safety and future regulatory compliance for potable reuse treatment plants and especially for those plants that do not use a reverse osmosis membrane-based treatment approach (e.g., membrane filtration/reverse osmosis/UV advanced oxidation process MF/RO/UVAOP).

3.2 Overview of State-of-the-Art Reuse

The diminishing availability of freshwater in many regions in the world continues to motivate research into water reuse. Water reuse is typically divided into non-potable and potable reuse. Non-potable reuse is typically used for irrigation, industrial, and other non-drinking uses.

Potable reuse is typically divided into indirect potable reuse (IPR) and direct potable reuse (DPR). This paper focuses on potable reuse – either IPR or DPR. Figure 3.1 presents examples of typical treatment trains for reuse aplications.

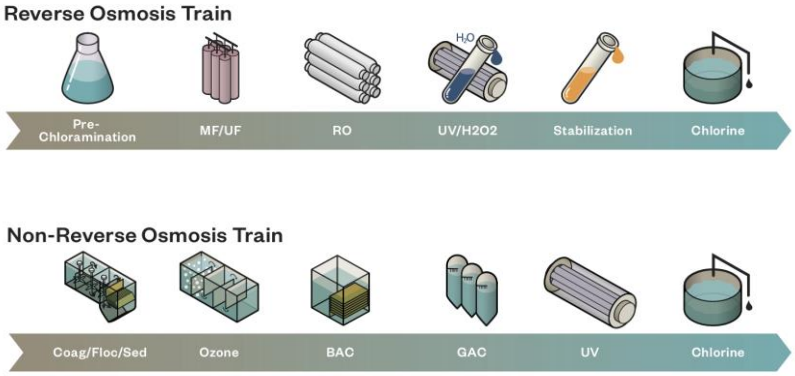

Figure 3.1 Schematics of Typical Treatment Process Trains Used in Water Reuse Applications. **Top:** Reverse Osmosis (RO) based treatment train with prechloramination, microfiltration/ultrafiltration (MF/UF), reverse osmosis (RO), UV-hydrogen peroxide (UV/H2O2), stabilization and an engineered storage buffer (ESB) with a chlorine residual. **Bottom:** non-RO based treatment train with coagulation/flocculation/sedimentation (Coag/Floc/Sed), ozone, biologically activated carbon (BAC), granular activated carbon (GAC), UV, and an ESB with chlorine residual.

One of the main concerns regarding the widespread application of potable water reuse is the neccesity for the system to protect humal health. This is especially true for DPR applications. When thinking about potable water reuse from a public health perspective, the main concerns are microbial and chemical contaminants. Sources of contamination in reuse systems include not only domestic users, but also industrial discharges. There are numerous reports on the characterization of contaminants in reuse systems. For example, concentrations of organic contaminants, although varied, are typically higher than what would be expected from any source water (Focazio et al., 2008). Pathogenic contamination is also significant (Amoueyan et al., 2017). Because in most cases is is not feasible to detect actual concentrations with online (i.e., real-time) monitoring of

specific pathogens, this aspect of water treatment also relies on the use of surrogat parameters to monitor treatment processes.

In addition to public health considerations, there are monitoring issues surrounding the efficient operations of potable reuse facilities that must be considered. These include, but are not limited to, variations in feed water quality (effluent from the wastewater treatment plant) that can cause membrane fouling, rapid variations in oxidant or coagulant demand, and changes in the efficacy of biological treatment. To ensure overall safety, the hazardous analysis and critical control point (HACCP) methodology is utilized in the planning and design of potable reuse facilities. The water qualty monitoring needs at reuse facilities encompass four distinct, but related, areas: microbial contaminants, chemical contaminants, operational needs, and data management and analytics interpretation as discussed in the following sections. As the field moves to expand DPR supplies, there needs to be attention on the operation of plants and the use of sensors to monitor operation.

This review focuses on the opportunities and challenges with respect to: (1) technologies for monitoring microbial contaminants; (2) technologies for monitoring chemical contaminants; (3) monitoring associated with operational needs; and (4) data management and analytics. The review includes proven conventional technologies as well as emerging and future potential technologies. The review concludes with thoughts on future outlook and recommendations with regards to contaminant monitoring, treatment system operation and data management and analytics in reuse systems moving forward.

3.3 Regulatory Drivers

The United States Environmental Protection Agency (USEPA) has not promulgated any regulations governing water reuse; its guidance (US EPA 2012 and 2017) provides some basic regulatory framework concepts and case studies, which are used in combination with reliance on the Safe Drinking Act regulations, but does not provide a regulatory path to potable reuse (Kadeli, 2012; Olivieri et al., 2020; USEPA, 2017a). Several states have developed or are in the process of developing reuse regulations including California, Texas, Florida, Colorado, and Arizona. Other states are also considering or moving forward with regulations. The most stringent DPR regulations to date are being developed by California State Water Board's Division of Drinking Water (DDW) which has issued the "A Proposed Framework of Regulating Direct Potable Reuse in California" (California State Water Resources Control Board (CSWRCB), 2019). The latest proposed framework is Addendum version 8-17-2021 and requires 20 log virus, 14 log *Giardia* and 15 log *Cryptosporidium* removal (CSWRCB, 2021). The framework also requires that any entity (or entities) that desire to practice DPR must specify a Direct Potable Reuse Responsible Agency (DiPRRA) which is a public water system that is responsible for using municipal wastewater for treatment and provides DPR project water directly for distribution, or for transmission to a water treatment plant prior to distribution. The DiPRRA must develop a monitoring plan that describes all monitoring that will be performed including source control monitoring, treatment process monitoring, and operational monitoring. The plan must also detail the calibration and verification of continuous on-line monitoring equipment associated with pathogen and chemical control points. The rationale for the monitoring plan is that the monitoring requirements for DPR projects are complex, and a written monitoring plan is required to ensure the monitoring is conducted as required (CSWRCB, 2019). For IPR the monitoring plans are

typically included in the operations plan. While several states continue to develop individual regulations, those provided by California are the most stringent and perscriptive and thus are the regulations that are referenced in the majority of this text.

3.4 Detection Technologies

For potable reuse water to be considered safe for public consumption it is imperative that microbiological and chemical contaminants are removed. Therefore, it is also critical to efficiently monitor contaminant removal by treatment processes in a manner that is acceptable for potable reuse systems. Similar to drinking and wastewater treatment, the acceptable level of contaminants is often very low leading to the need for analysis methods with high levels of precision (Thompson and Dickenson, 2020). However, because wastewater effluent serves as the source water for potable reuse, there is a potentially increased risk for the presence of contaminants in the water entering a potable reuse system (Nguyen et al., 2018). This necessitates find ways to monitor water conditions and contaminant removal in real-time to understand when barrier breakthroughs occur before the water leaves the potable reuse facility. Because it is often not possible for real-time analysis to measure specific contaminants directly, there is a need for surrogate parameters (Bailey et al., 2021; Dickenson et al., 2011, 2009; National Research Council, 2004; Olivieri et al., 2020; Thompson and Dickenson, 2020). Surrogate parameters are those which can indirectly monitor contaminant removal by direct correlation to the removal of indicator organisms/compounds (California Department of Public Health (CDPH), 2014). Indicator organisms/compounds are those that represent a family or class of human pathogens or compounds and are present at concentrations in which they can be reliably detected (Bailey et al., 2021; National Research Council, 2004; CDPH, 2014).

This section discusses several technologies, either currently available or that offer promise but require further development, that are capable of monitoring contaminant removal with a focus on those with real-time measurement capabilities. Because these approaches often measure contaminant removal indirectly, they are an assessment of barrier performance and do not discern concentrations of all contaminants. For example, turbidity measurements are typically used to monitor for microbiological contaminants (National Research Council, 2004), but may also indicate that breakthrough in chemical contamination is likely occurring (WHO, 2017). Therefore, several monitoring approaches and technologies can be used to monitor for both microbiological and chemical contaminants and these are presented in both section 3.1 and 3.2 (discussion of microbiological and chemical contaminant monitoring respectively). Additionally, offline and laboratory-based analysis (e.g., offline qPCR, mass spectroscopy etc.) is still needed to confirm the presence of specific contaminants and precise contaminant levels, however, these technologies are not presented as part of this review.

3.4.1 Microbiological Detection Technologies

Critical to the protection of public health during potable reuse treatment is the control of microbial pathogens, as even a momentary lapse could result in acute illness. As a result, state mandates pose strict requirements for microbial treatment (USEPA, 2017a). The need to achieve high levels of microbial removal poses challenges in monitoring the performance of treatment barriers. As outlined in the WRRF 11-06 report (Waller, 2014), the sensitivity of microbial methods would have to be improved by 25,000 to 100,000-fold. The report concluded “In other words, the near-term prospect of using direct pathogen measurements to confirm the microbial quality of treated water is essentially zero.” However, it is feasible for monitors to evaluate the performance of unit processes microbial removal using a variety of surrogate parameters. These

technologies focus on measurement of "barrier indicators" rather than indicators of specific pathogens.

When considering measures of microbial treatment performance, sensors can be divided into three categories 1) conventional technologies, 2) emerging technologies, and 3) potential technologies. Conventional technologies are sensors that are already widely used in the water industry and have extensive operational experience, whereas emerging technologies are sensors that have completed some research or pilot applications but do not yet have wide full-scale application. These technologies are promising but need further evaluation. Lastly, potential technologies are still in the developmental stage. These technologies may hold promise in the laboratory, but still need to be proven accurate and reliable in the field.

Conventional Technologies

Because of the difficulties in measuring pathogens in treated reclaimed water, most utilities are using conventional on-line measures of treatment performance (Fabbri and Bianco Prevot, 2021; Pepper and Snyder, 2016). These conventional measures include turbidity, ultraviolet absorbance/transmittance (UVA/UVT), conductivity, TOC, particle counting, ozone, chlorine sensors. Reviews of full-scale treatment plants in Perth, Australia, Sacramento, CA, Los Angeles County, CA, Orange County, CA, Tucson, AZ and others confirm that utilities valued the reliability and dependability of these analyzers, although for the case of microbiological contamination, these are all surrogate measurements (Pepper and Snyder, 2016).

Turbidity and Particle Counters. Turbidity is measured by the 90^{o} light scatter of particles in water and is most sensitive to particles in the size range of 0.1-0.5 μm (Morris, 1987). Similarly, particle counters measure the change in light transmittance through a fixed volume of liquid as a

result of particles blocking the light source with a typical minimum particle size detection of 500 nm (Ostarcevic et al., 2018). Therefore, these devices cannot be used to detect microbes directly but have a long history of use for monitoring water treatment plant filter performance. The equipment is reliable with proper maintenance and calibration. Laser turbidimeters coupled to intelligent interpretive algorithms can be used to establish baseline conditions for water quality and then recognize when changes in baseline conditions are indicative of altered water quality. The Texas Commission on Environmental Quality (TCEQ) has accepted laser turbidimetry as an alternative membrane monitor method for individual filter effluent measurements from membrane units providing pathogen removal (TCEQ, 2019). The performance of laser turbidimetry has been reported as most favorable for low pressure membrane applications, whereas the low particle counts typical in pretreated high-pressure membrane (RO) applications results in too few particles to measure high levels of particle removals (e.g., low LRVs). However, a major limitation of quantifying LRVs is related to the sensitivity of the instrumentation and low TOC in most high-pressure membrane applications.

TOC and UV-Vis Absorbance. TOC is a direct measure of all the organic carbon contained in a sample and is used to quantify the concentration of DOM. Ultraviolet-visible absorbance (UV-VIS) measures the absorbance of light by constituents dissolved in the water at specific wavelengths, most notably 254 nm (i.e., UV_{254}). Both are used as surrogates for barrier performance and can be used to monitor several treatment processes. Because both TOC and UV-VIS absorbance are also used to monitor processes for chemical contaminants for which the approach is similar, an expanded discussion of these parameters is provided in section 3.2.

Electrical Conductivity. Electrical conductivity (EC) is a measure of how readily electrons can pass through water and is used to quantify the total amount of charged species (i.e., ions) in water.

EC can be used as an indicator of membrane integrity, however, temperature, feed concentration, pressure, and fouling can all have an effect on permeate EC measurements. EC monitoring is useful when the feed water contains a relatively high concentration of salt that is efficiently rejected by an RO membrane. Due to the ease of implementation, conductivity monitoring is a common method for detection of integrity monitoring at full-scale for NF and RO systems, but the resolution of the method is low and can provide only up to 2 $\log_{10}$ removal when feed EC is around 20,000 µS/cm and permeate EC is 200 µS/cm. During pilot-scale evaluations at the Beenyup Wastewater Treatment Plant and Advanced Water Recycling Plant in Perth, Australia, TOC, turbidity, and conductivity sensors were useful to evaluate process control (Pepper and Snyder, 2016; van den Broeke et al., 2014).

Specific Ions. Measurement of the removal of specific ions such a sulfate or strontium has been used to demonstrate membrane integrity (Bernados, 2018; OCWD, 2021; Pype, 2015), but the selection of the specific ion depends on the natural abundance in the source water. Scale forming compounds such as $BaSO_4$ and $CaSO_4$, however, can alter the measured permeate sulfate concentration as well as adversely affect membrane performance. Removal efficiencies of sulfate and strontium across RO membranes of 3-4 logs has been consistently demonstrated (Bernados, 2018; OCWD, 2021; Pype, 2015) and regulators in Australia and California have approved the use of these ions for monitoring for demonstration of membrane performance.

Multiparameter Analysis. Commercial systems such as S::CAN Spectrolyzer, and multi sensor sondes (e.g., YSI 6920DW & 600DW-B, Hydraclam, Censar, Intellisonde, etc.) are available for multi-parameter analyses, but their applications are more limited. Challenges with conventional sensors include the management and analysis of the on-line data and aggregating the data streams to produce a multi-dimensional predictor of plant performance.

- Multi sensor sondes are available from a number of vendors for a wide variety of parameters. These devices allow multiple online analyzers to be incorporated into a single device and have been used for real-time monitoring for a variety of process control parameters, including ammonia, nitrate, dissolved oxygen, oxidation/reduction potential (ORP), chlorine, pH, temperature, chlorophyl A, rodamine, etc. (van den Broeke et al., 2014). With the deployment of a large number of sensors, routine calibration and quality control is important in maintaining reliable data.

- The S::CAN Spectrolyzer uses UV spectroscopy to generate a broadband picture of the overall water quality. Comparison of peaks in the signal before and after treatment can give an indication of contaminat removal. The units were used at the Woronora water treatment plant in South Africa for measurement of dissolved organic carbon with success. It was reported that the S::CAN units required minimal maintenance during the project and produced a generally high quality of data (van den Broeke et al., 2014). However, the limit of detection hampered the use of the instrument for measuring high levels of membrane performance (Pepper and Snyder, 2016).

Emerging Technologies

The list of emerging technologies is both evolving; this category is defined as technologies that have undergone independent research, demonstrated capability for process monitoring, and are ready for full scale demonstration and application. Table 3.1 provides an overview of some promising technologies.

Table 3.1 Emerging Microbiological Detection Technologies. A list of emerging microbiological detection technologies that are ready for full scale testing and implementation.

Technology	Description	Notes	Reference

Biosentry	Multi-angle light (MAL) scattering technology. Online real-time sensor that allows for continuous monitoring creating light patterns that vary depending on size and characteristics of target particles.	• Can be used to monitor bacterial removal by membrane and granular media filters.	(Pepper and Snyder, 2016)
Bio Scan	Measures biomarkers for viable bacteria and fungi (nicotinamide adenine dinucleotide and riboflavin) as well as proteins in microorganisms. A sensor is then used to identify the fluorescence emission.	• Interference due to the background fluorescence signal of the DOM is currently a challenge for widespread implementation. • WRFs' Reuse-11-01 project noted that the technology was not able to distinguish the difference between infective and killed *E. Coli*.	(Pepper and Snyder, 2016)
Flow Cytometers	Continuously monitors microorganisms in the process stream over a wide range of concentrations.	• The sensitivity of the method is not capable of determining the acceptable microbial quality of treated effluents, however, it can be used for total bacterial quantification in the field. • This technology is currently used for routine water-quality analysis by the Zurich Waterworks and several other Swiss and Dutch drinking water suppliers. • The Sentinel Monitoring Systems VBmicro flow cytometry provides a dection limit of <10 cells / 100 mL within 60 minutes. • Water Research Foundation project 5104 is evaluating DNA nanostructure surrogates that include fluorescently labeled oligonucleotide that allow for detection and quantification by flow cytometry without nucleic acid staining	(Besmer et al., 2014; Egli and Kotzsch, 2015; Hammes et al., 2012) http://www.sentinelmonitors.com/
Portable Fluorescence cell sorter/ counter	Uses 4-methyl-umbelliferone-β-D-glucuronide as a substrate which allowed the results to be easily compared to other traditional microbial methods.	• A portable handheld fluorescence detector was developed by Wildeboer et al. (2010) as a cell **sorter/counter** for the rapid detection of *E. coli* in water.	(Wildeboer et al., 2010)
Light Induced Fluorescence Emission (LIFE)	Uses high-energy deep-UV photons and deep neural nets to detect aromatic compounds including amino acids, proteins, DNA, microbial cells and their metabolites. ORB XYZ, Inc.	• Full scale trials by Anglian Water found that the sensor helped them to better understand their risk profiles, plan investigatory sampling and reduce time and operational costs. • The technology is currently being evaluated as part of a USBR-funded pilot plant project.	(https://www.usbr.gov/newsroom/#/news-release/4084).
LuminUltra	Test for total microbial content in water based on ATP levels produced by microbes.	• ATP is a useful surrogate because it is only associated with viable or recently viable cells. • Has strong potential as a surrogate parameter for analyzing microbial loads in test waters and for process control in treatment trains. • An on-line analyzer is available and an updated model is expected to be released in 2022.	(Pepper and Snyder, 2016)

Pulsed Fluorescence Marker	Fluorescent chemical tracers can be delivered as continuous feeds, pulses or as particles (microspheres).	• Fluorescent tracers have been widely reported for RO systems in order to assess virus removal or to determine LRVs. • fluorescence can be affected by the presence of chlorinated oxidizing agents, UV light and temperature and the correlation between the tracers and solid particles such as viruses and other pathogens is limited. • Fluorescent tracers can be delivered as continuous feeds, pulses or as particles (microspheres). • WRRF-09-06b concluded that the technology needs additional full-scale application.	(Frenkel and Cohen, 2014) (Ostarcevic et al., 2018) (Yoon, 2019)

The commonality of these emerging technologies is the need for more full-scale application and experience. To improve the industry acceptance of these technologies, there needs to be more information on the long-term performance and reliability of the instruments at the demonstration scale. Potential interferences must be well understood and be manageable. For these technologies to monitor critical processes, utilities must have confidence in the stability and quality of the data. Instruments that require frequent calibration or maintenance will not meet the reliability criteria of most utilities.

Potential Technologies

The list of potential technologies is essentially limitless as innovations in integrity testing continue to develop. The commonality in these technologies is that they require additional research to improve the sensitivity and reliability, before they could be realistically used for process monitoring. Table 3.2 provides an overview of these technologies.

Table 3.2. Potential Microbiological Detection Technologies. A list of potential microbiological detection technologies that require additional research to improve the sensitivity, reliability, or full-scale applications before they could be realistically used for process monitoring.

Technology	Description	Notes	References
Direct Microbial Testing	qPCR or other molecular assay	• A variety of targets have been proposed (e.g., phage, human and plant viruses, etc.)	(Tandukar et al., 2020; Yasui et al., 2021)

		• These assays are limited by the need to concentrate massive amounts of water to achieve the necessary limits of detection. • Microfluidic chip (lab-on-a-chip) technology is developing but still requires preconcentration. • The CRENAME (Concentration Recovery Extraction of Nucleic Acids and Molecular Enrichment) is a developing technology for molecular enrichment by whole genome amplification but requires 4 hours and is subject to inhibitors in the water.	
Indigenous Metagenomics	Hornstra et al. (2019) used metagenomics to identify indigenous viruses in a Dutch water supply and developed qPCR primers for a set of four viruses that were present in high numbers.	• The concentration of viruses were sufficient to demonstrate greater than 7 log removal through the plant. • Examination of three rivers and a lake in the Netherlands, Germany, and Belgium detected the viruses at levels greater than 1.8×10^8 gene copies per liter. The researchers reported that removal of the naturally occurring viruses was comparable to the results of the spiked MS2 bacteriophage. • It remains to be seen if these indigenous viruses are preset at high levels in all source waters, but the approach to use metagenomics to scan for naturally occurring viruses could be used in other locations. • The study is significant in that it provides a natural biological indicator for membrane integrity testing	(Hornstra et al., 2019)
Evanescent wave fiber optic sensors	Use a laser spectrofluorometer to detect an evanescent wave that is excited over a sample.	• The sensors can be highly customized to detect a range of pathogens and can be integrated into existing systems enabling the potential for online testing using flow-through systems. • Systems are currently susceptible to interference from background matrices. • Examples include the RAPTOR fiber optic biosensor and whispering gallery mode microlasers. Both technologies currently have operational	(Leskinen and Lim, 2008; Taitt et al., 2005; Vollmer, 2010)

		challenges that curtail widespread implementation	
Acoustic Wave Biosensors	Consist of a metal electrode that mechanically generate acoustic waves through water.	• Biochemical interactions with target microbes result in changes in the acoustic wave that are detected and then analyzed with output signals related to the type and concentration of microbe in the medium.	(Rocha-Gaso et al., 2009)
Surface Plasmon Resonance Biosensors	Based on a change in refractive index of a metallic surface irradiated with a light source reflected at an angle defined by the type and amount of target bacteria in the solution.	• The sensitive instrumentation, however, is limited by environmental exposure.	(Wei et al., 2007)
Piezoelectric Sensors	Measure changes in mass, resonance deflection on a quartz sensor once microbes bind to an antibody attached the surface.	• Current applications exist for food systems, but applications are developing environmental monitoring, biological tests, and technological processes.	(Kuchmenko and Lvova, 2019)
Quantum Dots	Linked to DNA. Probes capture and concentrate DNA from specific targets and are then detected using fluorescence resonance energy transfer.	• The system requires specialized personnel to operate the bench-scale systems and is relatively expensive.	(Zhang and Hu, 2010)
Carbon Nanotubes	Carbon nanotubes can be functionalized with specific receptors to specifically bind and report the detection of a wide array of environmental contaminants.	• Incorporated into biosensors • Still challenged with nonspecific binding, particle size variation, aggregation, and the inability to differentiate viable organisms.	(Vikesland and Wigginton, 2010)
Raman Spectroscopy	Non-invasive and reagent-free method that has been successfully applied to identify, differentiate, and classify pathogenic microorganisms based on their unique spectroscopic signatures.	• In surface-enhanced Raman spectroscopy, microorganisms are identified by the spectra produced by the surface of the organism following reaction with antibodies.	(Szabo, 2010)
Forrier Transform Infrared Spectroscopy	Infrared light interacts with various organic functional groups to identify bacteria.	• A major drawback of this method is that the molecular composition of microorganisms depends on various metabolic and environmental factors.	(Zhuang et al., 2020)

This brief overview of current, emerging, and potential techniques for microbial membrane integrity monitoring is expanded in Appendix A. The limitations and complexities of some techniques reduces the opportunities for application.

Most exciting of these potential technologies is the work of Hornstra et al. (2019) because it provides the potential to measure indigenous viruses in the feed water as a measure of direct microbial removal. Additional research is needed to determine the applicability of the existing set of naturally occurring viruses to a variety of source waters (Hornstra et al., 2019). Even if additional metagenomic work is needed to identify other indigenous viruses, developing a broader set of primers to measure indigenous viruses for a variety of sources water would result in a valuable tool for directly measuring microbial removals for treatment processes. Although on-line qPCR concentration and processing is a technology still in development, periodic testing for the removal of indigenous viruses could be a useful complement to other conventional and emerging on-line technologies.

3.4.2 Chemical Detection Technologies

The other aspect associated with the safety of water reuse is the presence of chemical contaminants – both regulated chemicals (e.g., regulated inorganic compounds, disinfection byproducts (DBPs) etc.) as well as "chemicals of emerging concern" (CECs) (Keller et al., 2022; Thompson and Dickenson, 2020). Some regulated chemicals such as total nitrogen (TN) are present in concentrations high enough to measure directly (Drewes et al., 2018). Other regulated contaminants, such as regulated DBPs are present in low concentrations, but the prevention and control of their formation is well understood. For example, in the case of trihalomethanes (THMs) and haloacetic acids (HAAs), precursor water conditions have been related to TOC concentration and chlorine dose, both of which can be monitored directly (Edzwald et al., 1985; Nikolaou et al., 2004; Nikolaou and Lekkas, 2001).

CECs represent a group of contaminants typically present at trace levels, and the information on their occurrence, prevention, and monitoring is more limited (Thompson and

Dickenson, 2020). There are numerous reports documenting the wide occurrence of CECs in wastewater, and the performance of various unit operations for removal. More recently, emphasis has been shifting to non-target analysis of contaminants in wastewater, acknowledging the reality that thousands of compounds are present, and as more compounds are introduced, more will be present in water reuse systems (Singer et al., 2016). The California Water Resources Control Board, in guidance from 2018, identified a list of 489 CECs, while only recommending that three different representative compounds are selected and monitored as indicators of potential human health (CSWRCB, 2018). It is reasonable to expect that more will be found as the use of non-targeted analysis expands and as we recognize the occurrence of transformation products from oxidative treatments (Drewes et al., 2018).

While the intention of this section is to cover the monitoring for all chemical contaminants (TOrCs, inorganic contaminants, metals etc.), the primary focus is on CECs due to the need for a better understanding of their occurrence, prevention, and monitoring. However, it should be understood several regulated organic compounds (i.e., atrazine, NDMA etc.) and regulated organic DBPs can be grouped with CECs under the category of trace organic contaminants (TOrCs), and that the monitoring approaches discussed in the context of CECs apply to other TOrCs as well.

Table 3.3. Potential Chemical Contaminant Surrogates. A list of potential chemical contaminant surrogate categories and specific metrics/ parameters.

Sensor Category/ Type	Metric/ Parameter	Description	Notes	Reference
TOC	TOC	Measurement of TOC concentration.	Only represents simple concentration and cannot be used to characterize DOM in sample. Limitations from limits of detection.	(CDPH, 2014)
UV-VIS Absorbance/Transmittance (UVA/UVT)	UV_{254}	Measurement of UV absorbance at 254 nm	Used to detect the presence of aromatic DOM.	(Edzwald et al., 1985)

			Can be related to the concentration of DOM.	
	$SUVA_{254}$	UV254 per TOC. Calculated as the UV254 absorbance divided by TOC concentration	Provides relative aromaticity of DOM present in sample.	(Edzwald et al., 1985)
	E2:E3	Ratio of absorbance at 254 to 365 nm	Relates to average molecular size.	(Summers et al., 1987)
Fluorescence	Total Fluorescence	Calculated as the sum of total fluorescence emission, by integrating emission spectra, at a given excitation wavelength	Integration of multiple emission wavelengths results in increased signal intensity, but the measurement is somewhat coarse.	(Song et al., 2021)
	Fluorescence Peak Regions	Fluorescence intensity in different regions of an excitation emission matrix (EEM). Relevant regions include: Peak A Peak C Peak T	Specific peak regions have been related to DOM source and composition.	(Coble et al., 1990)
	Quantum Yield	Provides relative fluorescence efficiency of sample media Calculated as the integration of fluorescence emission at a given excitation wavelength divided by absorbance at the	Intrinsic parameter found to be reliable in differentiating between sources of DOM.	(Ulliman et al., 2020)
	PARAFAC	Statistical decomposition of fluorescence components.	Can discern the concentrations of specific fluorescence components which can be related to DOM source and composisiton, but likely not realistic to incorporate into online sensors.	(Wünsch et al., 2017)
ECD	EDC	Measure of the remaining oxidant demand of DOM.	Can be correlated to contaminant abatement during ozone processes.	(Song et al., 2021)
Nitrate	Nitrate Formation	Measurement of nitrate formed during ozonation.	Nitrate is formed during the reaction between DON and ozone. Can be related to contaminant abatement.	(Chon et al., 2015)

TOC

CEC quantification necessitates the use of sample preparation steps, followed by analysis by mass spectrometry, which is costly and not feasible for continuous monitoring in any water production facility. There are no widely accepted methods to monitor CECs in reuse facilities, and given the complex matrix, it is unlikely that applications will be developed for monitoring single compounds. Technologies based on the measurement of a toxicological response may be better suited for application to reuse systems, but even then, there has been limited development work and even more limited ability to apply the results to meaningful action by operations teams. Consequently, water reuse facilities have been relying on the measurement and characterization of TOC (from wastewater origin) to indirectly monitor for undesirable constituents present in influent streams (e.g. CECs) and as a means to evaluate the performance of unit treatment processes. The TOC in reuse applications is better described as effluent organic matter (EfOM). In applications considering potable reuse, TOC is most likely a combination of EfOM and NOM from traditional supplies.

The premise is that by reducing TOC in the product water, human exposure to CECs (and pathogens) that may threaten human health will also be reduced. For example, the State of California requires TOC not to exceed 0.5 mg/L averaged over 20 weeks (CDPH, 2014) and Environmental Protection Agency (EPA) guidelines for IPR recommend a TOC limit of 2 mg/L (Kadeli, 2012). However, TOC is a bulk parameter that provides no information regarding the origin of the organic matter (i.e., DOM from natural sources or EfOM from wastewater origin) and may not have enough sensitivity at low TOC values (<0.2 mg/L) to indicate the presence of low molecular weight compounds, such as 1,4 dioxane and *n*-nitrosodimethylamine (NDMA). With respect to monitoring RO, TOC monitoring can only provide a rejection of around 99.75%

(2.6 log10) and may require different analyzers for the feed and permeate waters (Ostarcevic et al., 2018). Additionally, while oxidative processes such as ozonation and UV/AOP are capable of degrading CEC's, they may only achieve partial oxidation rather than complete mineralization (i.e., oxidize compounds to CO_2). When this occurs, it is possible that the overall measured TOC remains relatively constant following an oxidative process and is therefore not representative of contaminant removal. For example, Yu et. al., found that following UV/H_2O_2 doses required to achieve 50%, 70%, and 90% removal of 18 selected organic contaminants, the measured change in TOC, measured using both offline (combustion catalytic oxidation method) and online chemical-based (UV/ persulfate method) instrumentation, was always less than 10% (Yu et al., 2015). As a result of these limitations, a better approach would be to monitor the *quality* of the TOC present in influent streams rather than the concentration. For example, the ability to differentiate DOM from EfOM would allow reuse plants to have an online surrogate for wastewater levels and as a corollary, CECs.

Optical Surrogates

Recently, the use of sensor-based technologies, capable of quantifying different optical metrics rapidly and at high sensitivity levels with minimal sample volume or sample preparation, are gaining attention as tools to monitor in real-time the quality of the TOC (Carstea et al., 2016; Henderson et al., 2009; Hu et al., 2016; Hudson et al., 2007; Ruhala and Zarnetske, 2017). Notably, most of these sensors rely on the use of UV-Vis or fluorescence spectroscopy, which essentially characterize the chromophoric DOM (that which absorbs UV light) and fluorescent DOM. Numerous optical parameters have been developed using absorbance and fluorescence measurements to differentiate EfOM from DOM. Some of these parameters have been evaluated for reuse applications as well. For example, the maximum or integrated fluorescence intensities

within pre-defined excitation and emission regions (Coble, 1996) and components identified in parallel factor analysis (PARAFAC) have been used as optical surrogates for EfOM or organic contaminants coexisting with EfOM (Baker, 2001; Carstea et al., 2010; Hur and Cho, 2012; Riopel et al., 2014; Rock et al., 2019; Sgroi et al., 2017). Absorbance-based parameters including UV254, SUVA254, spectral slope, and others have been used for DOM source discrimination as reviewed by (Li and Hur, 2017).

A common approach and justification for optical parameter selection is to rely on correlations observed in previous studies that have been conducted in a specific experimental context. For example, fluorescence Peak T has been widely used as a surrogate for EfOM since marine studies observed "protein-like" DOM, more specifically amino acids tyrosine and tryptophan, to fluoresce in the same region as Peak T (Yamashita and Tanoue, 2003). However, other studies have demonstrated that the measured fluorescence of Peak T may not be unique to "protein-like" DOM due to polyphenols, and the fluorescence signature of these amino acids is strongly quenched by other DOM moieties (Maie et al., 2007; Wang et al., 2015). These studies question whether the most common, contemporary optical parameters should continue to be prioritized, or if a broader screening process is needed to justify parameters used for quantitative analysis. Optical parameters have also been used for assessments about the performance of unit operations. For example, UV254 has been used as a surrogate for performance of advanced oxidation processes for the removal of CECs, either via ozone- or UV-based AOPs (Wert et al., 2007). In the Yu et. al. (2016) study, the authors found that while TOC concentration changed only minimally following oxidation by UV/H_2O_2, online optical-based TOC, UV254, and total fluorescence (TF) sensors detected much more significant change at levels up to ~20%, 30%, and 45% respectively, and allowed for the calculation of meaningful correlations between the

contaminant removal detected by on-line sensors compared to analysis by liquid chromatography – mass spectroscopy.

Unlike the measurement of TOC, sensor-based technologies are customizable and, therefore, may have the potential to optically determine the relative contribution of wastewater to the overall TOC (Ruhala and Zarnetske, 2017). However, the use of sensor technology needs to be well calibrated against known potential biases and sources of error. For example, a recent study evaluated the potential use of optical parameters for differentiating DOM and EfOM in water reuse applications (Ulliman et al., 2020). They proposed a methodology that identified optical parameters that could detect statistically significant compositional differences between source water DOM and EfOM, independent of overall TOC values and without limited susceptibility to instrument biases (e.g. inner filtering effects for fluorescence measurements). The criteria developed included: (1) capacity of a specific optical property to measure changes in TOC character (i.e., between EfOM and DOM), independent of concentration. This criterion essentially looked for intrinsic properties; (2) the ability of an optical parameter to reliably differentiate between DOM and EfOM, considering Type I and II (false positive and false negative) errors, and the magnitude of a change in a specific optical property; (3) limited impact of instrumental artifacts (e.g., inner filter effects) during implementation.

The criteria were applied to 26 parameters that were measured in paired source water and conventionally treated wastewater samples from sites with varied spatial and temporal conditions. Two parameters, apparent fluorescence quantum yield measured at excitation 370 nm and fluorescence peak ratio A:T, met the above criteria across all sites, suggesting that these two parameters could be considered for further assessment for potential implementation. None of the other 24 parameters evaluated were shown to provide a reliable assessment of the degree of

wastewater EfOM influence. This is a promising area of future work that could ultimately lead to the development of appropriate surrogates for CECs in reuse applications.

Other Metrics

Other metrics that have shown promise as a surrogate to monitor CEC's, specifically with respect to ozonation processes are DOM electron donating capacity (EDC) and nitrate formation (Chon et al., 2015; Song et al., 2017, 2021; Wenk et al., 2013). During ozone treatment, ozone directly oxidizes contaminants, but also produces OH• that further oxidize contaminants. Some contaminants have been found to be highly reactive with ozone while others are recalcitrant and must be oxidized by OH• for removal. However, OH• are short-lived and it is therefore difficult to directly monitor combined oxidation impact from ozone and OH• during ozone processes (Elovitz and von Gunten, 1999). Additionally, ozone processes can lead to form disinfection byproducts (DBPs) such as bromate and N-nitrosodimethylamine (NDMA) (Andrzejewski et al., 2008; Wert et al., 2007). Therefore, it is important to properly monitor ozone processes for both contaminant removal and DBP formation.

While CEC's are often present at levels too low to directly measure, it is known that DOM competes directly with CEC's for oxidation, thus monitoring the oxidant demand of DOM can be used as a surrogate for the oxidation of CEC's. EDC (also referred to electron donating moiety (EDM) measurement) is a measure of how many electrons can be donated during chemical reactions (e.g., oxidation by ozone) and can be used as a measure for oxidant demand (Chon et al., 2015; Wenk et al., 2013; Wu et al., 2020). Monitoring nitrate formation may also be a useful surrogate as nitrate is formed in the reaction between ozone and amino acids that contribute to the composition of dissolved organic nitrogen (DON). Therefore, DON (as a fraction of overall DOM) also competes with CEC's for oxidation(Song et al., 2017).

Currently, UV-absorbance (i.e., UV_{254}) is often used to monitor oxidation processes as chromophoric DOM moieties, react readily with oxidants, often resulting in nonhomophobic products (i.e., UV-absorbance is abated). However, chemical reaction pathways during ozone processes are complex. It is possible that additional chromophoric compounds are formed, meaning compounds are potentially oxidized faster that UV-absorbance is abated, as well as the fact that individual specific contaminants are oxidized at different rates. Oxidation of contaminants and DOM during ozone treatment (as well as the abatement of UV_{254} and EDC, and the formation of nitrate) have also been observed to occur in two distinct phases with significantly different reaction rates (Chon et al., 2015; Song et al., 2021). Therefore, it may be difficult to monitor contaminant removal with UV-absorbance alone. Because EDC is related to oxidant demand, it represents another option to monitor ozone processes. Chon et. al. analyzed the abatement of six contaminants (17α-ethinylestradiol (EE2), carbamazepine (CBZ), atenol (ATE), bezafibrate (BZF), ibuprofen (IBU), and *p*-chlorobenzoic acid (PCBA)) that were spiked into secondary wastewater and treated with ozone. These authors found that four (ATE, BZF, IBU, and pCBA) were more accurately correlated to EDC decline, and two (EE2 and CBZ) were more accurately correlated to UV_{254} decline (Chon et al., 2015). In a similar study that analyzed five of the same contaminants (EE2, CBZ, BZF, IBU, and PCBA), the authors found that correlations were similar for both nitrate formation and UV_{254} abatement (Song et al., 2017).

As mentioned, it is also important to monitor the formation of additional contaminants (i.e., DBPs) during ozone treatment including N-nitrosodimethylamine (NDMA) (Andrzejewski et al., 2008; Schmidt and Brauch, 2008) and bromate (Wert et al., 2007). While the EPA does not currently regulate NDMA levels in drinking water, it does require that NDMA is monitored as it is a known carcinogen (*USEPA*, 2017). In the Song et. al., (2017) study, authors demonstrated that

nitrate formation has potential as useful surrogate for monitoring NDMA formation potential (NDMA-FP), which in turn is a surrogate for total NDMA precursor compounds (Song et al., 2017). These authors found that with increasing specific ozone doses (mg O_3/mg DOC) of a wastewater effluent, NDMA-FP compounds decreased while nitrate (both total nitrate and nitrate from dissolved organic nitrogen (DON)) increased, and that these observations were well correlated with each other. This suggests that NDMA-FP compounds are at least partially the same as those that form nitrate and nitrate formation is therefore potentially useful as a surrogate to monitor NDMA formation during ozone processes. In the Chon et. al. study, authors found that the relative residual EDC was more accurately correlated to bromate formation following ozonation compared to the correlation between bromate formation and the relative residual UVA_{254} (Chon et al., 2015).

3.5 Operations

The successful operation of a potable water advanced treatment facility must manage risk to public health and at the same time be operated reliably and efficiently so as possible to maintain the viability as an option for augmenting the drinking water supply. This highlights the importance of the "Four Rs": redundancy, reliability, robustness, and resilience (Pecson et al., 2015). In balancing these goals, the protection of public health is paramount and must always be the primary focus. A framework that has been widely adopted to support public health protection is the hazard analysis and critical control point (HACCP) process.

Initially developed for the food industry, HACCP is a logical, scientific process control system designed to identify, evaluate, and control hazards. Its purpose is to put in place process controls that will detect and correct deviations in quality processes at the earliest possible opportunity. It focuses on performance and quality monitoring and maintaining the barriers of

treatment, rather than on end of pipe sampling and treatment. Fundamental to the process is the identification of critical control points (CCPs) which are defined as points in the treatment process that are specifically designed to reduce, prevent, or eliminate a human health hazard and for which controls exist to adequately validate the proper performance of that process. Most importantly, these points can be monitored, and if they are not operating within prescribed limits, corrective action can be taken.

When viewed holistically, the HACCP methodology provides an additional two "R"s: response (the action taken by an operator or automated control), and reporting (the identification of critical monitors that report the information needed to trigger a response). In this way, HACCP establishes not only the level of treatment required for potable reuse but also the operational management that is critical and integral to the proper functioning and maintenance of the process and the regulatory acceptance of potable reuse.

Other points that are important to the treatment process, but are not directly related to the protection of public health, are often labelled as critical operating points (COPs). This elevates them to a level of importance for operational consideration however are distinct from those required to protect public health.

3.5.1 Critical Control Points (CCPs)

(Walker et al., 2016) identified CCPs and corresponding critical monitors for both an RO-based advanced treatment system as well as a carbon adsorption-based system. In both cases the goal was to meet drinking water quality standards (USEPA primary MCLs) and pathogenic log removal targets of 12-10-10 (virus, *Giardia* and *Cryptosporidium)* consistent with a 1 in 10,000 annual risk of infection per capita. Figure 3.2 provides an example where the reverse osmosis

process barrier has been identified as a CCP, a conductivity analyzer is used to monitor the CCP and general steps that are taken if the barrier fails.

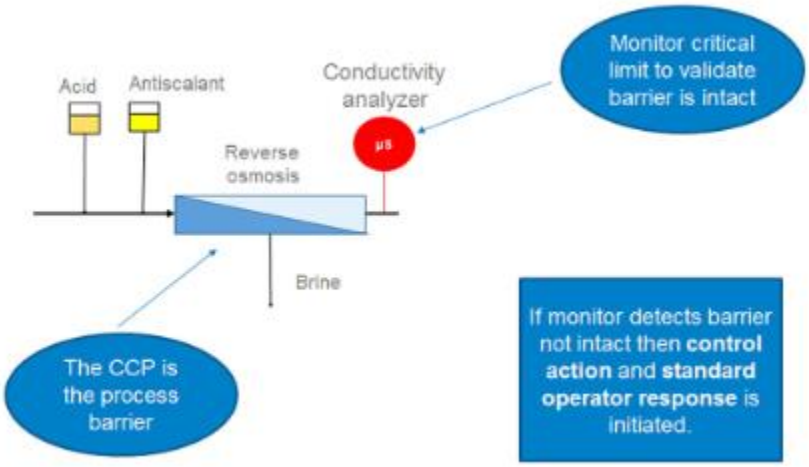

Figure 3.2: Reverse Osmosis Critical Control Point. An Example of a reverse osmosis process as a critical control point and electrical conductivity as a critical monitor, adapted from Walker et. al., 2016

For each CCP, there is a reliance on either a direct or surrogate measurement verified in most cases with online continuous or high frequency operational monitoring as the critical monitor. An important exception is the membrane integrity test which is usually a daily discrete test performed on each MF/UF unit. For each of these monitors, the important operational considerations include: (1) reliability – do the monitors often break down or drift from calibration, requiring either unplanned or burdensome routine maintenance; (2) operability – do the monitors require significant calibration, have many moving parts, and require significant operator attention as part of normal operation; (3) cost – are monitors cost effective, or is investment better spent with additional barriers of treatment; (4) sufficient representation – do monitors produce data that is sufficiently representative of water conditions and contaminant removal during reuse treatment? Each of these considerations is summarized in in Table 3.4.

Reliability

If monitoring systems are unreliable, there is a risk of being unaware of performance degradations or failures that can pose serious health risks. WRRF 13-03 "Critical Control Point Assessment to Quantify Robustness and Reliability of Multiple Treatment Barriers of a DPR Scheme", Walker et al. (2016) considered two methods to examine the reliability of monitors. A first method utilized computer simulations, with a second using the Risk Priority Number (RPN) model. The Risk Priority Number approach assigns a numeric score to steps in a process which quantify the likelihood that a failure will occur (i.e., occurrence index), the severity of harm or damage to personnel or equipment resulting from a failure (i.e., severity index), and the likelihood that a failure will not be detected (i.e., detection index). Using instrument vendor product specification information, the computer simulation method identified TOC as a higher risk analyzer relative to others in the treatment train. By contrast, the RPN methodology determined that while the TOC analyzer had a higher risk of failure, the disinfection process and associated analyzers had a greater impact on potential risk (Walker et al., 2016).

This report was limited to the use of manufacturer supplied reliability information and not based on actual operating experience at potable reuse facilities. There will be value in further work based on actual operating experience to better identify monitoring weak points. For new instruments or analyzers under consideration, an initial review of manufacturer reliability should be considered along with considerations for gathering in field reliability data.

An additional consideration for analyzers includes response time. Analyzers may have a nearly continuous output that is updated multiple times per second, or they can be configured in a semi batch combination of flushing, reagent addition, reaction, and measurement which can delay the response of the instrument for several minutes as the sample is processed. Further, the method

of sampling for instruments may delay the response. Sample sensors may be placed in line or connected by a sample line between the process and the analyzer and the sensor delays response time and may cause erroneous readings if the sample line loses flow.

Operability and Cost

The level of calibration and maintenance required for analyzers can be a significant burden for operational resources. In many cases, the successful management may require specialist instrument technicians either employed directly by the utility or provided under and external contract. The level of effort for calibration and verification was included in zero based staffing assessments for advanced treatment systems as part of WRRF 13-13 (Chapter 5).

Cost of analyzers, parts and maintenance are also key considerations for utilities. Particularly where smaller facilities are considering potable reuse, significant analyzer cost may prove prohibitive.

Sufficient Representation

Finally, it is important to consider the extent to which technologies can effectively monitor contaminant removal across a process. This is of particular importance for treatment barriers in which observed removal by direct measurement (for example via microbial challenge tests through membrane processes) has consistently shown a higher degree of removal than a practical (and currently available) CCP monitor can achieve. A key example is the reverse osmosis process, which due to limitations of electrical conductivity monitoring or TOC monitoring cannot provide sufficient resolution to ascertain beyond 1.5 to 2 log microorganism removal, whereas challenge test studies have demonstrated up to 6 log removal at that same barrier. Other membrane processes such as MF/UF and membrane bioreactors (MBR) also likely “under count” microbiological removal at those barriers due to the limitations of monitoring.

Table 3.4. Important Operational Considerations for Selecting Monitoring Technologies.

Critical Operational Management Points	Operational Consideration	Description
Critical Control Point (CCP)	Reliability	Do monitors often break down or drift out of calibration, require frequent or unplanned maintenance?
	Operability	Do the monitors require significant calibration, have many moving parts, and require significant operator attention as part of normal operation?
	Cost	Are monitors cost effective, or is investment better spent with additional barriers of treatment? Facilities should consider not only initial cost but also cost to maintain and operate sensors.
	Sufficient Representation	Do monitors produce data that is sufficiently representative of water conditions and contaminant removal during reuse treatment?
Critical Operating Point (COP)	NA	Points in a treatment system that are critical to monitor for consistent system performance but do not directly impact public health.

3.5.2 Critical Operating Points (COPs)

In addition to CCPs, which are focused solely on the protection of public health, operations must also consider how to manage consistent system performance to provide good control of ancillary processes that support the CCP barriers (chemical dosing, pre-straining, fouling management), minimization of energy consumption and protection of assets. Performance monitoring is critical in each of these areas also. As useful addition to the CCP process, Critical Operating Points (COPs) are important to the treatment process but do not directly impacting public health (Walker et al., 2016). COPs are often identified and used to highlight important processes and associated monitoring. Examples include pH correction as a part of RO pretreatment or BAC filter flow rate.

Potable reuse facilities are designed and operated as highly automated systems. Operations must be diligent in ensuring that the control and automation system in which the monitor is integrated work correctly and interact effectively to: (1) proactively review performance to anticipate problems before they occur; (2) respond effectively to alarms and shutdown conditions;

(3) provide a thorough investigation of why the problem occurred and transfer lessons learned to improve future operations; (4) return systems safely and effectively to service in a timely manner.

The response time can be significantly influenced by the operating principles of the critical monitor. Sampling frequency is an important consideration. Some analyzers (such as pressure, turbidity, and electrical conductivity) provide an effective continuous reading. Deviations will be quickly identified, and automated corrective action can be taken rapidly. By contrast, an analyzer that discretely samples every 10 or 15 minutes will incur a delay before a deviation is identified, with a commensurate delay in response. A particular challenge is seen with MF/UF systems which validate microbiological removal capability with a discrete daily membrane integrity test. For each unit, a deviation may not be identified for up to 24 hours. In direct potable reuse systems, where engineered storage is required to provide response time, the response time of monitors may have a significant impact on the required storage size and consequently, project capital cost.

3.6 Data Management and Analytics

Implementing and monitoring CCPs and COPs requires fast and accurate data collection, analysis, and response. To achieve these goals, industrial control systems are being integrated with modern data management systems, cloud services (i.e., highly scalable, remote computing resources and web-based visualizations), and algorithms to better detect failures and optimize operations. These technologies are constantly evolving as startups, software companies, and open source programmers drive innovation in their respective fields. To help align these technologies with the needs of potable reuse, both commercial and open-source software products are reviewed and trends, challenges, and opportunities are discussed below.

3.6.1 Software Terminology

To clarify terminology for open source and commercial software, key definitions and common terms are described in the following paragraphs. **Open source software** refers to tools for which the underlying code is publicly available. All software is created using a **programming language**, which is a set of rules and commands that developers can issue to a computer to perform tasks. Examples of popular programming languages include C++, JavaScript, and Python. Many programming languages enable software developers to import **software packages**—a set of tools that developers can use to improve the quality and reduce the effort to write code. For instance, a developer may import a plotting tool that enables them to create data visualizations. Open source software packages enable people to build on each other's work anywhere in the world, accelerating innovation in data management, analysis, and software development. Open source projects may be used to create commercial products but some open source projects limit use to individual or academic developers. Examples of open source software are listed in Table 3.6.

Platforms, applications ("apps"), and add-ons are common components of commercial software in the water sector. An **application** is a program that is installed on a computer or mobile device, such as a weather app on a phone or a word processor on a laptop. Software vendors often create a **platform** on which applications are hosted. For instance, an asset management software company may develop a proprietary platform with options for their clients to buy applications for work orders, level of service calculations, field data collection, and CCTV data analysis. A utility may connect their data to this platform and select among the available applications, with the flexibility to add or subtract apps to meet their needs. Within an application, a vendor might also sell **add-ons**—premium features (e.g., an optimization toolkit) for an extra cost.

Commercial Software

A brief list of commercial software for water and wastewater treatment and industrial automation is detailed in Table 3.5. These products come from a range of software vendors, including those that traditionally sell treatment equipment and water quality sensors (e.g., Hach and Suez) and companies focused solely on software and integration (e.g., GoAigua, Autodesk (Innovyze), and WaterClick). These products address the following needs in potable reuse: 1) data management and monitoring, 2) analytics, and 3) equipment or sensor health monitoring.

Data management and monitoring products integrate multiple data streams—e.g., SCADA, LIMS (laboratory information management system), and field data—into a central location, visualize data, and provide alerts and alarms for operators. In addition to real-time data visualization and notifications, software products often include features to generate automated reports that can be sent to regulators and other stakeholders. The products listed in Table 3.5 tend to host data in the cloud rather than on-premises, provide web-based visualizations of the data, and have more modern, customizable user interfaces. Regardless of the details of the implementation, data management provides the foundation on which data analytics applications are built.

Data analytics can be divided into full-service and self-service offerings. Self-service analytics software—such as Alteryx and TrendMiner—are industry agnostic software tools that provide low-code or code-free methods to manage, visualize, and analyze data. This type of software empowers users with limited programming experience to perform sophisticated analyses and may be appropriate for utilities that want to do data analytics in-house but do not have the resources available to hire a data analyst or data scientist. In contrast, companies that offer full-service analytics often perform data integration and data science tasks for their customers. Many Full-service analytics vendors have a subscription payment plan, also known as an “as-a-service” business model. Software-as-a-Service and Data-as-a-Service models are all increasingly common

for licensing software and outsourcing the data management. This financing approach shifts capital expenses to operations and maintenance costs, which has required many utilities to rethink their procurement and capital planning procedures. It is also reducing the burden on utility staff to learn new software and manage and analyze data.

Equipment and sensor health monitoring are a growing need in drinking water and reuse applications where public health protection is paramount and highly dependent upon the sensors being used. Data analytics products can only provide meaningful predictions when they receive good data. Sensor drift and failure are common and can produce data that does not represent reality. In potable reuse, these data quality failures can lead to potential public health impacts. To proactively identify sensor maintenance needs, some products provide a virtual log of maintenance activities and may flag suspicious sensors. Other products extend this maintenance tracking to equipment health more broadly, alerting staff about common issues such as excessive pump vibrations.

Table 3.5. Commercial Data Analytics Products. Commercial products for data management and monitoring, equipment or sensor health management, and analytics for water and wastewater treatment.

Company	Products	Product Detail on Website	Data Management and Monitoring	Analytics	Equipment or Sensor Health Management	Notes
ABB	Ezlink Connect	Moderate			X	Sensor monitoring application
Alteryx	Analytic Process Automation (APA) Platform	High	X	X		Self-service analytics platform
Autodesk (Innovyze)	Emagin	Low	X	X	X	Process flow diagrams and historical data are used to train machine learning algorithms
Aveva	Unified Operations Center	Low	X	X	X	Enterprise management platform
Aveva (OSIsoft)	PI System: PI Core, PI Cloud, PI Edge	High	X	X		Data management for industrial operations
Fontus Blue	Decision Blue	Low	X	X		Services include operator decision support tools (e.g., Virtual Jar Test)
GE	CIMPLICITY	Low	X	X		Industrial automation system that can integrate with Python for advanced analytics
GE	SmartSignal	Low	X	X	X	Industrial automation platform (not specific to water)
Hach (Danaher)	Claros	High	X	X	X	Water intelligence system, field collection, and sensor management
Hach (Danaher) / Aquatic Informatics	WaterTrax	Moderate	X			Cloud-based data management tool
Idrica	GoAigua	Moderate	X	X	X	Enterprise management platform
IOSight	iGreen, iWT, iWWT, and iDetect	High	X	X	X	Data integration and analytics platform for water sector
Kando	Kando	Low	X	X		Wastewater collections system monitoring
Plutoshift	Operational Data Platform (ODP)	Low	X	X	X	Industrial automation platform (not specific to water)

Company	Products	Product Detail on Website	Data Management and Monitoring	Analytics	Equipment or Sensor Health Management	Notes
Royal HaskoningDHV	Aquasuite Platform: OPIR, PURE, MINE, Analytics	High	X	X	X	Analytics platform that has been piloted for water reuse applications
s::can	ana::tool, moni::tool, and vali::tool	High	X	X	X	Tools work with both s::can and 3rd party sensors
Software AG (TrendMiner)	TrendMiner	High	X	X	X	Self-service industrial analytics tool
Suez	InSight	Low	X	X	X	Asset performance management tool
Suez (eRIS)	eRIS	Moderate	X	X		Data integration and analytics tool
Veolia	AQUAVISTA: Portal, Insight, Assist, and Plant	Moderate	X	X	X	Enterprise management platform
Xylem	Vue	Low	X	X	X	End-to-end digital solutions platform
WaterClick	Waterly	High	X		X	Platform as a Service tools for small and medium sized utilities

Table 3.6. Open Source Python Packages for Time Series Forecasting and Anomaly Detection. Adapted from (Bhatnagar et al., 2021).

Software Package	Developers	Prediction / Forecasting	Anomaly Detection	Reference	Code Repository
alibi-detect	Seldon		X	(Looveren et al., 2019)	https://github.com/SeldonIO/alibi-detect
Kats	Facebook	X	X		https://github.com/facebookresearch/Kats
Statsmodels	Open Source Community	X			https://github.com/statsmodels/statsmodels
gluon-ts	Amazon Web Services	X		(Alexandrov et al., 2020, 2019)	https://github.com/awslabs/gluon-ts
Merlion	Salesforce	X	X	(Bhatnagar et al., 2021)	https://github.com/salesforce/Merlion
RRCF	University of Michigan		X	(Bartos et al., 2019)	https://github.com/kLabUM/rrcf
STUMPY	TD Ameritrade		X	(Law, 2019)	https://github.com/TDAmeritrade/stumpy
Greykite	Linkedin	X	X	(Hosseini et al., 2021b, 2021a)	https://github.com/linkedin/greykite
Pecos	Sandia National Labs		X	(Klise, 2016; Klise and Stein, Joshua S., 2016)	https://github.com/sandialabs/pecos
Prophet	Facebook	X	X		https://github.com/facebook/prophet
pmdarima	Open Source Community	X	X		https://github.com/alkaline-ml/pmdarima

Open Source Software

In contrast to commercial software, open source packages are free and often have licenses that permit both commercial and private use, modification, and distribution. For many years, open source projects have been led by volunteers, academics, and federal agencies, but recently, large corporations like Microsoft and Facebook have taken on leadership roles. For profit companies often participate in open source projects to better understand their competition, to incorporate open source ideas into commercial software, identify talented programmers, and attract employees that want to solve difficult programs (Lerner and Tirole, 2001).

Open source software included in the review were time series data analytics packages (Table 3.6) available in Python—a popular programming language for data science. Time series data are observations recorded over time, a common format for treatment data. Time series analyses include forecasting future values (i.e., prediction) and detecting anomalies in the data. These tools are based on many of the same principles behind CANARY, water distribution event detection software developed by federal agencies for public health protection (Hart et al., 2007). However, the software packages in Table 3.6 have much broader applications for time series analysis. Because these open source packages are widely used and build upon prior work, they are high-quality in terms of computational efficiency, accuracy, and usability. For this reason, these packages will likely serve as the computation engine for many commercial products and customer solutions for the water sector, including potable reuse.

3.6.2 Machine-Learning

Software packages and machine learning can also aggregate multiple data streams and potentially detect process failures that may not be easily recognized by individual sensors. Additionally, incorporating machine learning into individual sensors may be especially helpful for

technologies such as fluorescence sensors where data can be difficult to interpret. For example, "Peak T" (i.e., tryptophan-like) fluorescence has been used as a surrogate for EfOM and microbial growth/activity (Hudson et al., 2007; Yamashita and Tanoue, 2003) but can also be due to compounds and moieties present in NOM and not representative of amino acids (Maie et al., 2007). Recently, Bedell and coworkers study incorporated machine learning with an online in-situ tryptophan-like fluorescence sensor to detect potential fecal exposure (Bedell et al., 2022, 2020). In these studies, machine learning was used to determine when elevated tryptofan-like fluorescence (TLF) signals were due specifically to the presence of *E. coli* and not the presence of other compounds that exhibit TLF fluorescence, both in the laboratory and when employed in a surface water. Similar investigations are recommended to increase the effectiveness of using similar fluorescence sensors in reuse systems where machine learning can help to deal with issues such as low signal (especially in the case of monitoring RO processes) and variations in signals due to inert compounds rather than contaminants. As sensor technology continues to be developed it is likely that some future sensors may present similar nuances.

3.6.3 Challenges in Data Management

It should be noted that there are several notable challenges with data management that need to be addressed both functionally as well as from a humanistic perspective. In order to properly harness data, one must adopt standards and understanding around data governance, database organization, data transfer, data engineering, and systems architecture to ensure secure, seamless flow of data. This is partly solved by having knowledgeable information technology staff and systems architects who can create or modify the system to meet the requirements. However, there is a humanistic side that includes both the fear of cybersecurity incidents and the misunderstanding of security and personal behavior that may lead to over-compensation at the expense of innovation

(Kennison and Chan-Tin, 2020; Nelson and Madnick, n.d.; Renaud et al., 2021). Thus, proper management of cybersecurity and network architecture must be coupled with education and management of fears and expectations around security controls and risks/vulnerabilities that should be managed.

3.7 Future Outlook and Recommendations

As reuse becomes more widely employed in the future years, there will be a growing need for the use of monitoring sensors, proper identification of CCPs and effective use and operation of sensors, and effective management and interpretation of process data. Specifically with regards to DPR in which there is minimal to no environmental buffer between treated wastewater and advanced treatment before redistribution to the drinking water distribution system, there is a greater concern that contaminants can enter the distribution system. During DPR, if a breakthrough occurs, there is a greater risk that contaminants will be quickly distributed to the public drinking water. This section summarizes the key findings of this review and provides recommendations for the future incorporation and operation of sensor technology, and efficient management of the data produced by them.

3.7.1 Detection Technologies

The current conventional technologies that are widely used for microbial detection are turbidity, conductivity, measurement of specific ions, and commercially available multi-parameter analysis systems. These technologies should be considered fundamental to reuse facility operation. Emerging and promising technologies were outlined in Tables 3.1-2. While these technologies currently require further development, research, and testing before implementation, they represent possible monitoring solutions in the future. The measurement of indigenous viruses in feed and permeate waters is particularly promising. These viruses are present in much greater

concentrations that target pathogenic contaminants and can be used as a surrogate for target contaminant monitoring (Hornstra et al., 2019). Future research is recommended to progress all emerging and promising sensor technologies towards full-scale use.

With respect to chemical detection, specifically CEC's, absorbance and fluorescence based optical sensors offer the most current and future promise. From absorbance and fluorescence, several metrics continue to be developed that can characterize the quality of NOM (i.e., TOC) present in water and detect changes that correlate to contaminant removal. Targeted fluorescence surrogates especially represents an area with potential for significant improvement (Korak and Arias-Paic, 2016) as it has been demonstrated that fluorescence can potentially be tailored to monitor specific contaminants and treatment processes (Anumol et al., 2015; Gerrity et al., 2012; Yu et al., 2015). The continued development of these targeted surrogates is recommended as a focus area for future research. Additionally, both absorbance and fluorescence surrogates can be used to monitor microbial contaminants as well. Surrogates including spectral slope, E2:E3 ratio and protein-like fluorescence can be related to microbial growth and activity (Fox et al., 2017; Helms et al., 2008; Hudson et al., 2007; Korak and Arias-Paic, 2016).

Finally, while TOC sensors are currently used to monitor both microbial and chemical contaminants in several treatment processes, users should be aware of their limitations. These limitations include limit of detection issues, especially when used to monitor processes such as RO as effluent waters are expected to have exceedingly low TOC concentrations, and the lack of ability to characterize TOC quality. The development of a sensor that combines TOC and optical based detection (i.e., absorbance and fluorescence) is particularly intriguing. This type of sensor could then be used to combine TOC, absorbance, and fluorescence to determine additional metrics

such as SUVA and fluorescent quantum yield (Ulliman et al., 2020), and possibly eliminate the need for multiple individual sensors in same location.

3.7.2 Operations

If sensors are to accomplish their job of accurately monitoring water quality, operational considerations must be taken into account. It is recommended that the HACCP process be adapted and applied to water reuse facilities as a methodological framework to guide operational management. This process creates a standard approach to identify CCP's in a treatment system, thus informing where sensor technology will be most essential. In combining typical RO and non-RO based treatment processes (Figure 3.1), available treatment technologies (sections 3.1.1. and 3.2), and guidance from previous reports WRF 09-03 and WRF 13-03, Table 3.7 displays a recommended monitoring approach for continuous/online sensors (Tchobanoglous, 2015; Walker et al., 2016):

Table 3.7: Recommended Sensor Monitoring Approach for Typical RO and Non-RO Based Treatment Trains

RO-based Treatments	**Recommended Monitoring**
Pre-Chloramination	Total (combined chlorine)
MF/UF	Turbidity
RO	EC and TOC
UV/H_2O_2	UV and UVT sensors,
Stabilization	pH, TDS, alkalinity, hardness, chemical dose
ESB - Chlorination	Effluent free chlorine residual

Non-RO-based Treatments	**Recommended Monitoring**
Coag/Floc/Sed	Coagulant dose, TOC, turbidimeter
Ozone	UV sensors
BAC	Turbidity, pre and post TOC
GAC	Turbidity, TOC
UV	UV sensors, UVT
ESB - Chlorination	Effluent free chlorine residual

Once CCPs and the required forms of monitoring have been identified, the sensor technology selection process should be guided by considerations of reliability, operability, cost, and sufficient representation. It is recommended that sensor manufacturers also make these

considerations as future sensors are developed. For example, some sensors include self-cleaning mechanisms that cut down on required maintenance, improving reliability and operability. Ideally, sensors should be relatively easy to operate and interpret data, perform reliably without the need for frequent maintenance, and be available at affordable costs.

3.7.3 Data Management and Analytics

Other industries will continue to drive improvements to data management and analytics in both commercial and open source software products. These innovations will allow the potable reuse sector to manage and analyze data more efficiently, driving improvements in water quality and operational reliability. Competition for skilled data workforce across sectors, state-specific requirements, data quality issues, cybersecurity and data privacy concerns, and unknown market potential, however, present barriers to realizing that potential.

A shift from local data storage and computing (i.e., on-premises) to the cloud is at the heart of modern data workflows. By shifting to the cloud, utilities can increase or decrease their data storage based on their needs and their IT staff can spend less time managing aging hardware. By storing data remotely, it streamlines data sharing and collaboration. Some utilities still require software vendors and consultants to enter their SCADA Network to access online analyzer data. Because SCADA Networks are not connected to the internet, there are significant inefficiencies for collaborators to work within that system. By securely pushing data out of the SCADA Network and connecting it to cloud storage, the data is available via the web to those that have been granted access. Once in the cloud, the ease of data sharing—both internally and externally—is improved dramatically.

Ultimately, the success of data-driven approaches depends on whether organizations feel the data is secure and that it is trustworthy. The risk of cybersecurity attacks on public and private

agencies continues to increase and utilities are a potential target. Organizational and customer information is most vulnerable, but an intrusion to process control systems, although unlikely, present public health risks. In response to growing threats, the US government passed American Water Infrastructure Act of 2018 was passed, requiring all drinking water utilities to assess cybersecurity threats and documentation priority countermeasures, and established the Cybersecurity & Infrastructure Security Agency (CISA) in the same year. Due to the public health consequences of a failure in potable reuse and reliance of high-frequency data, implementing best practices in network architecture and security policies is essential.

In addition to managing cybersecurity threats, potable reuse systems must proactively manage data quality. Many utilities suffer from poor data quality for two reasons: 1) measurement error often due to lack of sensor maintenance and 2) sensors reporting misleading values when processes are not in production (e.g., when a membrane cleaning is occurring). Although an operator may be able to identify sensor drift or recognize that a system is not in production, an algorithm may require more explicit instructions during training on the types of errors and the sources of those errors. If sensors are reliably and consistently maintained and measurements of non-production data are removed, data quality can be improved. This paves the way for more sophisticated tools and strengthens trust in the system.

To operationalize these tools, potable reuse systems need people and organizations to develop and implement the software. To drive software development for potable reuse, the market for these products needs to be reliable and consistent for companies to build tools that meet the unique needs of the industry, such as HACCP. In addition to software development hurdles, utilities have difficulty hiring and retaining staff with the data skills required to use the software.

Without a concerted effort by a utility to create data teams, utilities may need to rely on outsourcing data analytics work to subscription services.

3.8 Conclusion

As the need for reuse projects grows, this will also fuel the need for better sensor technology. As the need for expanded reuse operations become more significant, it is clear that utilization of sensor technology is imperative. To ensure the proper operation of sensor technology, it is important that reuse facilities and sensor and data management technology manufacturers embrace the need for ongoing communication and cooperation. Reuse facilities should be prepared to dedicate time and effort to developing a detailed understanding of sensor technologies, while sensor manufacturers prepare to aid reuse facilities in the installation and operation. When compared to typical drinking and wastewater treatment, water reuse relies more heavily on sensors and online data. Reuse facilities should also plan to use additional resources, for the employment, operation, and management of sensor technology and data.

Chapter 4

DOM Molecular Weight Fractionation and Fluorescence Quantum Yield Assessment Using a Coupled In-Line SEC Optical Property System

**** Note: The research in this chapter has been published as follows:***
Hanson, B.; Wunsch, U.; Buckley, S.; Fischer, S.; Leresche, F.; Murphy, K.; D'Andrilli, J.; Rosario-Ortiz, F. L. DOM molecular weight fractionation and fluorescence quantum yield assessment using a coupled in-line SEC optical property system. A*CS Environmental Science and Technology: Water*, **2022**, 2, 12, 2491-2501

4.1 Introduction

Dissolved organic matter (DOM) is composed of a diverse mixture of compounds originating from the molecular remnants of plants, animal materials, and microbial exudates. DOM represents a major part of the global carbon cycle and is an important factor in numerous chemical and physical processes in natural and engineered systems.[1,2] For example, DOM serves as a substrate for microbial growth and can complex with metals and organic pollutants, impacting their fate in natural waters.[3,4] Additionally, DOM impacts water treatment processes, including reactions with chlorine, resulting in the formation of disinfection byproducts, some of which are harmful to humans if consumed.[5,6] However, due to the complex chemical composition of DOM, determination of its characteristics relies on the development and application of numerous analytical methods.[7]

One property that has received considerable attention in the study of DOM is its average molecular weight and the overall size distribution of sub-components. Although molecular weight (MW) can be assessed using different techniques (e.g., vapor pressure osmometry, field flow

fractionation and high resolution mass spectrometry[8–12]), most assessments are based on the use of size exclusion chromatography (SEC).[13–15] SEC can be used to determine the *apparent* MW (AMW) distribution of DOM. Determination of the AMW (in contrast to *absolute* molecular weight) is based on the fact that the separation is not strictly due to molecular weight, but instead based on hydrodynamic size, which is affected by solution chemistry and non-ideal interactions within the SEC-column.[16] Applications of SEC for the study of DOM include systems where quantification is based on carbon, nitrogen, or optical properties, therefore offering different qualitative and quantitative information about the samples.[13]

The application of fluorescence spectroscopy for the study of DOM has gained significant attention over the past 30 years.[17–20] Three dimensional fluorescence excitation emission matrices (EEMs) are popularly used to distinguish source origin and inform physicochemical properties of DOM.[20–23] While fluorescence offers the possibility to collect signals with high sensitivity and relative simplicity,[24–26] the specific chemical components responsible for DOM fluorescence have yet to be identified.[27] Understanding the chemical characteristics of the main types of fluorophores within DOM would help to address deficiencies in fluorescence analysis, such as spectral overlap between fluorophores and the impacts of local environments on fluorescence signals (see section S-3 in the supplemental information for an expanded discussion on expected chemical groups responsible for absorbance and fluorescence of DOM). Insights into fluorophores highlight fluorescence properties that are sensitive to differences in DOM source and composition and inform how they can be applied, such as the use of DOM fluorescence as a surrogate for wastewater impact.[28]

One fluorescence-based metric, the fluorescence quantum yield (Φ_f), describes the fraction of photons reemitted via fluorescence relative to the number of absorbed photons.[29,30] Φ_f is an

intrinsic parameter (i.e., independent of concentration), and has been used to characterize the optical properties of DOM in different environments.[28,31–35] For example, Φ_f differentiated between effluent organic matter (EffOM) and naturally occurring DOM in wastewater blends with greater statistical power than other optical metrics.[28] Differentiation was ultimately possible because different fluorophores and chromophores existed at different relative abundances in each type of DOM.

While Φ_f is a sensitive measure used to quantify the unique fluorescence efficiencies of compounds, only the *apparent* Φ_f value of DOM can be determined for bulk-water samples by traditional fluorescence spectroscopy. This is because DOM represents a mixture of absorbing and fluorescing compounds summed by one *apparent* Φ_f value, where typical bulk values are in the order of 1-3% and are suppressed by nonfluorescing chromophores.[26,31–33,36] Therefore, to use Φ_f to further characterize the DOM mixture it would be useful to fractionate bulk-water DOM from which varying Φ_f intensities can be observed for a single sample. It was reported previously that fluorescence to absorbance ratios are MW dependent and that this ratio is greatest for smaller MW fractions.[37–39] Boyle and coworkers also found that, among several DOM samples, the Φ_f increased with decreasing sample MW.[40] From these studies it can be seen that: (i) Φ_f varies between fractions of a given DOM sample, and (ii) Φ_f is likely correlated to DOM MW. It should be noted that throughout the rest of this text, "Φ_f" refers to *"apparent fluorescent quantum yield".*

This study presents a SEC system in which Φ_f is calculated in-line as a function of AMW while in-line total organic carbon (TOC) concentrations measurements are used to identify the presence of spectroscopically undetectable DOM. To do this, dissolved organic carbon concentration (DOC), absorbance, and fluorescence, were combined with a SEC system so that each signal was essentially collected simultaneously as a function of AMW during analysis. To

demonstrate the application of the SEC system to characterize the Φ_f distribution within DOM, data are presented on the analysis of several DOM samples, consisting of riverine samples and ozonated DOM isolates. The goal of using this system was to better understand the fundamental properties of fluorescence in DOM, while also allowing the investigation of changes to fluorophores across a processing mechanism in natural and engineered systems.

4.2 Materials and Methods

4.2.1 Instrumentation

The SEC system was comprised of an Agilent 1260 high performance liquid chromatography (HPLC) setup that included an Agilent 1200 Series Vacuum Degasser, Agilent 1200 Series G1310A Isocratic Pump, Agilent 1260 Infinity Series G1315D Diode Array Detector (DAD), Agilent 1260 Series Infinity II Fluorescence Detectors (FLD) and a Sievers M9 TOC Analyzer. Absorbance and fluorescence signals were recorded directly by the Agilent OpenLab software (Rev. C01.09). An Agilent Universal Interface Box II was utilized to transfer data from the TOC analyzer to the Agilent software in voltage units, which were later converted to DOC concentration ($mg_C\ L^{-1}$) (see SI, Text S-1.2.3) for a detailed description of conversion). Note that because samples were filtered through 0.45 µm polyethersulfone (PES) filters, analysis results from the TOC analyzer can be considered DOC. A schematic of the instrumental setup for the SEC system is shown in Figure 4.1.

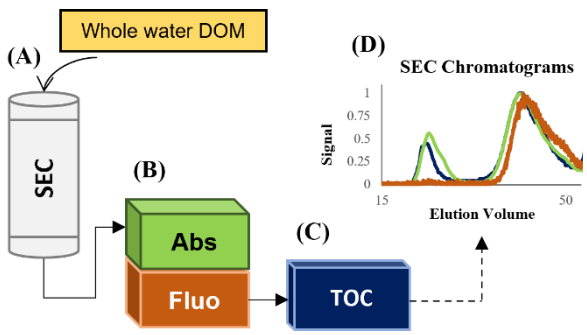

Figure 4.1. Schematic of the Size Exclusion Chromatography System. Bulk water samples are injected into the size exclusion chromatography (SEC) column (A). After eluting from the column, sample passes through the absorbance (Abs) and fluorescence (Fluo) detectors (B) and then travel to the Sievers M9 Total Organic Carbon (TOC) analyzer (C). The in-line coupled system allows for the determination of multiple optical metrics of the dissolved organic matter (DOM) based on apparent molecular weights (AMW), including Φ_f (D).

The size-based separations were achieved using a Toyopearl HW-50S column (internal diameter (ID) 20 mm x 25 cm, 92 mL total volume). Samples were injected via an Agilent Technologies 1100 Series G1328B Manual Injector Assembly with Rheodyne 7725i Injection Valve and 2 mL injection loop. The mobile phase consisted of phosphate buffer (0.0016M Na_2HPO_4, 0.0024M NaH_2PO_4, and 0.031M Na_2SO_4, pH 6.8, ionic strength 0.1M, see Appendix, Table A.1 for a full list of chemicals used and their sources) that was pumped at a flow rate of 1 mL min^{-1}. This mobile phase composition aimed to reduce unwanted column interactions and follows the methods of Her and co-workers.[14,41] The Agilent DAD was set to scan from 200-700 nm in 2-nm increments, and the Agilent FLD was operated in multi-emission scan mode at λ_{ex} = 350 nm, λ_{em} = 350-700 nm at 5-nm increments. These settings were required for accurate spectral corrections (e.g., inner-filter effect corrections) and calculation of Φ_f for the different MW fractions of the DOM.

To properly align the different detector signals, salicylic acid (a single compound with well-described absorbance and fluorescence spectra)[21,29,31,32,42] was injected at a concentration of 5 mg L^{-1} and peak elution volumes were then used to account for inter-detector volume between absorbance, fluorescence, and DOC detectors. On average, the volumetric difference between the absorbance and fluorescence detectors was approximately 0.05 mL and 2.8 mL between the absorbance and DOC detectors.

All SEC analyses lasted 150 min (total elution volume of 150 mL). Although all of the compounds should theoretically have eluted well before 150 min (void volume and bed volumes for the system were approximately 23 mL and 75 mL), compounds can experience non-ideal interactions causing them to elute after the bed volume.[13,14,43,44] Thus, extra time was utilized to ensure all detectors returned to baseline. Data from the beginning of the run (i.e., before the elution of any compounds) as well as the end of the run (i.e., after the elution of all compounds and all detectors had returned to baseline) were treated as blanks to apply baseline corrections. Following Her, 2003, the SEC column was initially calibrated with polyethylene glycols (PEG) to ensure results were comparable to previous studies (data not shown).[41] However, discrete molecular weight values or cutoffs were not provided because of the relative nature of SEC. That is, molecular separation is dependent on hydrodynamic size and is affected by solution chemistry and non-ideal interactions within the SEC-column, resulting in differing AMW estimations and AMW distributions.[14,16,43–46] In addition commonly used calibration standards (e.g., polysterene sulfonates and PEGs)[14,43] are uniform compounds while DOM is a complex mixture of chemically diverse compounds.[45] Therefore, in this study, chromatographic results were presented in terms of elution volume and interpreted qualitatively with respect to AMW (i.e., small, medium, large AMW regions).

Bulk-water characteristics were measured for all samples using a spectrophotometer (Hach DR 6000; Hach, Company, CO, USA), a spectrofluorometer (Horiba Jobin Yvon Fluoromax-4; Horiba, Japan), and a DOC analyzer (Sievers M5310C DOC analyzer; Suez Water Technologies, CO, USA). A full description of the analysis methods is included in the Appendix, Table A.3.

4.2.2 Samples

A total of nine natural water samples were collected from a subsection of Boulder Creek that flows through the City of Boulder, Colorado, and suburban land surrounding the city, as well as South Boulder Creek near the junction with Boulder Creek (see Appendix, Figure A.1 for exact sample locations). Samples were collected in 250 mL pre-washed and combusted glass bottles, wrapped in foil to exclude light, stored in coolers on ice, and immediately transported to the University of Colorado Boulder. All samples were passed through prewashed 0.45 μm pore size polyethersulfone (PES) filters and transferred into pre-washed and combusted 40 mL amber vials for storage at 4 °C in the dark until analysis. Prior to analysis, 15 mL aliquots of each sample were spiked with ~1 mL of a concentrated mobile phase solution (0.016M Na_2HPO_4, 0.024M NaH_2PO_4, and 0.031M Na_2SO_4), added dropwise, to match the ionic strength and pH of the mobile phase of the column. In this way, samples are essentially constituted in mobile phase and non-ideal interactions are suppressed as samples exchange into the mobile phase while entering the column after injection.

DOM fulvic acid isolates were obtained from the International Humic Substances Society (IHSS, St. Paul, MN, USA). Suwannee River Fulvic Acid (SRFA, 2S101F) was used as the sample to verify method accuracy and Pony Lake Fulvic Acid (PLFA, 1R109F) was used for ozonation experiments. Stock solutions of ~100 $mg_C\ L^{-1}$ were prepared in 100 mM phosphate buffer (pH 6.8) for each isolate. The solutions were stirred continuously for 24 hours and then filtered with ultrapure water prewashed 0.45 μm (PES) filters. The exact carbon concentration was measured using a Sievers M5310C DOC analyzer.

For the ozonation experiments, pure oxygen was fed to an ozone (O_3) generator model TG-40 (Ozone Solutions) and the obtained O_3/oxygen gas mixture was bubbled into a 2 °C water

jacketed 2 L glass reactor filled with ultrapure water. The obtained (O_3) stock solution had a concentration of ≈ 45 mg_{O3} L^{-1} that was measured spectrophotometrically using a 0.2 cm pathlength quartz cell with an absorbance value of 3200 M^{-1} cm^{-1} at λ=260 nm.[47] Appropriate amounts of the O_3 stock solution were added to 5mg_C L^{-1} PLFA samples to create various specific ozone doses (0.05, 0.1 and 0.2 $mmol_{O3}$ $mmol_C^{-1}$), similar to ozonation steps in drinking or wastewater treatment (0.36−1.16 mg_{O3} mg_C^{-1}).

4.2.3 Method development

Development of Correction Factors for Fluorescence Detector

Before utilizing the data from the fluorescence detector to calculate Φ_f, the spectral bias of monochromators and charge-coupled device detectors had to be considered by applying correction factors. Typically, correction factors are generated by comparing National Institute of Standards and Technology (NIST) certified data of fluorescence standards, such as NIST SRM2942-4 or Rhodamine-B, to the uncorrected fluorescence spectra.[29,48] However, such standards are most commonly solid blocks or come pre-filled into sealed cuvettes, and are incompatible with HPLC detector cells with non-standard dimensions and low volumes. Therefore, this study utilized a method whereby a sample EEM is measured without prior separation (i.e. the analytical column was removed from the system) at a very low flow rate (0.025 mL min^{-1}). The low flow rate allows enough time to collect measurements for a single fraction across multiple excitation wavelengths (while entire emission spectra are measured by the Agilent 1260 Infinity Fluorescence Detector). The obtained spectra were then compiled into a SEC-based EEM and compared against the EEM measured on a calibrated stand-alone fluorometer. In our study, the Agilent 1260 Infinity Fluorescence Detector data were compared to the calibrated Horiba Jobin Yvon Fluoromax-4, using SRFA (2S101F) as the standard. Appendix, Figure A6 shows the obtained correction factors.

Verification of In-line Fluorescence Data

Comparisons of the corrected SRFA EEM measured using the in-line method to the corrected SRFA EEM measured on the reference benchtop fluorometer were made to verify the adequacy of the correction factors (Figure 4.2). Corrected fluorescence spectra were highly similar at wavelengths with strong emission fluorescence intensities (i.e. λ_{ex}=250-400nm and λ_{em}=350-500nm), while in low emission intensity regions < 350nm, SEC-based EEM signals were relatively noisy. Because the noise occurs in regions where fluorescence signal is typically weak (λ_{ex}>400 nm and λ_{em}>550 nm), and not in the wavelengths used for Φ_f calculations, the calculated Φ_f are not significantly impacted.

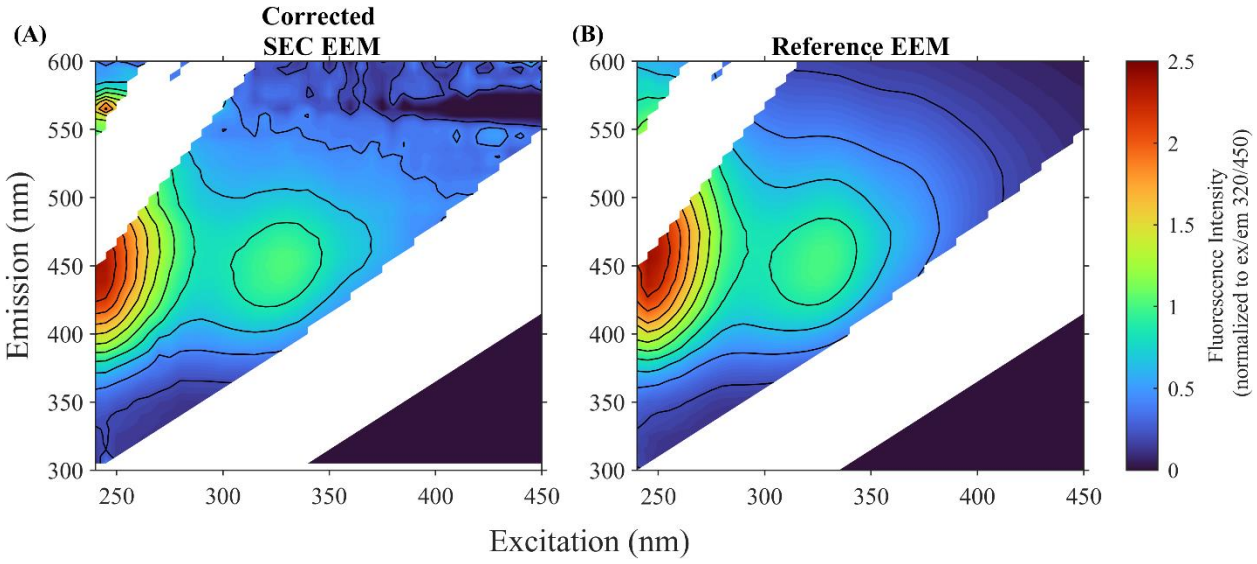

Figure 4.2. Corrected Suwannee River Fulvic Acid Sample EEMs. Corrected Suwannee River Fulvic Acid (SRFA) sample EEMs from the inline SEC-fluorescence detector (A) and the off-line benchtop fluorometer (B). Excitation wavelengths are plotted on the x-axis and emission wavelengths are plotted on the y-axis. Both EEMs fluorescence intensities (FI) were normalized to excitation 320 and emission 450 nm for a spectral comparison.

Additionally, correction factors were applied to a second reference standard analyzed by the SEC system, quinine sulfate, for which its fluorescence spectrum is well defined. Quinine

sulfate has a fluorescence excitation/emission maximum at 347 nm and 455 nm respectively, and well characterized emission in the range of 400-530 nm.[48] The fluorescence spectrum of quinine sulfate overlaps strongly with fluorescence emission of DOM, especially at λ_{ex}=350 nm which was the excitation wavelength chosen for this study. For these reasons, quinine sulfate is a good reference standard for DOM research, and commonly used in the field.[21,29] Quinine sulfate was prepared at a concentration of 10 mM in 0.1N H_2SO_4 and analyzed by the SEC absorbance and fluorescence detectors, using 0.1N H_2SO_4 as mobile phase. Because the SEC column is limited to a pH range of 2-13, this analysis was conducted with the column removed from the system. Results are displayed in Figure 4.3, where the emission spectrum of quinine sulfate is closely replicated, with all data points falling within the error range of the reference spectrum.

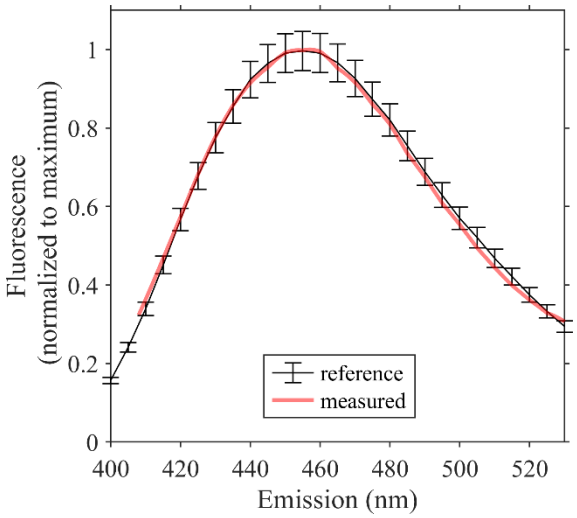

Figure 4.3. Comparison of Quinine Sulfate Fluorescence Emission Spectra. A comparison of the corrected SEC quinine sulfate (QS) fluorescence emission spectrum (red) from the inline detector to a referenced spectrum (black). Emission spectra were obtained at λ_{ex} = 350 nm. Fluorescence intensities were normalized to the peak maximum to account for differences in concentration (y-axis).

Verification of In-line Φf Calculation

As previously stated, Φ_f is defined as the ratio of the number of photons emitted via fluorescence to the number of absorbed photons. The value of Φ_f for a compound is calculated by comparison to a standard for which the absolute Φ_f is known.[29,30] Standards are typically pure compounds for which the Φ_f yield does not vary with excitation wavelength. While quinine sulfate dissolved in H_2SO_4 is often used for this purpose,(Cawley et al., 2015; Del Vecchio and Blough, 2004; Ulliman et al., 2020c; Wünsch et al., 2015; Würth et al., 2011) this solution is not compatible with the SEC column (see section 2.3.2). In this study, salicylic acid was used as a Φ_f standard as it is well characterized,(Pozdnyakov et al., 2009; Wünsch et al., 2015) can be readily dissolved in the SEC mobile phase, and thus can be analyzed under the typical instrumental conditions described in Section 2.1. The Φ_f values were calculated following eq. 1(Cawley et al., 2015)

$$\frac{\Phi_{fDOM}}{\Phi_{fSA}} = \frac{\int_0^\infty I_{DOM}(\lambda_{ex})d\lambda_{em}}{A_{DOM}(\lambda_{ex})} \times \frac{A_{SA}(\lambda_{ex})}{\int_0^\infty I_{SA}(\lambda_{ex})d\lambda_{em}} \quad (1)$$

where $\Phi_{f,DOM}$ and $\Phi_{f,SA}$ are the Φ_f for DOM and salicylic acid respectively, $A_{DOM}(\lambda_{ex})$ and $A_{SA}(\lambda_{ex})$ are the absorbance values of DOM and salicylic acid (at the fluorescence excitation wavelength), $I_{DOM}(\lambda_{ex})$ and $I_{SA}(\lambda_{ex})$ indicate the fluorescence intensities at the excitation wavelength and are integrated across the range of emission wavelengths ($d\lambda_{em}$). A 5 $mg_C\ L^{-1}$ standard of salicylic acid was prepared in mobile phase and analyzed by the SEC system under the same conditions described in section 2.1, and results were compared to the Φ_f reference value for salicylic acid.

The measured Φ_f for salicylic acid agrees well with a reference value of 36%,(Pozdnyakov et al., 2009; Wünsch et al., 2015) with deviations less than 4.8% of the reference value (Figure 4.4). Notably, during data processing, Φ_f was calculated only when absorbances were above 0.5 $cm^{-1}10^{-3}$; below this threshold, data were noisy and Φ_f was unreliable. This was an important

limitation for analyzing samples with very low concentrations (i.e., natural water samples, as shown below).

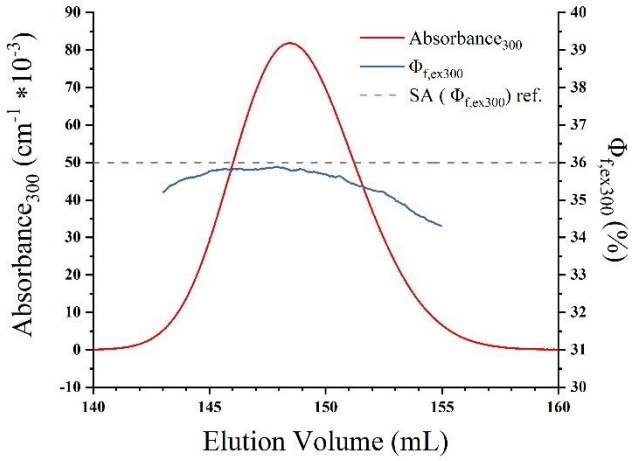

Figure 4.4. Absorbance and Fluorescence Quantum Yield SEC Chromatograms for Salicylic Acid. Elution volume in mL is plotted on the x-axis, absorbance and percent fluorescent quantum yield (Φ_f) values are plotted on the primary and secondary y-axes respectively. The red line shows the chromatogram of absorbance at 300 nm, the blue line shows Φ_f at λ_{Ex} = 300 nm. The reference value for $\Phi_{f,Ex=300}$ is 36 %,(Pozdnyakov et al., 2009) and is shown by the grey dashed line.

Verification of Method Accuracy

SRFA was analyzed at two concentrations (5.1 $mg_C\ L^{-1}$ and 21.5 $mg_C\ L^{-1}$) to verify method accuracy. Specifically it was verified that: (i) SEC chromatographic profiles of the same material are invariant with concentration (i.e., elution volume remains constant); (ii) DOC, absorbance, and fluorescence signals are proportional to concentration for the same sample at different concentrations,(P. G. Coble et al., 2014; Gardner et al., 2005); (iii) Φ_f is independent of concentration(Ulliman et al., 2020c) (Figure 4.5). Tucker Congruence Coefficients (TCC) were calculated to compare the normalized chromatograms of the 5.1 $mg_C\ L^{-1}$ sample to that of the 21.5 $mg_C\ L^{-1}$ for each signal. These TCC values were determined to be 0.998, 0.993, and 0.999 for DOC, absorbance, and fluorescence respectively, indicating excellent agreement (TCC > 0.95 indicates two components can be considered equal)(Lorenzo-Seva and ten Berge, 2006) between

normalized chromatograms of the two concentrations (Figure 4.5.E-G) (refer to SI Text S-2.4 for TCC calculations). The chromatographic peak maximum ratios of DOC, absorbance, and fluorescence (ratios of SRFA chromatographic maximums of two concentrations) for SRFA concentrations are 0.237, 0.242, and 0.257 respectively, representing errors of 3.5, 1.4, and 4.8% (see SI S-2.5 for percent error calculations). The Φ_f profiles for the different SRFA concentrations overlay each other indicating that the same Φ_f values were calculated for elution volumes ~32-42 mL. However, in Figure 4.5.D, at ~42 mL, Φ_f began to differ between the two concentrations. This results from improved resolution and accuracy of the fluorescence and absorbance signals at higher sample concentration, and not to a change in Φ_f, which is an intrinsic property. Thus, for the 5.1 $mg_C\ L^{-1}$ standard, Φ_f signal increased to ~2.5% (at ~45 mL) where it remained (for elution volumes > 45 mL) though signal variance increased. For the 21.5 $mg_C\ L^{-1}$ standard, two distinct Φ_f peaks were seen at ~45 mL and ~52 mL before the signal variance increased.

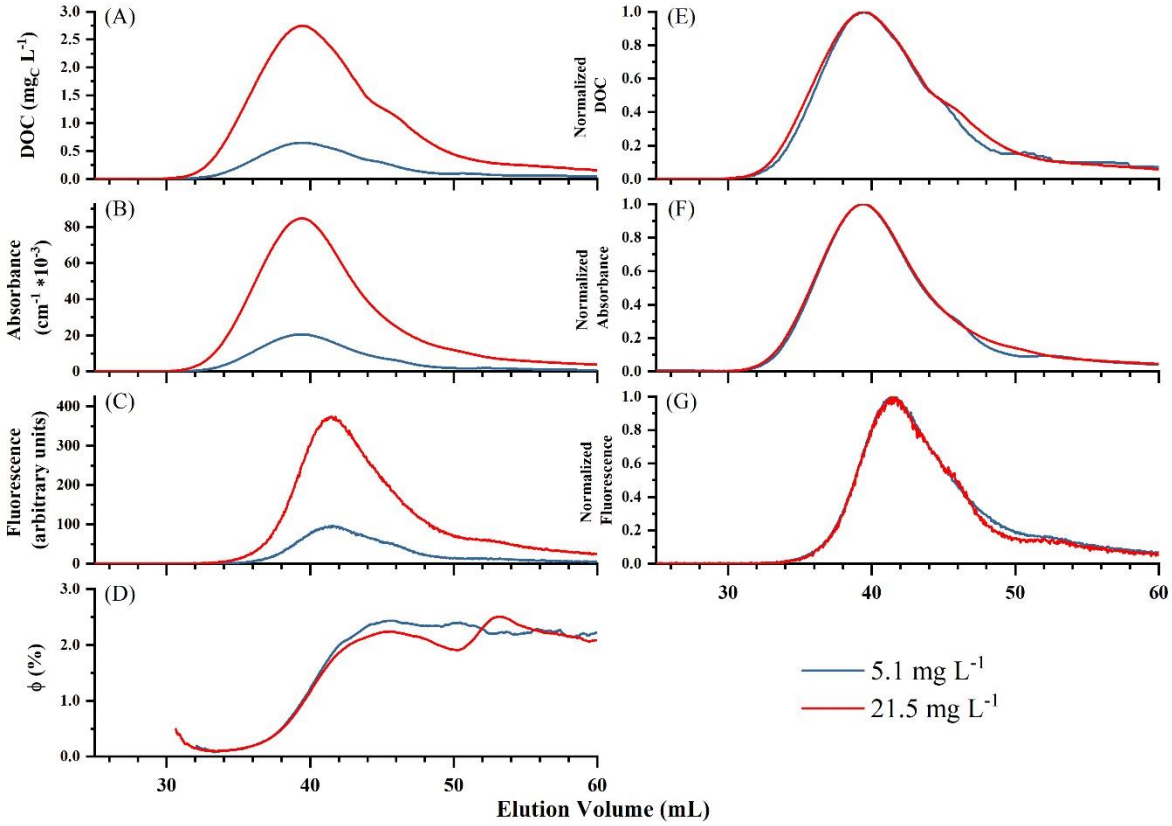

Figure 4.5. SEC chromatograms for SRFA at 5.1 and 21.5 mg_C L^{-1}. SEC chromatograms from the inline system for Suwannee River Fulvic Acid (SRFA) samples with bulk water [DOC] of 5.1 and 21.5 mg_C L^{-1}). (A) Dissolved organic carbon (DOC), (B) Absorbance (λ=350 nm), (C) Fluorescence (λ_{ex}=350 nm, λ_{em}=390-700 nm), and (D) Fluorescent quantum yield. (E), (F), and (G) show DOC, Absorbance, and Fluorescence chromatograms normalized to the emission peak maximum. Red chromatogram lines show SRFA (21.5 mg_C L^{-1} L^{-1}) and blue chromatogram lines show SRFA (5.1 mg_C L^{-1}). Absorbance was obtained at 350 nm, fluorescence and Φ_f were obtained at λ_{Ex} = 350 nm.

4.3 Results and Discussion

4.3.1 Applications of the SEC System for the Quantification of Φ_f Distribution

Boulder Creek Surface Water

The SEC-Φ_f method was applied to assess the Φ_f distribution for aqueous samples collected from Boulder creek. Figure 4.6 shows the DOC, absorbance, fluorescence, and Φ_f as a function of AMW for a subset of three Boulder Creek samples (SEC data for the additional Boulder Creek and South Boulder Creek samples are provided in Appendix Figure A.8.A-B and bulk water data for all Boulder Creek and South Boulder Creek samples in Appendix Figures A.2-A.5, Tables A.2-A.3). The SEC chromatograms using the DOC detector showed two distinct peaks occurring in elution volume ranges of ~20-30 mL and ~35-50 mL. At sample locations further downstream (streamflow direction is from BC-AF to BC-75th), DOC concentration of both peaks (and thus overall DOC concentration) increased (Figure 4.6). The stream section where BC-AF, BC-61st, BC-75th samples were taken, flows through an urban corridor of the city of Boulder, therefore, it is likely that a complex combination of anthropogenic inputs are responsible for the observed increases in DOC concentrations downstream.(Kaushal and Lewis, 2003; Murphy, 2003)

Absorbance chromatograms also displayed two distinct peaks within 20-30 mL and 35-50 mL, while fluorescence chromatograms show one peak within 35-50 mL. For the remainder of the discussion, the absorbance peaks within 20-30 mL and 35-50 mL will be referred to as "large AMW" and "medium to small AMW" peaks, respectively. Thus, chromophoric compounds (absorbing at 350 nm) contributed to both peaks, while fluorophores (excited at 350 nm) were constrained to the medium to small AMW peak. It has been reported elsewhere that, upon fractionation by AMW, a distinction is observed between large AMW fractions with high absorbance (i.e., the fluorescence:absorbance ratio is small), and small AMW fractions with

intense fluorescence (i.e., the fluorescence:absorbance ratio is large).(De Haan and De Boer, 1987; Stewart and Wetzel, 1980) Interestingly, in the medium to small AMW peak, where absorbance and fluorescence signals are greatest, the absorbance and fluorescence peaks vary much less between samples than the DOC, indicating the differences between DOC chromatograms were largely due to nonchromophoric DOM (i.e., spectroscopically invisible).

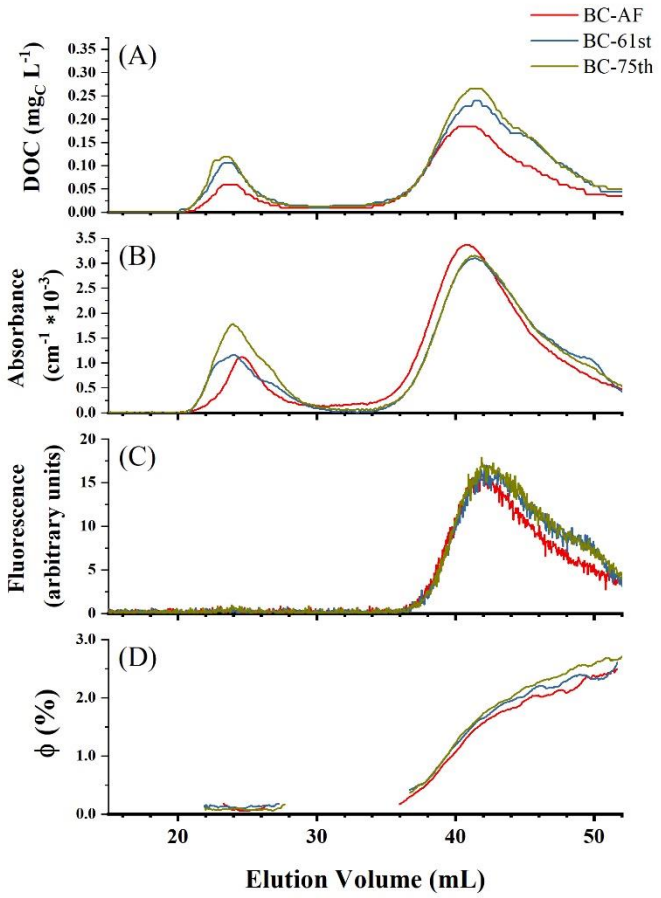

Figure 4.6: SEC Chromatograms for Boulder Creek Water Samples. (A) Dissolved Organic Carbon (DOC), (B) Absorbance (λ=350 nm), (C) Fluorescence (λ_{ex}=350 nm, λ_{em}=390-700 nm), and (D) Fluorescent quantum yield (Φ_f). Φ_f was not calculated when absorbance was below 0.5 $cm^{-1}10^{-3}$. Red lines show the sample from Boulder Creek at 61st Street (BC-61st), blue lines show the sample from Boulder Creek at Arapahoe Avenue (BC-AF), and yellow lines show the sample from Boulder Creek at 75th Street (BC-75th). Absorbance was measured at 350 nm, fluorescence and Φ_f were measured at λ_{Ex} = 350 nm.

The Φ_f results for Boulder Creek samples are shown in Figure 4.6.D. The Φ_f was calculated in the elution volume range in which absorbance intensities were above 0.5 $cm^{-1}\times10$. Across

elution volumes ~35-53 mL, Φ_f increased from <0.5% to ~2.5% for smaller AMW fractions (earlier elution volumes) relative to larger AMW fractions (later elution volumes), where bulk water Φ_f values for the same samples were determined to be 0.97-1.39% (Appendix, Figure A.5). These data indicate that although most absorbance and fluorescence (as a fraction of the overall DOM absorbance and fluorescence) occurred between 38-46 mL (where signal intensities increased to a chromatographic maximum at ~40-42 mL before decreasing with increasing elution volumes), the Φ_f values continued to increase with increasing elution volumes of medium to small AMW fractions.

Prior research has been dedicated to understanding the structural properties of chromophores and fluorophores within DOM.(Coble, 1996b; Gardner et al., 2005; McKnight et al., 2001b; Stedmon et al., 2003) Although some correlations on the structural identities of these optically active species (phenols, quinones, etc.) have been made,(Aiken, 2014; D'Andrilli et al., 2013b; Maie et al., 2007; Reynolds, 2003; Stubbins et al., 2014) their distribution within the DOM molecular size continuum is not well understood.(McKay, 2020a; Wünsch et al., 2015) The data presented here provides the first direct evidence of a clear separation between weakly fluorescing species present at higher concentrations (thus observed with relatively higher fluorescence and lower Φ_f signal intensities) eluting between 38-46 mL, as opposed to highly fluorescing species which dominate the lower AMW fractions, though their overall mass contributions are smaller (observed with lower fluorescence and higher Φ_f signal intensities). This de-coupling between numerous weakly fluorescent fractions with relatively larger AMW, and fewer highly fluorescent fractions with relatively lower AMW, matches well with other work where the Φ_f MW distribution was assessed.(Boyle et al., 2009; De Haan and De Boer, 1987; Stewart and Wetzel, 1980) It should

be noted that this study analyzed the AMW distribution of Φ_f only at λ_{Ex} = 350 nm. Future studies may benefit from exploring the relationship at other relevant λ_{Ex}.

Figure 4.7 displays SEC-based DOC, absorbance, fluorescence, and Φ_f chromatograms for one Boulder Creek sample (BC 75th) to help understand the qualitative DOM behavior observed for Φ_f. While the absorbance trace closely mirrored the DOC in both shape and elution volume, fluorescence material with smaller AMWs eluted with a similar, but slightly offset size distribution. This suggests that within the medium to small AMW range, as the AMW decreased, DOM fluorescence increased relative to absorbance at λ_{ex}=350 nm. This observation highlights the ability of SEC measurements to provide a more in-depth understanding of the complex composition of DOM, with respect to Φ_f.

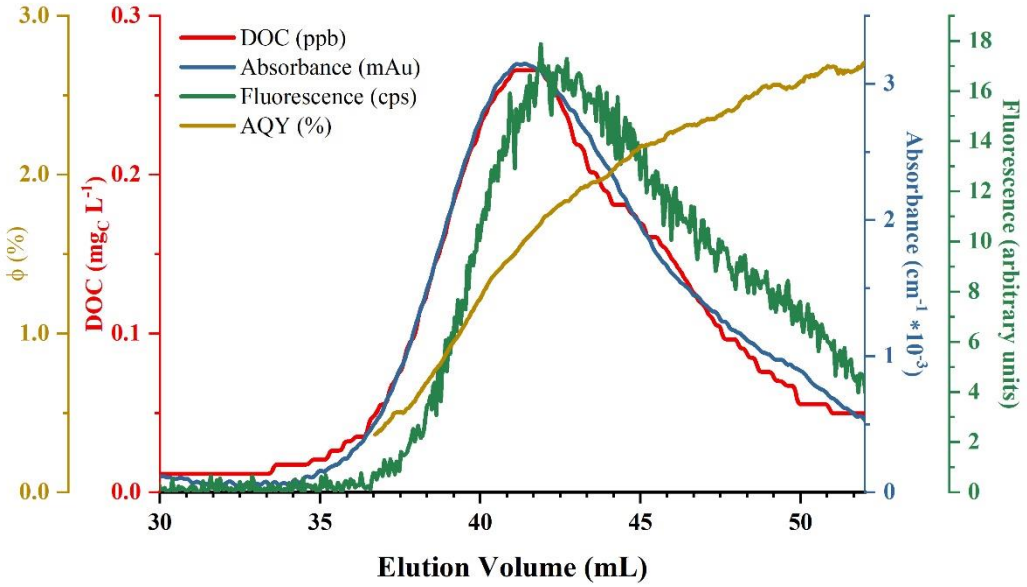

Figure 4.7: SEC Chromatograms for Boulder Creek Sample BC-75th. Elution volume range 30-52mL represents the medium to low apparent molecular weight (AMW) range. Dissolved Organic Carbon (DOC), absorbance (λ=350 nm), fluorescence (λ_{ex}=350 nm, λ_{em}=390-700 nm), and Φ_f are plotted on the red, blue, green, and yellow y-axes, respectively. Absorbance was measured at 350 nm, fluorescence and Φ_f were measured at λ_{Ex} = 350 nm.

Impact of Ozonation on PLFA

Section 3.1.1 presented an application of this method along a biogeochemical gradient. In this section, we describe the impact of a chemical process (ozonation) on DOM properties and Φ_f. Solutions of PLFA (5 $mg_C\ L^{-1}$) were ozonated at ozone doses of 0.05, 0.1, and 0.2 $mmol_{O3}\ mmol_C^{-1}$. Previous research indicates that ozonation of PLFA induces a decrease in absorbance and fluorescence, but an increase in Φ_f.(Leresche et al., 2021, 2019) Upon ozonation, bulk water DOC changes only minimally,(Nöthe et al., 2009) but low AMW products are formed such as formaldehyde, acetaldehyde, or oxalic acid,(Hammes et al., 2006) that should be observable by the SEC-DOC detector. The fact that DOC, absorbance, fluorescence, and Φ_f all change as a result of ozonation, suggests that SEC coupled with DOC, absorbance, and fluorescence detection would prove a valuable tool to follow the changes induced by ozonation.

With increasing ozone doses, a decrease in absorbance and fluorescence in PLFA was observed (Figure 4.8.B-C). The DOC chromatograms indicate that there was a reduction in large AMW compounds (< ~40 mL), and a simultaneous increase in smaller AMW compounds (~40-53 mL) with formation of two distinct lower AMW peaks at ~45 and ~52 mL (Figure 4.8.A,E). Additionally, the normalized (to the maximum) absorbance and fluorescence chromatograms are presented in Figure 4.8.E-F. Interestingly, while both absorbance and fluorescence values across the associated chromatograms decreased, the normalized data revealed that with increasing ozone dose, the absorbance trace shifted to lower AMW, while the fluorescence trace remained roughly distributed over the same AMW range. As a result, the SEC-Φ_f showed a larger increase for large AMW molecules (~33-40 mL) while the increase was less significant for smaller AMW (> ~40 mL) (Figure 4.8.D). Previous research observed increasing bulk Φ_f with increasing ozone doses.(Leresche et al., 2019) This observation is confirmed here in more detail, in which the increase is particularly marked for the high AMW fraction (< ~40 mL).

Ozonation of phenols leads to the formation of ring-opening products, indicating that carbon-carbon bonds can be broken by ozonation.(Tentscher et al., 2018) The DOC chromatograms indicate that ozonation induces a fragmentation of DOM molecules, an observation that concords with the breaking of carbon-carbon bonds and the aforementioned appearance of low AMW products such as formaldehyde, acetaldehyde, and oxalic acid.(Hammes et al., 2006) The remaining fluorescence after ozone treatment is indicative of functional groups that are not as reactive with ozone, and could include terpeniods or phenols with a high pK_a (the deprotonated form of phenol being more reactive by ≈ 4-6 orders of magnitude towards ozone). An example of such a phenol is salicylic acid, which has a pK_a for the phenolic moieties of 13.4.(von Sonntag and von Gunten, 2012)

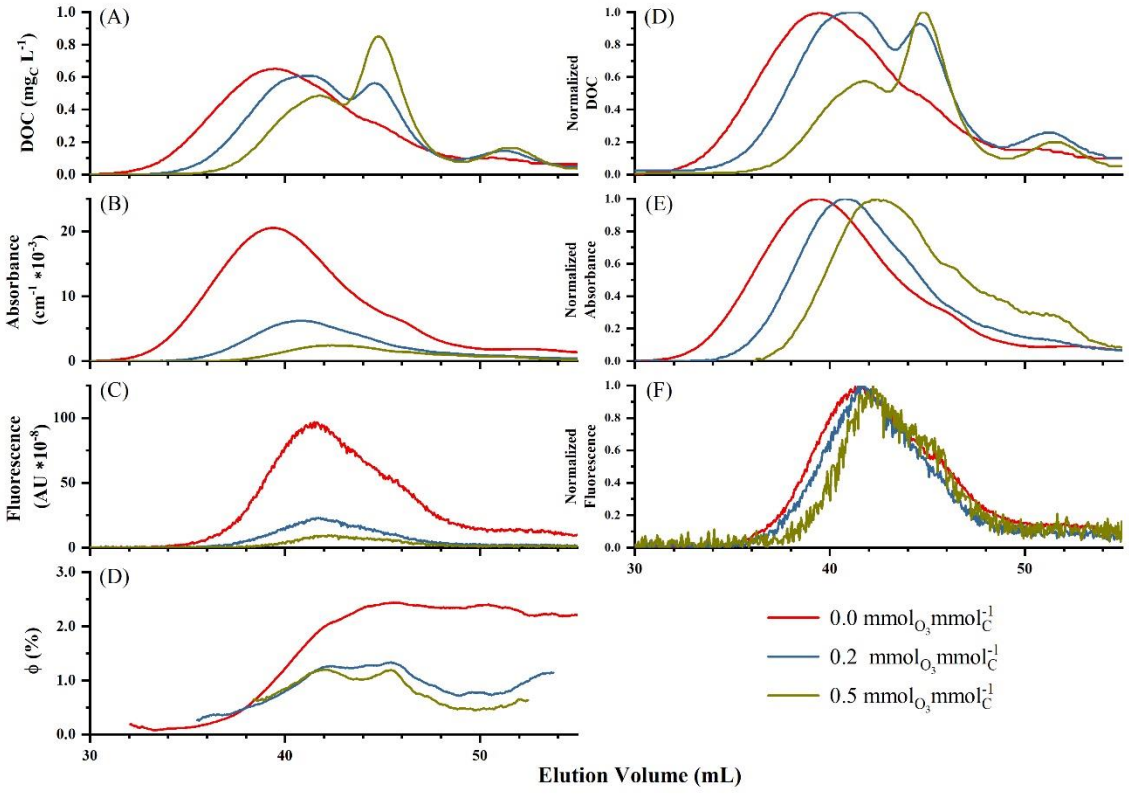

Figure 4.8 SEC Chromatograms for PLFA Treated with Ozone. **Left:** Dissolved Organic Carbon (DOC), absorbance (λ=350 nm), fluorescence (λ_{ex}=350 nm, λ_{em}=390-700 nm), and Φ_f chromatograms for Pony Lak fulvic acid (PLFA) with a bulk water [DOC] of 5 $mg_C\ L^{-1}$ samples treated with ozone. (A) DOC ($mg_C\ L^{-1}$), (B) Absorbance, (C) Fluorescence, and (D) Fluorescent quantum yield chromatograms. **Right:** Normalized absorbance and fluorescence chromatograms for PLFA treated with ozone. (D) DOC chromatograms normalized to the peak maximum. (E) Absorbance chromatograms normalized to the chromatogram peak maximum (i.e., normalized to 1). (F) Fluorescence chromatograms normalized to the chromatogram peak maximum. **All plots:** The red line shows untreated PLFA, the yellow line shows PLFA ozonated at a dose of 0.05 $mmol_{O3}\ mmol_C^{-1}$, the blue line shows PLFA ozonated at a dose of 0.1 $mmol_{O3}\ mmol_C^{-1}$, and the green line shows PLFA ozonated at a dose of 0.2 $mmol_{O3}\ mmol_C^{-1}$. Chromatograms were plotted as a function of elution volume (mL).

Further Potential Applications

Although the focus of this work was on calculating the Φ_f for AMW fractions from SEC analysis, the system as developed, could be used to calculate a variety of additional optical parameters. Examples that have previously been used in the investigation of bulk water DOM include: $SUVA_{254}$, spectral slopes, specific fluorescence, fluorescence indices, and fluorescence peak ratios.(Baker, 2001; Edzwald et al., 1985; Hansen et al., 2016; Helms et al., 2008; Huguet et al., 2009; McKnight et al., 2001b; Parlanti, 2000) Coupling these metrics with SEC analysis would lead to a more complete understanding of physiochemical properties of DOM as a function of MW. Additionally, recent work by Ulliman et al. (2020) proposed a methodology to evaluate the potential for several parameters (e.g., Φ_f, fluorescence peak ratios A:C and C:T, fluorescence peak T intensity, and fluorescence index) to differentiate natural DOM from EffOM using several paired samples.(Ulliman et al., 2020c) A similar methodology can be applied to the same parameters coupled with SEC. Because SEC fractionates samples by size, it reduces the complexity of DOM with respect to bulk water analysis. We suggest that future work using this system could investigate whether this reduced complexity extends to other freshwater, marine, and soil porewaters, leading to a greater ability to differentiate DOM qualitative changes and DOM sources. Furthermore, this

method provides a means by which highly fluorescent size fractions of DOM can be identified for more detailed analyses of carbon quality and its changes through different processing mechanisms. This system was specifically developed to capture different fractions for further off-line biological and chemical analysis at the molecular level using other analytical techniques (e.g., high resolution mass spectrometry and nuclear magnetic resonance spectroscopy).

4.4 Conclusion

This study developed a novel in-line method for the determination of Φ_f as a function of AMW using a SEC system coupled with DOC, absorbance, and fluorescence. This method provides useful and important information regarding DOM characterization, especially regarding fluorescence properties, something that still is considered to be a black-box in the DOM characterization community. The development and validation of instrument-specific correction factors for the SEC-fluorescence detector were needed to produce accurate fluorescence emission spectra. We calculated the Φ_f with the help of a salicylic acid standard, confirmed method accuracy by varying concentrations, and monitored chemical processing effects of ozonation for different AMW DOM fractions. Φ_f of the DOM in natural water and fulvic isolate samples followed a characteristic profile whereby Φ_f increased with decreasing AMW. However, the profile of PLFA DOM changed following ozonation, suggesting SEC-based Φ_f tracks important fundamental changes to DOM composition.

For all sample sets, a close investigation of all chromatographic results (fluorescence, absorbance, and DOC) individually is especially useful in the qualitative understanding of sample composition and chromatographic behavior. For example, the natural water samples and the isolates analyzed in this study showed that larger AMW fractions with lower Φ_f correspond with higher DOC concentrations while smaller AMW fractions with higher Φ_f correspond with lower

concentrations. While DOM components with higher Φ_f will contribute more to observed bulk fluorescence than components with lower Φ_f relative to their abundances, bulk water Φ_f values are weighted more heavily to lower SEC-based Φ_f (<1.5%) due to higher abundances (i.e., concentration). Additionally, by comparing the SEC-DOC to SEC-absorbance and SEC-DOC to SEC-fluorescence signals, it can be understood which fractions contain DOM that is chromophoric and fluorophoric and which fractions are not, providing more detail than is detected by bulk water absorbance and fluorescence analysis alone. Finally, it is proposed that future studies could utilize this method to differentiate between sources of OM (e.g., natural organic matter from diverse ecosystems and EffOM), and to identify highly fluorescent components for isolation and further detailed investigation.

Chapter 5

A Demonstration of the Conservative Mixing Behavior of DOM Optical Properties and Molecular Size Following Source Blending

5.1 Introduction

Dissolved organic matter (DOM) is a complex mixture of organic molecules resulting from the breakdown of higher organic species (plants, animals, microbes). DOM plays important roles in both natural and engineered systems where it is referred to as natural organic matter (NOM) and effluent organic matter (EfOM), respectively (Bauer et al., 2013b; Thomas S. Bianchi, 2011). For example, in surface waters, NOM is the main absorber of light and can also complex with metals and organic contaminants, impacting their fate and transport in the environment (Azam et al., 1983b; Ravichandran, 2004b). During water treatment processes, DOM can increase fouling rates of membrane filtration processes and can react with chlorine used for disinfection purposes, resulting in the production of harmful products known as disinfection byproducts (DBP's) (Christman et al., 1983).

In addition to understanding interactions with different environments, the study of DOM is important for its use as a surrogate for other the natural and anthropogenic constituents in water. The use of DOM as a surrogate is possible because DOM is ubiquitously present in all waters (both natural and treated) and it is typically present at concentrations several times higher than the concentration of individual constituents of interest. For example, the removal of DOM can be related to the removal of target pathogens and chemical contaminants during treatment processes

(Dickenson et al., 2009; Gerrity et al., 2012), where the measurement of specific pathogens and contaminants cannot be easily measured by methods that are feasible for treatment scenarios. These surrogate applications are especially intriguing for potable reuse and "de facto" reuse scenarios.

Although bulk DOM concentration (and thus removal) can be measured by analysis of total organic carbon (TOC), and dissolved organic carbon (DOC), these metric provides no information regarding the *quality* of DOM. Analyzing properties such as absorbance and fluorescence (i.e., optical properties), and molecular size provide additional characterization in terms of DOM source and composition (Coble, 1996b; P. G. Coble et al., 2014; Summers et al., 1987a). For example, absorbance at 254 nm is known to increase DOM aromaticity (Edzwald et al., 1985). It is known that aromatic DOM is preferentially removed by coagulation processes during water treatment. Fluorescence signatures of DOM have been related to the precursor material of DOM. For example, fluorescence signals at an excitation wavelength ($\lambda_{f,ex}$) of ~280 nm and emission wavelength ($\lambda_{f,em}$) of ~350 nm are often associated with DOM of microbial origins whereas signal at $\lambda_{f,ex}$ of ~280 nm and $\lambda_{f,em}$ of ~450 nm is associated with allochthonous DOM, or DOM composed of humic substances that are transported to aquatic systems from where the DOM is sampled(P. G. Coble et al., 2014; Findlay and Sinsabaugh, 2003; Maie et al., 2007; Yamashita and Tanoue, 2004, 2003). Complementary, molecular size impacts DOM transport in natural environments and removal during treatment (Perdue and Ritchie, 2003b). For example, membrane filtration processes (i.e., microfiltration and ultrafiltration) selectively remove large molecular weight fractions of DOM, whereas smaller fractions pass through filters (Ignatev and Tuhkanen, 2019).

In order for photophysical metrics to inform source and compositional inferences, the fundamentals of these properties must be well understood. However, there is currently a debate as

to the fundamental mechanisms that control these processes (McKay, 2020a). While it has been established that the spectroscopic characteristics of DOM are source specific, it is not understood whether these properties are a sum of the characteristics of individual DOM components, or if there are interactions between DOM molecules that impact the observed signals. According to the fundamental principles of Beer Lambert Law and fluorescence quantum yield (Equations 1-5), in ideal systems (non-interacting molecules) the measured absorbance and fluorescence for mixtures of compounds are a superposition (i.e., simple addition) of the absorbance and fluorescence of individual components. One of the leading arguments against superposition is the suspected occurrence of charge transfer interactions between DOM moieties (i.e., molecules or functional groups within molecules). Charge transfer refers to electronic interactions occurring between DOM chromophores (i.e., the components of DOM that absorb light), forming donor-acceptor (DA) complexes in which the resulting observed spectroscopic properties are uniquely different compared to a linear combination of the individual components (Del Vecchio and Blough, 2004, 2004; McKay et al., 2018; McKay, 2020a).

Similar to the uncertainty surrounding optical properties properties of DOM, the mechanisms that control observed molecular size distributions are also debated. It is unknown whether size distributions are true observations of the mix of individual compounds or if smaller compounds group together in conglomerates and are thus observed to be large (Capasso et al., 2020; Guetzloff and Rice, 1994; Jones and Bryan, 1998; Piccolo, 2001). Methods that have been used to estimate average molecular sizes and distributions of DOM include size exclusion chromatography (SEC), vapor pressure osmometry (VPO), cryoscopy (CRY), field flow fractionation (FFF), and ultrafiltration (UF) (Aiken and Malcolm, 1987; Perdue and Ritchie, 2003b). However, the results vary from one method to another resulting from the fact that they are

analyzing different properties related to DOM. For example, colligative methods (e.g., VPO, CRY), are based on the relationship between a solvent property (e.g., melting/boiling points, vapor pressure) and the solvent mole fraction and tend to yield lower estimates of molecular weight. Non-colligative properties (e.g., SEC, FFF, UF) are based on the physical properties of the solute molecules (e.g., molecular size, molecular shape) and have yielded higher estimates of molecular weight.

In addition to fundamental understanding, establishing whether observed spectroscopic properties and size distributions result from the linear superposition of individual components or affected by interactions has significant impacts for the ability to use DOM characterization as a practical surrogate, such as the fate and transport of other constituents in natural and treated systems and for source differentiation, especially in the case of *de facto* reuse (Ulliman et al., 2020b). These assumptions become especially important in instances when molecular size and optical properties are used as surrogates for contaminant removal or water treatment operational control, as misinterpretations may increase the risk to human health due to misinformed decisions.

This study investigates whether the blending of DOM sources follows mass balance properties as a function of molecular size using 3 detectors. Multiple detectors are used to differentiate chromophores and fluorophores, which represent only a fraction of the entire DOM pool. DOM sources are blended in pairs in controlled ratios. If optical spectra and molecular size chromatograms are a superposition of individual components, then it is hypothesized that applying mass balances to the end-member sources should predict the spectra of any mixture. Therefore, each blending ratio was modelled and compared against observed chromatograms to determine whether or not the ideal mass balance assumptions hold true within in the context of analytical reproducibility to assess the limitations.

5.2 Materials and Methods

5.2.1 DOM sources and Experimental Matrix

Source Selection

This study analyzed a pair of aquatic DOM sources (Table 1-2) that were blended in binary mixtures in ratios according to Table 5.3. Both sources, Suwannee River Humic Acid (SRFA) and Suwannee River Fulvic Acid (SRFA) were DOM isolates from the International Humic Substances Society (IHSS). DOM isolates were chosen as predominant source material due to the ability to control the experimental conditions with respect to DOC and optical density and for broad use in the DOM research community. See Tables 5.1-5.3 for details regarding the blending scenarios.

Sample and Blend Preparation

To prepare stock solutions at a target concentration of 80 milligrams carbon per liter (mg_C L^{-1}), ~16 mg of dry isolate were dissolved in 100 mL of Type I water and stirred for 24 hours at room temperature. Solutions were filtered through pre-combusted 0.7 μm GF/F filters. Stock solutions were adjusted to a pH of 6.8 using NaOH to match the pH of the SEC mobile phase. Assuming a concentration of 80 mg_C L^{-1}, three separate dilutions of each stock solution were prepared at a nominal concentration of 3 mg_C L^{-1} and analyzed by an offline Sievers M5310 DOC Analyzer and Cary-4000 Spectrophotometer to determine the actual concentration and optical density of the stock solution. Sample blends were created according to the ratio scheme outlined in Table 5.3 with binary mixtures with variable proportions of each end member. For each blend pair, two scenarios were created. The first scenario mixed end members targeting a constant [DOC], and the other scenario targeted a constant optical density of 0.15 measured at 300 nm for each blending series. These scenarios deliberately created challenging scenarios where only composition changes, independent of nominal [DOC] and optical density at a fixed wavelength.

Blend solutions were prepared gravimetrically in 120 mL pre-combusted amber bottles, and pH was adjusted after blending as necessary to pH 6.8. Bottles were capped and refrigerated until analysis. Prior to analysis, a 20 mL aliquot of each sample was spiked with ~1 mL of a concentrated mobile phase solution (0.016 M Na_2HPO_4, 0.024 M NaH_2PO_4, and 0.03 1M Na_2SO_4), to match the ionic strength and pH of the mobile phase of the SEC column. By matrix matching the samples to the eluent, non-ideal interactions are suppressed as samples disperse into the mobile phase after injection (Her et al., 2002b). Exact volumes of added spike were recorded to calculate impact on overall concentrations and ratio percentages.

Table 5.1. Sources of DOM and References Used in Blends

DOM Source	Reference
Suwannee River Fulvic Acid (SRFA)	2S101F
Suwannee River Humic Acid (SRHA)	2S101H

Table 5.2. Experimental Matrix of DOM Blending Pairs

Blend Pairs	
DOM Source 1	DOM Source 2
SRFA	SRHA

Table 5.3. Summary of Blend Ratios. The table shows a summary of various blend ratios that were used for every blend pair in the study. Numbers in the left most column are used for referencing the various blends in the text.

Blending Ratios		
Ratio Numbers	% Contribution Source 1 (Blended by or UV_{300})	% Contribution Source 2 (Blended by or UV_{300})
1	100	0
2	90	10
3	80	20
4	70	30
5	50	50
6	30	70
7	20	80
8	10	90
9	0	100
10 (duplicate of 6)	70	30

5.2.2 Data Collection

The SEC system was an Agilent 1260 high performance liquid chromatography (HPLC) setup that included an Agilent 1200 Series Vacuum Degasser, Agilent 1200 Series G1310A Isocratic Pump, Agilent 1260 Infinity Series G1315D Diode Array Detector (DAD), Agilent 1260 Series Infinity II Fluorescence Detectors (FLD) and a Sievers M9 DOC Analyzer. Absorbance and fluorescence signals were recorded directly by the Agilent OpenLab software (Rev. C01.09). An Agilent Universal Interface Box II was utilized to transfer data from the DOC analyzer to the Agilent software in voltage units, which were later converted to [DOC] ($mg_C\ L^{-1}$) (see SI, Text S-1.2.3) for a detailed description of conversion). Size-based separations were achieved using a Toyopearl HW-50S column (internal diameter (ID) 20 mm x 25 cm, 92 mL total volume). Samples were injected via an Agilent Technologies 1260 Series G7129A Autosampler configured with a 900 µL analytical head and multi-draw injection kit to allow for injection volumes of up to 1.8 mL.

All sample blends were analyzed by the SEC system described in Section 2.1. During analysis, the SEC system was operated at a flow rate of 1 mL/min using 1.8 mL injection volumes, the largest injection volume possible for the system). The elution time for each sample was 150 min to ensure all detectors returned to baseline. For all analyses, the DOC detector measured DOC concentration ([DOC]) at 4 second intervals. The Agilent DAD detector scanned from 200-700 nm in 2-nm increments. For fluorescence analysis, each samples were analyzed twice, once at each excitation wavelength (λ_{ex} 275 nm and λ_{ex} 350 nm). Emission spectra were collected from the excitation wavelength up to 700 nm at 5 nm increments. Absorbance and fluorescence emission spectra were collected at ~0.3 second intervals, producing a absorbance and fluorescence emission spectra at each chromatographic elution volume data point. From the spectral data, specific

wavelengths were extracted to create two-dimensional chromatograms at specific absorbance or fluorescence emission wavelengths. Chromatograms were also plotted for total fluorescence (TF), representing the integrated fluorescence intensity . Since each sample was analyzed twice for different excitation wavelengths, chromatograms were measured in duplicate on the DOC and UV detectors, as those data acquisition parameters are independent of the fluorescence excitation wavelength. During data processing, elution volumes of each detector were aligned, baseline corrections were performed, and fluorescence data was spectrally corrected following the methods of Hanson and coworkers (Hanson et. al., 2022). All corrections were preformed using MATLAB.

5.2.3 Fundamental Equations for Optical Signals and Mass Balance

To determine if blending two DOM sources follows conservative mixing principles (i.e., non-interacting chromophores/fluorophores), equations describing the relationship between the concentration of DOM present and the optical response. Equation 1 defines absorbance (A) as a function of the incident light intensity (I_0) and transmitted intensity (I). Beer-Lambert Law (Equation 1) defines absorbance as proportional to the decadic molar absorption coefficient (ε), molar concentration (c), and cell pathlength (d). Since DOM is a mixture of multiple unique molecules that could absorb light at a given wavelength, ε represents the apparent molar absorbance coefficient of the mixture, and the concentration of DOM present is represented by the bulk carbon concentration. Equation 1 shows that *A* is proportional to c, if the apparent ε is unaffected by the presence of other DOM sources in the blended samples.

(1) $$A = log\frac{I_0}{I} = \varepsilon cd$$

Similarly, the combination of Beer-Lambert Law and the apparent fluorescence quantum yield describe the relationship between fluorescence intensity and concentration. Equation 2 shows that fluorescence intensity (F) is proportional to the intensity of light absorbed ($I-I_0$) and the

fluorescence quantum yield (Φ), which describes the fraction of light absorbed emitted as fluorescence. Using Napierian conventions, Equation 3 defines the intensity of light absorbed in terms of concentration (c), Napierian molar absorption coefficient (k), and fluorescence quantum yield (Φ). Applying a series expansion, Equation 3 can be approximated as Equation 4 when the product kcd is small. This linearizing approximation leads to a proportional relationship between fluorescence intensity and concentration. This proportionality not only assumes that the truncated error from the series expansion is small, but that the intrinsic photophysical properties (Φ and k) are unaffected by the presence of another DOM source in blended samples.

(2) $$F = \Phi(I - I_0)$$

(3) $$(I - I_0) = 1 - e^{-kcd}$$

(4) $$(I - I_0) \approx kcd$$

(5) $$F \approx \Phi kcd$$

If the optical properties (i.e., ε, k and Φ) and molecular size distribution of one DOM source are unaffected by the presence of a second DOM source, then mass balances that incorporate Equations 1 and 5, should predict the SEC chromatogram of blends with varying ratios of each DOM source. Equations 6-9 develop the general equation (equation 10) to predict the SEC chromatograms for blended samples. Equations 6 and 7 are mass balances on water and DOM mass, respectively,

(6) $$v_{blend} = v_1 + v_2 + v_{DI}$$

(7) $$c_{blend} v_{blend} = c_1 v_1 + c_2 v_2$$

where *v* and *c* represent the volume and concentration, respectively. The subscripts "1", "2" and "blend" represent DOM source 1, DOM source 2 and the blended samples, respectively. The DOM sources are either concentrated stock solutions or EfOM as collected. In the case of concentrated stock solutions, additional deionized water (v_{DI}) is added, which is assumed to have negligible background DOM concentrations for the mass balance calculations. Equations 8 and 9 shows that the total concentration of DOM in the blended sample is a function of DOM source concentration and the fractional volume (f_1 and f_2) that the DOM sources to the final blended solution.

(8) $$c_{blend} = c_1 \frac{v_1}{v_{blend}} + c_2 \frac{v_2}{v_{blend}}$$

(9) $$c_{blend} = c_1 f_1 + c_2 f_2$$

If the DOM in each source is unaffected by its blending with another DOM source, then the optical responses should be proportional to the contribution of each DOM source to the blended sample. Under these ideal assumptions, Equations 1 and 4 show that the optical response (absorbance or fluorescence) is proportional to the concentration. To illustrate for absorbance at a single wavelength, equation 10 postulates that, for non-interacting chromophores, the absorbance of the blended sample is the superposition (i.e., summation) of the absorbance of the two sources at the actual concentration present in the blended sample ($A_{1,blend}$ and $A_{2,blend}$). Note that the concentration of a DOM source in the blended solution ($c_{1,blend}$ and $c_{2,blend}$) will be less than the original source if there is mixing with another source.

(10) $$A_{blend} = A_{1,blend} + A_{2,blend}$$

Since absorbance is proportional to concentration, the absorbance contribution from an individual source (e.g., $A_{1,blend}$) depends on the absorbance of the source solution (e.g., A_1) and the fractional contribution of that material to the blended sample (e.g., f_1). Equation 11 applies

Beer-Lambert law to Equation 10. Leveraging the mass balance in equation 9, the concentration of a DOM after dilution is the source concentration times the fractional volume contribution, whish in equation 12. Substituting equation 12 into equation 11 shows that the absorbance of the blended solution is summation of the source absorbance (e.g., A_1) weighted based on the fractional contributions by volume.

(11) $$A_{blend} = \varepsilon_1 c_{1,blend} d + \varepsilon_2 c_{2,blend} d$$

(12) $$c_{1,blend} = f_1 c_1 \text{ and } c_{2,blend} = f_2 c_2$$

(13) $$A_{blend} = f_1(\varepsilon_1 c_1 d) + f_2(\varepsilon_2 c_2 d)$$

(14) $$A_{blend} = f_1 A_1 + f_2 A_2$$

A similar derivation can be applied to fluorescence, using equation 5. Equation 14 and its equivalent for fluorescence can be generalized as equation 15, showing that the optical signal of the blend (sig_{blend}) is the weighted summation of the source materials (sig_1 and sig_2).

(15) $$sig_{blend} = f_1 sig_1 + f_2 sig_2$$

This application of mass balances and fundamental photophysical principles only applies if the chromophores/fluorophores do not interact with the newly introduced DOM such that the intrinsic photophysical parameters (i.e., ε, k, Φ) change. Testing the validity of this assumption is a core objective of this study to determine if SEC can reveal non-ideal interactions as a function of molecular size and photophysical characteristic.

Chromatograms were smoothed using a cubic spline function to evaluate the central tendency independent of noise. The fluorescence chromatograms consistently had higher noise and an example of smoothing is shown in Figure 5.1. The chromatograms of the end members were

smoothed prior to applying Equation 15 to predict the chromatogram of the blended sample. The measured chromatograms of the blended samples were also smoothed prior to comparing the measured and predicted chromatograms. An error analysis assessed the variability in the raw data and repeatability between duplicates to objectively determine when predicted and actual chromatograms showed systematic differences.

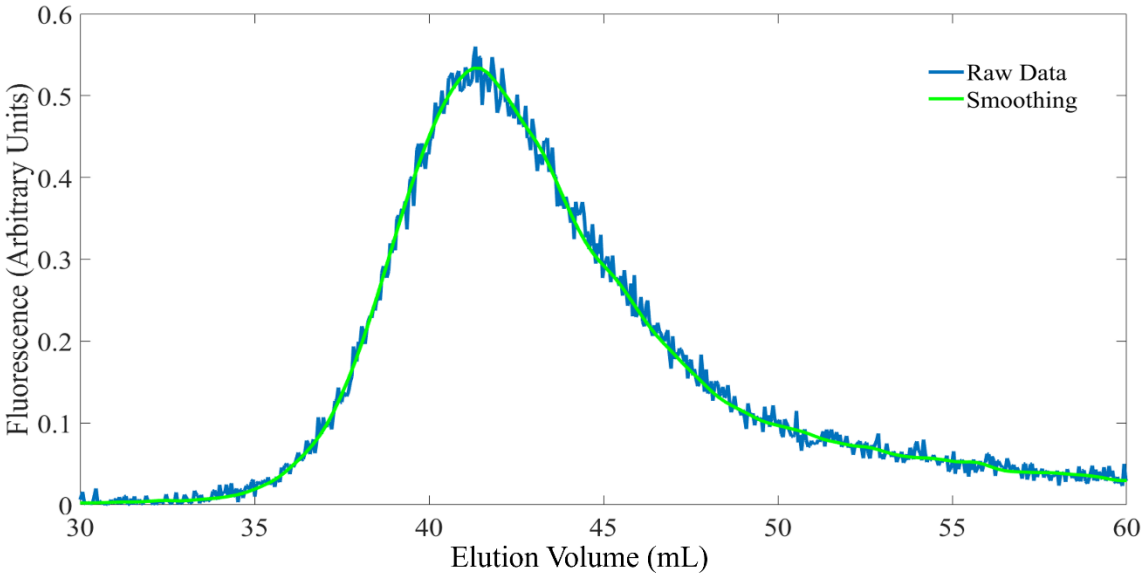

Figure 5.1. Fluorescence Chromatogram Smoothing. Sample: SRFA/SRHA Blend by constant UV_{300}, Excitation 350 nm, 100% SRFA. A comparison of raw fluorescence chromatogram (blue) to the smoothed chromatogram (green).

For all blend pairs, equation 15 was applied to smoothed chromatograms to predict the chromatograms for DOC, absorbance at wavelengths (λ_{Abs}) of 275 and 350 nm, total fluorescence (TF) at λ_{Fex} 275 nm and 250 nm, and apparent fluorescence quantum yield (Φ_F) at the same λ_{Fex} wavelengths. Total fluorescence is the integrated fluorescence intensity at a set λ_{Fex}. These predictions yield two-dimensional chromatograms with elution volume on the x-axis, which is the elution time normalized by the volumetric flowrate. Since full absorbance and fluorescence emission spectra are also measured at each elution volume, equation 15 was also applied to predict

the spectra at each volume, producing a three-dimensional plot where the optical signal (z-axis) is a function of both elution volumes (x-axis) and wavelength (y-axis). Figure 5.2 shows an example workflow of using the chromatographic data from end members (Figure 5.2, Top) to predict the chromatographic data of intermittent blends (Figure 5.2, Middle). These predictions are overlaid with measured chromatograms of the blended samples (Figure 5.2, Bottom).

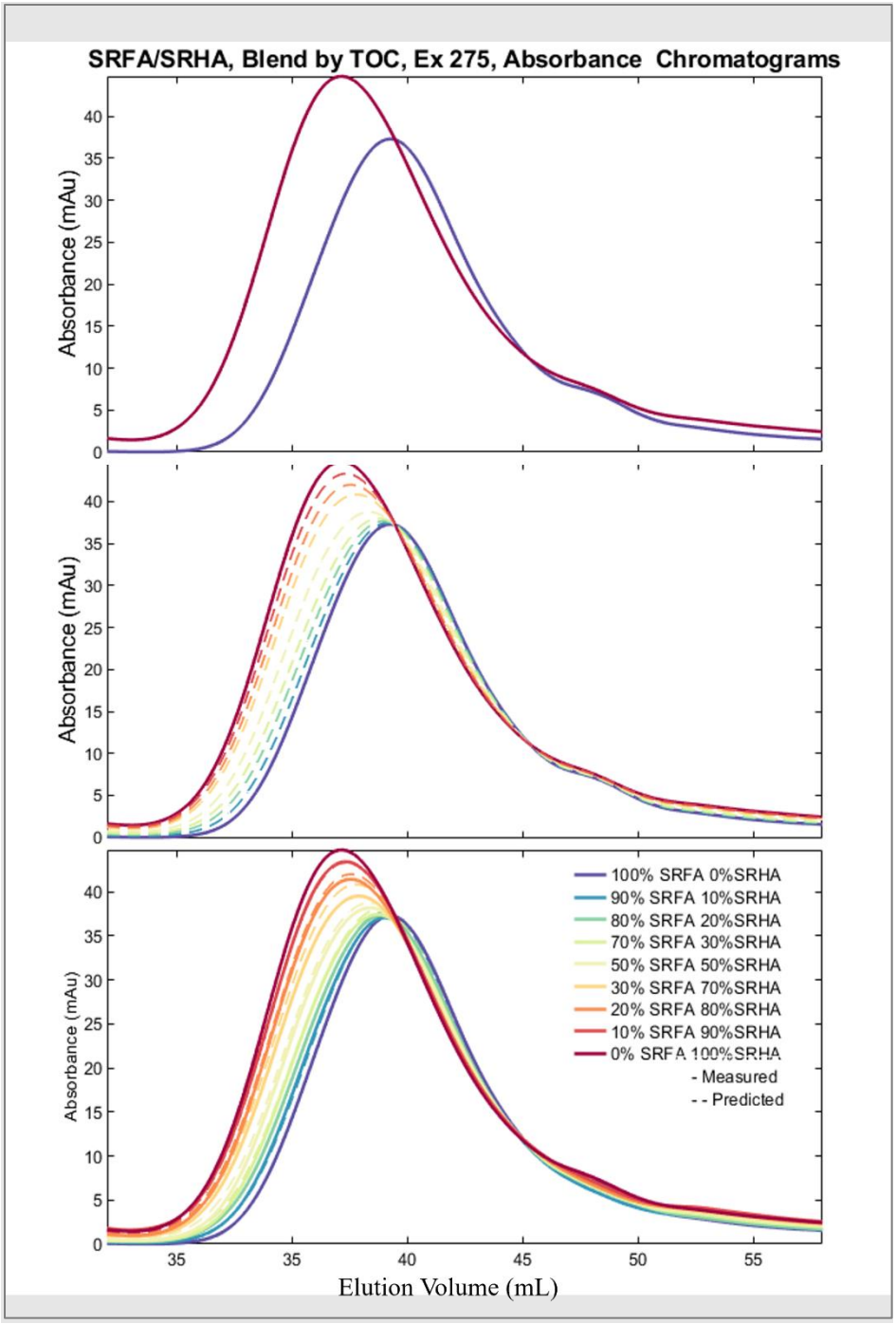

Figure 5.2. Workflow of Predicted Blend Sample Chromatograms from End Member Data. Predicted and measured absorbance chromatograms of the SRFA/SRHA blend at constant DOC (nominal [DOC] = 3 mg/L). Absorbance of all chromatograms was measured or predicted at 275 nm. **Top:** Measured absorbance chromatograms for the blend end members (samples containing 100% NLFA and 100% NLNOM). **Middle:** Measured chromatograms from the blend end members and predicted chromatograms for intermittent blend ratios (samples containing 10-90% of SRFA and SRHA). **Bottom:** Predicted and measured chromatograms for all blend ratios (i.e., end members and intermittent blends).

In addition to evaluating chromatograms at all elution volumes, three commonly used metrics were calculated that represent an entire chromatogram with a single data point, rather than evaluated at every elution volume. The metrics include number average (M_n), weight average (M_w), and polydispersity (P_d), and chromatogram integration using equations 16–18 (Striegel et al., 2009). The measured and predicted values for each metric were compared to see how well the metrics of the end member could predict the metric of the blended sample. Equations 16-18 were used to calculate M_n, M_w and P_d respectively:

(16) $$M_n = \frac{\sum_{i=1}^{N} h_i}{\sum_{i=1}^{N} (h_i/V_i)}$$

(17) $$M_w = \frac{\sum_{i=1}^{N} (h_i V_i)}{\sum_{i=1}^{N} h_i}$$

(18) $$P_d = \frac{M_w}{M_n}$$

where h_i represents the detector response at a given elution volume, V_i. For intermittent blends, the predicted values of all metrics were calculated from the predicted chromatograms. In calculating these metrics time and detector response thresholds were assigned based on the following: Raw DOC data captured by Chemstation is in mV which occurs in a step-like behavior where the step increment is equal to 10 ppb and is considered the signal noise. These thresholds served as a boundary within which data was evaluated and data outside of the boundary discarded for the sake of metric calculations. The minimum threshold was set to 70 ppb representing a limit of quantification (LOQ) equal to a signal to noise ratio of 7:1. Average noise in the absorbance and fluorescence baseline signal were found to be 0.5 milli absorbance units (mAu) and 0.0025 arbitrary fluorescence units respectively, and the LOQ threshold was set to 2 mAu and 0.01 arbitrary fluorescence units respectively. Notes mAu is equal to $cm^{-1}x10^{-3}$.

5.2.4 Assessment of Variability

An analysis of experimental and instrumental variability is necessary to identify when the measured and predicted chromatograms show systematic deviations, which may be indicative of non-ideal photophysical behaviors. The experimental and analytical variability was assessed by running two different types of duplicates. One of the blends was prepared twice (Blend Ratios 6 and 10) to assess the expected error from both preparing and analyzing the same blend. The end members were analyzed in duplicate, spaced out at the beginning and end of the sequence to analyze instrumental variability and drift.

Several approaches were used to objectively compare measured and predicted data to assess if blending of DOM sources follows fundamental mass balance properties. The absolute error between measured and predicted chromatograms was calculated by subtracting both chromatograms. The relative percent error was calculated by dividing absolute error at each elution volume by the predicted detector response at that same elution volume. Based on replicate data (data not shown), ±5% relative error thresholds were used to evaluate the matching accuracy of two-dimensional chromatograms. Absolute and relative errors were determined for three-dimensional data, however they were used to qualitatively evaluate regions where systematic error occurred (i.e., ±5% thresholds were not applied). Absolute errors were calculated for M_n, M_w, and P_d which and were evaluated relative to the range of the end member metric values. To summarize the performance of metric values, whose error was less than 5% of the end member range were considered to be an accurate match and the number of samples in a given batch were reported. For example, if the range of M_n values between end members was 2 mL, samples with an absolute M_n error of <0.1 mL were considered an accurate match. Matching accuracy of integrated values were assessed as a function of their relative error.

5.3 Results and Discussion

Two (2) pairs of DOM sources were tested to evaluate whether conservative mixing occurred with respect to molecular size and optical properties. One of the pairs (blend 1, Table 5.2) used 2 IHSS isolates and the other (blend 2, Table 5.2) used one isolate and one wastewater derived EfOM. The selection of end members represent DOM from various backgrounds. The first pair represents DOM fractions obtained from XAD-fractionation that are widely studies within the research community. The second pair represents a more realistic *de facto* reuse scenario.

5.3.1 Characterization of End Members

End members SRFA and SRHA display similar chromatographic features with detectable signals between elution volumes 30-60 mL for all signals (DOC, absorbance, and fluorescence) (Figure 5.3). DOC chromatograms show a large broad peak beginning at a low elution volume bound (30 mL) representing a larger apparent molecular weight (AMW) peak. Around 46-52 mL, there is a lower AMW peak that appears as a rider peak on the larger AMW peak leading to poor chromatographic resolution between these features. At 275 and 350 nm, absorbance chromatograms show a similar broad, larger AMW peak but lack the lower AMW rider peak. However, below 254 nm, the smaller AMW rider peak is observed, suggesting that the moieties contributing to the smaller AMW peaks in the DOC chromatogram include small, aromatic compounds (vida infra). Finally, the fluorescence chromatograms also show a single broad chromatographic peak without any smaller AMW rider peaks.

From the SRHA to SRFA end members, M_n and M_w increased for DOC (40.170 to 42.213 mL and 40.805-42.674 mL for M_n and M_w respectively) and absorbance (39.27-40.847 mL and 40.148-41.382 for M_n and M_w respectively) but were relatively constant for fluorescence (43.515-43.576 mL and 44.022-44.179 mL for M_n and M_w respectively). P_d decreased for DOC (1.016-

1.011) and absorbance (1.022-1.013) but was again constant for fluorescence (1.012-1.014). Because molecular size decreases with increasing elution volume, SRFA has a size distribution shifted to smaller AMW. DOC and absorbance chromatograms of SRFA are closer to a log-normal distribution (where a P_d value of 1 represents a log-normal distribution), agreeing with (Pavlik and Perdue, 2015b).

While M_n and M_w values are similar for DOC and absorbance chromatograms, the range of absorbance values (1.568 and 1.234 mL for M_n and M_w respectively) were generally smaller compared to DOC (2.043 and 1.869 mL for M_n and M_w respectively) suggesting the end member absorbance distributions are closer to one another than DOC (Table 5.4). For all isolates, fluorescence M_n and M_w values had higher elution volumes compared to both DOC and absorbance, showing that FDOM fractions are primarily composed of smaller compounds, agreeing with previous research (Hanson et al., 2022; Wünsch et al., 2018). The range of M_n and M_w values between end members was smaller for fluorescence (~0.5 mL) compared to absorbance and DOC (~2-2.5 mL). Therefore, there is more homogeneity in the FDOM size distribution, which is also visually apparent in Figure 5.3 (third row). Greater similarity in FDOM chromatograms over DOC and CDOM agrees with previous studies (Hanson et al., 2022; Wünsch et al., 2018).

Table 5.4. Summary of Chromatogram SEC Metrics for End Members. **Note:** M_n and M_w values are in units of milliliters (mL) and P_d values are unitless.

	DOC			UV 275 nm			TF at Ex 275 nm		
Isolate	Mn (mL)	Mw (mL)	Pd	Mn (mL)	Mw (mL)	Pd	Mn (mL)	Mw (mL)	Pd
SRFA	42.213	42.674	1.011	40.847	41.382	1.013	43.576	44.179	1.014
SRHA	40.170	40.805	1.016	39.279	40.148	1.022	43.515	44.022	1.012

P_d values were slightly greater than 1.0 for all end member isolates (and all blended samples) indicating that all isolates were close to log-normally distributed but slightly skewed toward lower molecular weight compounds. Also characterizing DOM by SEC, Cabaniss and coworkers postulated that the skew towards lower AMW results from a combination of geochemical reactions during DOM processing, such as precipitation, volatilization, and microbial processing, that preferentially removes the largest and smallest compounds from the original DOM pool (Cabaniss et al., 2000; Striegel et al., 2009). In the case of DOM isolates, the methods used for resin isolation and concentration by reverse osmosis also preferentially select for a more homogenous size distribution than the original sample (Thurman and Malcolm, 1981). These authors and others have also noted that some amount of tailing is typically observed for many forms of HPLC analysis due to nonideal behavior (Cabaniss et al., 2000; Striegel et al., 2009).

5.3.2 Comparison of Predicted and Measured Data

For each blending combination, the measured chromatogram was compared to the predicted one for 7 signals, shown side-by-side in Figure 5.3, which includes DOC, absorbance at two wavelengths, total fluorescence at two excitation wavelengths, and apparent fluorescence quantum yield at two excitation wavelengths. For each of these 7 signals, systematic differences were evaluated by calculating the absolute and relative percent error for each metric. This section details that analysis for one blend (SRFA/SRHA) and then distinct differences with the MRNOM/EfOM blend are highlighted.

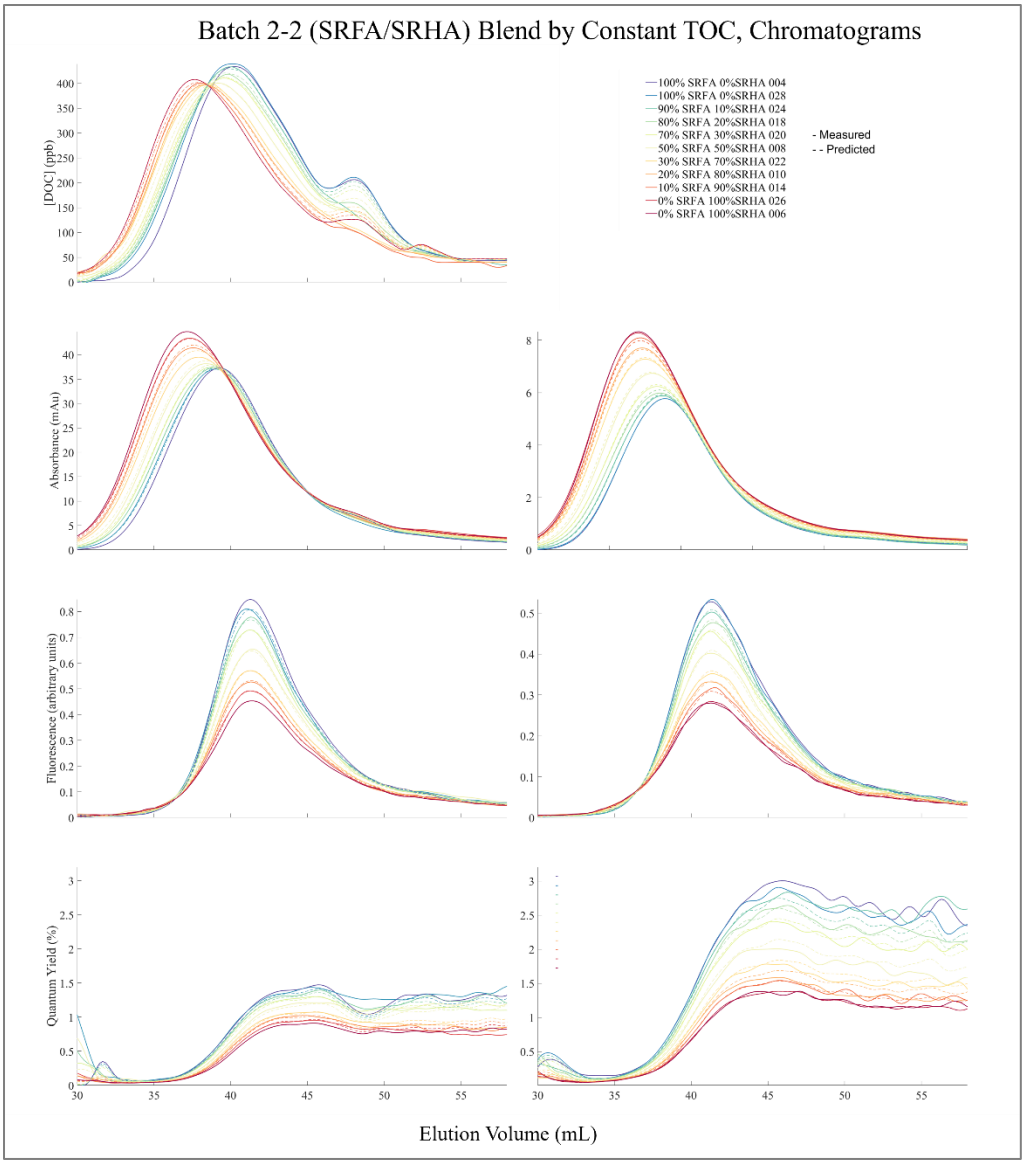

Figure 5.3. Chromatograms for the SRFA/SRHA Blend at Constant DOC. **LEFT (top to bottom):** DOC (ppb); Absorbance at 275 nm (mAu, cm^{-1}); Fluorescence at Ex: 275 nm, Em: Total Fluorescence 315-520 nm (Arbitrary Units); Fluorescence Quantum Yield at Ex: 275 nm (%). **RIGHT (top to bottom):** Absorbance at 350 nm (mAu cm^{-1}); Fluorescence at Ex: 350 nm, Em: Total Fluorescence 390-580 nm (Arbitrary Units); Fluorescence Quantum Yield at 350 nm (%).

Dissolved Organic Carbon

The measured and predicted DOC chromatograms were in good agreement showing a systematic gradient in both AMW distribution and signal magnitude between the end members (Figure 5.4, Top). Between elution volumes 37 and 46 mL, encompassing the main peak, the absolute error in [DOC] was ≤ 10 ppb for all but one blended sample, representing ≤ 3% relative error. For elution volumes lower than 36 mL, relative errors increased above 5% for all samples but relative errors are expected to increase as [DOC] signal decreases. The absolute error was ≤ 20 ppb for all but one sample, which was ≤ 25 ppb. An increase in relative error (17-37%) was also observed above 52 mL as the DOC signal decreased, but the absolute errors were ≤ 25 ppb. Above elution volumes of 57 mL, an unexpected peak in [DOC] signal occurred (data not shown) for several samples likely from IC rather than DOC. Although an IC peak was not observed in the end member samples, IC may have been introduced during pH adjustment while stirring. As a result, an upper bound was applied at 57 mL (elution volume), above which the true [DOC] signal cannot be separated from the [IC] chromatograms.

Interestingly, the measured data deviated significantly from the predicted in the elution volume range of 45-52 min (Figure 5.4, Top). Although the end member samples show a defined rider peak, this peak was less pronounced than predicted or absent in the blended samples. This behavior was reproducible in both blend versions (constant DOC and constant UV). In this region, absolute errors were found to increase to maximums 26-71 ppb representing a relative error of 16-37%.

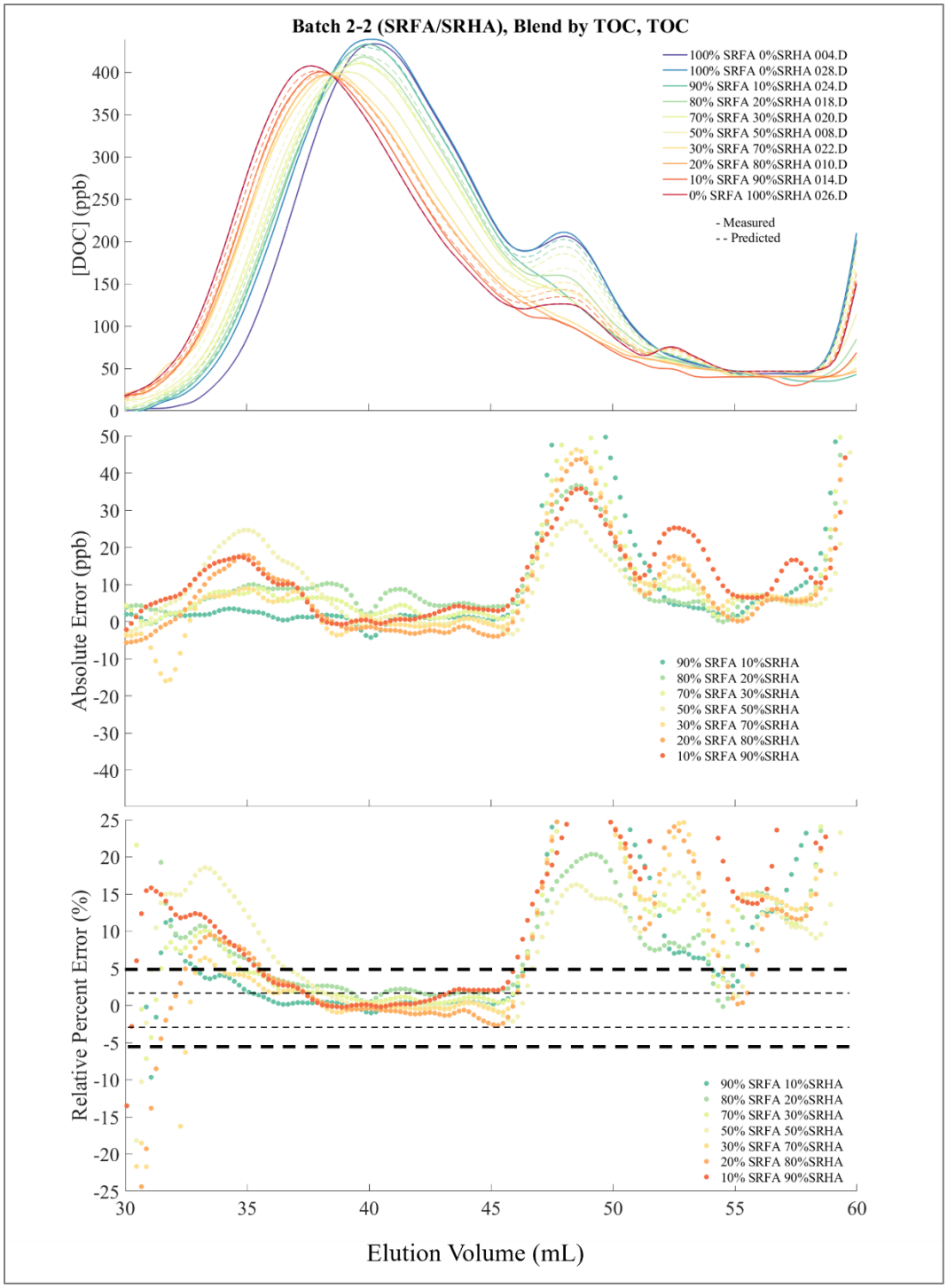

Figure 5.4. SRHA/SRFA Blend at Constant DOC: DOC Chromatograms and Chromatogram Error. **Top:** DOC chromatograms (ppb). **Middle:** Absolute error of DOC chromatograms (ppb). **Bottom:** Relative percent error of DOC chromatograms (%).

With respect to the calculated metrics, calculated M_n, M_w, and integrated area were less than predicted values and did not follow a unidirectional gradient between the end members as expected from the SEC chromatograms (Figure B.8). In total (i.e., total number of intermittent blend samples for the blend by DOC and blend by UV combined), 3 and 4 out of 16 samples (for M_n and M_w respectively) had errors that fell within 5% of the range in of SRFA and SRHA values. The relative error in integrated area ranged from ~4-7%. Additionally, the M_n and M_w of some intermediate blends were outside the range of the end members. The poor prediction of the size distribution is due to the suppression or absence of the rider peak at 47-52 mL elution volume, which will shift averages to lower elution volumes (larger molecular sizes). Observing sizes outside the range of the end members demonstrates the limitations of interpreting M_n and M_w, because the specific features chromatograms are lost. The impact of the rider peaks on the M_n and M_w metrics is also amplified because the initial range between the end members is small (~2.5 mL) compared to the range across which the samples elute (~30 mL). These metrics would be less sensitive to rider peaks if the initial difference between end members was greater. The sensitivity and its negative impact on prediction ability illustrates that these metrics should not be considered in isolation without interpreting the chromatogram features.

For both chromatographic data and calculated metrics, trends in error were not observed with respect to the percent of each end member in a given sample which suggests that the observed error was not due to interaction (with the exception of the 45-52 mL range which is further discussed below).

In comparing blends versions (i.e., comparing the blend prepared at a constant DOC to the blend at constant UV_{300}), the range in [DOC] magnitudes between end members were more similar for the blend at constant [DOC] than for the constant UV_{300} (Figure 5.4 and B.1). The similarity

in the constant DOC batch is intuitive as all samples contain the same overall [DOC]. Therefore, the area under the DOC chromatograms (i.e., integration) is the same for all samples in this blend version. The difference in the constant UV_{300} batch occurs because SRHA has a higher $SUVA_{300}$ than SRFA. Therefore, in the constant UV_{300}, the [DOC] of the 100% SRFA sample must be greater than that of the 100% SRHA sample for the total UV_{300} to match. The difference in [DOC] is observed in chromatogram data as the [DOC] at all elution volumes increases for the incremental blends with increasing percent SRFA (i.e., SRFA contributes relatively more [DOC] to the total sample [DOC] than SRHA).

The relative error in [DOC] between 37-47 mL was very similar between the two blend versions, however in the constant UV_{300} blend, at elution volumes lower than 37 mL, there was significant error, exceeding 25% for all but 2 samples (Figure 5.4 and B.1). The reason for this may be related to the decreasing signal strength with increasing percentage of SRHA in samples of the blend at UV_{300}. The SRHA end member sample (i.e., 100% SRHA) has the lowest [DOC] across all elution volumes of the chromatogram and the greatest proportion of chromatographic data that occurs near or below the LOQ. Increased error in the end member would propagate through the predicted data of intermittent blends and may explain the increased error of all intermittent samples in this blend.

Absorbance

Absorbance chromatograms for all end member pairs and blend types (constant DOC and constant UV) were analyzed at 275 and 350 nm (Figures 5.5-5.6 and B.2-B.3). The absorbance chromatograms followed similar trends to that of DOC chromatograms where the highest accuracy and precision was found near the chromatographic peak and error increased in the tail regions. However, results show better matching accuracy with respect to the absorbance signals. The

relative errors remained within ±5% between 33-47 mL (i.e., near the peak) for both blends and both wavelengths (275 and 350nm) which is a larger range of high accuracy (where relative chromatographic errors within ±5% were considered to be high accuracy) compared to the DOC detector. At elution volumes 30-33 mL the error was greater for both blend versions at 275 nm compared to 350 nm (Figures 5.5-5.6, B.2-B.3). This is possibly explained by the following: because the absorbance is higher at 275 nm across all elution volumes compared to 350 nm, when the signal begins to increases from baseline toward the peak (~30-33 mL), the increase in chromatographic slope occurs more rapidly (i.e., greater increase in y-axis value per x-axis increment) at 275 nm compared to 350 nm and the more dramatic change (i.e., more rapidly increasing chromatographic slope) may lead to larger error. Increased relative error was also observed in the 47-52 mL range (5-15%) at both absorbance wavelengths. This trend is similar to the behavior in the [DOC] chromatograms and discussed further in Section 5.3.4. At 275 nm, the metric values for 10 and 8 out of 16 samples (M_n and M_w respectively) were within 5% of the range between SRFA and SRHA and 14 and 10 out of 16 samples (M_n and M_w respectively) fell within this range at 350 nm (Figures B.9-B.10 and B.11-B.12). The relative error in integrated values ranged from ~0.3% to 2.2% (i.e., high matching accuracy of integration values for all samples).

Finally, Figure 5.7 demonstrates that in addition to chromatograms at a given wavelength, absorbance spectra at a given elution volume can be extracted from three-dimensional data SEC-absorbance data. The top subplot of Figure 5.7 shows the three-dimensional for the “70% SRFA 30% SRHA” sample from the blend by DOC (the same three-dimensional data is available for all predicted and measured samples). The horizontal and vertical white dashed lines show the points where respective chromatograms and spectra were extracted. Chromatograms and spectra from the same wavelength and elution volume were then extracted from all other samples in the same blend

and plotted in the middle and bottom subplots (chromatograms and spectra respectively) of Figure 5.7. The bottom subplot of Figure 5.7 shows the spectra extracted at elution volume 38 mL. From a qualitative visual inspection of the spectral data (Figure 5.7, Bottom), the predicted and measured data had a high matching accuracy at elution volume 38 mL. The matching accuracy of spectral data is expected to follow similar trends as the chromatographic data. For example, 38 mL represents an elution volume near peaks of all chromatograms in this plot (Figure 5.7, Bottom) and thus high matching accuracy is expected. As such, the matching accuracy of the spectral data is expected to be poor at elution volumes near the chromatographic tails (e.g. 30-33 mL), where increased error is observed in the chromatographic data. While an example from these elution volumes is not shown, the same extraction process could be performed to investigate the spectral data in these ranges.

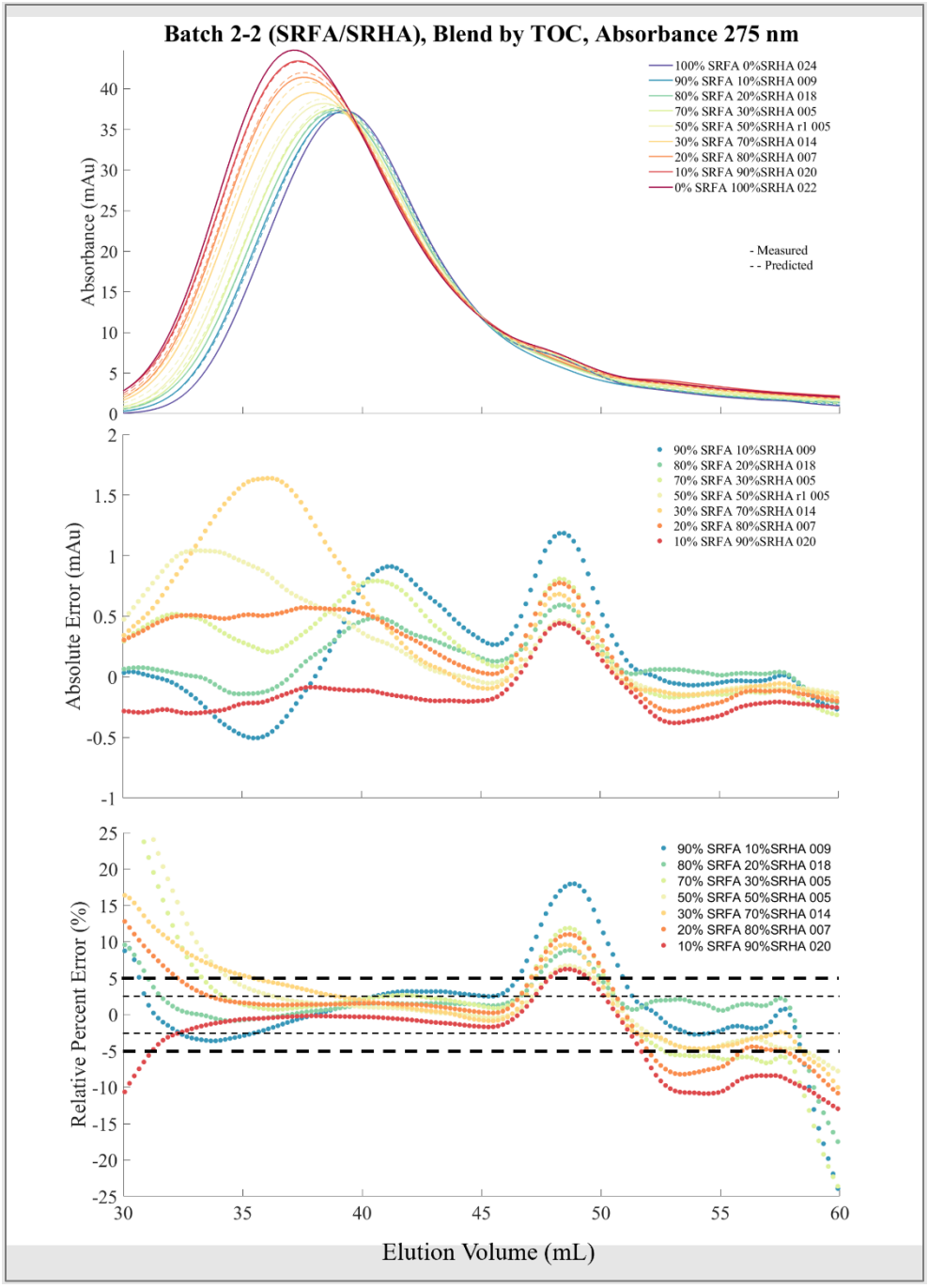

Figure 5.5. SRFA/SRHA Blend at Constant DOC: Absorbance 275 nm Chromatograms and Error. **Top:** Absorbance chromatograms at 275 nm (mAu). B Absolute error of absorbance chromatograms at 275 nm (mAu). **Bottom:** Relative percent error of absorbance chromatograms at 275 nm (%).

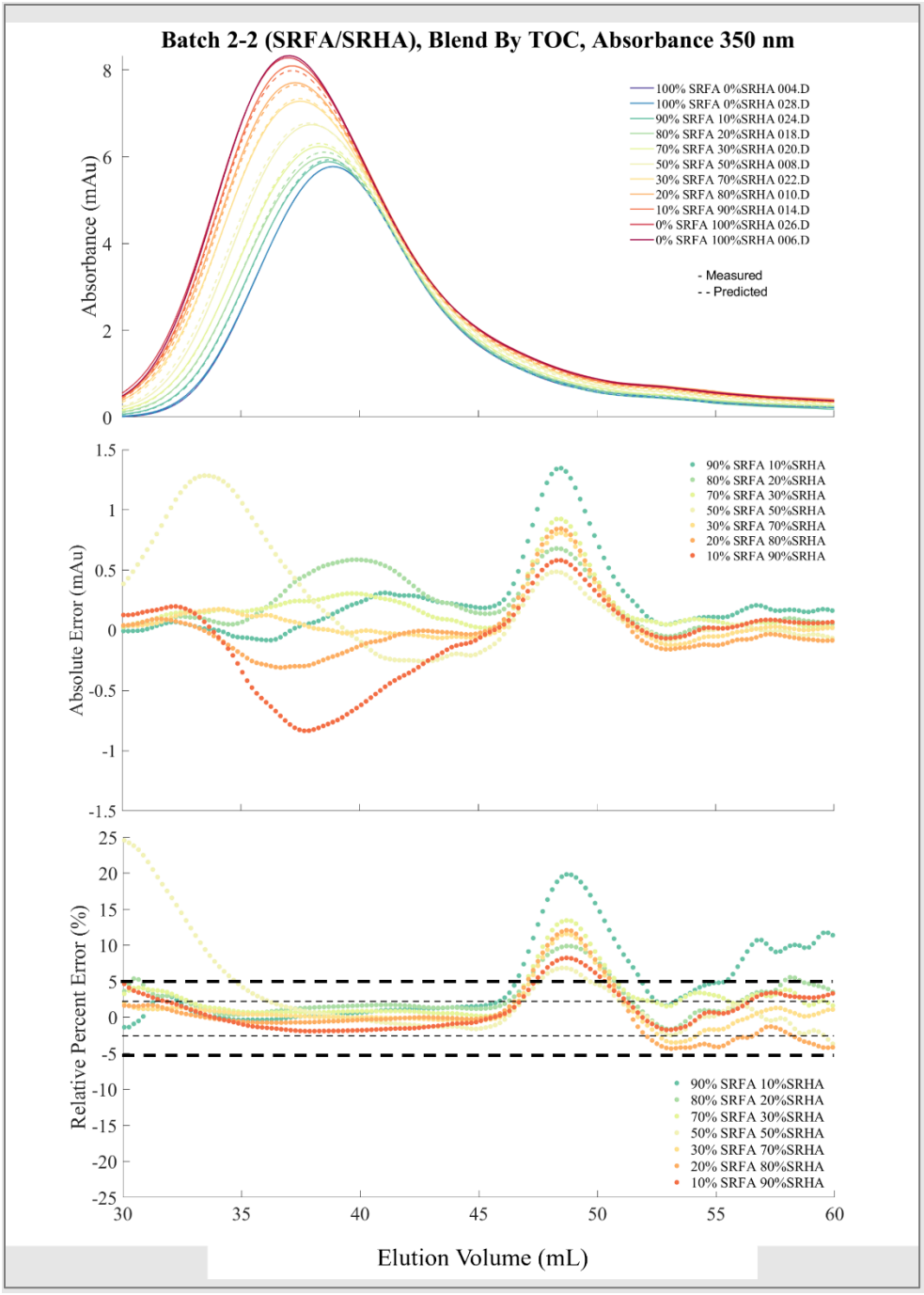

Figure 5.6. SRHA/SRFA Blend at Constant DOC: Absorbance Chromatograms at 350 nm and Chromatogram Error. **Top:** Absorbance chromatograms at 350 nm (mAu). **Middle:** Absolute error of absorbance chromatograms at 350 nm (mAu). **Bottom**: Relative percent error of absorbance chromatograms at 350 nm (%).

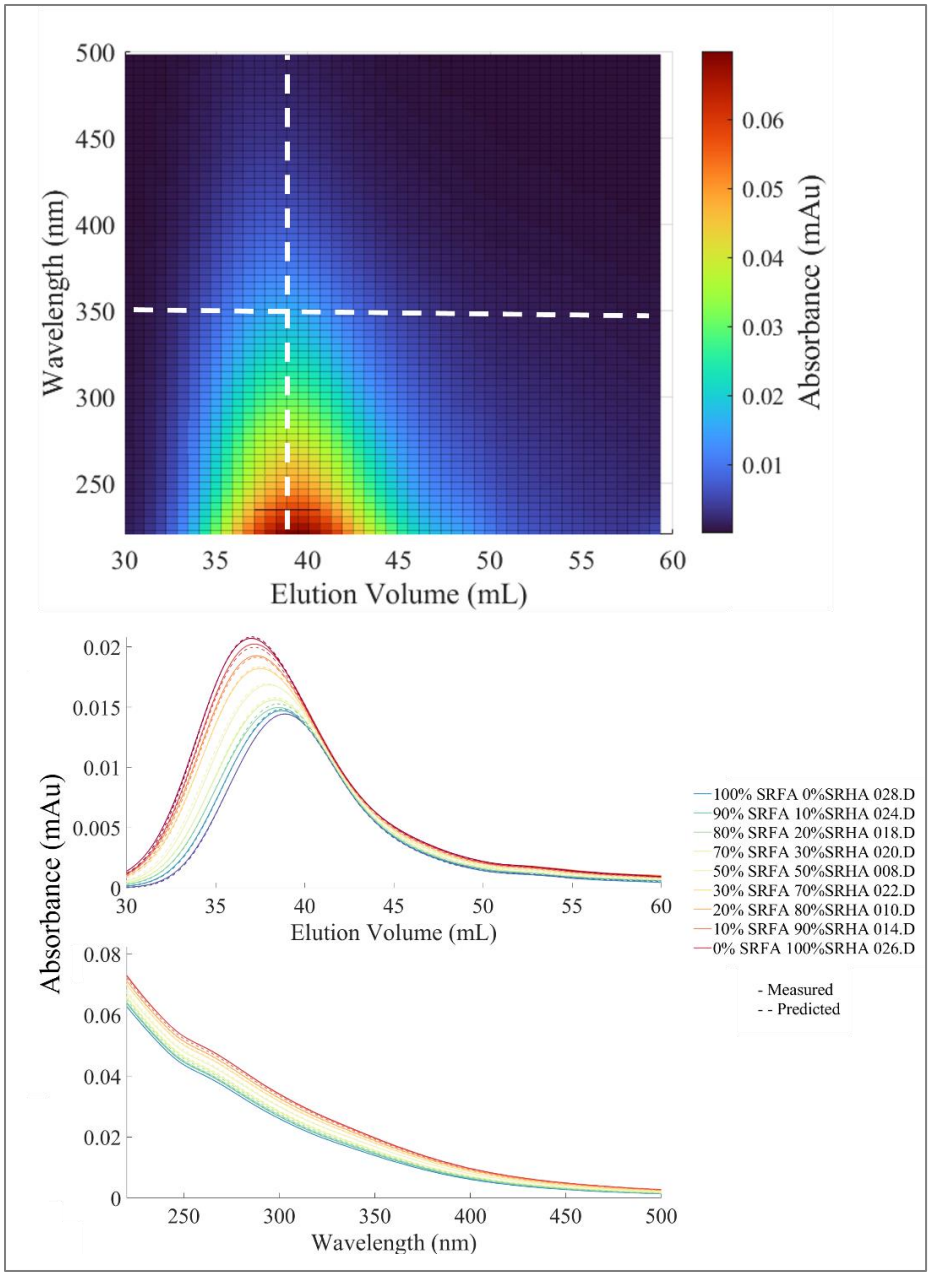

Figure 5.7. Extraction of Absorbance Chromatograms and Spectra from Three-Dimensional Data. **Top:** 70% SRFA 30% SRHA (blend at constant DOC) 3-dimensional SEC-Absorbance plot. Vertical and horizontal dashed white lines show the elution volume and wavelength where chromatograms and spectra were extracted from respectively. **Middle:** Absorbance chromatograms at 350 nm (mAu) extracted from 3-dimensional data. **Bottom:** Absorbance spectra (220-500 nm) extracted from 3-dimensional data.

Fluorescence

Fluorescence chromatograms were analyzed at λ_{Fex} 275 and 350 nm (Figures 5.8-5.9 and B.4-B.5). The chromatograms shown in the top Figure 5.8 (top subplot) and 5.9 (top subplot) represent the TF (i.e., integrated emission spectra) at the given λ_{Fex}. For both blend versions and both excitation wavelengths, there was a high matching accuracy between measured and predicted data was observed for both blend versions and both λ_{Fex}. Relative error remained below 5% for elution volumes 35-53 mL at both excitation wavelengths. This demonstrates that the reduced/missing signal between 47-52 mL was not detected by fluorescence detectors resulting in the largest range of high accuracy compared to absorbance and [DOC]. The absolute error decreased near the chromatographic tails and increased slightly near the chromatographic maximum. Error within a given sample was more scattered around the predicted data compared to [DOC] and absorbance chromatograms. The previous two explanations can likely be explained by the noise in the original signal where the signal to noise ratio was relatively lower compared to [DOC] and absorbance (this is discussed further in Section 3.4.). The matching accuracy of M_n, M_w, and P_d values are not reported for fluorescence chromatograms. These metrics are less prescriptive for fluorescence chromatograms (compared to DOC and absorbance) because as there is very little shift in the chromatographic distribution between end members (SRFA and SRHA). However, integrated values, which are a function of detector response (i.e., fluorescence intensity), demonstrated high matching accuracy with errors ranging from <1-3% (Figures B.11-11 and B.16-17).

Similar to the process of extracting chromatograms and spectra from three-dimensional data that was discussed in for the absorbance data above (i.e., the process shown in Figure 5.7), a similar process can be performed using three-dimensional fluorescence data. An example of this

is shown in Figure 5.10. There are two key differences to note for when this process is perfomed on three-dimensional fluorescence data: (i) Only fluorescence emission spectra can be extracted from three-dimensional fluorescence data as the analysis is conducted at a fixed λ_{Fex} (see the bottom subplot of Figure 5.10 for an example); (ii) the chromatograms extracted are at a single λ_{Fem} (Figure 5.10, Middle) where the chromatographic data in Figures 5.8-5.9 and B.4-B.5 represent TF. For the example shown in 5.10, a qualitative visual evaluation suggests that both chromatograms at λ_{Fem} 340 (middle subplot) and spectra at 41 mL (bottom subplot) have high matching accuracy.

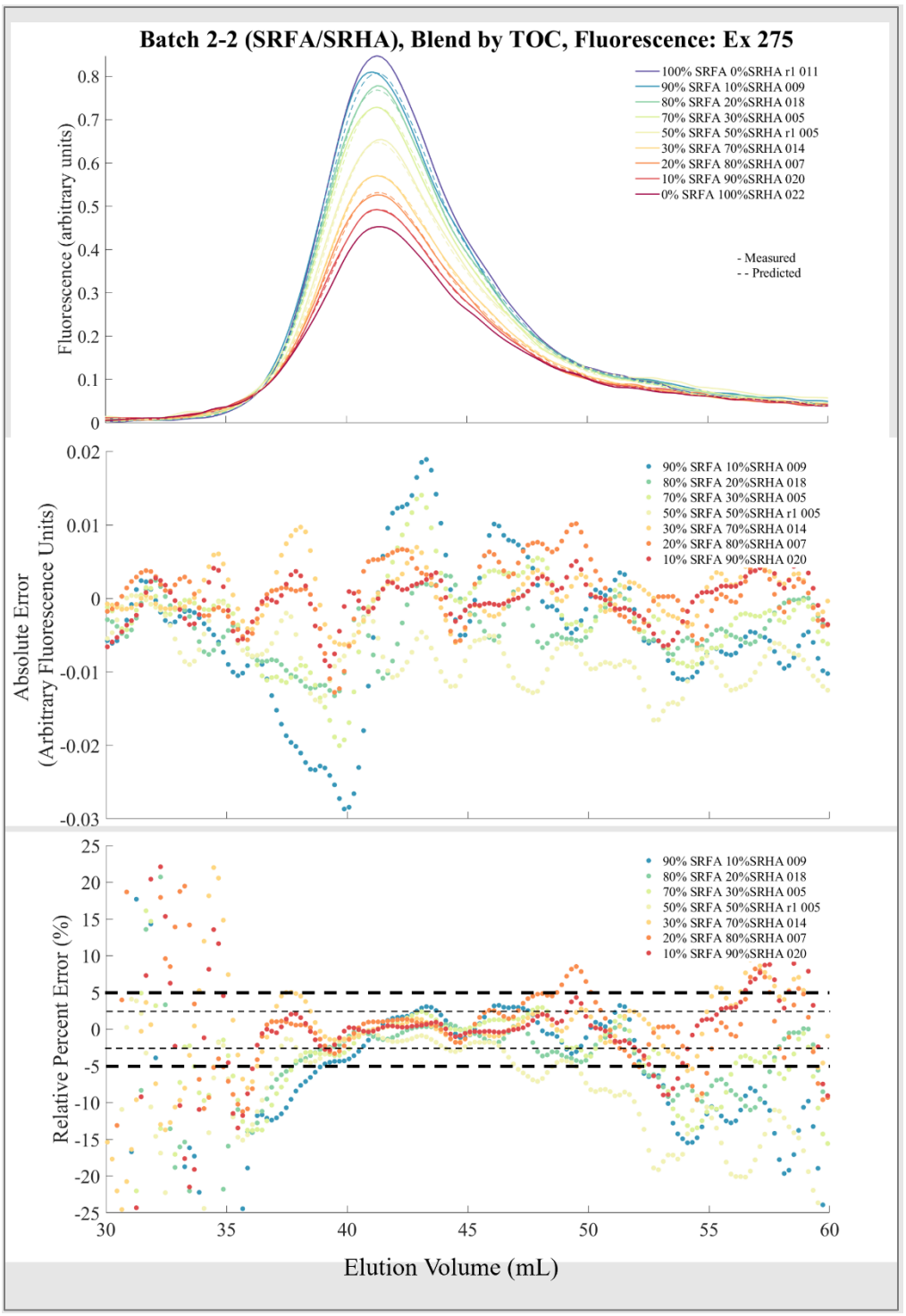

Figure 5.8. SRFA/SRHA Blend at Constant DOC: λ_{Fex} 275 nm Fluorescence Chromatograms and Error. **Top:** Fluorescence chromatograms at excitation 275 nm (Arbitrary Units). **Middle:** Absolute error of fluorescence chromatograms at excitation 275 nm (Arbitrary Units). **Bottom:** Relative percent error of fluorescence chromatograms at excitation 275 nm (%).

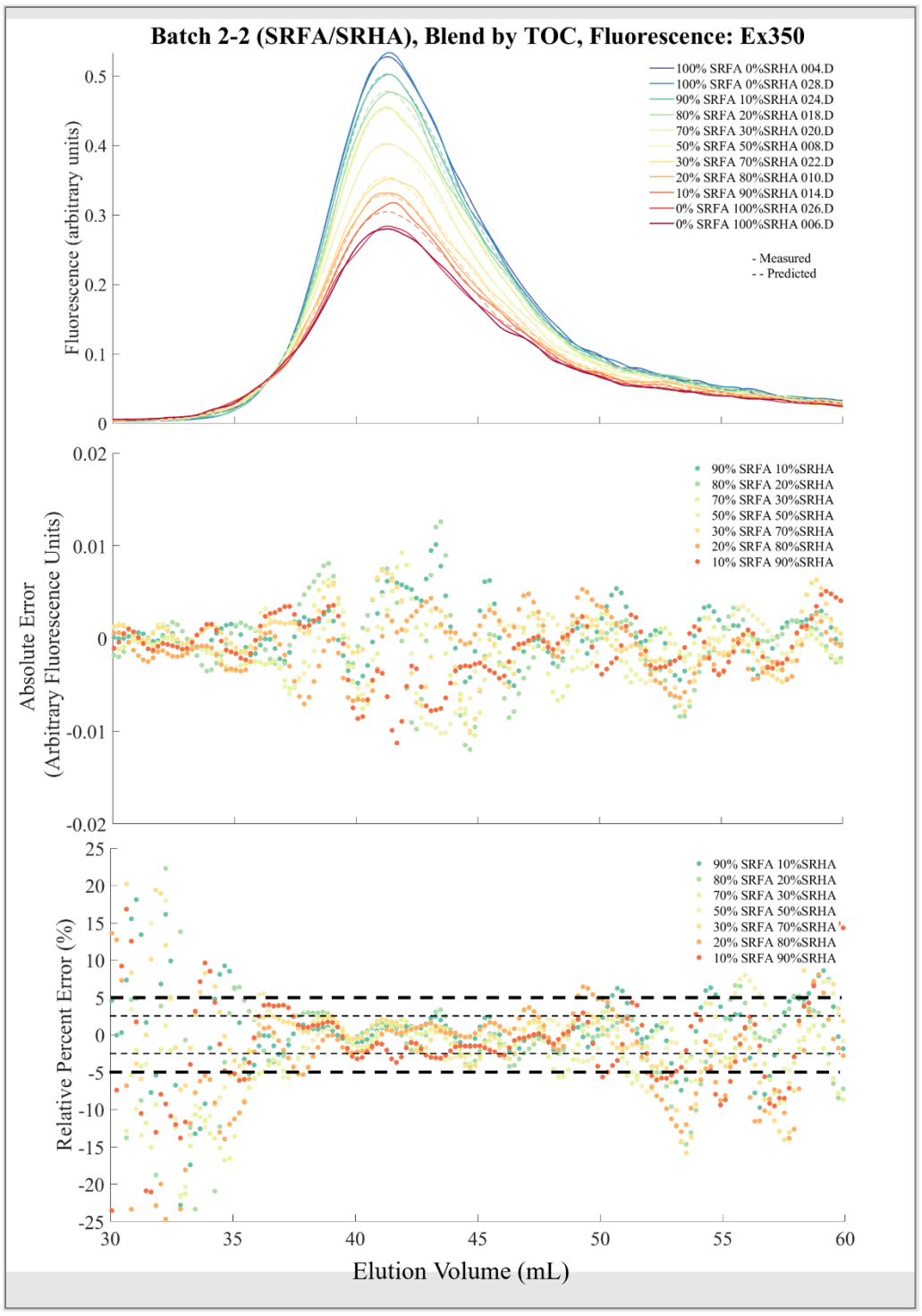

Figure 5.9. SRFA/SRHA Blend at Constant DOC: λ_{Fex} 350 nm Fluorescence Chromatograms and Error. **Top:** Fluorescence chromatograms at excitation 350 nm (Arbitrary Units). **Middle:** Absolute error of fluorescence chromatograms at excitation 350 nm (Arbitrary Units). **Bottom:** Relative percent error of fluorescence chromatograms at excitation 350 nm (%).

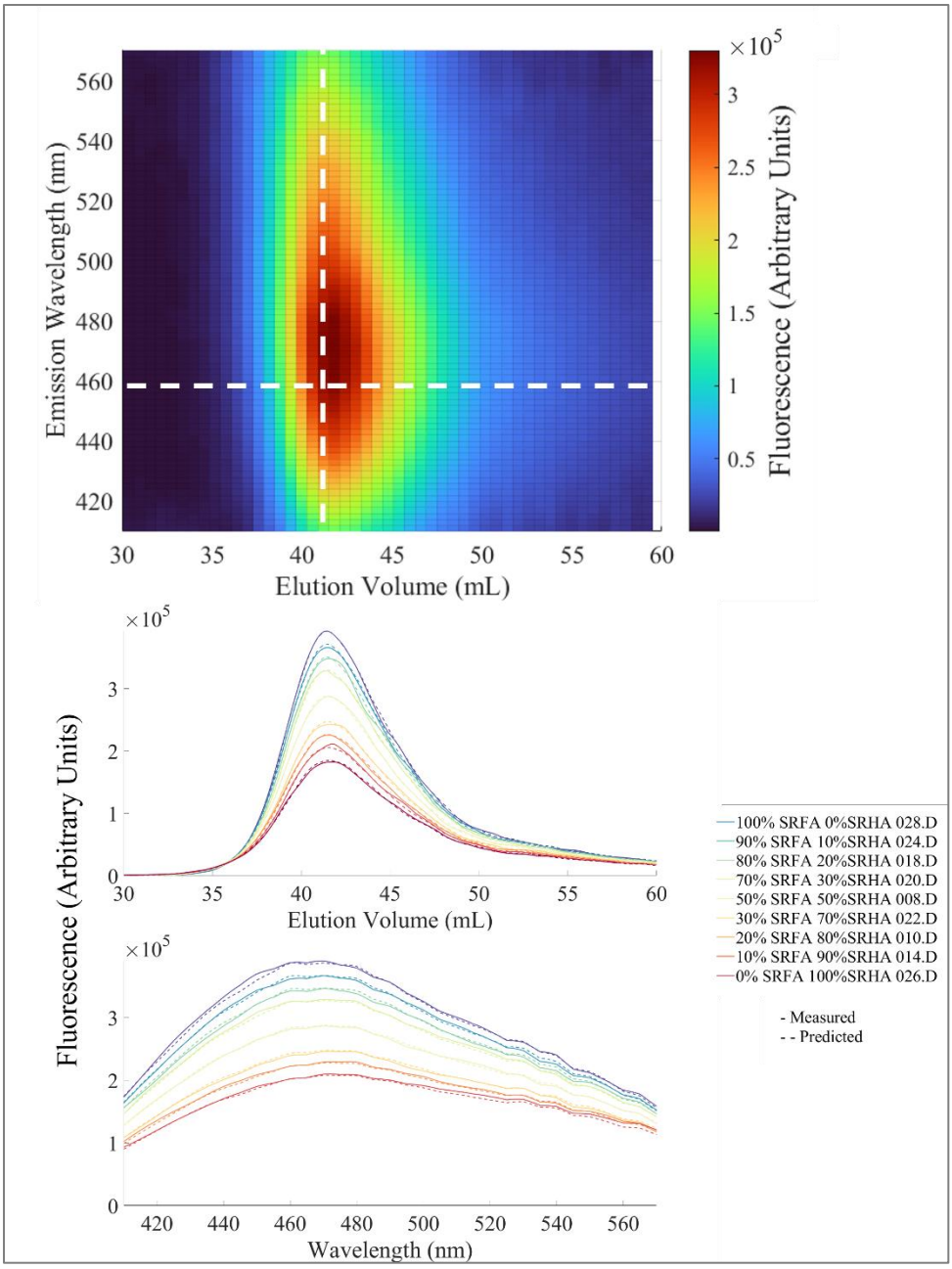

Figure 5.10. Extraction of Fluorescence Chromatograms and Emission Spectra from Three-Dimensional Data. **Top:** 70% SRFA 30% SRHA (blend at constant DOC, λ_{Fex} 350 nm) 3-dimensional SEC-fluorescence plot. Vertical and horizontal dashed white lines show the elution volume and wavelength where chromatograms and spectra were extracted from respectively. **Middle:** Fluorescence chromatograms at excitation 350 nm, emission 460 nm (Arbitrary Units) extracted from 3-dimensional data. **Bottom:** Absorbance spectra (220-500 nm) extracted from 3-dimensional data.

Fluorescence Quantum Yield.

Φ_F quantum yield chromatograms were calculated at λ_{Fex} 275 and 350 nm (i.e., Φ_{F275} and Φ_{F350}). Relative errors were within ±5% between elution volumes between 36-47 mL at λ_{Fex} 275 nm and 37-49 mL for λ_{Fex} 350 nm (Figures 5.11-5.12). Because the Φ_F calculation involves fluorescence and absorbance, error was propagated from both absorbance and fluorescence chromatograms. For example, systematic error was observed in the 47-52 mL range of the Φ_{F275} chromatograms which must result from the systematic error that occurred in the absorbance chromatograms for the same elution volume range. However, the impact of propagation was not dramatic as Φ_F error mostly fell within ±5% in the same regions as absorbance and fluoresce (i.e., the Φ_F chromatogram error did not increase significantly compared to the absorbance and fluorescence). Because the profile of Φ_F chromatograms were not traditional chromatographic peaks (where the signal increases from baseline to peak and returns to baseline), metrics were not calculated for this data.

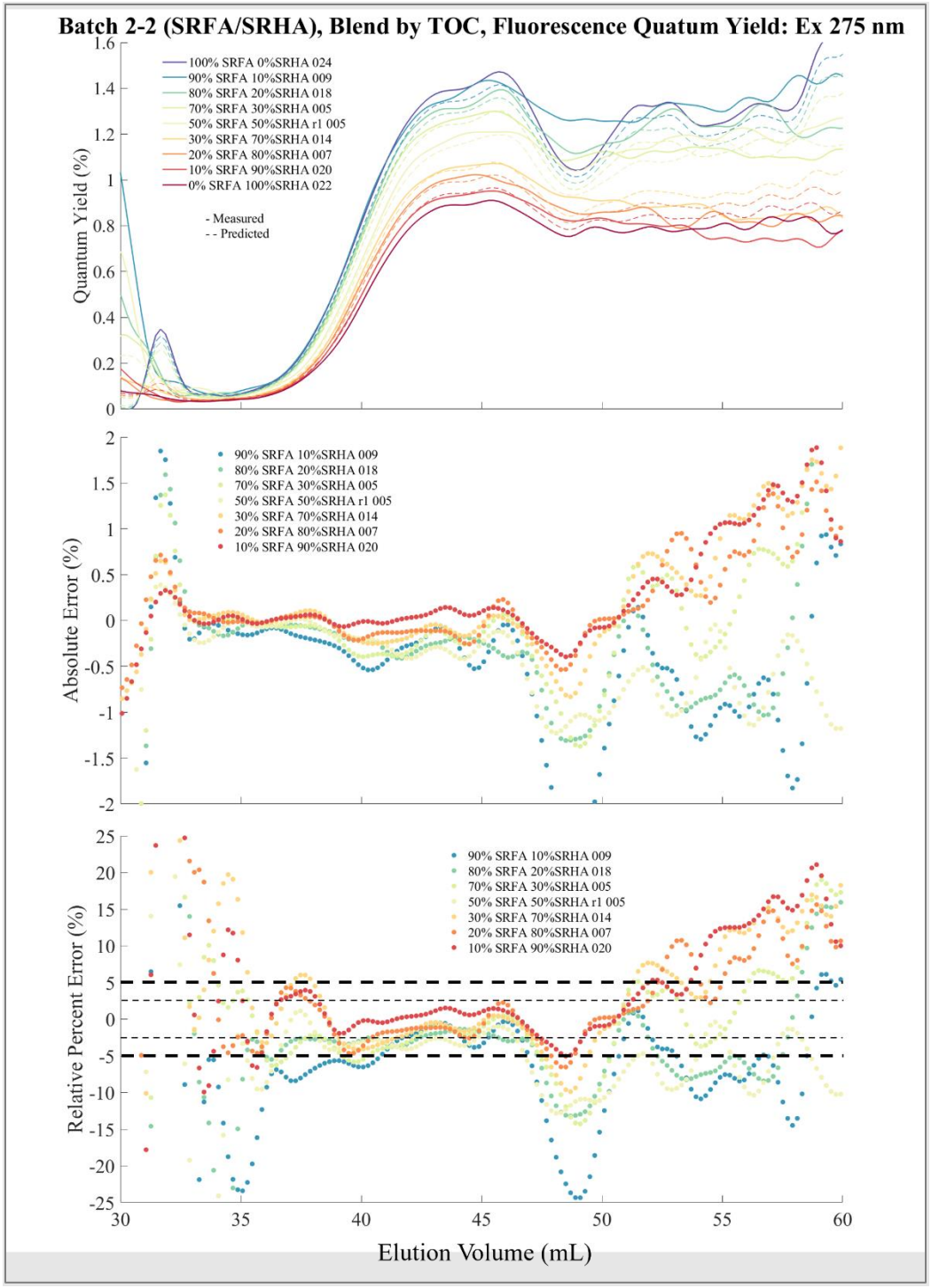

Figure 5.11. SRFA/SRHA Blend at Constant DOC: λ_{Fex} 275 nm Φ_F Chromatograms and Error. **Top (a):** Fluorescence quantum yield chromatograms at excitation 275 nm (%). **Middle (b):** Absolute error of fluorescence quantum yield chromatograms at excitation 275 nm (%). **Bottom (c):** Relative percent error of fluorescence quantum yield chromatograms at excitation 275 nm (%).

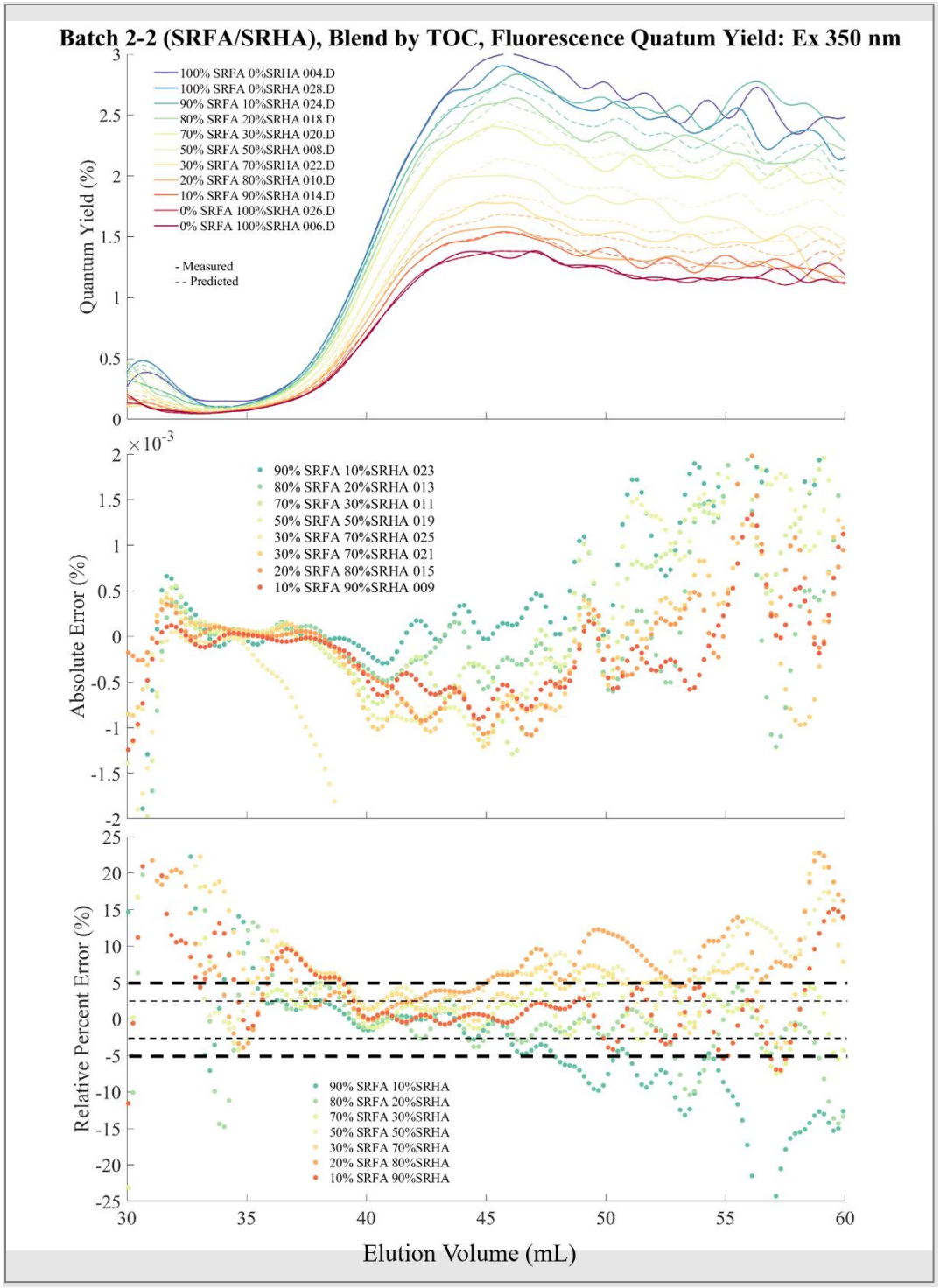

Figure 5.12. SRFA/SRHA Blend at Constant DOC: λ_{Fex} 350 nm Φ_F Chromatograms and Error. **Top:** Fluorescence quantum yield chromatograms at excitation 350 nm (%). **Middle:** Absolute error of fluorescence quantum yield chromatograms at excitation 350 nm (%). **Bottom:** relative percent error of fluorescence quantum yield chromatograms at excitation 350 nm (%).

5.3.3 Discussion

This section is intended to discuss additional comparisons between the detectors and what the implications of the data trends are with respect to the interpretation of conservative mixing. All four chromatographic signals (i.e., DOC, absorbance, fluorescence, and quantum yield) demonstrated good matching between measured and predicted data, with the highest accuracy (i.e., lowest relative error) near the DOC, absorbance, and fluorescence chromatographic peaks (Figures 5.4-5.6, 5.8-5.9, 5.11-5.12, and B.1-B.7). Because quantum yield is a combination of fluorescence and absorbance signals, this data was also most accurate near the absorbance and fluorescence chromatographic peaks. In comparing data from the three SEC detectors (i.e., DOC, absorbance, and fluorescence), DOC was the least accurate in terms of matching between measured and predicted data, demonstrated by the chromatographic error and error in metric values across all blend versions (i.e., constant DOC and constant UV_{300}). The reason for this is primarily related to the reduced or missing signal in the elution volume range 47-52 mL, where the largest deviations between measured and predicted values were found in the DOC is most sensitive. Relative errors are greatest in DOC chromatographic data and leads to greater error in the metrics compared to absorbance and fluorescence. Another consideration is the IC peak that appears in DOC chromatograms beginning at 57 mL but is not present in fluorescence or absorbance data. While SRFA and SRHA elute almost entirely before 57 mL, the IC peak could me more impactful to the interpretation of data for samples with small components that elute in this range. Finally, the DOC instrument is connected downstream from the main HPLC-SEC system components (i.e., pump, autosampler, column, SEC-DAD, and SEC-FLD discussed in Section 2.2). High pressure tubing is used to link the SEC-autosampler, SEC-column, SEC-DAD, and SEC-FLD, however, the DOC has custom internal tubing that cannot be changed. The Sievers M9 DOC analyzer is traditionally

used for offline bulk water analysis and a special configuration is utilized to connect to the SEC system. In this configuration, flow travels through the custom internal DOC instrument tubing segments, some of which have larger internal diameters compared to the high-pressure tubing used between the autosampler and FLD. The changes in internal diameter result in peak spreading and likely introduces variability as samples flow from the FLD to the DOC. Despite increased error compared to absorbance and fluorescence data, the measured DOC chromatographic and metric data follow the general trend of the predicted data and suggests that conservative mixing did occur with respect to the overall molecular size distribution.

For both absorbance and fluorescence accuracy was highest near the chromatographic peak (where lower relative errors were observed) while the precision was higher in the chromatographic tail regions (i.e., lower absolute error), accuracy was highest near the chromatographic peak. This is likely explained by the fact that when signal is low, the absolute variability (i.e., absolute error) is also expected to be low compared to the variability of a strong signal. However, for a weak signal, small deviations from expected values result can still result in high relative error (compared to a strong signal). Aside from chromatographic tails, the matching accuracy of absorbance and fluorescence suggests conservative mixing was generally observed for all blend versions.

One additional consideration regarding fluorescence data is the raw signal noise. The signal to noise ratio is higher for the raw signal of fluorescence compared to absorbance and DOC, meaning that the impact of the smoothing function is relatively greater for fluorescence data. A comparison of the raw and smoothed fluorescence signals is shown in Figure 5.1. The impact of the signal noise in the raw data is an important consideration in terms of reliably differentiating between incremental blends, especially for cases in which the end member signals are highly similar. In a hypothetical scenario, as end member fluorescence signals approach each other, the

signal noise from adjacent incremental blends will eventually overlap. When overlap is observed in the raw signals, the ability of this detector to reliably differentiate between blend samples must be questioned (even if overlap does not occur between smoothed signals). Therefore, the following should be considered when using this method to differentiate between DOM sources: (1) raw data should always be inspected as signal overlap may not be apparent in smoothed data; (2) the fluorescence detector may require greater relative differences between end member signals (compared to DOC and absorbance) to avoid signal overlap.

Finally, like the DOC, absorbance, and fluorescence signals, the matching accuracy of Φ_F data also suggests that conservative mixing was observed. However, unlike DOC, absorbance, and fluorescence, Φ_F is an internal property, meaning it is independent of concentration (Boyle et al., 2009; Cawley et al., 2015; Del Vecchio and Blough, 2004; Ulliman et al., 2020b; Wünsch et al., 2015). Therefore, when measured at the same fluorescence excitation wavelength, the end member Φ_F values are same for both blend versions (see the top subplot in Figures 5.11 and B.6, and the top subplot of Figures 5.12 and B.7). This property may be especially useful for blending scenarios in which concentration cannot be controlled (see discussion regarding source differentiation applications below). It should also be noted that Φ_F also relies on the performance of two detectors. As discussed in Section 5.3, Φ_F error results from the propagation of error from absorbance and fluorescence data. Therefore, in using this method, Φ_F data should never be considered on its own without considering the accuracy and error of both the absorbance and fluorescence data first.

Finally, one complication of assessing the matching accuracy of predicted and measured blend data and the ability to reliably differentiate between intermittent blends is that the difference in signal intensity between different blend ratios is not constant. For example, Figure 5.1, shows the convergence of chromatograms for all samples converge at early elution volumes, representing

low apparent molecular sizes and at all elution volumes greater than the peak maximums. A convergence at one or both chromatographic tails (i.e., the earliest and latest elution volumes of the chromatogram) was observed for most signals in all blends.

Deviations from Conservative Mixing

While conservative mixing was generally observed for all signals (DOC, absorbance, fluorescence and Φ_F), deviations from this behavior were observed in the 47-52 mL elution volume range in the DOC and absorbance chromatograms. As discussed in Section 5.3, these deviations result from the fact that DOC and absorbance chromatograms show a rider peak eluting between 47-52 mL for the SRFA and SRHA end member samples which was absent from the measured chromatograms of intermittent blends. Figure 5.13 shows a combination of DOC, absorbance and fluorescence data and highlights the observations of each detector between 47-52 mL. The top subplot shows the DOC chromatograms from the blend by DOC where differences between measured and predicted data can clearly be seen between 47-52 mL. Subplots in the left column of the second and third rows show an example of the measured three-dimensional absorbance and fluorescence data respectively (these subplots also appear in Figures 5.7 and 5.10). Subplots in the right column of the second and third rows are three-dimensional subtraction plots that show the relative percent error of the measured data (for absorbance and fluorescence respectively) in the subplots on the left. These error subtraction plots were generated by subtracting the measured three-dimensional data from predicted three-dimensional data and dividing by the measured three-dimensional data. The subplots in the right column can be used to assess for regions of error in absorbance and fluorescence data with respect to molecular size, absorbance spectra and fluorescence emission spectra. Together, Figure 5.13 demonstrates that the deviation from expected behavior was observed by the DOC and absorbance detectors but not the fluorescence

detector (in agreement with the data shown in Figures 5.4-5.6 and 5.8-5.9). It is also important to note that with respect to the absorbance detector, deviation was observed across the wavelength range of 220-300 nm and relative percent errors increased with decreasing wavelength. These findings suggest that the DOM fraction observed to elute in the end member samples but not the intermittent blends can be characterized as relatively low molecular size compounds that weakly absorb between 220-300 nm (suggesting they have low levels of aromaticity), and the absence of fluorescent components. Note that the absorbance truly extends to 200 nm, but wavelengths between 200 and 220 nm are not shown in Figure 5.13.

To better understand why the differences in predicted and measured data occurred, the characteristics of the DOM compounds that typically elute in this range (47-52 mL) need to be understood. A previous study observed a similar rider peak for DOM sources and characterized it as being composed of low molecular weight acids (Huber et al., 2011b). It is also known that many DOM samples contain some fraction of small, highly hydrophobic compounds that are retained by SEC-columns as they experience hydrophobic interactions with the column packing material (Her et al., 2002b; Huber et al., 2011b). Other research has demonstrated that simple aromatic ring structures with hydroxy and methoxy groups may also be retained as these molecules are more comfortable when associated with the column packing material than they are in a polar, aqueous environment such as the SEC mobile phase (Amy et al., 1987; R. S. Swift and Posner, 1971). Based on size alone, small, highly hydrophobic compounds as well as simple aromatic ring structures could be expected to elute in the 47-52 mL elution volume range. Therefore, some retention of compounds that should elute in this range may also be expected. What is not clear is why only the SRFA and SRHA end member samples show the elution of a peak in this range and

not the intermittent blends. This trend was repeatable and was observed for both blend versions in the DOC and absorbance and chromatographic data.

In summary, the SEC results suggest that conservative mixing did occur with respect to optical properties and molecular size distribution for nearly all DOM fractions. The notable exception was a portion of the material eluting between 47-52 mL. Aside from this deviation, trends in error were generally a function of signal strength (where relative error increased with decreasing signal strength), and there were no observed systematic trends with respect to the percent of each end member in blend sample which suggests that the observed error was not due to interaction. As such, the findings of this study are in support of the superposition model (see Section 5.1) with respect to the blending of DOM sources. However, it is important to also note that these results do not inform whether interactions occur within a given DOM source. It is therefore possible that interactions impact the characteristic optical properties observed for DOM sources.

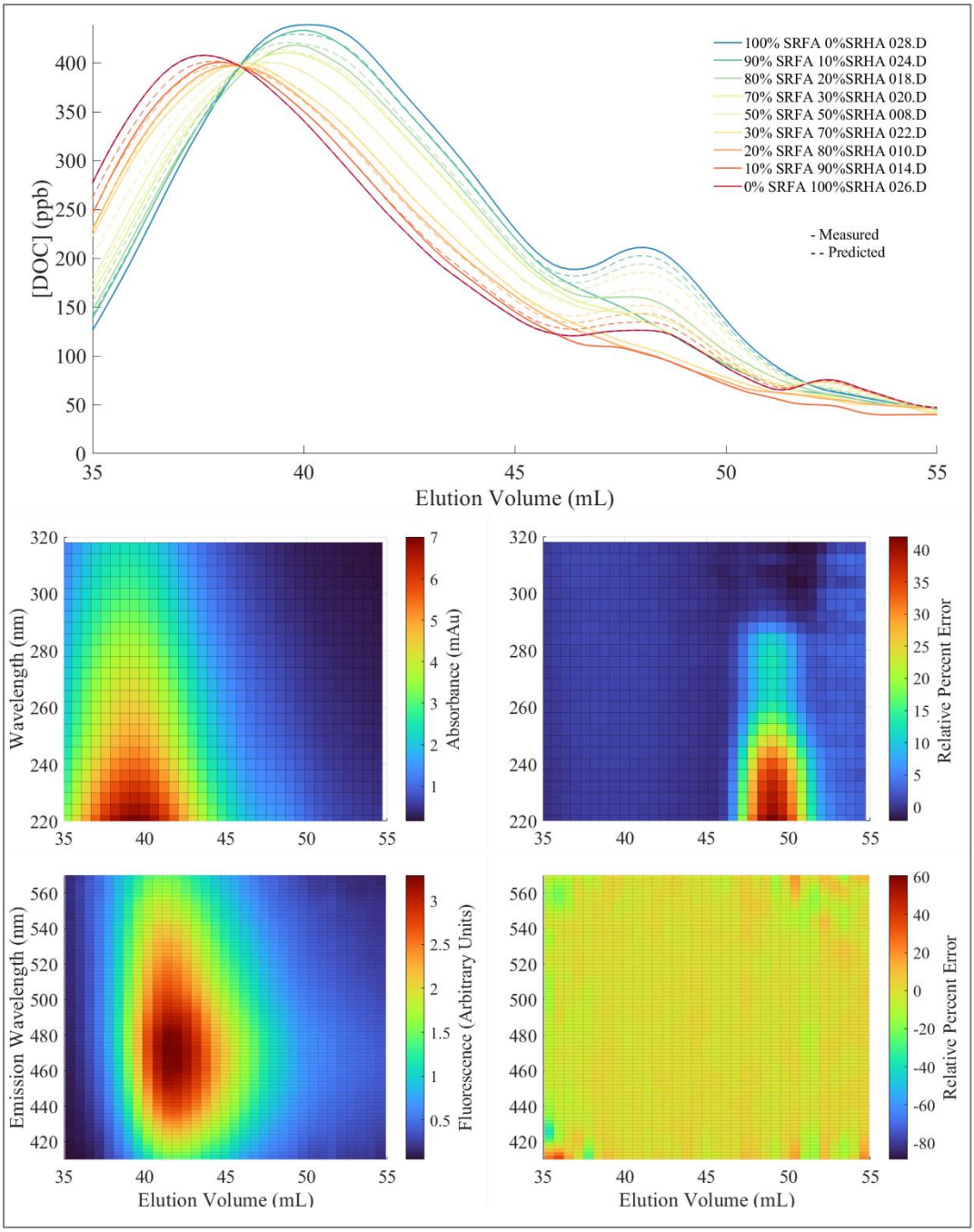

Figure 5.13. SRFA/SRHA Blend at Constant DOC: Comparison of DOC Chromatograms to 3-Dimensional SEC-Absorbance and SEC-Fluorescence. **Top:** DOC chromatograms from the SRFA/SRHA, blend at constant DOC. **Middle (Left to Right):** 70% SRFA 30% SRHA 3-dimensional SEC-absorbance; **(c)** 70% SRFA 30% SRHA 3-dimensional SEC-absorbance relative percent error. **Bottom (Left to Right):** 70% SRFA 30% SRHA 3-dimensional SEC-fluorescence (Ex: 350 nm); 70% SRFA 30% SRHA 3-dimensional SEC-fluorescence (Ex: 350 nm) relative percent error.

Source Differentiation Applications

While the conservative mixing behavior observed in this study provides insight to fundamental questions regarding the chemical behavior of DOM with respect to size distribution and optical properties, it also provides support for the use of these properties and DOM source differentiation in real-world water quality applications. Several scenarios exist in which differentiating between multiple water sources are important for the protection of human health. For example, the source waters for many drinking water treatment systems are impacted treated wastewater effluent discharged upstream (i.e., de-facto reuse). The percentages of wastewater effluent in these water sources are known to vary spatially and temporally and can be hard to predict. The results of this study suggest that optical properties and molecular size distribution can be used to differentiate sources of DOM based on compositional differences. However, important considerations must be made before these properties can effectively be utilized.

While conservative mixing was generally observed by all metrics used for analysis, the magnitude of signal shifts between incremental blends were specific to given blend versions and wavelength and DOM. For example, in the blend at constant DOC, absorbance decreased with increasing SRFA percentage at all elution volumes, and the incremental shifts were smaller at 275 nm (i.e., the SRFA and SRHA end member signals were more similar to each other at this wavelength) compared to 350 nm, while the opposite trend was found in the blend at constant UV_{300} (i.e., absorbance increased with increasing SRFA percentage and the incremental shifts). In this example, the gradient of incremental shifts are dictated by end member absorbance spectra and SUVA values which highlights the need to develop detailed end member characterizations (with respect to molecular size and optical properties) to inform which metrics will be most effective.

In a previous study which systematically evaluated optical based metrics for their ability to reliably differentiate between surface water and wastewater (Ulliman et al., 2020b), the authors found Φ_F at λ_{Fex} 350 nm to be the only metric capable of reliably differentiating between the sources. (Boyle et al., 2009; Cawley et al., 2015; Del Vecchio and Blough, 2004; Ulliman et al., 2020b; Wünsch et al., 2015). In the current study, results showed that the range in Φ_F values between end members was larger at λ_{Fex} 350 nm compared to λ_{Fex} 275 nm, suggesting λ_{Fex} 350 nm may be better for reliably differentiating between incremental blend ratios. However, at 275 nm (and λ_{Fex} 275 nm with respect to fluorescence) the magnitude of absorbance and fluorescence signals were stronger compared to 350 nm. This may suggest that in a scenario where concentration (and thus magnitude of absorbance and fluorescence signals) cannot be controlled, Φ_F at λ_{Fex} 275 nm could be advantageous if end member sources have weak absorbance and fluorescence signals. From this perspective, Φ_F at λ_{Fex} 275 and 350 nm both have potential advantages and disadvantages, reinforcing the importance of end member characterization.

5.4 Conclusion

In summary, the results of this study provide a fundamental demonstration of the conservative mixing behavior with respect to DOM optical properties and molecular size following the blending of DOM sources. This conclusion is supported by data from each SEC detector (i.e., DOC, absorbance, and fluorescence) and the calculated quantum yield trace. These findings suggest that interactions are not occurring following the mixing of DOM sources and that signals of blended samples can be reliably predicted from the signals of individual source. One exception to the observed conservative mixing was found in the elution volume range between 47-52 mL, where the [DOC] and absorbance chromatograms observed that a shoulder peak present in both SRFA and SRHA end members did not occur in the intermittent blends. The reasons for this are

currently not clear and future research should investigate this further. Aside from the 47-52 mL ranges, matching accuracy was generally found to be the highest near the chromatographic peaks where the relative error in measured data remained within ±5% of the predicted data for all detectors. Absorbance, fluorescence, and Φ_F, were found to have better accuracy than DOC. However, other factors such as the fluorescence signal noise should be considered when evaluating matching accuracy. In general, differences in matching error between detectors was relatively minor and all support the observation of conservative mixing. Finally, the results of this research provide fundamental support for the use of molecular size and optical properties in DOM source differentiation and future research should attempt to advance such applications toward real-world scenarios.

Chapter 6

Advancements in the Understanding of Protein-like Fluorescence in Paired Surface Water-Wastewater Samples

6.1 Introduction

Dissolved organic matter (DOM) is ubiquitous in all waters and plays important roles in natural and engineered systems. In surface and groundwaters, DOM impacts to the fate and transport of metals and organic contaminants and in engineered systems, control of DOM is critical to preventing the formation of harmful disinfection byproducts, namely trihalomethanes and haloacetic acids (Christman et al., 1983; Edzwald et al., 1985; P. C. Singer, 1999). The ubiquity and concentration at which DOM is typically found (in natural and treated waters) has resulted in the investigation of DOM as a surrogate for other water constituents present in low conditions and not easily measured (Dickenson et al., 2009; Edzwald et al., 1985; Gerrity et al., 2012; Pepper and Snyder, 2016). While DOM is complex, its specific chemical composition is linked to its the sources from which it is derived (Coble, 2007, 1996b; McKnight et al., 2001b). For example, microbially derived aquatic DOM is created in the water source in which it is found (i.e., autochthonous) while plant derived DOM is generally transported from the location it is produce to the water source in which it is found (i.e., allochthonous)(P. G. Coble et al., 2014; Findlay and Sinsabaugh, 2003). Additionally, organic matter derived from wastewater effluent (i.e., effluent organic matter, EfOM) contains both natural organic matter (NOM) and compounds from

anthropogenic contributions (Ulliman et al., 2020b), both of which are transformed by wastewater treatment processes which includes microbial activity (Dickenson et al., 2011; Singer et al., 2016).

The analysis of the optical properties of DOM (i.e., absorbance and fluorescence) continues to be widely used when studying DOM due to their high sensitivity and relative simplicity when compared to other analytical techniques such as high-resolution mass spectrometry or nuclear magnetic resonance (NMR). Several relationships have been developed between relating optical metrics to DOM composition. In particular, commonly occurring DOM fluorescence peaks have been linked to DOM source material. For example, fluorescence Peaks A and C are thought to be related to humic-like substances of allochthonous DOM where Peaks B and T are thought to be related to protein like material of microbially derived DOM.

The link between fluorescence Peaks B and T and microbially derived DOM primarily results from the spectral similarity between Peaks B and T and amino acids tyrosine and tryptophan respectively. Peak B and tyrosine have fluorescence excitation/emission (Ex/Em) maxima 275/305 nm and Peak T and tryptophan have and Ex/Em maxima of 275/340 nm (Coble, 1996b; Maie et al., 2007; Yamashita and Tanoue, 2003). Because of the similarity between Peaks B and T, and tyrosine and tryptophan and because amino acids are the subcomponents of protein molecules the term “protein-like” fluorescence has been adapted to generally represent Peaks B and T (Coble, 1996b). In addition to the spectral similarity, previous studies have in fact correlated the Peak B and T signals with the presence of amino acids. For example, Yamashito and Tanoue found that Peaks B and T correlated with hydrolysable amino acid content (Yamashita and Tanoue, 2003).

While Peaks B and T have been correlated to microbially derived DOM, the relationship is not always straightforward. For example, it is known that other fluorophores found in DOM,

such as polyphenols, can also fluoresce in the same regions as peaks B and T (P. G. Coble et al., 2014). As such, it should be understood that "protein-like" fluorescence refers only to a region of Ex/Em wavelengths and should not imply that the composition includes amino acids or proteins. Additionally spectral overlap that exists between Peaks B and T and A, and it is known that Peak A fluorescence can quench "protein-like" fluorescence, especially that of Peak B (P. G. Coble et al., 2014; Maie et al., 2007; Wang et al., 2015). Finally, another study found that DOM leached from grass, leaves, and needles initially contained mostly Peaks B and T fluorescence, but that after exposure to microbial cultures, Peak B and T decreased while Peaks A and C increased (D'Andrilli et al., 2019).

A better fundamental understanding of Peaks B and T is especially important with regards to the characterization of EfOM fluorescence, as it relates to many applications including sensor technology for water reuse applications. In many treatment systems, treated wastewater is discharged into surface waters which then serve as the source for downstream drinking water treatment facilities (R. K. Henderson et al., 2009b; Ulliman et al., 2020b). EfOM fluorescence is a potentially useful surrogate for the contributions of wastewater effluent to surface water (see Uliman et al., 2020 for a recent analysis of the potential use of optical metrics to assess EfOM in reuse systems). However, a key component of this is the relationship between microbial activity and "protein-like" fluorescence and that knowledge gaps still exist in this regard.

In this study we aim to further the understanding of organic matter fluorescence Peaks B and T fluorescence by analyzing the DOM in a paired surface water and wastewater effluent, using bulk water spectroscopy and an SEC system with coupled with absorbance and fluorescence detectors. Individual fractions representing large and medium-to small sized fractions were collected from the SEC system and analyzed with an offline fluorescence to investigate the

potential impacts of quenching and peak overlap to Peak B and T fluorescence. A biofiltration system was then used to isolate and characterize microbially derived DOM. These results provide further necessary information for the development of optical sensors for tracing DOM in biogeochemical settings.

6.2 Materials and Methods

6.2.1 Samples

Surface Water and Wastewaters

A surface water sample was collected from Boulder Creek (BCSW) at 40.052^{o}, -105.178627^{o} in a clean 250 mL glass bottle. Wastewater was provided by the Boulder Wastewater Treatment (Boulder, CO) facility prior to UV disinfection, initially collected in a 55-gallon drum from which an aliquot was transferred to a 1 L amber glass bottle. This location of Boulder Creek is between the point where Boulder Creek water is drawn into the wastewater facility and where wastewater effluent is discharged back to the surface water meaning and was chosen to be representative of the NOM present in the wastewater effluent samples. Wastewater sample "BWW1" was collected in February 2023. After collection, samples were transported to the laboratory where they were immediately filtered through pre-combusted GF/F filters into amber glass bottles and refrigerated in the dark until analysis.

All samples were spiked with a concentrated SEC mobile phase (0.016M Na_2HPO_4, 0.024M NaH_2PO_4, and 0.031M Na_2SO_4) to match the 0.1M ionic strength of the mobile phase (checked with a conductivity probe to ensure match).

SEC Fraction Collection. Specific size fractions of BCSW and BWW1 were collected into separate 40 mL glass amber bottles following separation by the SEC system at the

fluorescence detector effluent (see Section 2.2. for SEC system description). Subsequent runs were used to collect the fractions individually, as well as a total-run sample (referred to as FT), collected from the starting elution volume of Fraction 1 (F1) to the ending elution volume of Fraction 2 (F2), for BCSW and BWW1. Additionally, aliquots of F1 and F2 representing the fractional contribution (based on elution volume) to the total-run sample, were re-combined post collection, (referred to as Fraction Combined or FC, see Section 3.1 for further discussion). All of the samples collected from the SEC system were then analyzed with offline bulk water optical spectroscopy instrumentation to generate absorbance spectra and fluorescence excitation emission spectra (EEMs).

The reasons for collecting F1, F2, FT, and FC are as follows: i) Previous studies have found that Peak B fluorescence is found in all SEC fractions (whereas Peaks A and C are only found in the medium-to-small fractions) (Maie et al., 2007). However, significant spectral overlap exists between Peak B and Peak A (P. G. Coble et al., 2014) and it is difficult to discern between these fluorescence peaks using SEC data alone. If chromatograms only observe a single excitation and emission wavelength. Three-dimensional SEC-FLD data shows that the tail of Peak A fluorescence extends into the Peak B region even for samples in which no Peak B and T fluorescence are present. Note that this statement is not to suggest Peak B and T fluorescence is not occurring in F2, only that the data can be better resolved if the fractions are collected and analyzed separately with benchtop fluorometer. ii.) Previous studies have also suggested that Peak B and T fluorescence is quenched by Peaks A and C fluorescence, suggesting these fluorophore groups are interacting. Analyzing collected fractions with a benchtop fluorometer will help to understand the accuracy of the interpretations made by the SEC-FLD data, and to better understand the impact of quenching. To further analyze the impacts of quenching, the EEMs of F1 and F2 can be mathematically

superimposed (FS) and compared to FT and FC by EEM subtraction and calculation of relative percent error. Theoretically, if no quenching occurs, these EEMs will be identical to one another.

Biofiltration

The biofiltration experiment was performed using glass column packed with sand media. A 55-gal drum of wastewater effluent was collected from the Boulder Wastewater Treatment Facility and transported to the University of Colorado, Environmental Engineering Department on May 23rd, 2023 where it was filtered using a 0.45 μm polyethersulfone (PES) membrane filter back into a 55-gal drum and then refrigerated in the dark at until analysis. Please note the wastewater collected for the biofiltration experiment was a separate batch from that used in the fractionation experiments discussed previously. Prior to loading onto the column, influent wastewater was prepared as follows: 3 L aliquots were collected in amber colored glass bottles and pre-chlorinated to 8.1 milligrams chlorine per liter (mg_{Cl}/L). Pre-chlorinated aliquots were then allowed to sit in amber colored glass bottles until the chlorine residual decreased to <0.05 mg_{Cl}/L. Remaining chlorine residual was then diluted by mixing pre-chlorinated aliquots with an equal volume of raw wastewater effluent (i.e., aliquots that were not pre-chlorinated). Following dilution, the mixed volumes (i.e., perchlorinated aliquot mixed with raw effluent aliquots) were loaded into a clear 10 L glass carboy that served as the influent reservoir to the sand column. This influent wastewater preparation was repeated daily for the duration of the experiment. Wastewater was loaded onto the sand filtration column from at an HLR of 4 mL/min, using a peristaltic pump continuously for 18 days to allow for the growth of a biofilm on the sand media. Samples were collected from both the influent and effluent of the filtration column on days 1, 8 and 18 into 500 mL amber bottles. Influent samples were collected for each day of sampling to monitor for changes to the EfOM stock (i.e., wastewater effluent that was pre-filtered and stored). Influent and effluent samples can

then be compared for each day to monitor for changes to the EfOM characterization that occur across the filtration process. To remove any particulate that had eluted from the column, 100 mL aliquots of each sample were re-filtered using pre-rinsed 0.45 μm GF/F filters into 100 mL amber colored glass bottles. Samples were stored, refrigerated in the dark until analysis. All samples were analyzed with the SEC-system and system conditions described in Section 6.2.2.

The purpose of the biofiltration experiment is to isolate and characterize microbially derived DOM. Previous studies have been used to generate biofilm life cycle models (Sauer et al., 2022). In the early stages of a biofilm life cycle planktonic cells attach to a media surface (i.e., reversible and irreversible attachment), where they mature into cell clusters and then cell colonies (i.e., maturation I and II respectively) (Petrova and Sauer, 2009; Sauer et al., 2022, 2002). During the attachment and maturation stages changes to the EfOM characterization are not expected to be observed as new, microbially derived DOM is not being released from the biofilm.

Once a mature biofilm has formed, cells and biofilm matrix detach from the biofilm in a process known as dispersion. Dispersion can occur either actively, where the microbes produce extracellular enzymes that degrade either the biofilm matrix or biofilm substrate (Kaplan, 2010; Lappin-Scott and Bass, 2001; Stoodley et al., 2001), or passively where portions of biofilm are detached by hydrodynamic shear (Sauer et al., 2022). In relation to the current study, material released from the biofilm during the detachment phase will include microbially derived DOM. The microbially derived DOM can then be characterized by comparing the effluent sample to the influent sample (where detached biofilm material and microbial cells were not present). Please note that intact cells and particulate matter was removed by filtering following sample collection and data is therefore representative of the microbially derived DOM remaining in the sample. Typically, biofiltration is utilized to remove organic matter and contaminants from a source water.

To achieve removal, columns are regularly backflushed to remove material that has detached from the biofilm. However, because the purpose of this experiment was to isolate microbially derived DOM, the column was intentionally not backflushed before sample collection.

6.2.2 Instrumentation

Size Exclusion Chromatography

The SEC system was an Agilent 1260 high performance liquid chromatography (HPLC) setup that included an Agilent 1200 Series Vacuum Degasser, Agilent 1200 Series G1310A Isocratic Pump, Agilent 1260 Infinity Series G1315D Diode Array Detector (DAD), Agilent 1260 Series Infinity II Fluorescence Detectors (FLD) and a Sievers M9 DOC Analyzer. Absorbance and fluorescence signals were recorded directly by the Agilent OpenLab software (Rev. C01.09). The DAD detector collected absorbance spectra from 200-700 nm in 2 nm increments. The fluorescence detector analyzed samples at an excitation wavelength of 280 nm and collected emission spectra in the wavelength range of 280-600nm in 1 nm increments. The FLD bandpass is fixed at 20 nm and cannot be adjusted. An Agilent Universal Interface Box II was utilized to transfer data from the DOC analyzer to the Agilent software in voltage units, which were later converted to [DOC] ($mg_C\ L^{-1}$) (see SI, Text S-1.2.3) for a detailed description of conversion). Size-based separations were achieved using a Toyopearl HW-50S column (internal diameter (ID) 20 mm x 25 cm, 92 mL total volume). Samples were injected via an Agilent Technologies 1260 Series G7129A Autosampler configured with a 900 µL analytical head and multidraw injection kit to allow for injection volumes of up to 1.8 mL. All sample analyses were conducted for 150 min to ensure the elution of all matter from the SEC column, allowing all detectors to return to baseline prior to the next injection. One blank run consisting of mobile phase was injected between each sample analysis.

Bulk Water Spectroscopy

Bulk water DOM absorbance spectra were measured on a Hach DR 6000 (Hach Company, CO, USA) spectrophotometer using 1 cm quartz cuvettes for a wavelength range of 200-800 nm. Lamp output was verified on a Holmium reference cell. All sample spectra were blank corrected with conductivity and pH-adjusted deionized water that matched the adjustment necessary to the individual samples. UV-Visible absorbance spectra were collected to calculate absorbance metrics of carbon normalized specific UV absorbance at 254 and 280 nm ($SUVA_{254}$ and $SUVA_{280}$) and slope ratio (Table A.2).

EEMs were collected using a Horiba Jobin Yvon Fluoromax-4 (Horiba, Japan). EEMs were produced over an excitation wavelength range of 240–450 nm over 10 nm increments and an emission range of 300–600 nm over 2 nm increments in a 1-cm quartz cuvettes. Fluorescence spectra were collected with an excitation and emission bandpass set to 5 nm and integration time of 0.25 in signal/reference ratio mode.

Data Correction

Inner-filter effects were corrected using the corresponding absorbance spectra (Lakowicz, 2006). EEMs were normalized by the Raman peak area of deionized water (resistivity ≥18.2MΩ-cm), collected at an excitation wavelength of 350 nm during the time of EEM collection (Lawaetz and Stedmon, 2009). Corrected EEMs are presented in normalized Raman Units (RU). Lastly, EEMs were also blank corrected with deionized water adjusted to the conductivity and pH of the SEC mobile phase (6.8 mS/cm and pH = 6.8). First and second order Rayleigh-scattering were corrected for by blank subtraction followed by interpolation across the excised EEM area. All EEM corrections were performed using MATLAB.

SEC-fluorescence data was corrected following the methods of Hanson and coworkers (Hanson et al., 2022). SEC and bulk water data were both corrected and processed using MATLAB.

6.3 Results and Discussion

6.3.1 Surface Water and Wastewater Characterization

For both waters, F1 is unique in that Peak B and T is the only type of fluorescence present and Peak A fluorescence was only observed in F2. The F2 EEM clearly shows that Peak B and T fluorescence is present in that fraction as well and is also supported by SEC data (Figure 6.3, left column, second row). In the SEC chromatograms (Figures 6.1-6.2), F1 Peak B fluorescence appears as a sharp, narrow peak eluting between 20 and 30 mL in both the surface water and wastewater. However, based on previous studies this peak contains material that only travels through the column void space (Her et al., 2002b; Huber et al., 2011b). The compounds within this peak are not further separated based on size and it is not possible to possible to observe the true chromatographic shape of this material. F2 Peak B and T fluorescence elutes as a low intensity, broad peak from 37-52 mL in BCSW and 37-68 mL in the wastewater. Because F2 molecules do enter column pore space, the chromatographic shape is observed. These observations agree with SEC fluorescence data from previous studies (Maie et al., 2007).

While the focus of this research is primarily on the behavior of Peak B and T fluorescence, there is spectral overlap with Peak A, and previous studies have found Peak B and T quenching by Peak A, thus characterization of Peak A in these samples is related. As mentioned previously, Peak A was observed only in F2 where it co-occurs with Peak B and T. However, there are significant differences in the F2, Peak A, chromatographic profiles between the two waters. The

BWW1 F2 Peak A is broad and with noticeable minor peaks at 50 mL and 65 mL. The profile in BCSW is slightly shifted to higher molecular sizes compared to BWW1 and occurs as a relatively sharper peak occurring at 38-53 mL with a second minor peak occurring at 55-65 mL.

Comparing the contributions of the fluorescence peaks (i.e., comparing the contributions of Peak A and the contributions of Peaks B and T) in each water to each other also highlights the differences between the waters. In BWW1, the magnitude of Peak B fluorescence in F1 is ~3 times that of BCSW. Interestingly, in F2 the intensities of Peak A components are relatively similar between the two waters, though BWW1 contains additional lower molecular size components that do not appear in BCSW. This is especially highlighted in the 3-D SEC plots (Figure 6.2).

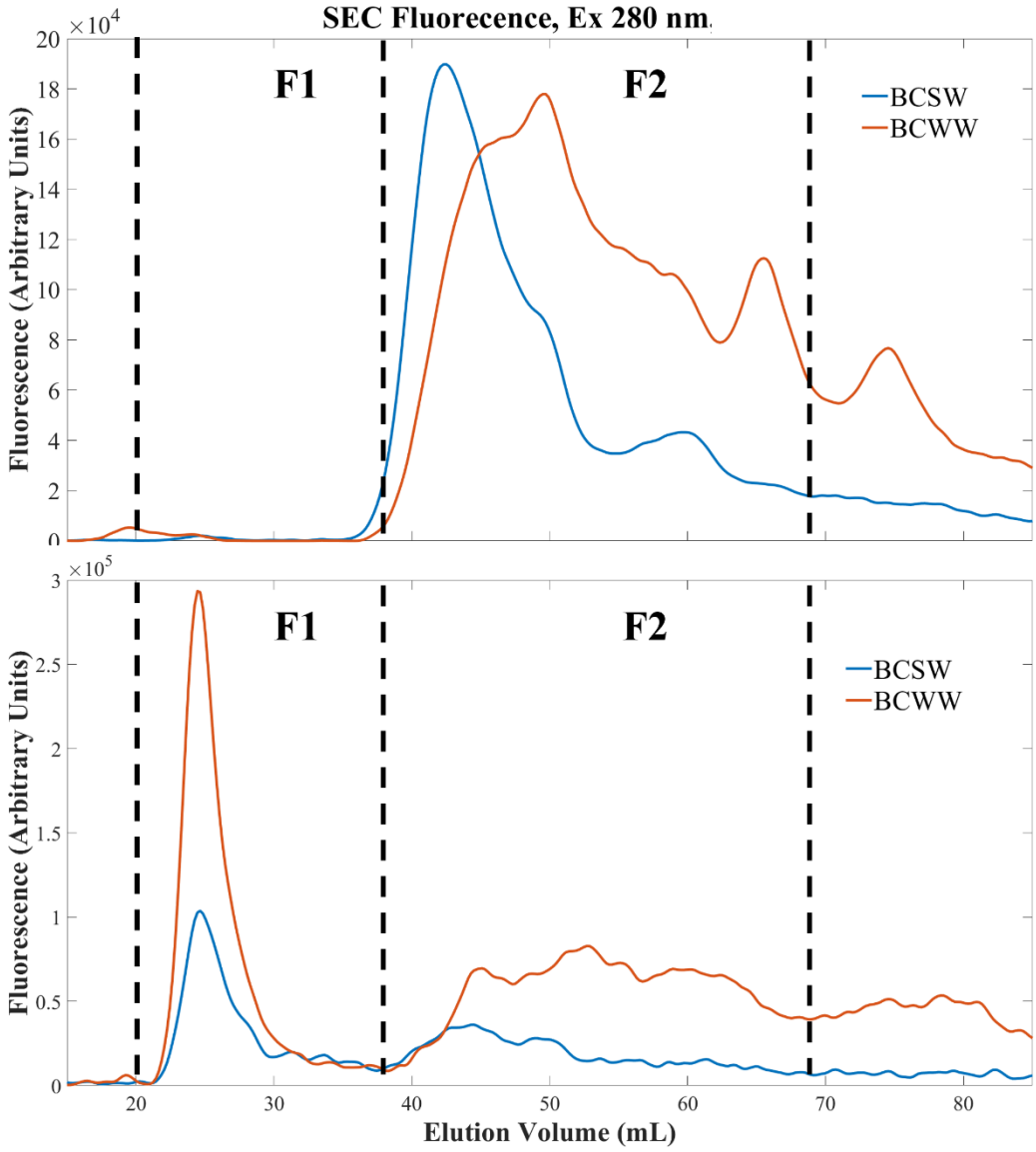

Figure 6.1 Surface Water and Wastewater SEC-Fluorescence Chromatograms. **Top:** Ex/Em 280/450 nm. **Bottom**: Ex/Em 280/335 nm. The wastewater sample (BWW1) is represented by the orange line and the surface water (BCSW) is represented by the blue line. The vertical dashed lines represent the cutoff times used for fraction collection: F1 was captured from 18-37 mL and F2 was collected from 37-68 mL.

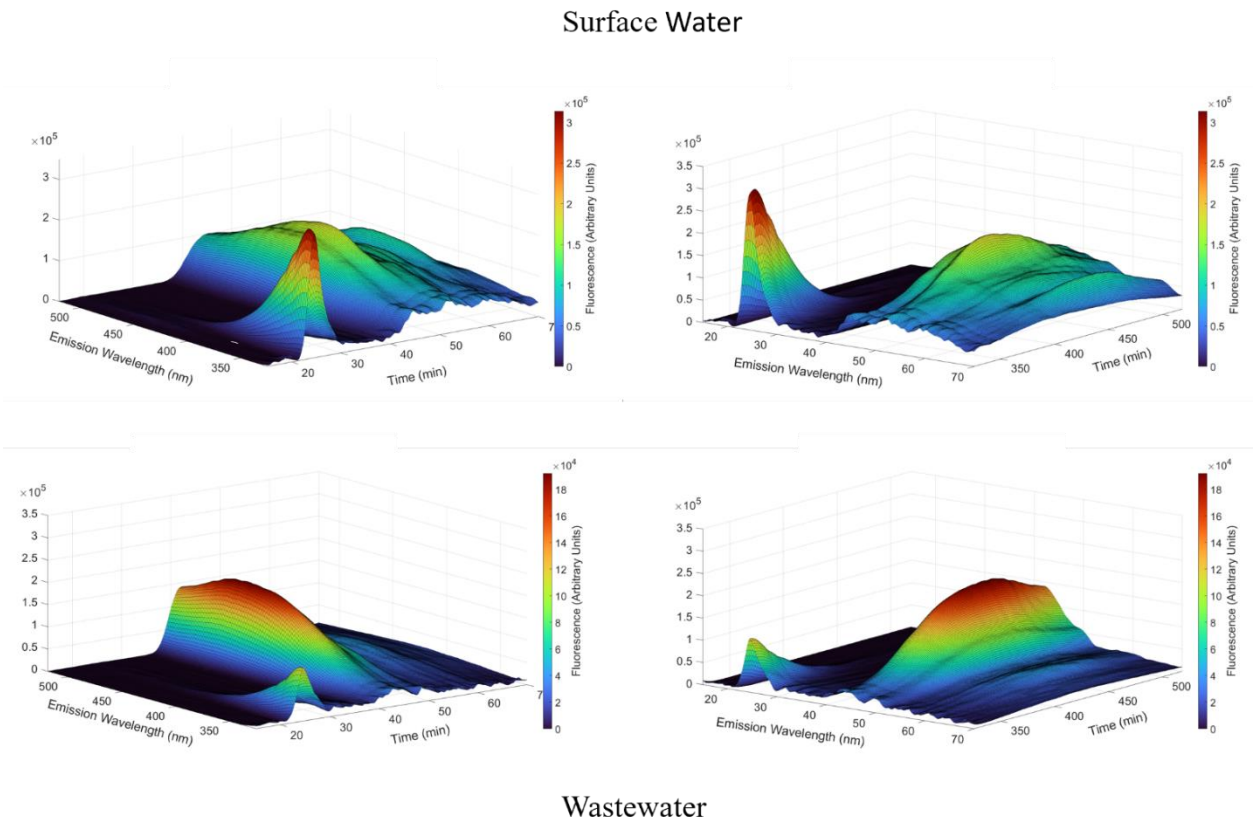

Figure 6.2 3-D Surface Water and Wastewater SEC-Fluorescence Chromatograms. **Top:** Surface water sample (BCSW). **Bottom**: Wastewater Sample (BWW1) The wastewater sample (BWW1). The left and right columns are rotated angles of the same plots in a given row (note the shifting of the x and y axis with the rotation). All data was obtained from the SEC-FLD at Ex/Em 280/325-520 nm.

6.3.2 Fraction Analysis

A preliminary run was used to define cutoff elution of 18-37 min. and 37-70 min for fractions F1 and F2 respectively. For both waters, FT, FC, and FS (Figure 6.3, left column) EEM comparisons showed low relative error. Error was characterized by random noise and no systematic behavior (where systematic behavior would suggest potential interaction). This demonstrates that FT, FC, and FS are equal to one another and there is no observable interaction between F1 and F2 when in the presence of one another. Several studies have found that Peak B and T fluorescence is quenched by that of Peak A (Wang et. al. 2015). The lack of interaction between F1 and F2 in the current study suggests that Peak A (in F2) does not quench the fluorescence of Peak B and T in F1. It should be noted the current study cannot explicitly confirm quenching of Peak B and T in F2, only that it does not occur in that of F1. It is therefore likely that Peak B and T fluorescence in F1 and F2 result from fluorophores of a different respective chemical composition. Maie and coworkers found that Peak B and T in the large molecular size fraction correlated to DON likely related to amino acids, while that of fraction 2 did not, based on their SEC data (Maie et al., 2007). Regardless of the specific explanation, this is useful in the interpretation of Peak B and T fluorescence especially if the fluorescence of either fraction can be related to microbial activity.

By extracting the data at Ex/Em 280/320 nm from the BWW1 EEM, the contributions of Peak B fluorescence in F1 and F2 to the overall Peak B fluorescence contained in FT, FC, or FS (Figure 6.3, right column, row 2) was approximated to be 35% and 65% respectively. However, integrating the Ex/Em 280/320 nm chromatogram across the elution volumes used to define F1, F2, and FT (shown by the red lines in Figure 6.2) collection resulted in approximations of 24.4% and 75.5% for F1, F2, and FT, respectively. This is explained by the fixed bandwidth of 20 nm

resulting in the broadening of fluorescence spectra, compared to the benchtop fluorometer which has a bandwidth that is controllable and set to 5 nm during analysis. The broadening increases the spectral overlap of Peak A into Peak B and T in the SEC data. Failing to consider this could result in interpretations of inflated fluorescence intensities (i.e., larger bandwidths broaden fluorescence spectra and increase the amount of light reaching the detector at a given wavelength (Lakowicz, 2006)) and highlights the utility of collecting fractions for further analysis with a benchtop instrument. Moreover, care needs to be taken when drawing conclusions from SEC-FLD spectra especially when single Ex/Em pair chromatograms are used and in comparisons made between SEC and benchtop instrument fluorescence data.

Despite the error, chromatogram integrations can still be used estimate *relative* contributions of each fluorescence peak to the samples, and the results can be used to better understand how these samples compare, and thus some of the potential impacts of wastewater treatment with respect to DOM fluorescence. The Peak B and T contributions of F1 and F2 to the total Peak B and T in BCSW are 49.1% and 51.9% respectively, meaning the contribution of Peak B and T in F1 to the total sample Peak B and T is relatively higher compared to that of BWW1. However, from integrating F1 in the Ex/Em 280/335 nm chromatogram for each sample, the magnitude of Peak B and T fluorescence in F1 in BWW1 is 2.25 times that of BCSW (Figure 6.1, Bottom). In F2, the peak intensities of Peak A in the Ex/Em 280/450 nm chromatogram, are relatively similar between the two waters, though BWW1 contains additional lower molecular size components that do not appear in BCSW (Figure 6.1, Top). These additional components are more clearly seen in the 3-D SEC plots (Figure 6.2). By integrating F2 in the Ex/Em chromatograms (Figure 6.1, Top) the Peak A fluorescence of BWW1 is 1.53 times that of BCSW. In comparing the Ex/Em 280/335 and 280/450 chromatogram integrations, the ratios of Peak B and T in F1 to

Peak A in F2 are 29.3% and 37.5% for BCSW and BWW1 respectively. Finally, the total Peak B and T fluorescence (i.e., integration of F1+F2 in the Ex/Em 280/335 nm chromatogram) represents 36.5% and 45.7% of the combined total Peak A, and B and T fluorescence (i.e., combined total of integration of F1+F2 in Ex/Em 280/335 and Ex/Em 280/450 nm chromatograms) the for BCSW and BWW1 respectively.

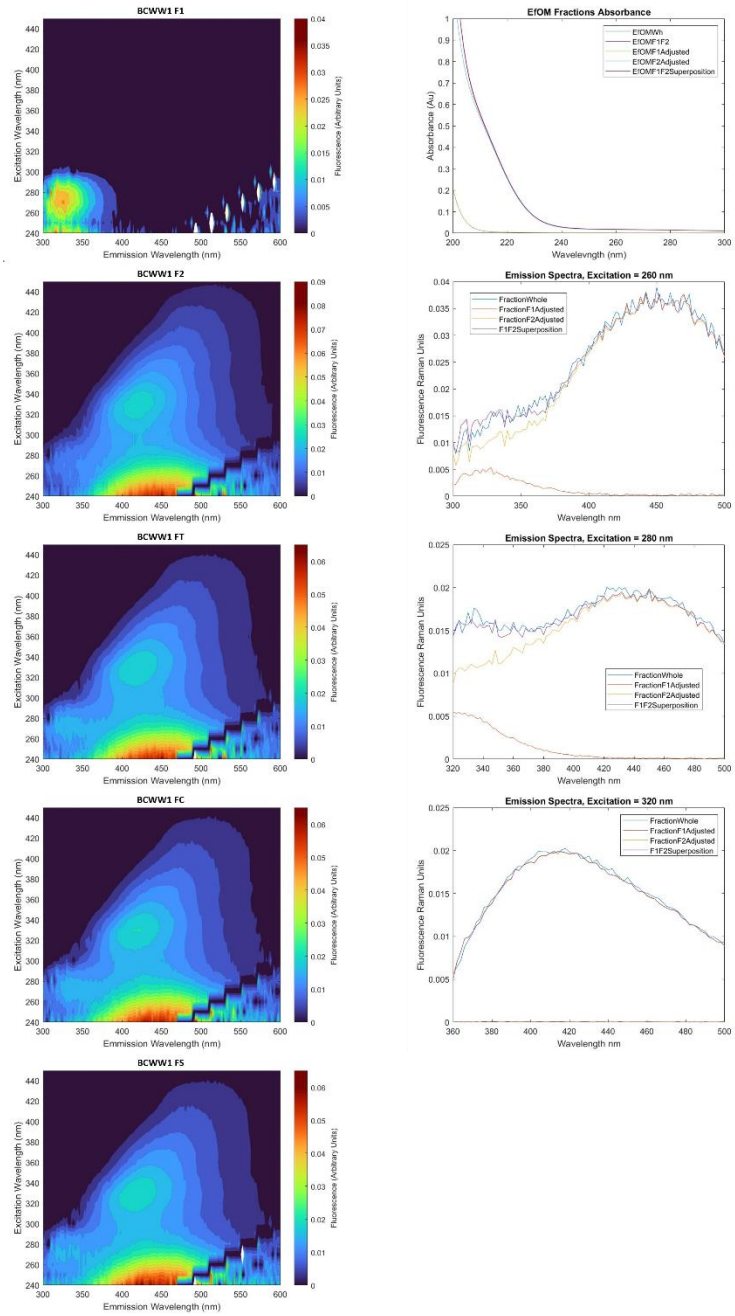

Figure 6.3 Bulk Water Spectra of a Fractionated Wastewater Sample. **Left (Top to Bottom):** Fraction 1 (F1) collected from SEC at elution volumes 18-37 mL; Fraction 2 (F2) collected from SEC at elution volumes 37-68 mL); Entire SEC run (FT) collected from 18-67 mL; Fractions F1 and F2 re-combined post collection (FC) based on elution volume ratios of each fraction to the total elution volume (i.e., 18-68 mL); Superimposed fractions (FS): F1 and F2 EEMs multiplied by their fractional contribution to FT based on elution volume. **Right (Top to Bottom):** Absorbance spectra; Fluorescence spectra Em/Ex 260/300-500 nm; Fluorescence spectra Em/Ex 280/320-500 nm; Fluorescence spectra Em/Ex 320/360-500 nm; The 2-D spectra plots (i.e., right side) show FT, F1 adjusted (F1 multiplied by fractional contribution to FT) , F2 adjusted (F2 multiplied by fractional contribution to FT), and FS.

6.3.3 Biofiltration

Results from the biofiltration experiment are shown in Figures 6.4-6.7 which display DOC, absorbance, and fluorescence chromatograms for all biofilter influent and effluent samples. Absorbance chromatograms at 280 nm (UV_{280}), fluorescence chromatograms at Ex/Em 280/340 nm ($F_{280/340}$) and 280/350 nm ($F_{280/450}$) were extracted from 3-dimensional SEC-DAD and SEC-FLD data respectively (Figures 6.4-6.6). $F_{280/340}$ and $F_{280/450}$ chromatograms suggest that the characterization of EfOM is similar for the separate batches of wastewater used for the biofiltration (Figure 6.1) and the fractionation experiments (Figure 6.6). As such, the terms F1 and F2 will again be used to describe the large (elution volumes 20-30 mL) and medium-to-small (30-55 mL) SEC fractions respectively. In addition to the characterization described in Section 6.3.1, the DOC and UV_{280} chromatograms in Figures 6.4-6.5 show that the F1 peak produced a relatively stronger DOC peak compared to UV_{280} and that both detectors show a strong F2 peak. The SEC-based characterization of EfOM analyzed in this study agree with the results of a previous study where the authors observed a strong F1 peak and weak F2 peak at fluorescence Ex/Em 278/253 (i.e., Peak B and T fluorescence), a relatively stronger DOC F1 peak compared to that of absorbance, and a strong F2 peak detected by DOC and absorbance (Her et al., 2003b).

Influent sample chromatograms from each day demonstrate that minimal changes occurred to the EfOM stock over the course of the experiment. In comparing data between influent and effluent samples from a given day, chromatograms from all detectors show that minimal changes occurred to the EfOM between column influent and effluent for samples collected on 5/28 and 6/04 both in terms of molecular size and optical property characterization. The lack of changes to the molecular size distribution and optical properties between influent and effluent samples suggest that the biofilm was still in the attachment and maturation stages of the biofilm cycle and

the dispersion (i.e., detachment of material from the biofilm) was not occurring. Comparing the influent and effluent chromatograms for the samples collected on 6/14 show increases in the F1 peak for the DOC, UV_{280}, and $F_{280/340}$ (Figures 6.4-6.7). To quantify the changes in EfOM characterization across the biofilter, percent increases were calculated in reference the influent signal with the following:

$$(\%\ increase = \frac{(sig_{inf} - sig_{inf})}{sig_{inf}} \quad (1)$$

where sig_{inf} and sig_{eff} are the chromatographic signals (i.e., DOC, absorbance, or fluorescence) of the influent and effluent samples respectively. Interestingly, for the F1 peak, the DOC and UV_{280} signals increased by 37.1 and 37.8% respectively, while the $F_{280/340}$ signal increased by 130.1%. No changes were seen were observed by any of the signals for the smaller molecular sizes (elution volumes 30-55 mL) including the $F_{280/450}$, in which the chromatogram lacks a large molecular size peak and only detected compounds of lower molecular sizes. Therefore, the increase in $F_{280/340}$ in the 5/28 effluent sample (compared to the influent sample on the same day) likely suggests that the biofilm had reached the dispersion stage of its life cycle. As cells and biofilm matrix detached from the biofilm microbially derived DOM was dispersed into the column effluent.

Together, the results of the biofiltration study demonstrates that the microbially derived DOM released from the biofilm (i.e., during the dispersion phase of the biofilm life cycle) can be characterized as large molecular size compounds that contain components that highly fluorescent Peak B and T fluorophores. Both $F_{280/340}$ $F_{280/450}$ chromatograms also suggest that the microbially derived DOM does not contain compounds that fluoresce in the range of Peaks A and C which are generally related to humic-like materials. Maie and coworkers found the concentration of dissolved organic nitrogen ([DON]) to be correlated to the $F_{280/325}$ in the large molecular size fraction (but

not in the smaller fractions) and suggested that while cautious interpretation is needed, $F_{280/325}$ could potentially be used as a surrogate for [DON] in waters where microbial activities control [DON] (Maie et al., 2007). From the results of Maie and coworkers, and the fact that biofilms are known to be composed of large proteinaceous compounds (Flemming et al., 2007), it is hypothesized that the $F_{280/340}$ of the microbially derived DOM dispersed from the biofilm is likely related to the fluorescence of certain amino groups that are components of proteinaceous material. Additionally, fluorescent free amino acids, which are small compounds in comparison to proteinaceous material, do not appear to have contributed to the composition of the microbially derived DOM dispersed from the biofilm.

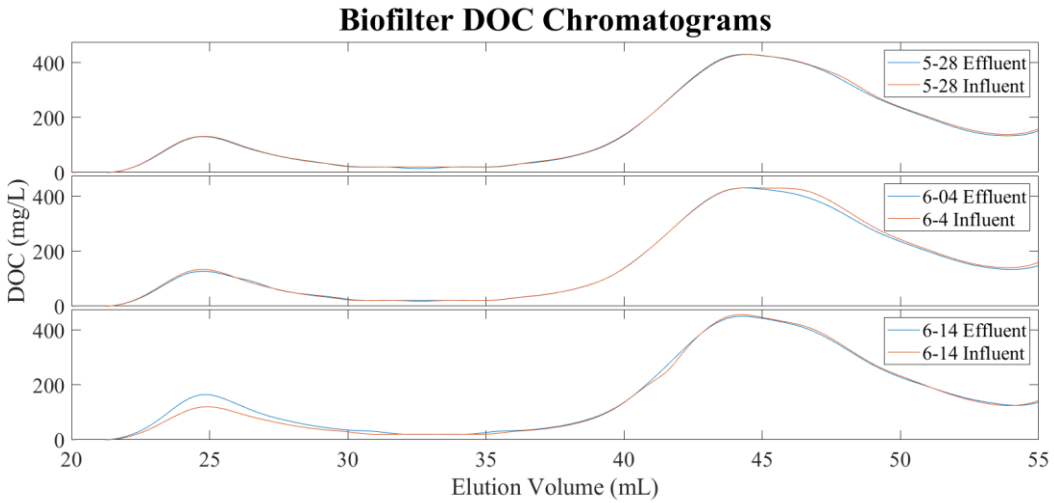

Figure 6.4 Biofilter Influent and Effluent DOC Chromatograms. **Top:** DOC chromatograms for biofilter influent and effluent samples collected on 5/28/2023. **Middle**: DOC chromatograms for biofilter influent and effluent samples collected on 6/04/2023. **Bottom:** DOC chromatograms for biofilter influent and effluent samples collected on 6/14/2023. For all plots elution volume is plotted on the x-axis and [DOC] (mg/L) is plotted on the y-axis. Orange lines represent influent samples and blue lines represent effluent samples.

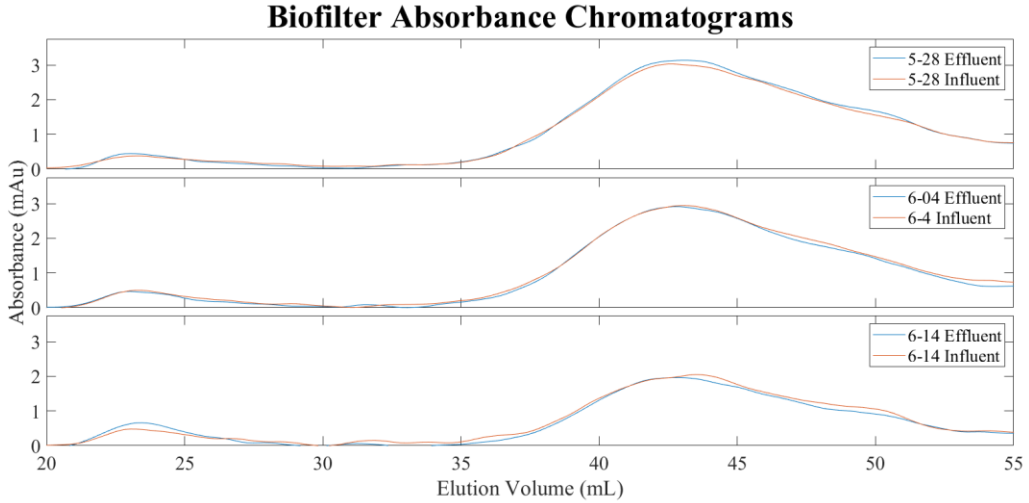

Figure 6.5 Biofilter Influent and Effluent Absorbance 280 nm Chromatograms. **Top:** Absorbance 280 nm chromatograms for biofilter influent and effluent samples collected on 5/28/2023. **Middle**: Absorbance 280 nm chromatograms for biofilter influent and effluent samples collected on 6/04/2023. **Bottom:** Absorbance 280 nm chromatograms for biofilter influent and effluent samples collected on 6/14/2023. For all plots elution volume is plotted on the x-axis and absorbance 280 nm (mAu) is plotted on the y-axis. Orange lines represent influent samples and blue lines represent effluent samples.

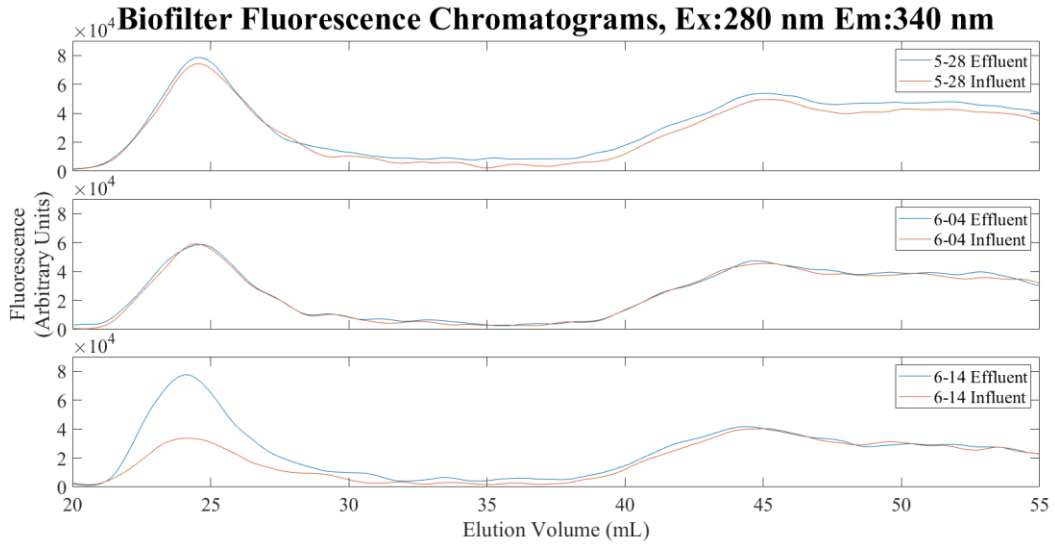

Figure 6.6 Biofilter Influent and Effluent Fluorescence Ex/Em: 280/340 nm Chromatograms. **Top:** Chromatograms for biofilter influent and effluent samples collected on 5/28/2023. **Middle**: Chromatograms for biofilter influent and effluent samples collected on 6/04/2023. **Bottom:** Chromatograms for biofilter influent and effluent samples collected on 6/14/2023. For all plots elution volume is plotted on the x-axis and Fluorescence Ex/Em: 280/340 nm (arbitrary units) is plotted on the y-axis. Orange lines represent influent samples and blue lines represent effluent samples.

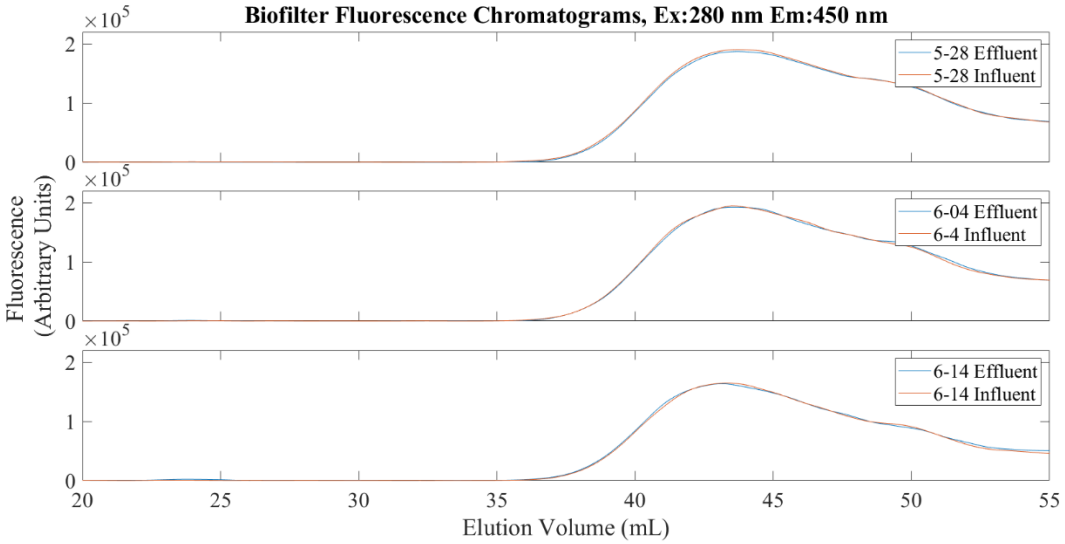

Figure 6.7 Biofilter Influent and Effluent Fluorescence Ex/Em: 280/450 nm Chromatograms. **Top:** Chromatograms for biofilter influent and effluent samples collected on 5/28/2023. **Middle**: Chromatograms for biofilter influent and effluent samples collected on 6/04/2023. **Bottom:** Chromatograms for biofilter influent and effluent samples collected on 6/14/2023. For all plots elution volume is plotted on the x-axis and Fluorescence Ex/Em: 280/450 nm (arbitrary units) is plotted on the y-axis. Orange lines represent influent samples and blue lines represent effluent samples.

6.3.4 Discussion

The results discussed in Section 6.3.1-6.3.2 demonstrated that the EfOM in BWW1 contains a relatively higher ratio of Peak B and T to Peak A compared to the NOM in BCSW. Similarly, when F1 and F2 from the NOM and EfOM samples are compared, there is a greater difference in the total fluorescence (i.e., integrated emission spectra at Ex 280) of F1 compared to F2. Because it can be assumed that more microbial activity occurs during wastewater processes compared to natural surface waters, these results may point to a correlation between Peak B and T fluorescence and microbial activity. This correlation was also supported by results from the biofiltration experiment, where microbially derived DOM dispersed from the biofilm was characterized as large molecular sized compounds that fluoresce specifically in the Peak B and T range.

While it is important to avoid the assumption that the microbially derived DOM from a biofilter will have the same characterization as that which is derived from wastewater treatment, it is known that free floating biofilm aggregates form in the absence of surface attachment during activated sludge processes (Sauer et al., 2022; Trego et al., 2021). These free-floating aggregates (i.e., granular sludge) are known to be composed of extracellular polymeric substances (EPS), similar to that of an attached biofilm (Gao et al., 2011). Additionally, Jarusutthirak and Amy used SEC to analyze the soluble microbial products (SMP) formed in a sequencing batch reactor designed to simulate activated sludge processes. The SMP (which likely include the contents of lysed microbial cells and EPS from biofilm aggregates), were composed of large molecular size compounds, with minor contributions of medium-to-small sized compounds, with low absorbance at 254 nm.

The occurrence of biofilm aggregates and the size distributions of SMP (shown by Jarusutthirak and Amy) suggest that similarities likely exist between the composition of microbially derived DOM from wastewater processes (e.g., activated sludge) and microbially derived DOM dispersed from biofiltration processes. Furthermore, the findings in this study provide support for the link between "protein-like" fluorescence and microbial activity. Future studies should investigate whether Peak B and T fluorescence signals can specifically be used as surrogates to differentiate between wastewater and surface water, whether they are indicative of the presence of microbiological and chemical contaminants, and how these signals can be utilized by online fluorescence sensors used during water treatment and especially in water reuse systems.

6.4 Conclusion

The investigation of a paired surface water and wastewater effluent pair using a SEC system coupled with DOC, absorbance, and fluorescence detectors revealed the Peaks B and T fluorescence in the large molecular sized components of the EfOM sample were responsible for the increase in total Peak B and T fluorescence compared to the surface water NOM. Large and medium-to-small fractions were collected from the SEC system and analyzed with an offline fluorescence to investigate the potential impacts of fluorescence quenching and peak overlap. While the F1 Peak B and T fluorescence was not found to be quenched by Peak A fluorescence, peak overlap was determined to impact perceived fluorescence peak signals. A biofiltration experiment demonstrated that changes to the characterization of EfOM were not observed during the aggregation and maturation stages of a biofilter. During the dispersion stage, when microbial cells and biofilm matrix detach from the biofilm, microbially derived DOM was isolated and its composition was characterized as large molecular sized compounds with highly fluorescent Peak B and T fluorophores similar to that which are found the EfOM F1 fraction. These findings are

valuable as they support potential link between Peak B and T fluorescence and microbial activity and will be important for the development of optical sensors use for monitoring during water reuse applications.

Chapter 7

Conclusions

In summary, the research presented in this thesis investigates the use of molecular size and optical properties to characterize dissolved organic matter (DOM), focusing on knowledge gaps and deficiencies that currently exist in this field of research. Findings from a literature review on monitoring techniques in potable water reuse (Chapter 4) suggest there is a need to shift toward online/in situ monitoring techniques. The use of optical properties in sensor-based technologies are among the most promising approaches in this regard. While several optical sensors are available today, more work is required for these technologies to see their potential. Thus, it is critical to advance the understanding of fundamental behaviors of DOM optical properties and how they can be used to for DOM characterization in terms of source and composition.

In Chapter 1, the size exclusion chromatography system (SEC) system paired with absorbance, fluorescence, and dissolved organic carbon (DOC) detection demonstrates the ability to observe DOM optical properties as a function of molecular size. These size-based relationships yield new information regarding the fundamental components of DOM. For example, the SEC-based fluorescence quantum yield (Φ_F) results suggest the most highly fluorescent fraction of DOM are related to small size fractions (Φ_F up to ~2.5-3%) which are generally present in lower abundance compared to larger, weakly fluorescing fractions ($\Phi_F \leq 1.5\%$) and a steady increase in Φ_F was observed as molecular size decreased. The observed range in Φ_F (<0.5-3%) within individual samples may provide benefit in the use of SEC-Φ_F for DOM source differentiation compared to bulk Φ_F where one value (typically ranging from 1-3%) is calculated for each sample.

Results from Chapter 5 demonstrate the conservative mixing behavior of DOM optical properties and molecular size when DOM sources are blended. These findings suggest that interactions are not occurring following the mixing of DOM sources and that signals of blended samples can be reliably predicted from the signals of individual source. Matching accuracy was generally found to be the highest near the chromatographic peaks where the relative error in measured data remained within ±5% of the predicted data for all detectors. Absorbance, fluorescence, and Φ_F, were found to have better accuracy than DOC. However other factors, such as the fluorescence signal noise, should also be considered when evaluating matching accuracy. In general, differences between the error of each detector were relatively minor and results from all of the measured signals (i.e., DOC, absorbance, fluorescence, and Φ_F) support the observation of conservative mixing. This fundamental understanding is critical if DOM optical properties are to be used as surrogates for source differentiation in real world scenarios as misinterpretations of data may negatively impact human health.

In Chapter 6, results verified that "protein-like" fluorescence occurred in the medium-to-low molecular weight fraction of the paired surface and wastewater samples. This agrees with similar observations made in a previous study on estuarian samples (Maie et. al., 2007). However, it was found that the spectral overlap from Peak A likely influences quantitative calculations of "protein-like fluorescence" in the medium-to-low molecular weight fraction based on SEC-data, especially in cases where chromatograms from single excitation/emission pairs are used for interpretation. Comparisons of EEMs for separate fractions collected from the SEC system suggest quenching (or other interactions) did not occur between the "protein-like" fluorescence in the large molecular weight fraction and Peak A ("humic-like") fluorescence in the medium-to-low molecular weight fraction. This is important to understand as previous studies hypothesized that

"protein-like" fluorescence in the large molecular size fraction is linked to the presence of amino acid groups in proteinaceous material and may be related to microbial activity. In comparing the surface water and wastewater data, the most significant differences are found in the small molecular size fractions (low end of the medium-to-low molecular size fraction, F2, that was collected). In this size range, additional SEC-peaks containing predominantly Peak A fluorescence were observed in the EfOM sample but not in the surface water NOM. While it is unclear if these peaks result from microbial activity or anthropogenic inputs, these results suggest this region of chromatographic data could be informative in differentiating between surface water and wastewater effluent. Finally, the biofiltration experiment demonstrated that the microbially derived DOM dispersed from the biofilm could be characterized as large molecular sized compounds with strong protein-like fluorescence signals. These results provide support for the link between protein-like fluorescence and microbial activity which needs to be understood for the development of fluorescence-based sensors for monitoring in water treatment systems.

Overall, the findings will help to advance the use of optical properties and molecular size in real world water treatment scenarios. Research presented in Chapters 3-6 all provide important information with regards to the fundamental understanding of DOM optical properties, especially with regards to source differentiation. With respect to the development of optical sensor probes, these devices are currently much simpler than benchtop spectrophotometers and fluorometers and are often restricted to measuring one absorbance wavelength or a single fluorescence excitation/emission wavelength pair. Future work must continue to investigate the fundamental understandings of DOM optical properties for their potential to be realized in applied water treatment settings.

Chapter 8

Future Work

There are several avenues in which future work can expand on the research presented in this thesis. The size exclusion chromatography fluorescence quantum yield (SEC-Φ_f) method developed in Chapter 4 is utilized in Chapters 5 and 6 where a second fluorescence excitation wavelength (λ_{Fex}) of 275 nm (note λ_{Fex} 280 nm was used in Chapter 6, however λ_{Fex} 275 and 280 nm will yield very similar information) was investigated. Future studies should evaluate other λ_{Fex} and determine which would be the most optimal for application of this method. One of the drawbacks of using λ_{Fex} 350 nm is that the absorbance and fluorescence detector responses (i.e., signal magnitude) are relatively weak compared to lower wavelengths. Weaker signals are generally subject to increased error because SEC-Φ_f is not calculated below absorbance values of <0.5 mAu (this cutoff was used to avoid the consideration of inaccurate Φ_f values). Therefore, weaker signals also decrease the elution volume range for which SEC-Φ_f is calculated. However, lower λ_{Fex} wavelengths introduce the possibility of SEC-Φ_f capturing multiple fluorescence peaks (e.g., i.e., Peaks A and C or Peaks A and B/T) (P. G. Coble et al., 2014) simultaneously due to the spectral overlap that typically exists between peaks. When this occurs, it is not initially clear which fluorophore groups are responsible for measured Φ_f values and is problematic for relating Φ_f to DOM source and composition. Such cases require additional inspection and cautious interpretation.

Future work should also seek to characterize the changes to SEC-Φ_f following multiple treatment processes. In Chapter 6, ozonation of dissolved organic matter (DOM) is presented as

an example of this and a later study used the method to further the understanding of the relationship between Φ_f and singlet oxygen Φ (Φ_{O1}) following ozonation (Buckley et al., 2023). Similar investigations can be applied to other chemical treatment processes such as UV-advanced oxidation (i.e., UV-AOP) or to understand the removal of chromophores and fluorophores by physical processes such as microfiltration and ultrafiltration (MF and UF respectively). A better fundamental understanding of how treatment processes impact DOM is needed if DOM is to be used a surrogate for the removal of contaminants (see Chapter 3.3 for examples of the use of optical properties as surrogates for specific contaminants).

The research presented in Chapter 5 provides a fundamental demonstration of the conservative mixing of molecular size and optical properties during the blending of DOM sources. Future work should investigate DOM source differentiation in applied/real world scenarios where DOM properties are used to determine the contributions of multiple source waters after they are mixed (e.g., the contribution of discharged wastewater effluent to a receiving surface water). These investigations would have to consider additional processes (other than blending) that impact DOM properties, such as photobleaching in surface waters, and would require verification by a separate metric (i.e., direct measurement of another water constituent that is also representative of the source contributions). Additionally, differentiation between other DOM pools, such as algal organic matter (AOM) or DOM that leaches from soil impacted by forest fires (i.e., pyrogenic organic carbon), would also be valuable as algal blooms and forest fires are known to impact water quality.

Following the results of Chapter 6, future work should further investigate how microbial activity in specific environments impacts the size-based fluorescence in scenarios where microbial activity can be closely monitored/controlled. For example, D'Andrilli and coworkers exposed

DOM leached from leaves, needles, and grass to microbial cultures that were prepared in a laboratory setting (D'Andrilli et al., 2019). While these authors only analyzed bulk water samples, the inclusion of an SEC system in similar studies would help to understand how various types of microbial activity or microbial conditions are related to "protein-like" fluorescence in specific size fractions.

Finally, in general relation to the ideas discussed in this thesis (i.e., not related to the findings of a specific chapter), future work should include development of SEC-based PARAFAC methods. Several previous studies have used PARAFAC to decompose individual fluorescence peaks from EEM data (D'Andrilli et al., 2019; R.K. Henderson et al., 2009; Murphy et al., 2013), and at least one study applied PARAFAC to SEC-fluorescence data to decompose the size-based fluorescence peaks for a single sample (Wünsch et al., 2017) across all λ_{Fex} and λ_{Fem} captured in an EEM. The latter study required the same sample to be analyzed several times, applying a different λ_{Fex} during each analysis. A simplified method could potentially be used to focus on the decomposition of overlapping size-based fluorescence peaks at single λ_{Fex} wavelengths. This would be useful in situations where the same fluorescence peaks are seen in multiple fractions or where multiple fluorescence peaks are found in the same size fraction (both situations were observed in the surface and wastewater effluent samples that were analyzed in Chapter 6).

Bibliography

Aiken, G.R., Malcolm, R.L., 1987. Molecular weight of aquatic fulvic acids by vapor pressure osmometry. Geochimica et Cosmochimica Acta.

Aiken, G., 2014. Fluorescence and Dissolved Organic Matter: A Chemist's Perspective, in: Baker, A., Reynolds, D.M., Lead, J., Coble, P.G., Spencer, R.G.M. (Eds.), Aquatic Organic Matter Fluorescence, Cambridge Environmental Chemistry Series. Cambridge University Press, New York, NY, pp. 35–74. https://doi.org/10.1017/CBO9781139045452.005

Alexandrov, A., Benidis, K., Bohlke-Schneider, M., Flunkert, V., Gasthaus, J., Januschowski, T., Maddix, D.C., Rangapuram, S., Salinas, D., Schulz, J., Stella, L., Türkmen, A.C., Wang, Y., 2019. GluonTS: Probabilistic Time Series Models in Python.

Alexandrov, A., Benidis, K., Bohlke-Schneider, M., Flunkert, V., Gasthaus, J., Januschowski, T., Maddix, D.C., Rangapuram, S., Salinas, D., Schulz, J., Stella, L., Turkmen, A.C., Wang, Y., 2020. GluonTS: Probabilistic and Neural Time Series Modeling in Python. Journal of Machine Learning Research 21, 1–6.

Amoueyan, E., Ahmad, S., Eisenberg, J.N.S., Pecson, B., Gerrity, D., 2017. Quantifying pathogen risks associated with potable reuse: A risk assessment case study for Cryptosporidium. Water Research 119, 252–266. https://doi.org/10.1016/j.watres.2017.04.048

Amy, G.L., Collins, M.R., Kuo, C.J., King, P.H., 1987. Comparing Gel Permeation Chromatography and Ultrafiltration for the Molecular Weight Characterization of Aquatic Organic Matter. Journal - American Water Works Association 79, 43–49. https://doi.org/10.1002/j.1551-8833.1987.tb02782.x

Andrzejewski, P., Kasprzyk-Hordern, B., Nawrocki, J., 2008. N-nitrosodimethylamine (NDMA) formation during ozonation of dimethylamine-containing waters. Water Research 42, 863–870. https://doi.org/10.1016/j.watres.2007.08.032

Anumol, T., Sgroi, M., Park, M., Roccaro, P., Snyder, S.A., 2015. Predicting trace organic compound breakthrough in granular activated carbon using fluorescence and UV absorbance as surrogates. Water Research 76, 76–87. https://doi.org/10.1016/j.watres.2015.02.019

Appiani, E., Page, S.E., McNeill, K., 2014. On the Use of Hydroxyl Radical Kinetics to Assess the Number-Average Molecular Weight of Dissolved Organic Matter. Environ. Sci. Technol. 48, 11794–11802. https://doi.org/10.1021/es5021873

Azam, F., Fenchel, T., Field, J.G., Gray, J.S., Meyer-Reil, L.A., Thingstad, F., 1983. The Ecological Role of Water-Column Microbes in the Sea. Marine Ecology Progress Series 10, 257–263. https://doi.org/10.3354/meps010257

Bailey, E.S., Hopkins, M., Casanova, L., Sobsey, M.D., 2021. Evaluating Fecal Indicator and Pathogen Relationships in Sewage Impacted Surface Waters to Blend with Reclaimed Water for Potable Reuse in North Carolina. Pathogens 10, 1603. https://doi.org/10.3390/pathogens10121603

Baker, A., 2001. Fluorescence Excitation−Emission Matrix Characterization of Some Sewage-Impacted Rivers. Environ. Sci. Technol. 35, 948–953. https://doi.org/10.1021/es000177t

Bartos, M., Mullapudi, A., Troutman, S., 2019. rrcf: Implementation of the Robust Random Cut Forest algorithm for anomaly detection on streams. JOSS 4, 1336. https://doi.org/10.21105/joss.01336

Bauer, J.E., Cai, W.-J., Raymond, P.A., Bianchi, T.S., Hopkinson, C.S., Regnier, P.A.G., 2013. The changing carbon cycle of the coastal ocean. Nature 504, 61–70. https://doi.org/10.1038/nature12857

Bedell, E., Sharpe, T., Purvis, T., Brown, J., Thomas, E., 2020. Demonstration of Tryptophan-Like Fluorescence Sensor Concepts for Fecal Exposure Detection in Drinking Water in Remote and Resource Constrained Settings. Sustainability 12, 3768. https://doi.org/10.3390/su12093768

Bedell, E., Harmon, O., Fankhauser, K., Shivers, Z., Thomas, E., 2022. A continuous, in-situ, near-time fluorescence sensor coupled with a machine learning model for detection of fecal contamination risk in drinking water: Design, characterization and field validation. Water Research 220, 118644. https://doi.org/10.1016/j.watres.2022.118644

Bernados, B., 2018. Reverse Osmosis for Direct Potable Reuse in California: Reverse Osmosis for Direct Potable Reuse in California. Journal - American Water Works Association 110, 28–36. https://doi.org/10.5942/jawwa.2018.110.0006

Besmer, M.D., Weissbrodt, D.G., Kratochvil, B.E., Sigrist, J.A., Weyland, M.S., Hammes, F., 2014. The feasibility of automated online flow cytometry for in-situ monitoring of microbial dynamics in aquatic ecosystems. Front. Microbiol. 5. https://doi.org/10.3389/fmicb.2014.00265

Bhatnagar, A., Kassianik, P., Liu, C., Lan, T., Yang, W., Cassius, R., Sahoo, D., Arpit, D., Subramanian, S., Woo, G., Saha, A., Jagota, A.K., Gopalakrishnan, G., Singh, M., Krithika, K.C., Maddineni, S., Cho, D., Zong, B., Zhou, Y., Xiong, C., Savarese, S., Hoi, S., Wang, H., 2021. Merlion: A Machine Learning Library for Time Series.

Bianchi, T.S., 2011. The role of terrestrially derived organic carbon in the coastal ocean: A changing paradigm and the priming effect. Proceedings of the National Academy of Sciences 108, 19473–19481. https://doi.org/10.1073/pnas.1017982108

Boyle, E.S., Guerriero, N., Thiallet, A., Vecchio, R.D., Blough, N.V., 2009. Optical Properties of Humic Substances and CDOM: Relation to Structure. Environ. Sci. Technol. 43, 2262–2268. https://doi.org/10.1021/es803264g

Bruccoleri, A., Pant, B.C., Sharma, D.K., Langford, C.H., 1993. Evaluation of primary photoproduct quantum yields in fulvic acid. Environ. Sci. Technol. 27, 889–894. https://doi.org/10.1021/es00042a011

Cabaniss, S.E., Zhou, Q., Maurice, P.A., Chin, Y.-P., Aiken, G.R., 2000. A Log-Normal Distribution Model for the Molecular Weight of Aquatic Fulvic Acids. Environ. Sci. Technol. 34, 1103–1109. https://doi.org/10.1021/es990555y

Capasso, S., Chianese, S., Musmarra, D., Iovino, P., 2020. Macromolecular Structure of a Commercial Humic Acid Sample. Environments 7, 32. https://doi.org/10.3390/environments7040032

Carstea, E.M., Baker, A., Bieroza, M., Reynolds, D., 2010. Continuous fluorescence excitation–emission matrix monitoring of river organic matter. Water Research 44, 5356–5366. https://doi.org/10.1016/j.watres.2010.06.036

Carstea, E.M., Bridgeman, J., Baker, A., Reynolds, D.M., 2016. Fluorescence spectroscopy for wastewater monitoring: A review. Water Research 95, 205–219. https://doi.org/10.1016/j.watres.2016.03.021

Catalá, T.S., Reche, I., Álvarez, M., Khatiwala, S., Guallart, E.F., Benítez-Barrios, V.M., Fuentes-Lema, A., Romera-Castillo, C., Nieto-Cid, M., Pelejero, C., Fraile-Nuez, E., Ortega-Retuerta, E., Marrasé, C., Álvarez-Salgado, X.A., 2015. Water mass age and aging driving chromophoric dissolved organic matter in the dark global ocean. Global Biogeochemical Cycles 29, 917–934. https://doi.org/10.1002/2014GB005048

Cawley, K.M., Korak, J.A., Rosario-Ortiz, F.L., 2015. Quantum Yields for the Formation of Reactive Intermediates from Dissolved Organic Matter Samples from the Suwannee River. Environmental Engineering Science 32, 31–37. https://doi.org/10.1089/ees.2014.0280

CDPH, 2014. Regulations Related to Recycled Water, California Code of Regulations. California Department of Public Health.

Chon, K., Salhi, E., von Gunten, U., 2015. Combination of UV absorbance and electron donating capacity to assess degradation of micropollutants and formation of bromate during ozonation of wastewater effluents. Water Research 81, 388–397. https://doi.org/10.1016/j.watres.2015.05.039

Christman, R.F., Norwood, D.L., Millington, D.S., Johnson, J.Donald., Stevens, A.A., 1983. Identity and yields of major halogenated products of aquatic fulvic acid chlorination. Environ. Sci. Technol. 17, 625–628. https://doi.org/10.1021/es00116a012

Coble, P.G., Green, S.A., Blough, N.V., Gagosian, R.B., 1990. Characterization of dissolved organic matter in the Black Sea by fluorescence spectroscopy. Nature 348, 432–435. https://doi.org/10.1038/348432a0

Coble, P.G., 1996. Characterization of marine and terrestrial DOM in seawater using excitation-emission matrix spectroscopy. Marine Chemistry 51, 325–346. https://doi.org/10.1016/0304-4203(95)00062-3

Coble, P.G., 2007. Marine Optical Biogeochemistry: The Chemistry of Ocean Color. Chem. Rev. 107, 402–418. https://doi.org/10.1021/cr050350+

Coble, P.G., Lead, J., Baker, A., Reynolds, D.M., Spencer, R.G.M. (Eds.), 2014. Aquatic Organic Matter Fluorescence, Cambridge Environmental Chemistry Series. Cambridge University Press, New York, NY. https://doi.org/10.1017/CBO9781139045452

Conte, P., Piccolo, A., 1999. High pressure size exclusion chromatography (HPSEC) of humic substances: Molecular sizes, analytical parameters, and column performance. Chemosphere 38, 517–528. https://doi.org/10.1016/S0045-6535(98)00198-2

Cory, R.M., McKnight, D.M., 2005. Fluorescence Spectroscopy Reveals Ubiquitous Presence of Oxidized and Reduced Quinones in Dissolved Organic Matter. Environ. Sci. Technol. 39, 8142–8149. https://doi.org/10.1021/es0506962

CSWRCB, 2018. A Proposed Framework for Regulating Direct Potable Reuse in California. California State Water Resources Control Board.

CSWRCB, 2019. Proposed Framework of Regulating Direct Potable Reuse In California, Second Edition. California State Water Resources Control Board.

CSWRCB, 2021. A Proposed Framework of Regulating Direct Potable Reuse In California Addendum version 8-17-2021. California State Water Resources Control Board.

D'Andrilli, J., Foreman, C.M., Marshall, A.G., McKnight, D.M., 2013. Characterization of IHSS Pony Lake fulvic acid dissolved organic matter by electrospray ionization Fourier transform ion cyclotron resonance mass spectrometry and fluorescence spectroscopy. Organic Geochemistry 65, 19–28. https://doi.org/10.1016/j.orggeochem.2013.09.013

D'Andrilli, J., Junker, J.R., Smith, H.J., Scholl, E.A., Foreman, C.M., 2019. DOM composition alters ecosystem function during microbial processing of isolated sources. Biogeochemistry 142, 281–298. https://doi.org/10.1007/s10533-018-00534-5

D'Andrilli, J., Silverman, V., Buckley, S., Rosario-Ortiz, F.L., 2022. Inferring Ecosystem Function from Dissolved Organic Matter Optical Properties: A Critical Review. Environ. Sci. Technol. 56, 11146–11161. https://doi.org/10.1021/acs.est.2c04240

De Haan, H., De Boer, T., 1987. Applicability of light absorbance and fluorescence as measures of concentration and molecular size of dissolved organic carbon in humic Lake Tjeukemeer. Water Research 21, 731–734. https://doi.org/10.1016/0043-1354(87)90086-8

Del Vecchio, R., Blough, N.V., 2004. On the Origin of the Optical Properties of Humic Substances. Environ. Sci. Technol. 38, 3885–3891. https://doi.org/10.1021/es049912h

Dickenson, E.R.V., Drewes, J.E., Sedlak, D.L., Wert, E.C., Snyder, S.A., 2009. Applying Surrogates and Indicators to Assess Removal Efficiency of Trace Organic Chemicals during Chemical Oxidation of Wastewaters. Environ. Sci. Technol. 43, 6242–6247. https://doi.org/10.1021/es803696y

Dickenson, E.R.V., Snyder, S.A., Sedlak, D.L., Drewes, J.E., 2011. Indicator compounds for assessment of wastewater effluent contributions to flow and water quality. Water Research 45, 1199–1212. https://doi.org/10.1016/j.watres.2010.11.012

Drewes, J.E., Anderson, P., Denslow, N., Jakubowski, W., Olivieri, A., Schlenk, D., Snyder, S., 2018. Monitoring Strategies for Constituents of Emerging Concern (CECs) in Recycled Water. California State Water Recources Control Board.

Edzwald, J.K., Becker, W.C., Wattier, K.L., 1985. Surrogate Parameters for Monitoring Organic Matter and THM Precursors. Journal - American Water Works Association 77, 122–132. https://doi.org/10.1002/j.1551-8833.1985.tb05521.x

Egli, T., Kotzsch, S., 2015. Flow Cytometry for Rapid Microbiological Analysis of Drinking Water: From Science to Practice, an Unfinished Story, in: Flow Cytometry in Microbiology: Technology and Applications. Caister Academic Press, United Kingdom, pp. 175–216.

Elovitz, M.S., von Gunten, U., 1999. Hydroxyl Radical/Ozone Ratios During Ozonation Processes. I. The R ct Concept. Ozone: Science & Engineering 21, 239–260. https://doi.org/10.1080/01919519908547239

Fabbri, D., Bianco Prevot, A., 2021. Analytical control in advanced oxidation processes: Surrogate models and indicators vs traditional methods. Microchemical Journal 171, 106799. https://doi.org/10.1016/j.microc.2021.106799

Fellman, J.B., Hood, E., Spencer, R.G.M., 2010. Fluorescence spectroscopy opens new windows into dissolved organic matter dynamics in freshwater ecosystems: A review. Limnology and Oceanography 55, 2452–2462. https://doi.org/10.4319/lo.2010.55.6.2452

Ferrari, G.M., Dowell, M.D., Grossi, S., Targa, C., 1996. Relationship between the optical properties of chromophoric dissolved organic matter and total concentration of dissolved organic carbon in the southern Baltic Sea region. Marine Chemistry 55, 299–316. https://doi.org/10.1016/S0304-4203(96)00061-8

Findlay, S.E., Sinsabaugh, R.L. (Eds.), 2003. Aquatic Ecosystems Interactivity of Dissolve Organic Matter, Aquatic Ecology. Elsevier Science, Samn Diego, CA.

Fischer, S.J., Gonsior, M., Chorover, J., Powers, L.C., Hamilton, A., Ramirez, M., Torrents, A., 2022. Biosolids leachate variability, stabilization surrogates, and optical metric selection. Environ. Sci.: Water Res. Technol. 8, 657–670. https://doi.org/10.1039/D1EW00320H

Flemming, H.-C., Neu, T.R., Wozniak, D.J., 2007. The EPS Matrix: The "House of Biofilm Cells." J Bacteriol 189, 7945–7947. https://doi.org/10.1128/JB.00858-07

Focazio, M.J., Kolpin, D.W., Barnes, K.K., Furlong, E.T., Meyer, M.T., Zaugg, S.D., Barber, L.B., Thurman, M.E., 2008. A national reconnaissance for pharmaceuticals and other organic wastewater contaminants in the United States — II) Untreated drinking water sources. Science of The Total Environment 402, 201–216. https://doi.org/10.1016/j.scitotenv.2008.02.021

Fox, B.G., Thorn, R.M.S., Anesio, A.M., Reynolds, D.M., 2017. The in situ bacterial production of fluorescent organic matter; an investigation at a species level. Water Research 125, 350–359. https://doi.org/10.1016/j.watres.2017.08.040

Frenkel, V., Cohen, Y., 2014. 2014 New Techniques for REal-Time Monitoring of Membrane Integrity for Virus Removal (Research Report No. WRF 09-06B). WateReuse, Alexandria, Virginia.

Gabor, R., Baker, A., McKnight, D.M., Miller, M., 2014. Fluorescence indices and their interpretation, in: Aquatic Organic Matter Fluorescence. Cambridge University Press, New York, NY, pp. 303–338.

Gao, D., Liu, L., Liang, H., Wu, W.-M., 2011. Aerobic granular sludge: characterization, mechanism of granulation and application to wastewater treatment. Critical Reviews in Biotechnology 31, 137–152. https://doi.org/10.3109/07388551.2010.497961

Gardner, G.B., Chen, R.F., Berry, A., 2005. High-resolution measurements of chromophoric dissolved organic matter (CDOM) in the Neponset River Estuary, Boston Harbor, MA. Marine Chemistry 96, 137–154. https://doi.org/10.1016/j.marchem.2004.12.006

Gerrity, D., Gamage, S., Jones, D., Korshin, G.V., Lee, Y., Pisarenko, A., Trenholm, R.A., von Gunten, U., Wert, E.C., Snyder, S.A., 2012. Development of surrogate correlation models to predict trace organic contaminant oxidation and microbial inactivation during ozonation. Water Research 46, 6257–6272. https://doi.org/10.1016/j.watres.2012.08.037

Green, S.A., Blough, N.V., 1994. Optical absorption and fluorescence properties of chromophoric dissolved organic matter in natural waters. Limnology and Oceanography 39, 1903–1916. https://doi.org/10.4319/lo.1994.39.8.1903

Guetzloff, T.F., Rice, J.A., 1994. Does humic acid form a micelle? Science of The Total Environment 152, 31–35. https://doi.org/10.1016/0048-9697(94)90548-7

Haddeland, I., Heinke, J., Biemans, H., Eisner, S., Flörke, M., Hanasaki, N., Konzmann, M., Ludwig, F., Masaki, Y., Schewe, J., Stacke, T., Tessler, Z.D., Wada, Y., Wisser, D., 2014. Global water resources affected by human interventions and climate change. Proc. Natl. Acad. Sci. U.S.A. 111, 3251–3256. https://doi.org/10.1073/pnas.1222475110

Hammes, F., Salhi, E., Köster, O., Kaiser, H.-P., Egli, T., von Gunten, U., 2006. Mechanistic and kinetic evaluation of organic disinfection by-product and assimilable organic carbon (AOC) formation during the ozonation of drinking water. Water Research 40, 2275–2286. https://doi.org/10.1016/j.watres.2006.04.029

Hammes, F., Broger, T., Weilenmann, H.-U., Vital, M., Helbing, J., Bosshart, U., Huber, P., Peter Odermatt, R., Sonnleitner, B., 2012. Development and laboratory-scale testing of a fully automated online flow cytometer for drinking water analysis. Cytometry 81A, 508–516. https://doi.org/10.1002/cyto.a.22048

Hansen, A.M., Kraus, T.E.C., Pellerin, B.A., Fleck, J.A., Downing, B.D., Bergamaschi, B.A., 2016. Optical properties of dissolved organic matter (DOM): Effects of biological and photolytic degradation. Limnology and Oceanography 61, 1015–1032. https://doi.org/10.1002/lno.10270

Hanson, B., Wünsch, U., Buckley, S., Fischer, S., Leresche, F., Murphy, K., D'Andrilli, J., Rosario-Ortiz, F.L., 2022. DOM Molecular Weight Fractionation and Fluorescence Quantum Yield Assessment Using a Coupled In-Line SEC Optical Property System. ACS EST Water 2, 2491–2501. https://doi.org/10.1021/acsestwater.2c00318

Hart, D., McKenna, S.A., Klise, K., Cruz, V., Wilson, M., 2007. CANARY: A Water Quality Event Detection Algorithm Development Tool, in: World Environmental and Water Resources Congress 2007. Presented at the World Environmental and Water Resources Congress 2007, American Society of Civil Engineers, Tampa, Florida, United States, pp. 1–9. https://doi.org/10.1061/40927(243)517

Hawkes, J.A., Sjöberg, P.J.R., Bergquist, J., Tranvik, L.J., 2019. Complexity of dissolved organic matter in the molecular size dimension: insights from coupled size exclusion chromatography electrospray ionisation mass spectrometry. Faraday Discuss. 218, 52–71. https://doi.org/10.1039/C8FD00222C

Helms, J.R., Stubbins, A., Ritchie, J.D., Minor, E.C., Kieber, D.J., Mopper, K., 2008. Absorption spectral slopes and slope ratios as indicators of molecular weight, source, and photobleaching of chromophoric dissolved organic matter. Limnology and Oceanography 53, 955–969. https://doi.org/10.4319/lo.2008.53.3.0955

Henderson, R.K., Baker, A., Murphy, K.R., Hambly, A., Stuetz, R.M., Khan, S.J., 2009. Fluorescence as a potential monitoring tool for recycled water systems: A review. Water Research 43, 863–881. https://doi.org/10.1016/j.watres.2008.11.027

Her, N., Amy, G., Foss, D., Cho, J., Yoon, Y., Kosenka, P., 2002. Optimization of Method for Detecting and Characterizing NOM by HPLC−Size Exclusion Chromatography with UV and On-Line DOC Detection. Environ. Sci. Technol. 36, 1069–1076. https://doi.org/10.1021/es015505j

Her, N., Amy, G., McKnight, D., Sohn, J., Yoon, Y., 2003. Characterization of DOM as a function of MW by fluorescence EEM and HPLC-SEC using UVA, DOC, and fluorescence detection. Water Research 37, 4295–4303. https://doi.org/10.1016/S0043-1354(03)00317-8

Hornstra, L.M., Rodrigues da Silva, T., Blankert, B., Heijnen, L., Beerendonk, E., Cornelissen, E.R., Medema, G., 2019. Monitoring the integrity of reverse osmosis membranes using

novel indigenous freshwater viruses and bacteriophages. Environ. Sci.: Water Res. Technol. 5, 1535–1544. https://doi.org/10.1039/C9EW00318E

Hosen, J.D., McDonough, O.T., Febria, C.M., Palmer, M.A., 2014. Dissolved Organic Matter Quality and Bioavailability Changes Across an Urbanization Gradient in Headwater Streams. Environ. Sci. Technol. 48, 7817–7824. https://doi.org/10.1021/es501422z

Hosseini, R., Yang, K., Chen, A., Patra, S., 2021a. A flexible forecasting model for production systems.

Hosseini, R., Yang, K., Patra, S., Rachit, A., 2021b. Greykite: a flexible, intuitive and fast forecasting library.

Hu, H.-Y., Du, Y., Wu, Q.-Y., Zhao, X., Tang, X., Chen, Z., 2016. Differences in dissolved organic matter between reclaimed water source and drinking water source. Science of The Total Environment 551–552, 133–142. https://doi.org/10.1016/j.scitotenv.2015.12.111

Huber, S.A., Balz, A., Abert, M., Pronk, W., 2011. Characterisation of aquatic humic and non-humic matter with size-exclusion chromatography – organic carbon detection – organic nitrogen detection (LC-OCD-OND). Water Research 45, 879–885. https://doi.org/10.1016/j.watres.2010.09.023

Hudson, N., Baker, A., Reynolds, D., 2007. Fluorescence analysis of dissolved organic matter in natural, waste and polluted waters—a review. River Research and Applications 23, 631–649. https://doi.org/10.1002/rra.1005

Huguet, A., Vacher, L., Relexans, S., Saubusse, S., Froidefond, J.M., Parlanti, E., 2009. Properties of fluorescent dissolved organic matter in the Gironde Estuary. Organic Geochemistry 40, 706–719. https://doi.org/10.1016/j.orggeochem.2009.03.002

Hur, J., Cho, J., 2012. Prediction of BOD, COD, and Total Nitrogen Concentrations in a Typical Urban River Using a Fluorescence Excitation-Emission Matrix with PARAFAC and UV Absorption Indices. Sensors 12, 972–986. https://doi.org/10.3390/s120100972

Hutta, M., Góra, R., Halko, R., Chalányová, M., 2011. Some theoretical and practical aspects in the separation of humic substances by combined liquid chromatography methods. Journal of Chromatography A 1218, 8946–8957. https://doi.org/10.1016/j.chroma.2011.06.107

Ignatev, A., Tuhkanen, T., 2019. Step-by-step analysis of drinking water treatment trains using size-exclusion chromatography to fingerprint and track protein-like and humic/fulvic-like fractions of dissolved organic matter. Environ. Sci.: Water Res. Technol. 5, 1568–1581. https://doi.org/10.1039/C9EW00340A

Jones, M.N., Bryan, N.D., 1998. Colloidal properties of humic substances. Advances in Colloid and Interface Science 78, 1–48. https://doi.org/10.1016/S0001-8686(98)00058-X

Kaplan, J.B., 2010. Biofilm Dispersal: Mechanisms, Clinical Implications, and Potential Therapeutic Uses. J Dent Res 89, 205–218. https://doi.org/10.1177/0022034509359403

Kadeli, L., 2012. 2012 Guidelines for Water Reuse. USEPA.

Kaushal, S.S., Lewis, W.M., 2003. Patterns in the Chemical Fractionation of Organic Nitrogen in Rocky Mountain Streams. Ecosystems 6, 483–492.

Keller, A.A., Su, Y., Jassby, D., 2022. Direct Potable Reuse: Are We Ready? A Review of Technological, Economic, and Environmental Considerations. ACS EST Eng. 2, 273–291. https://doi.org/10.1021/acsestengg.1c00258

Kennison, S.M., Chan-Tin, E., 2020. Taking Risks With Cybersecurity: Using Knowledge and Personal Characteristics to Predict Self-Reported Cybersecurity Behaviors. Front. Psychol. 11, 546546. https://doi.org/10.3389/fpsyg.2020.546546

Klise, K.A., 2016. Performance Monitoring using Pecos.

Klise, K.A., Stein, Joshua S., 2016. Automated performance monitoring for PV systems using pecos. Presented at the 2016 IEEE 43rd Photovoltaic Specialists Conference (PVSC), pp. 3431–3435. https://doi.org/10.1109/PVSC.2016.7750304

Korak, J.A., Dotson, A.D., Summers, R.S., Rosario-Ortiz, F.L., 2014. Critical analysis of commonly used fluorescence metrics to characterize dissolved organic matter. Water Research 49, 327–338. https://doi.org/10.1016/j.watres.2013.11.025

Korak, J.A., Rosario-Ortiz, F.L., Summers, R.S., 2015. Evaluation of optical surrogates for the characterization of DOM removal by coagulation. Environ. Sci.: Water Res. Technol. 1, 493–506. https://doi.org/10.1039/C5EW00024F

Korak, J., Arias-Paic, M., 2016. Monitoring Strategies for Direct Reuse of Reclaimed Water (Research No. 2016- 0365– 01). U.S. Department of the Interior, Bureau of Reclamation, Denver, CO.

Kuchmenko, Lvova, 2019. A Perspective on Recent Advances in Piezoelectric Chemical Sensors for Environmental Monitoring and Foodstuffs Analysis. Chemosensors 7, 39. https://doi.org/10.3390/chemosensors7030039

Lakowicz, J.R., 2006. Principles of Fluorescence Spectroscopy, 3rd ed. Springer, New York, NY.

Lappin-Scott, H.M., Bass, C., 2001. Biofilm formation: Attachment, growth, and detachment of microbes from surfaces. American Journal of Infection Control 29, 250–251. https://doi.org/10.1067/mic.2001.115674

Law, S., 2019. STUMPY: A Powerful and Scalable Python Library for Time Series Data Mining. JOSS 4, 1504. https://doi.org/10.21105/joss.01504

Lawaetz, A.J., Stedmon, C.A., 2009. Fluorescence intensity calibration using the Raman scatter peak of water. Appl Spectrosc 63, 936–940. https://doi.org/10.1366/000370209788964548

Leenheer, J.A., 2009. Systematic Approaches to Comprehensive Analyses of Natural Organic Matter. Annals of Environmental Science 3.

Leresche, F., McKay, G., Kurtz, T., von Gunten, U., Canonica, S., Rosario-Ortiz, F.L., 2019. Effects of Ozone on the Photochemical and Photophysical Properties of Dissolved Organic Matter. Environ. Sci. Technol. 53, 5622–5632. https://doi.org/10.1021/acs.est.8b06410

Leresche, F., Torres-Ruiz, J.A., Kurtz, T., Gunten, U. von, Rosario-Ortiz, F.L., 2021. Optical properties and photochemical production of hydroxyl radical and singlet oxygen after ozonation of dissolved organic matter. Environ. Sci.: Water Res. Technol. 7, 346–356. https://doi.org/10.1039/D0EW00878H

Leresche, F., Vialykh, E.A., Rosario-Ortiz, F.L., 2022. Computational Calculation of Dissolved Organic Matter Absorption Spectra. Environ. Sci. Technol. 56, 491–500. https://doi.org/10.1021/acs.est.1c06252

Lerner, J., Tirole, J., 2001. The open source movement: Key research questions. European Economic Review 45, 819–826. https://doi.org/10.1016/S0014-2921(01)00124-6

Leskinen, S.D., Lim, D.V., 2008. Rapid Ultrafiltration Concentration and Biosensor Detection of Enterococci from Large Volumes of Florida Recreational Water. Appl Environ Microbiol 74, 4792–4798. https://doi.org/10.1128/AEM.00052-08

Li, P., Hur, J., 2017. Utilization of UV-Vis spectroscopy and related data analyses for dissolved organic matter (DOM) studies: A review. Critical Reviews in Environmental Science and Technology 47, 131–154. https://doi.org/10.1080/10643389.2017.1309186

Looveren, V., Arnaud, K., Vacanti, J., Cobb, G., Scillitoe, O., Samoilescu, A., Roberts, 2019. Alibi Detect: Algorithms for outlier, adversarial and drift detection.

Lorenzo-Seva, U., ten Berge, J.M.F., 2006. Tucker's congruence coefficient as a meaningful index of factor similarity. Methodology: European Journal of Research Methods for the Behavioral and Social Sciences 2, 57–64. https://doi.org/10.1027/1614-2241.2.2.57

Maie, N., Scully, N.M., Pisani, O., Jaffé, R., 2007. Composition of a protein-like fluorophore of dissolved organic matter in coastal wetland and estuarine ecosystems. Water Research 41, 563–570. https://doi.org/10.1016/j.watres.2006.11.006

McAdams, B.C., Aiken, G.R., McKnight, D.M., Arnold, W.A., Chin, Y.-P., 2018. High Pressure Size Exclusion Chromatography (HPSEC) Determination of Dissolved Organic Matter Molecular Weight Revisited: Accounting for Changes in Stationary Phases, Analytical Standards, and Isolation Methods. Environ. Sci. Technol. 52, 722–730. https://doi.org/10.1021/acs.est.7b04401

McKay, G., Korak, J.A., Erickson, P.R., Latch, D.E., McNeill, K., Rosario-Ortiz, F.L., 2018. The Case Against Charge Transfer Interactions in Dissolved Organic Matter Photophysics. Environ. Sci. Technol. 52, 406–414. https://doi.org/10.1021/acs.est.7b03589

McKay, G., 2020. Emerging investigator series: critical review of photophysical models for the optical and photochemical properties of dissolved organic matter. Environ. Sci.: Processes Impacts 22, 1139–1165. https://doi.org/10.1039/D0EM00056F

McKnight, D.M., Boyer, E.W., Westerhoff, P.K., Doran, P.T., Kulbe, T., Andersen, D.T., 2001. Spectrofluorometric characterization of dissolved organic matter for indication of precursor organic material and aromaticity. Limnology and Oceanography 46, 38–48. https://doi.org/10.4319/lo.2001.46.1.0038

Morris, T.M., 1987. THE RELATIONSHIP BETWEEN HAZE AND THE SIZE OF PARTICLES IN BEER. Journal of the Institute of Brewing 93, 13–17. https://doi.org/10.1002/j.2050-0416.1987.tb04468.x

Mostafa, S., Korak, J.A., Shimabuku, K., Glover, C.M., Rosario-Ortiz, F.L., 2014. Relation between Optical Properties and Formation of Reactive Intermediates from Different Size Fractions of Organic Matter, in: Advances in the Physicochemical Characterization of Dissolved Organic Matter: Impact on Natural and Engineered Systems, ACS Symposium Series. American Chemical Society, United States, pp. 159–179. https://doi.org/10.1021/bk-2014-1160.ch008

Murphy, K.R., Stedmon, C.A., Waite, T.D., Ruiz, G.M., 2008. Distinguishing between terrestrial and autochthonous organic matter sources in marine environments using fluorescence spectroscopy. Marine Chemistry 108, 40–58. https://doi.org/10.1016/j.marchem.2007.10.003

Murphy, S.F., 2003. Comprehensive water quality of the Boulder Creek Watershed, Colorado, during high-flow and low-flow conditions, 2000 (USGS Numbered Series No. 03–4045), Comprehensive water quality of the Boulder Creek Watershed, Colorado, during high-flow and low-flow conditions, 2000, Water-Resources Investigations Report. U.S. Geological Survey, Reston, VA. https://doi.org/10.3133/wri034045

National Research Council, 2004. Indicators for Waterborne Pathogens. National Academic Press, Washington, D.C.

Nelson, N., Madnick, S., n.d. Studying the Tension Between Digital Innovation and Cybersecurity.

Nguyen, T., Westerhoff, P., Furlong, E.T., Kolpin, D.W., Batt, A.L., Mash, H.E., Schenck, K.M., Boone, J.S., Rice, J., Glassmeyer, S.T., 2018. Modeled De Facto Reuse and Contaminants of Emerging Concern in Drinking Water Source Waters: Modeled De Facto Reuse and Contaminants of Emerging Concern in Drinking Water Source Waters. Journal - American Water Works Association 110, E2–E18. https://doi.org/10.1002/awwa.1052

Nikolaou, A.D., Lekkas, T.D., 2001. The Role of Natural Organic Matter during Formation of Chlorination By-products: A Review. Acta hydrochimica et hydrobiologica 29, 63–77. https://doi.org/10.1002/1521-401X(200109)29:2/3<63::AID-AHEH63>3.0.CO;2-C

Nikolaou, A.D., Golfinopoulos, S.K., Lekkas, T.D., Kostopoulou, M.N., 2004. DBP Levels in Chlorinated Drinking Water: Effect of Humic Substances. Environ Monit Assess 93, 301–319. https://doi.org/10.1023/B:EMAS.0000016798.53163.43

Nöthe, T., Fahlenkamp, H., Sonntag, C. von, 2009. Ozonation of Wastewater: Rate of Ozone Consumption and Hydroxyl Radical Yield. Environ. Sci. Technol. 43, 5990–5995. https://doi.org/10.1021/es900825f

OCWD, 2021. Reverse Osmosis: Getting the Credit it Deserves.

Olivieri, A.W., Pecson, B., Crook, J., Hultquist, R., 2020. California water reuse—Past, present and future perspectives, in: Advances in Chemical Pollution, Environmental Management and Protection. Elsevier, pp. 65–111. https://doi.org/10.1016/bs.apmp.2020.07.002

Ostarcevic, E., Jacangelo, J., Gray, S., Cran, M., 2018. Current and Emerging Techniques for High-Pressure Membrane Integrity Testing. Membranes 8, 60. https://doi.org/10.3390/membranes8030060

Parlanti, E., 2000. Dissolved organic matter Fuorescence spectroscopy as a tool to estimate biological activity in a coastal zone submitted to anthropogenic inputs. Organic Geochemistry 17.

Pavlik, J.W., Perdue, E.M., 2015. Number-Average Molecular Weights of Natural Organic Matter, Hydrophobic Acids, and Transphilic Acids from the Suwannee River, Georgia, as Determined Using Vapor Pressure Osmometry. Environmental Engineering Science 32, 23–30. https://doi.org/10.1089/ees.2014.0269

Pecson, B.M., Trussell, R.S., Pisarenko, A.N., Trussell, R.R., 2015. Achieving Reliability in Potable Reuse: The Four Rs. Journal - American Water Works Association 107, 48–58. https://doi.org/10.5942/jawwa.2015.107.0047

Pepper, I.L., Snyder, S., 2016. Monitoring for reliability and process control of potable reuse applications. Water Environment and Reuse Foundation and IWA Publishing.

Perdue, E.M., Ritchie, J.D., 2003. 5.10 - Dissolved Organic Matter in Freshwaters, in: Holland, H.D., Turekian, K.K. (Eds.), Treatise on Geochemistry. Elsevier, Oxford, UK, pp. 273–318. https://doi.org/10.1016/B0-08-043751-6/05080-5

Petrova, O.E., Sauer, K., 2009. A Novel Signaling Network Essential for Regulating Pseudomonas aeruginosa Biofilm Development. PLoS Pathog 5, e1000668. https://doi.org/10.1371/journal.ppat.1000668

Peuravuori, J., Pihlaja, K., 1997. Molecular size distribution and spectroscopic properties of aquatic humic substances. Analytica Chimica Acta 337, 133–149. https://doi.org/10.1016/S0003-2670(96)00412-6

Piccolo, A., 2001. THE SUPRAMOLECULAR STRUCTURE OF HUMIC SUBSTANCES: Soil Science 166, 810–832. https://doi.org/10.1097/00010694-200111000-00007

Pozdnyakov, I.P., Pigliucci, A., Tkachenko, N., Plyusnin, V.F., Vauthey, E., Lemmetyinen, H., 2009. The photophysics of salicylic acid derivatives in aqueous solution. Journal of Physical Organic Chemistry 22, 449–454. https://doi.org/10.1002/poc.1489

Pype, M.-L., 2015. National Validation Guidelines for Water Recycling: Reverse Osmosis Membranes.

Ravichandran, M., 2004. Interactions between mercury and dissolved organic matter—a review. Chemosphere 55, 319–331. https://doi.org/10.1016/j.chemosphere.2003.11.011

Remucal, C.K., Cory, R.M., Sander, M., McNeill, K., 2012. Low Molecular Weight Components in an Aquatic Humic Substance As Characterized by Membrane Dialysis and Orbitrap Mass Spectrometry. Environ. Sci. Technol. 46, 9350–9359. https://doi.org/10.1021/es302468q

Renaud, K., Zimmermann, V., Schürmann, T., Böhm, C., 2021. Exploring cybersecurity-related emotions and finding that they are challenging to measure. Humanit Soc Sci Commun 8, 75. https://doi.org/10.1057/s41599-021-00746-5

Reynolds, D.M., 2003. Rapid and direct determination of tryptophan in water using synchronous fluorescence spectroscopy. Water Research 37, 3055–3060. https://doi.org/10.1016/S0043-1354(03)00153-2

Riopel, R., Caron, F., Siemann, S., 2014. Fluorescence Characterization of Natural Organic Matter at a Northern Ontario Wastewater Treatment Plant. Water Air Soil Pollut 225, 2126. https://doi.org/10.1007/s11270-014-2126-3

Rocha-Gaso, M.-I., March-Iborra, C., Montoya-Baides, Á., Arnau-Vives, A., 2009. Surface Generated Acoustic Wave Biosensors for the Detection of Pathogens: A Review. Sensors 9, 5740–5769. https://doi.org/10.3390/s90705740

Rock, C., Hoppe-Jones, C., Daniels, K., Brassil, N., Hooper, J., Vandegrift, J., Goldman, J., 2019. Assessment of Techniques to Evaluate Water Quality from Direct and Indirect Potable Reuse Facilities (No. WRF 4508). Water Research Foundation.

Ruhala, S.S., Zarnetske, J.P., 2017. Using in-situ optical sensors to study dissolved organic carbon dynamics of streams and watersheds: A review. Science of The Total Environment 575, 713–723. https://doi.org/10.1016/j.scitotenv.2016.09.113

Sandron, S., Rojas, A., Wilson, R., Davies, N.W., Haddad, P.R., Shellie, R.A., Nesterenko, P.N., Kelleher, B.P., Paull, B., 2015. Chromatographic methods for the isolation, separation and characterisation of dissolved organic matter. Environ. Sci.: Processes Impacts 17, 1531–1567. https://doi.org/10.1039/C5EM00223K

Sauer, K., Camper, A.K., Ehrlich, G.D., Costerton, J.W., Davies, D.G., 2002. Pseudomonas aeruginosa Displays Multiple Phenotypes during Development as a Biofilm. J Bacteriol 184, 1140–1154. https://doi.org/10.1128/jb.184.4.1140-1154.2002

Sauer, K., Stoodley, P., Goeres, D.M., Hall-Stoodley, L., Burmølle, M., Stewart, P.S., Bjarnsholt, T., 2022. The biofilm life cycle: expanding the conceptual model of biofilm formation. Nat Rev Microbiol 20, 608–620. https://doi.org/10.1038/s41579-022-00767-0

Schmidt, C.K., Brauch, H.-J., 2008. N,N -Dimethylsulfamide as Precursor for N -Nitrosodimethylamine (NDMA) Formation upon Ozonation and its Fate During Drinking Water Treatment. Environ. Sci. Technol. 42, 6340–6346. https://doi.org/10.1021/es7030467

Sgroi, M., Roccaro, P., Korshin, G.V., Vagliasindi, F.G.A., 2017. Monitoring the Behavior of Emerging Contaminants in Wastewater-Impacted Rivers Based on the Use of Fluorescence Excitation Emission Matrixes (EEM). Environ. Sci. Technol. 51, 4306–4316. https://doi.org/10.1021/acs.est.6b05785

Singer, P.C., 1999. Humic substances as precursors for potentially harmful disinfection by-products. Water Science and Technology 40, 25–30. https://doi.org/10.1016/S0273-1223(99)00636-8

Singer, H.P., Wössner, A.E., McArdell, C.S., Fenner, K., 2016. Rapid Screening for Exposure to "Non-Target" Pharmaceuticals from Wastewater Effluents by Combining HRMS-Based Suspect Screening and Exposure Modeling. Environ. Sci. Technol. 50, 6698–6707. https://doi.org/10.1021/acs.est.5b03332

Song, Y., Breider, F., Ma, J., von Gunten, U., 2017. Nitrate formation during ozonation as a surrogate parameter for abatement of micropollutants and the N-nitrosodimethylamine (NDMA) formation potential. Water Research 122, 246–257. https://doi.org/10.1016/j.watres.2017.05.074

Song, Z.-M., Xu, Y.-L., Liang, J.-K., Peng, L., Zhang, X.-Y., Du, Y., Lu, Y., Li, X.-Z., Wu, Q.-Y., Guan, Y.-T., 2021. Surrogates for on-line monitoring of the attenuation of trace organic contaminants during advanced oxidation processes for water reuse. Water Research 190, 116733. https://doi.org/10.1016/j.watres.2020.116733

Stedmon, C.A., Markager, S., Kaas, H., 2000. Optical Properties and Signatures of Chromophoric Dissolved Organic Matter (CDOM) in Danish Coastal Waters. Estuarine, Coastal and Shelf Science 51, 267–278. https://doi.org/10.1006/ecss.2000.0645

Stedmon, C.A., Markager, S., Bro, R., 2003. Tracing dissolved organic matter in aquatic environments using a new approach to fluorescence spectroscopy. Marine Chemistry 82, 239–254. https://doi.org/10.1016/S0304-4203(03)00072-0

Stedmon, C.A., Nelson, N.B., 2015. Chapter 10 - The Optical Properties of DOM in the Ocean, in: Hansell, D.A., Carlson, C.A. (Eds.), Biogeochemistry of Marine Dissolved Organic Matter (Second Edition). Elsevier Science, Netherlands, pp. 481–508. https://doi.org/10.1016/B978-0-12-405940-5.00010-8

Stewart, A.J., Wetzel, R.G., 1980. Fluorescence: absorbance ratios—a molecular-weight tracer of dissolved organic matter1. Limnology and Oceanography 25, 559–564. https://doi.org/10.4319/lo.1980.25.3.0559

Stoodley, P., Wilson, S., Hall-Stoodley, L., Boyle, J.D., Lappin-Scott, H.M., Costerton, J.W., 2001. Growth and Detachment of Cell Clusters from Mature Mixed-Species Biofilms. Appl Environ Microbiol 67, 5608–5613. https://doi.org/10.1128/AEM.67.12.5608-5613.2001

Striegel, A.M., Yau, W.W., Kirkland, J.J., Bly, D.D., 2009. Modern Size Exclusion Chromatography Practice of Gel Permeation and Gel Filtration Chromatography, Second Edition. ed. Wiley, Hoboken, NJ.

Stubbins, A., Lapierre, J.-F., Berggren, M., Prairie, Y.T., Dittmar, T., del Giorgio, P.A., 2014. What's in an EEM? Molecular Signatures Associated with Dissolved Organic Fluorescence in Boreal Canada. Environ. Sci. Technol. 48, 10598–10606. https://doi.org/10.1021/es502086e

Summers, R.S., Cornel, P.K., Roberts, P.V., 1987. Molecular Size distribution and Spectroscopic Characterization of Humic Substances. The Science of the Total Environment 62, 27–37. https://doi.org/10.1016/0048-9697(87)90478-5

Swift, R.S., Posner, A.M., 1971. GEL CHROMATOGRAPHY OF HUMIC ACID. Journal of Soil Science 22, 237–249. https://doi.org/10.1111/j.1365-2389.1971.tb01610.x

Szabo, J., 2010. Detection of Biological Suspensions Using Online Detectors in a Drinking Water Distribution System Simulator 26.

Taitt, C.R., Anderson, G.P., Ligler, F.S., 2005. Evanescent wave fluorescence biosensors. Biosensors and Bioelectronics 20, 2470–2487. https://doi.org/10.1016/j.bios.2004.10.026

Tandukar, S., Sherchan, S.P., Haramoto, E., 2020. Applicability of crAssphage, pepper mild mottle virus, and tobacco mosaic virus as indicators of reduction of enteric viruses during wastewater treatment. Sci Rep 10, 3616. https://doi.org/10.1038/s41598-020-60547-9

TCEQ, 2019. Clarification for the Use of an Alternative Technology to Monitor the Turbidity in Drinking Water Produced by Membrane Units at Public Water Systems in Texas.

Tchobanoglous, G., 2015. Framework for direct potable reuse. WateReuse Research Foundation, Alexandria, VA.

Tentscher, P.R., Bourgin, M., von Gunten, U., 2018. Ozonation of Para-Substituted Phenolic Compounds Yields p-Benzoquinones, Other Cyclic α,β-Unsaturated Ketones, and Substituted Catechols. Environ. Sci. Technol. 52, 4763–4773. https://doi.org/10.1021/acs.est.8b00011

Thompson, K.A., Dickenson, E.R.V., 2020. A performance-based indicator chemical framework for potable reuse. AWWA Water Science 2. https://doi.org/10.1002/aws2.1191

Thurman, E.M., Malcolm, R.L., 1981. Preparative isolation of aquatic humic substances. Environ. Sci. Technol. 15, 463–466. https://doi.org/10.1021/es00086a012

Trego, A.C., Mills, S., Collins, G., 2021. Granular biofilms: Function, application, and new trends as model microbial communities. Critical Reviews in Environmental Science and Technology 51, 1702–1725. https://doi.org/10.1080/10643389.2020.1769433

Ulliman, S.L., Korak, J.A., Linden, K.G., Rosario-Ortiz, F.L., 2020. Methodology for selection of optical parameters as wastewater effluent organic matter surrogates. Water Research 170, 115321. https://doi.org/10.1016/j.watres.2019.115321

USEPA, 2017a. 2017 Potable Reuse Compendium (Compendium No. 810 R 17 002). US Environmental Protection Agency.

USEPA, 2017b. Technical Fact Sheet – N-Nitroso-dimethylamine (NDMA) (Technical Fact Sheet No. EPA 505-F-17-005). US Environmental Protection Agency.

van den Broeke, J., Carpentier, C., Moore Colin, 2014. Compemdium of Sensors and Monitors and Their Use in the Global Water Industry. Water Environment Research Foundation, IWA Publishing.

Velapoldi, R.A., Tønnesen, H.H., 2004. Corrected Emission Spectra and Quantum Yields for a Series of Fluorescent Compounds in the Visible Spectral Region. Journal of Fluorescence 14, 465–472. https://doi.org/10.1023/B:JOFL.0000031828.96368.c1

Vikesland, P.J., Wigginton, K.R., 2010. Nanomaterial Enabled Biosensors for Pathogen Monitoring - A Review. Environ. Sci. Technol. 44, 3656–3669. https://doi.org/10.1021/es903704z

Vollmer, F., 2010. Optical microresonators: label-free detection down to single viral pathogens. SPIE Newsroom. https://doi.org/10.1117/2.1201002.002619

von Sonntag, C., von Gunten, U., 2012. Chemistry of Ozone in Water and Wastewater Treatment: From Basic Principles to Applications. IWA Publishing, London, UK. https://doi.org/10.2166/9781780400839

Wang, Z., Cao, J., Meng, F., 2015. Interactions between protein-like and humic-like components in dissolved organic matter revealed by fluorescence quenching. Water Research 68, 404–413. https://doi.org/10.1016/j.watres.2014.10.024

Walker, T., Stanford, B.D., Khan, S., Robillot, C., Snyder, S., Valerdi, R., Dwivedi, S., Vickers, J., 2016. Critical Control Point Assessment to Quantify Robustness and Reliability of Multiple Treatment Barriers of a DPR Scheme (No. WRF 13-03). Water Research Foundation.

Waller, S., 2014. Real-Time Monitoring Tools to Characterize Microbal Contaminants in Reclaimed Water: State-of-the-Science Assessment (No. 11– 06). Water Research Foundation, Alexandria, VA.

Wei, D., Oyarzabal, O.A., Huang, T.-S., Balasubramanian, S., Sista, S., Simonian, A.L., 2007. Development of a surface plasmon resonance biosensor for the identification of Campylobacter jejuni. Journal of Microbiological Methods 69, 78–85. https://doi.org/10.1016/j.mimet.2006.12.002

Weishaar, J.L., Aiken, G.R., Bergamaschi, B.A., Fram, M.S., Fujii, R., Mopper, K., 2003. Evaluation of Specific Ultraviolet Absorbance as an Indicator of the Chemical Composition and Reactivity of Dissolved Organic Carbon. Environ. Sci. Technol. 37, 4702–4708. https://doi.org/10.1021/es030360x

Wenk, J., Aeschbacher, M., Salhi, E., Canonica, S., von Gunten, U., Sander, M., 2013. Chemical Oxidation of Dissolved Organic Matter by Chlorine Dioxide, Chlorine, And Ozone: Effects on Its Optical and Antioxidant Properties. Environ. Sci. Technol. 47, 11147–11156. https://doi.org/10.1021/es402516b

Wert, E., Rosarioortiz, F., Drury, D., Snyder, S., 2007. Formation of oxidation byproducts from ozonation of wastewater. Water Research 41, 1481–1490. https://doi.org/10.1016/j.watres.2007.01.020

WHO, 2017. Water Quality and Health - Review of Turbidity: Information for regulators and water suppliers (Technical Brief No. WHO/FWC/WSH/17.01). World Health Organization.

Wigand, M.C., Dangles, O., Brouillard, R., 1992. Complexation of a fluorescent anthocyanin with purines and polyphenols. Phytochemistry 31, 4317–4324. https://doi.org/10.1016/0031-9422(92)80466-R

Wildeboer, D., Amirat, L., Price, R.G., Abuknesha, R.A., 2010. Rapid detection of Escherichia coli in water using a hand-held fluorescence detector. Water Research 44, 2621–2628. https://doi.org/10.1016/j.watres.2010.01.020

Wu, Q.-Y., Zhou, T.-H., Du, Y., Ye, B., Wang, W.-L., Hu, H.-Y., 2020. Characterizing the molecular weight distribution of dissolved organic matter by measuring the contents of electron-donating moieties, UV absorbance, and fluorescence intensity. Environment International 137, 105570. https://doi.org/10.1016/j.envint.2020.105570

Wünsch, U.J., Murphy, K.R., Stedmon, C.A., 2015. Fluorescence Quantum Yields of Natural Organic Matter and Organic Compounds: Implications for the Fluorescence-based Interpretation of Organic Matter Composition. Frontiers in Marine Science 2.

Wünsch, U.J., Murphy, K.R., Stedmon, C.A., 2017. The One-Sample PARAFAC Approach Reveals Molecular Size Distributions of Fluorescent Components in Dissolved Organic Matter. Environ. Sci. Technol. 51, 11900–11908. https://doi.org/10.1021/acs.est.7b03260

Wünsch, U.J., Stedmon, C.A., Tranvik, L.J., Guillemette, F., 2018. Unraveling the size-dependent optical properties of dissolved organic matter. Limnology and Oceanography 63, 588–601. https://doi.org/10.1002/lno.10651

Wünsch, U.J., Hawkes, J.A., 2020. Mathematical chromatography deciphers the molecular fingerprints of dissolved organic matter. Analyst 145, 1789–1800. https://doi.org/10.1039/C9AN02176K

Würth, C., Grabolle, M., Pauli, J., Spieles, M., Resch-Genger, U., 2011. Comparison of Methods and Achievable Uncertainties for the Relative and Absolute Measurement of Photoluminescence Quantum Yields. Anal. Chem. 83, 3431–3439. https://doi.org/10.1021/ac2000303

Yamashita, Y., Tanoue, E., 2003. Chemical characterization of protein-like fluorophores in DOM in relation to aromatic amino acids. Marine Chemistry 82, 255–271. https://doi.org/10.1016/S0304-4203(03)00073-2

Yamashita, Y., Tanoue, E., 2004. Chemical characteristics of amino acid-containing dissolved organic matter in seawater. Organic Geochemistry 35, 679–692. https://doi.org/10.1016/j.orggeochem.2004.02.007

Yasui, M., Iso, H., Torii, S., Matsui, Y., Katayama, H., 2021. Applicability of pepper mild mottle virus and cucumber green mottle mosaic virus as process indicators of enteric virus removal by membrane processes at a potable reuse facility. Water Research 206, 117735. https://doi.org/10.1016/j.watres.2021.117735

Yoon, S.-H., 2019. Potential and limitation of fluorescence-based membrane integrity monitoring (FMIM) for reverse osmosis membranes. Water Research 154, 287–297. https://doi.org/10.1016/j.watres.2019.02.001

Yu, H.-W., Anumol, T., Park, M., Pepper, I., Scheideler, J., Snyder, S.A., 2015. On-line sensor monitoring for chemical contaminant attenuation during UV/H2O2 advanced oxidation process. Water Research 81, 250–260. https://doi.org/10.1016/j.watres.2015.05.064

Zhang, C., Hu, J., 2010. Single Quantum Dot-Based Nanosensor for Multiple DNA Detection. Anal. Chem. 82, 1921–1927. https://doi.org/10.1021/ac9026675

Zhuang, J., Li, M., Pu, Y., Ragauskas, A., Yoo, C., 2020. Observation of Potential Contaminants in Processed Biomass Using Fourier Transform Infrared Spectroscopy. Applied Sciences 10, 4345. https://doi.org/10.3390/app10124345

Appendix

Appendix A

A-1 Materials and Methods

A-1.1 Chemicals

Table A.1 List Chemicals and Sources. Chemicals and sources used in the study. **Note:** IHSS refers to the International Humic Substances Society

Chemical	Source	Batch
Monosodium Diphosphate (NaH_2PO_4)	Sigma Aldrich	
Disodium hydrogen phosphate (Na_2HPO_4)	Sigma Aldrich	
Sodium Sulfate (Na_2SO_4)	Sigma Aldrich	
Sulfuric Acid (H_2SO_4)	Sigma Aldrich	
Salicylic Acid ($C_7H_6O_3$)	Sigma Aldrich	
Potassium Hydrogen Phthalate (KHP)		
Suwannee River Fulvic Acid (SRFA)	IHSS	2S101F
Pony Lake Fulvic Acid (PLFA)	IHSS	1R109F

A-1.2 Analytical Methods

UV-Visible absorbance spectra and fluorescence excitation emission matrices (EEMs) were measured to (i) compute spectral metrics on bulk water samples (including Φ_f) and (ii) verify optical properties of the size exclusion chromatography (SEC) system. Bulk water spectral measurements were conducted to verify in-line Φ_f determinations. All environmental samples were filtered with a DI flushed PES 0.45 um filter. Environmental samples and IHSS DOM isolates were adjusted to a conductivity = ~6.8 mS/cm and pH = 6.8 prior to optical analyses to match the pH and conductivity of the SEC mobile phase.

A-1.2.1 UV-Absorbance

Bulk water DOM absorbance spectra were measured on a Hach DR 6000 (Hach Company, CO, USA) spectrophotometer using 1 cm quartz cuvettes for a wavelength range of 200-800 nm. Lamp output was verified on a Holmium reference cell. All environmental sample and IHSS isolate spectra were blanked with conductivity and pH-adjusted deionized water that matched the adjustment necessary to the individual samples. UV-Visible absorbance spectra were collected to calculate absorbance metrics of carbon normalized specific UV absorbance at 254 and 280 nm ($SUVA_{254}$ and $SUVA_{280}$) and slope ratio (Table A.2).

A-1.2.2 Fluorescence

Fluorescence excitation emission matrices (EEMs) were collected using a Horiba Jobin Yvon Fluoromax-4 (Horiba, Japan). EEMs were produced over an excitation wavelength range of 240–450 nm over 10 nm increments and an emission range of 300–600 nm over 2 nm increments in a 1-cm quartz cuvettes. Fluorescence spectra were collected with an excitation and emission bandpass set to 5 nm and integration time of 0.25 in signal/reference ratio mode. EEM corrections of primary and secondary inner-filter effects, Raman water normalization, and blank subtraction were performed with MATLAB (Mathworks, MA) software.(Korak et al., 2014b) Briefly, inner-filter effects were corrected using the corresponding absorbance spectra.(Lakowicz, 2006) The dissolved organic carbon concentration (DOC) of isolates and environmental samples were at or adjusted to less than $< 10\ mg_C\ L^{-1}$ to reduce inner filter effects as well.(Hudson et al., 2007) EEMs were normalized by the Raman peak area of deionized water (resistivity ≥18.2MΩ-cm), collected at an excitation wavelength of 350 nm during the time of EEM collection.(Lawaetz and Stedmon, 2009) Corrected EEMs are presented in normalized Raman Units (RU). Lastly, EEMs were also blanked with deionized water adjusted to the conductivity and pH of the SEC mobile phase (6.8

mS/cm and pH = 6.8). First and second order Rayleigh-scattering were corrected for by blank subtraction followed by interpolation across the excised EEM area. Fluorescence metric references, definitions, and results of absorptivity metrics are reported in Table A.3. All spectral metrics were computed in MATLAB. Fluorescence Φ_f on bulk water EEMs were calculated for excitations of 240-450 nm with quinine sulfate (QS) in 0.1 N sulfuric acid as a reference. EEM Φ_f were computed in MATLAB following previously described standard methods.(McKay et al., 2018) Bulk water Φ_f data is presented in Figure A.5.

A-1.2.3 Total Organic Carbon

Bulk water total organic carbon (TOC) concentration was measured using a Sievers M5310C Total Organic Carbon (TOC) analyzer (Suez Water Technologies, CO, USA), independently of the in-line DOC detection connected to the SEC system. SEC-TOC results were analyzed by the Suez Sievers M9, which can be configured to an online mode of analysis, and then connected in-line to the HPSEC system following the absorbance and fluorescence detectors. Because the M9 is not an Agilent module (as were each of the other HPSEC components), data was transferred in real-time from the M9 to Agilent Chemstation Software in units of mV. These units are arbitrary with respect to TOC, and it is desired to convert them back to units of TOC concentration measured by the M9 ($mg_C\ L^{-1}$ or ppm). However, because the samples were all filtered through 0.45 μm PES filters, results from analysis by TOC instruments are referred to as DOC rather than TOC throughout the text. To generate a calibration curve, potassium hydrogen phthalate (KHP) was injected into the HPSEC system at several concentrations ranging from 0.05 – 10 $mg_C\ L^{-1}$. The peak measurements captured in Chemstation (mV) were then compared to the peak measurements of the raw data exported from the M9 instrument ($mg_C\ L^{-1}$ TOC) and a calibration factor was generated for the conversion.

A-1.2.4 Sample Collection

Natural water samples were collected from several locations along Boulder Creek (Boulder, CO USA), between the exit of Boulder Canyon (sample BC-100), and just before it crosses 75th Street, and from South Boulder Creek (SBC) just before the junction with Boulder Creek (see Figure A.1 for sample locations). Samples were collected in 250 mL bottles positioned pointing upstream at least 1 foot offshore with a minimum stream depth 6-8 inches. Glass bottles were DI rinsed and sample rinsed before samples were collected. Samples were filtered using 0.45 μm polyether sulfone (PES) filters. Filters were flushed using 300 mL of DI water and were sample rinsed prior to sample filtration to reduce carbon leaching from the filters. DI water was filtered, stored, and transported in the same method as described for the samples to account for possible error in field methods.

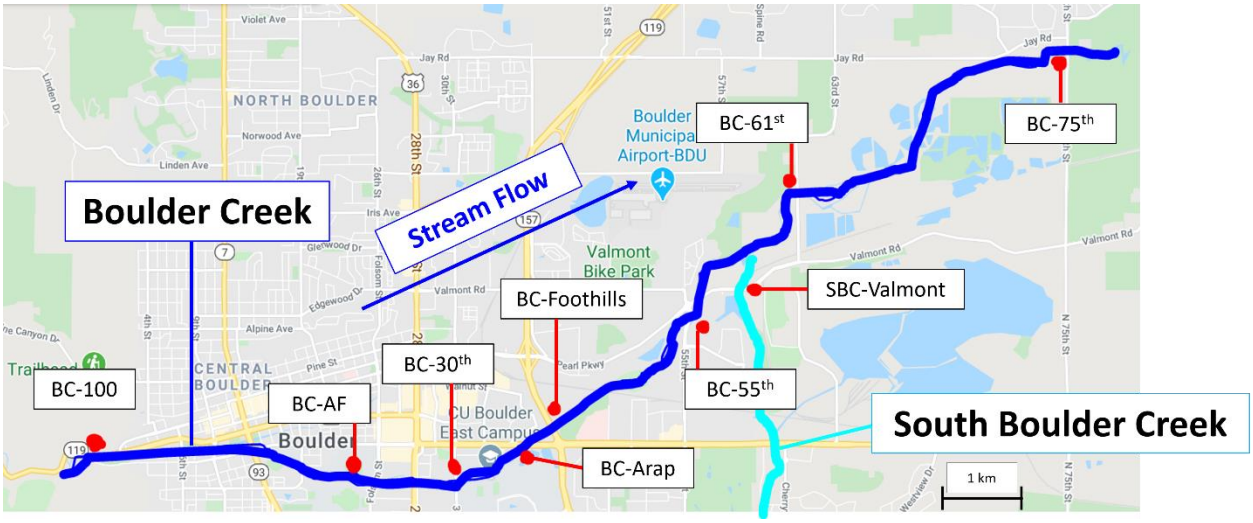

Figure A.1 Map of Boulder Creek and South Boulder Creek Sampling Locations (Boulder, CO, USA).

A-2 Results and Discussion

A-2.1 Bulk Water Analysis Results

Bulk water Boulder Creek DOC, absorbance scans and 3D EEMs were collected to characterize bulk samples by spectral metrics, compute Φ_f of bulk water DOM, and verify optical properties of the SEC system (Figures A.2-A.5, Tables A.2 and A.3). The $SUVA_{254}$ decreased from 2.09 to 1.50 moving from upstream to downstream Boulder Creek, suggesting some decreasing aromaticity with downstream flow, agreeing with previously observed $SUVA_{254}$ values of surface waters (Table A.2).(Hansen et al., 2016; Weishaar et al., 2003b) Additional optical metrics calculated include the E_2:E_3 ratio which was greatest downstream of the pond from South Boulder Creek at Valmont Road (SBC-Valmont) (Table A.2).(Peuravuori and Pihlaja, 1997) Peak A:C ratios offer a concentration independent metric to quantify changes across commonly observed fluorescence maxima.(Ulliman et al., 2020b) Changes in fluorescence index (FI), humification index (HIX), and A:C ratios did not vary notably from upstream to downstream sites (Table A.2). In contrast, both specific peaks A and C (fluorescence intensity divided by DOC concentration) increased moving downstream through the city of Boulder).

Table A.2 Absorbance Metrics for Boulder Samples. Absorbance metrics,(Helms et al., 2008; Peuravuori and Pihlaja, 1997; Stedmon et al., 2000; Weishaar et al., 2003b) and results for upstream Boulder Creek (BC-100) to downstream (BC-75th) samples collected through the city of Boulder. Properties of IHSS reference isolate Suwanee River Fulvic Acid (SRFA) are also reported.

DOM Sample	$SUVA_{280}$ ($L\ mg_C^{-1}\ m^{-1}$)	$SUVA_{254}$ ($L\ mg_C^{-1}\ m^{-1}$)	$E_2:E_3$	Spectral $Slope_{300-650}$	Slope Ratio Sr
BC-100	1.51	2.09	6.06	0.81	1.00
BC-AF	1.61	2.10	5.10	0.72	0.93
BC-30th	1.56	2.06	5.00	0.66	0.95
BC-Arap	1.64	2.20	5.22	0.64	0.88
BC-55th	2.17	1.63	5.18	--	0.95
SBC-Valmont	1.38	2.00	7.64	0.66	1.05
BC-61st		1.96		--	
BC-75th	1.12	1.50	5.88	0.52	0.87
SRFA	3.35	2.62	4.09	1.0	0.65

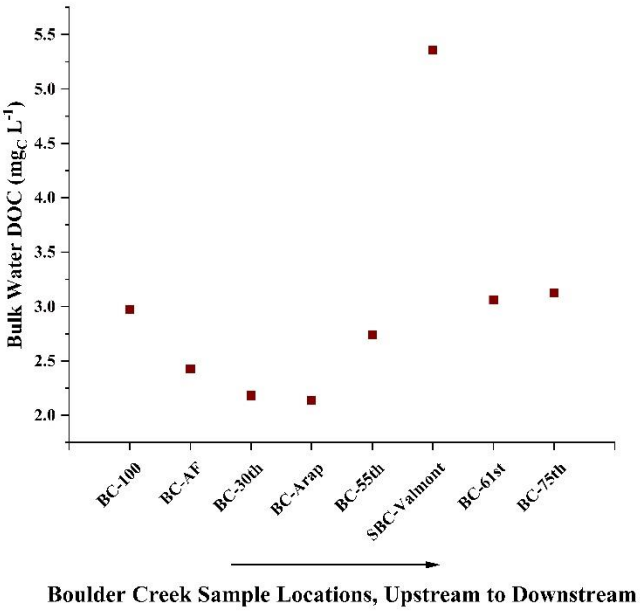

Figure A.2 Bulk Water DOC Data for Boulder Creek Samples. Bulk water dissolved organic carbon (DOC) concentrations along Boulder Creek. Input from a pond terminating South Boulder Creek near Valmont Road (SBC-Valmont) is also indicated.

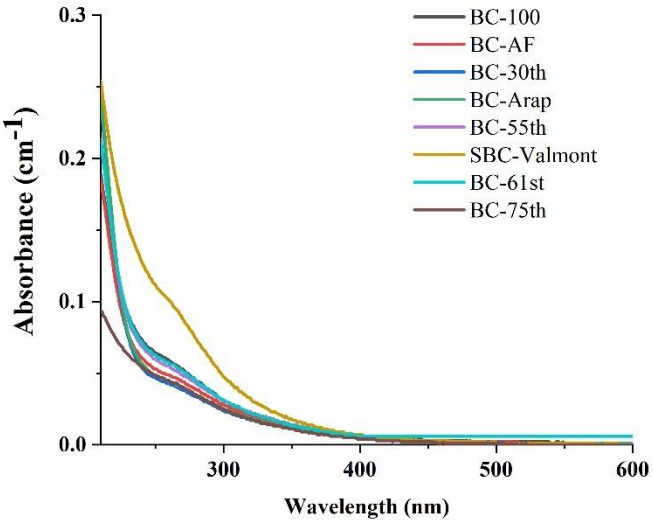

Figure A.3 Bulk water Absorbance Spectra for Boulder Creek Samples. Absorbance (cm^{-1}) scans of bulk water Boulder Creek (BC) samples from October 17, 2019 The legend is organized vertically from upstream to downstream locations.

Bulk water Boulder Creek EEMs indicated the presence of classically described "fulvic acid-like" and "humic acid-like" (peaks A and C, respectively) using the common labeling and descriptive schemes in Coble et al. 1990,(P. G. Coble et al., 1990) previously observed in freshwater ecosystems (Figure A.4).(Fellman et al., 2010; Ferrari et al., 1996; Gabor et al., 2014) Φ_f determined from EEMs increased in bulk water samples moving downstream (Figure A.5). EEM Φ_f has been previously shown to be a statistically robust, intrinsic optical measure that can distinguish wastewater and freshwater mixing.(Ulliman et al., 2020b)

Previous studies have examined biogeochemical drivers for changes in DOM of EEM-based Φ_f. Apparent Φ_f of DOM has been previously observed to increase with increased algal production (i.e., release of polyphenols), or DOM aging in oceanic water masses at depth, in connection to cumulative microbial metabolism.(Catalá et al., 2015; Ferrari et al., 1996) The

Boulder Creek transect sampled herein represents a freshwater carbon mass with short residence times. Therefore, it is possible that the increase in Φ_f is due to anthropogenic nutrient inputs from the surrounding urban and agricultural land, such as nitrogen and phosphorous, which may stimulate *in situ* algal and/or microbially produced DOM, or inputs of natural DOM of contrasting quality. South Boulder Valmont Pond outflow represented a source of greater DOC (Figure A.2) and higher EEM Φ_f at 350 nm (Figure A.5) than upstream sites – i.e., a pond input of greater residence time or algal/microbial production.

Table A.3 Fluorescence Metrics for Boulder Creek Samples. Fluorescence metrics,(Cory and McKnight, 2005; Hansen et al., 2016; McKnight et al., 2001b) fluorescence index (FI), humification index (HIX), EEMs peak intensities, and peak ratios for upstream Boulder Creek (BC-100) to downstream (BC-75th) samples collected through the city of Boulder. Properties of IHSS reference isolate Suwanee River Fulvic Acid (SRFA) are also reported.

DOM Sample	FI	HIX	Specific Peak A	Specific Peak C	A:C Ratio
BC-100	1.40	0.84	0.17	0.05	3.25
BC-AF	1.43	0.82	0.25	0.08	3.18
BC-30th	1.45	0.75	0.26	0.08	3.15
BC-Arap	1.45	0.86	0.29	0.09	3.19
BC-55th	1.47	0.81	0.33	0.10	3.41
SBC-Valmont	1.44	0.88	0.27	0.08	3.35
BC-61st	1.49	0.80	0.30	0.09	3.44
BC-75th	1.49	0.92	0.28	0.09	3.23
SRFA	1.27	0.89	0.44	0.15	5.15

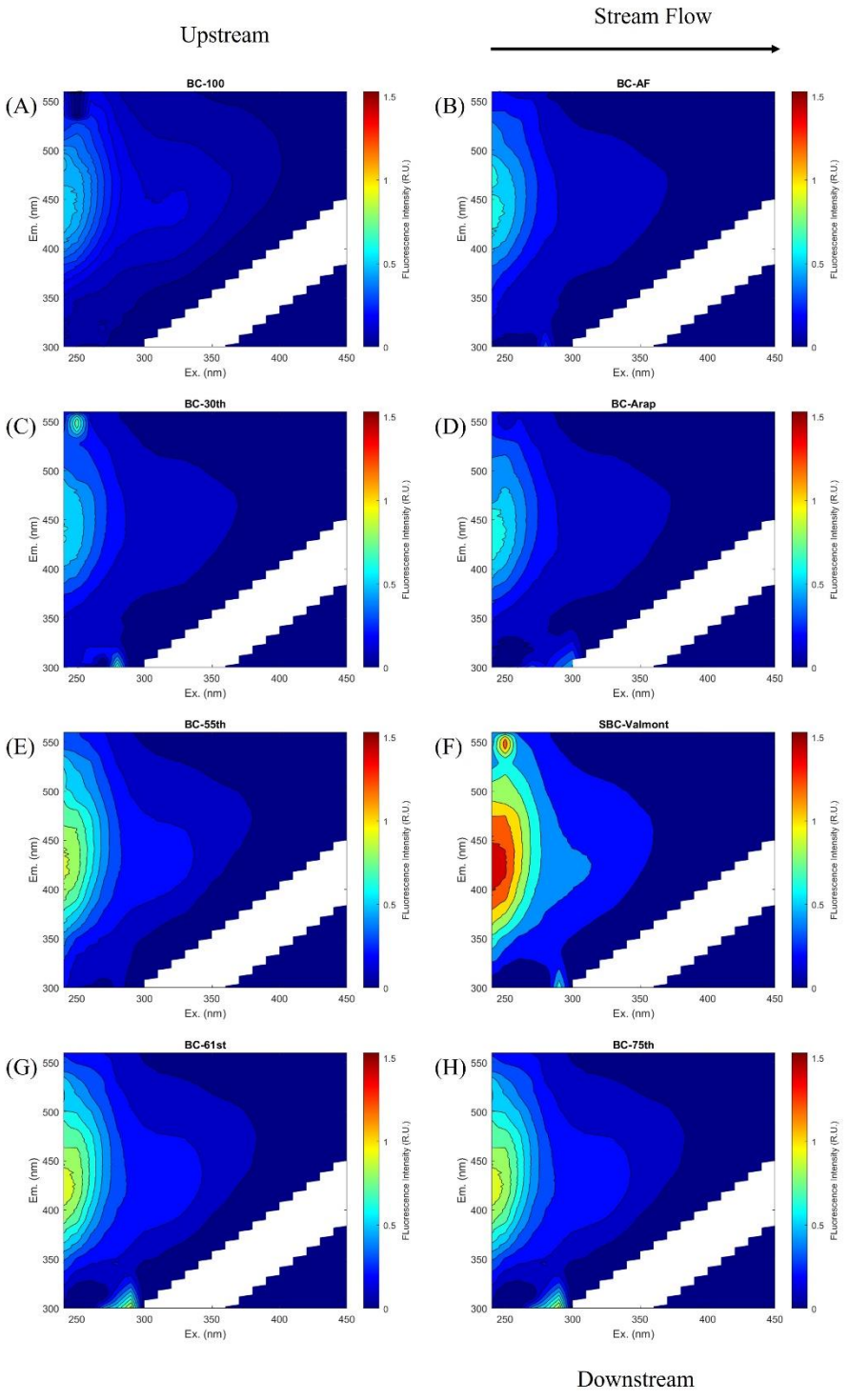

Figure A.4 Bulk Water EEMs for Boulder Creek Samples. Boulder Creek (BC) excitation emission matrices (EEMs) starting upstream at BC-100 (A) and flowing downstream to lower BC-75th (H). For all subplots, excitation wavelengths are plotted on the x-axis and emission wavelengths are plotted on the y-axis EEMs were measured on SEC-mobile phase adjusted (SEC-

spike corrected) bulk water samples. Two EEMs for sampling locations at 55th and 61st street denoted (*) were excluded from Φ_f analysis due to partial scatter corrections that interfered with Φ_f analyses. RU: Raman Units.

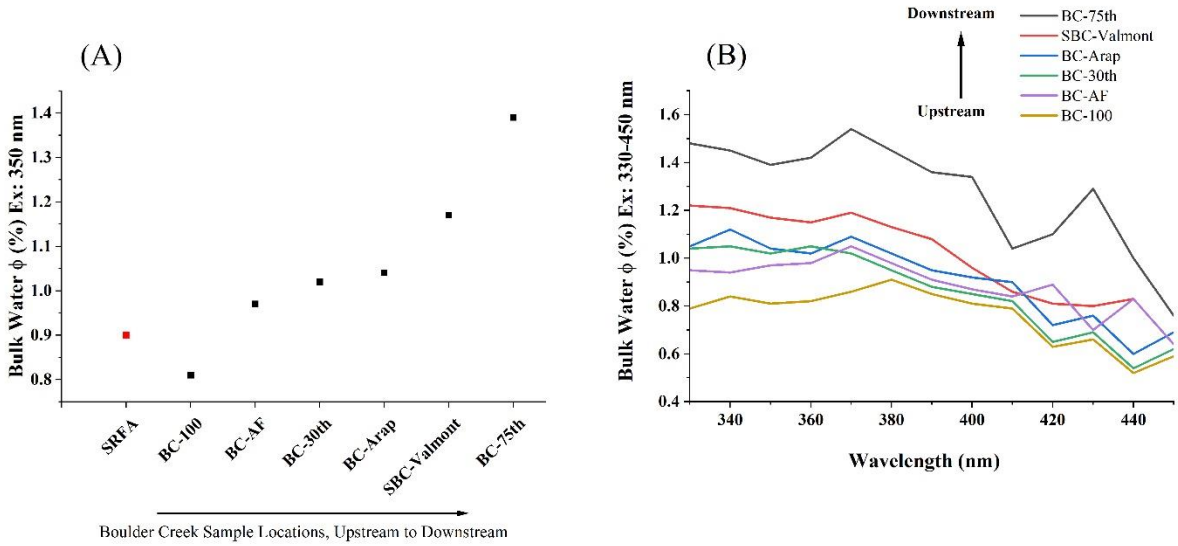

Figure A.5 Bulk Water Φ_F Data for Boulder Creek Samples. Boulder Creek Bulk Water Fluorescent Quantum Yields **A.** Bulk water apparent quantum yields (Φf) for unfractionated dissolved organic matter (DOM) along Boulder Creek (BC), through the city of Boulder collected on October 17, 2019. Input from a pond terminating tributary (South Boulder Creek) near Valmont Road (SBC-Valmont) is also indicated. **B.** Apparent Φf for bulk, unfractionated DOM over an excitation range of 240-450 nm along the Boulder Creek main stem transect, including the pond terminating tributary at Valmont input into lower Boulder Creek.

The bulk water EEMs showed that the apparent Φ_f of DOM increases with stream flow downstream, as urbanization increases. The in-line- Φ_f method provides additional information about the AMW distribution of higher- Φ_f signals entering the system. Increasing Φ_f with lower molecular weight fractions is shown in Figure 4.6 (main text). Based on Hosen et al. (2014), the elevated, low molecular weight Φ_f is likely due to autochthonous algal-produced DOM or microbial exudates (Hosen et al., 2014).

A-2.2 Correction Factors

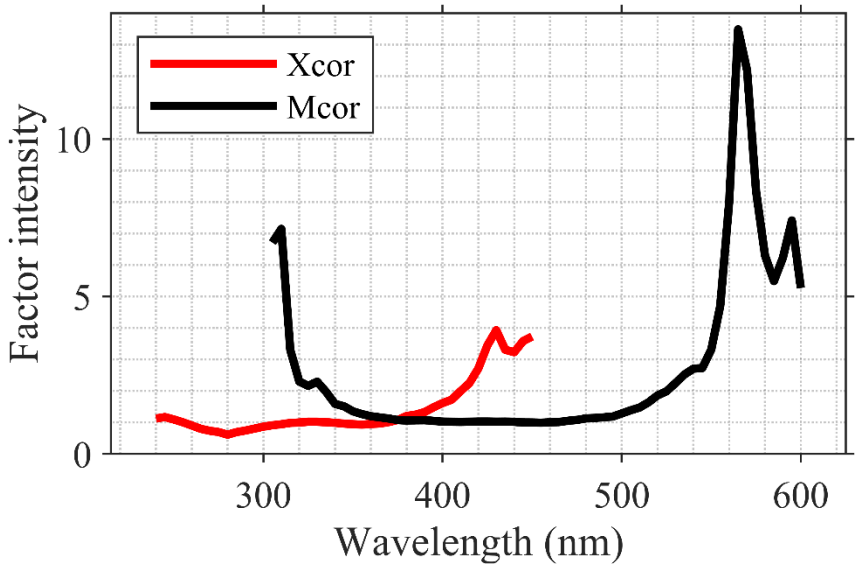

Figure A.6 Correction Factors Developed for the SEC-Fluorescence Detector. Correction factors were developed for the SEC-fluorescence detector by comparing EEMs of SRFA from the SEC-based fluorescence detector to that of an offline benchtop fluorescence detector. Excitation corrections are represented by "Xcor" and span 250-450nm. Emission corrections are represented by "Mcor" and span 300-600nm.

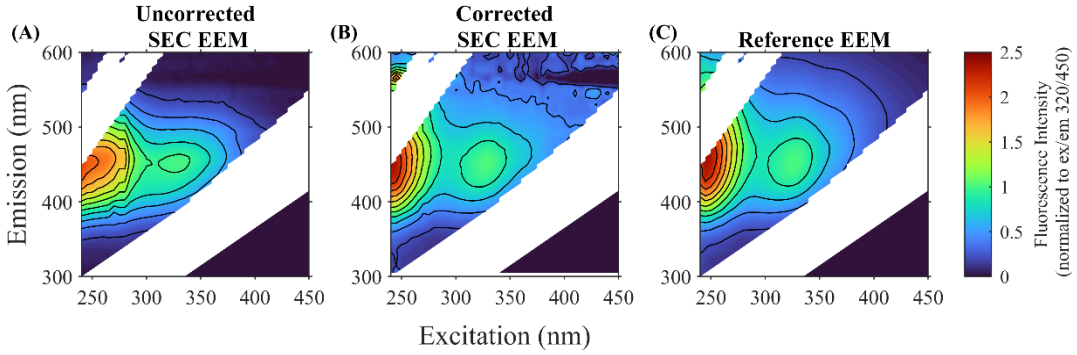

Figure A.7 Comparison of Three-dimensional SEC-Fluorescence Data After Spectral Corrections. Correction factors were applied to Suwannee River Fulvic Acid (SRFA) sample excitation emission matrices (EEMs). **A.** "Uncorrected SED EEM" represents the SRFA EEM generated from the inline SEC-fluorescence detector prior to applying correction factors. **B.** "Corrected SEC EEM" represents the SRFA EEM from the inline SEC-fluorescence detector after correction factors have been applied. **C.** "Reference EEM" represents SRFA EEM generated from a Fluoromax-4 benchtop fluorometer that applies built in correction factors. Excitation wavelengths (λ_{ex}) are plotted on the x-axis and emission wavelengths (λ_{em}) are plotted on the y-axis.

Figure A.7 shows the SRFA sample EEM from the inline SEC-fluorescence detector before and after correction factors are applied (Figure A.7A and A.7B, respectively) and a comparison of the corrected inline SEC-fluorescence detector EEM to a corrected EEM of the same sample from the offline benchtop fluorometer that applies built in correction factors (Figure A.7B and A.7C, respectively). This figure is similar to Figure 4.2 in the main text but also displays the SRFA EEM prior to correction factors being applied (Figure A.7A) for a visual demonstration of the impact of correction factors on inline SEC-fluorescence detector data.

A-2.3 Selection of Φ_f Wavelengths

Figure A.5 shows that for all samples, peak C Φ_f maximums (calculated from bulk water absorbance and fluorescence data) occurred between 325-375nm. This serves as justification for the choice of 350nm as the Φ_f wavelength for the SEC-method development. While Φ_f values at low wavelengths (240-250nm) do exceed those between 325-375nm, the low wavelength Φ_f represents a combination of multiple fluorophore groups (i.e., peaks A, B and/or T) for which individual Φ_f values are difficult to obtain without the use of a statistical deconvolution method such as parallel factor analysis.

A-2.4 Verification of Method Accuracy

Tucker Congruence Coefficient (TCC) were calculated as follows Lorenzo-Seva et. al. (2006) (Lorenzo-Seva and ten Berge, 2006):

eq A-1: $$r_c = \frac{\sum XY}{\sqrt{\sum X^2 \sum Y^2}}$$

where r_c is the Tucker Congruence Coefficient, X and Y are defined as column vectors and in this case represent the ordinate points of a chromatograms normalized to 1. When X and Y points of

individual chromatograms are taken across the same elution volume points (abscissa values), they can be used to compare the congruence of two individual chromatograms.

A-2.5 Percent Error

Percent error used to compare the peak maximum ratios of SRFA at 5.1 and 21.5 $mg_C\ L^{-1}$ (see main text 3.1.3) was calculated as follows:

eq A-3 : $$chromatographic\ maximum\ ratio = \frac{chromatographic\ max\ of\ SRFA\ at\ 5.1\ mg_C\ L^{-1}}{chromatographic\ max\ of\ SRFA\ at\ 21.5\ mg_C\ L^{-1}} = x_s$$

eq A-4 : $$x_{avg} = \frac{x_{s,DOC} + x_{s,absorbance} + x_{s,fluorescence}}{3}$$

eq A-5 : $$Percent\ \text{Error} = \left|\frac{x_{avg} - x_s}{x_{avg}}\right|$$

where x_s is the ratio of the chromatographic maximums of SRFA 5.1 $mg_C\ L^{-1}$ to SRFA $mg_C\ L^{-1}$ for a given signal (DOC, absorbance, and fluorescence) and x_{avg} is the is the mean ratio of all 3 signals.

A-2.6 Examination of DOM from Natural Sources – South Boulder Creek

SEC results from the South Boulder Creek-Boulder Creek (SBC-BC) Junction are shown in Figure A.8B. In large part, the behavior of the each of the individual chromatograms is very similar to that of the Boulder Creek samples (in terms of overall shape, and AMW distribution), including a similar characteristic in-line Φ_f profile. This suggests that the "humic-like" material contained in both BC and SBC likely contain similar fluorophores and is supported by the observed bulk fluorescence (Table A.3, Figure A.4). However, the SBC-Valmont sample (representative of SBC before the junction with BC Φ_f values are lower in intensity than the BC-Foothills sample (representative of BC before the junction with SBC), while the Φ_f values of BC-61st (representing BC and SBC following the junction), fall in between those of the separate bodies of water. These results suggest that using in-line Φ_f, it is possible, at least qualitatively, to detect differences in

DOM signatures contained in different bodies of water, waters receiving different inputs, and/or that of a mixture of the two. Understanding how this quality can be applied, the range of its sensitivity in other ecosystems, and whether it is more useful than other existing methods is beyond the scope of this research and is left to further investigations.

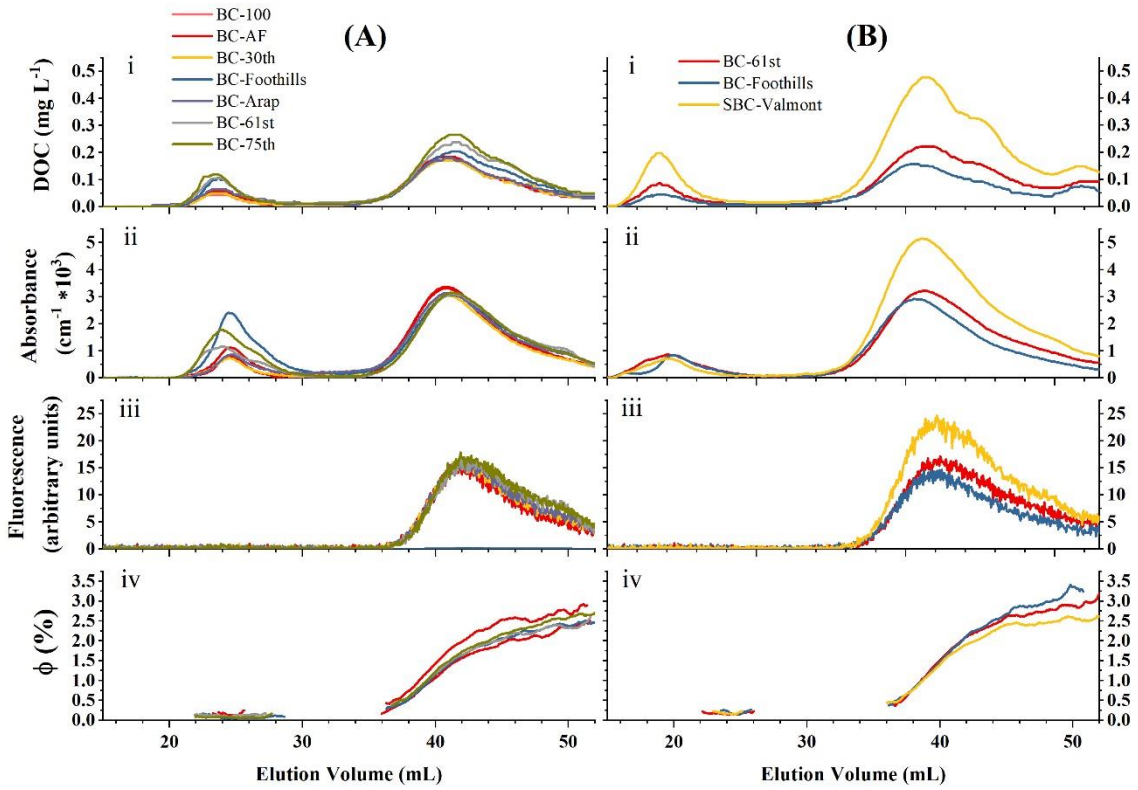

Figure A.8 Additional SEC chromatograms for Bolder Creek and South Boulder Creek Samples. Surface Water SEC Chromatograms **A.** Boulder Creek samples and **B.** South Boulder Creek (.B) natural water samples. **(A.B.i)** Dissolved Organic Carbon (DOC) concentrations, **(A.B.ii)** Absorbance (λ=350 nm), **(A.B.iii)** Fluorescence (λ_{ex}=350 nm, λ_{em}=390-700 nm), and **(A.B.iv)** Fluorescent quantum yield (Φ_f). Φ_f was not calculated when absorbance was below 0.5 mAu. The legends are organized vertically from upstream to downstream locations.

A-2.7 Impact of Ozone on PLFA

A weighted integration was performed to verify Φ_f of AMW fractions align with bulk water Φ_f, found by Leresche et al. (2019) (Table A,4).(Leresche et al., 2019) Various elution

volume intervals were selected as integration boundaries. The area under the absorbance chromatogram was integrated for each time interval and divided by the integration of the entire chromogram, represented by "Absorbance (%)". The Φ_f chromatogram was then integrated across the same time intervals to obtain the total in-line Φ_f in each fraction. Weighted in-line Φ_f values for each fraction were calculated by multiplying total in-line Φ_f values by corresponding UV (%) and then summed to calculate "reconstituted" Φ_f. Reconstituted in-line Φ_f represents a theoretical estimation of bulk water Φ_f values based on the in-line Φ_f data. Note that because in-line Φ_f are only calculated when absorbance is sufficiently high (> 0.5 $cm^{-1}*10^{-1}$), low stock solution concentrations may lead to variable results using this weighted integration method.

Table A.4: Weighted Integration of SEC-Fluorescence Quantum Yield. Absorbance chromatograms were integrated across boundaries defined by the elution volume interval and then divided by the integration of the entire chromatogram (all elution volumes) to obtain Absorbance %. Φ_f chromatograms were integrated across the same elution volume intervals and the integrated value for a given elution volume interval was multiplied by the Absorbance % of the same interval to obtain the "Weighted SEC- Φ_f". Reconstituted values represent the sum of values determined for each elution volume interval. In the far right column, previously reported values of bulk water Φ_f for ozonated SRFA are given.(Leresche et al., 2019)

Sample	Elution Volume Interval (minutes)	Absorbance Integration $(cm^{-1} * 10^{-3})^2$	Absorbance (%)	Weighed SEC- Φ_f	Φ_f Leresche et al., 2019(Leresche et al., 2019)
PLFA Ozone Dose 0.00 $mmol_{O3}$ $mmol_C^{-1}$	30 – 40	122.0	24.7%	0.4%	
	40 – 47.5	231.9	47.0%	1.7%	
	47.5 – 55	140.6	28.5%	2.4%	
	Reconstituted	494.5	100.1%	1.58%	1.45%
PLFA Ozone Dose 0.05 $mmol_{O3}$ $mmol_C^{-1}$	30 – 40	73.8	23.9%	0.8%	
	40 – 47.5	163.8	52.9%	1.9%	
	47.5 – 55	71.5	23.1%	2.6%	
	Reconstituted	309.1	99.9%	1.83%	1.86%
PLFA Ozone Dose 0.10 $mmol_{O3}$ $mmol_C^{-1}$	30 – 40	41.8	21.39%	1.32%	
	40 – 47.5	116.4	59.57%	2.04%	
	47.5 – 55	37.2	19.04%	2.66%	
	Reconstituted	195.4	100.0%	2.00%	1.29%
PLFA Ozone Dose 0.20 $mmol_{O3}$ $mmol_C^{-1}$	30 – 40	23.5	18.1%	1.6%	
	40 – 47.5	105.8	81.2%	2.2%	
	47.5 – 55	9.8	7.6%	2.8%	
	Reconstituted	139.1	106.8%	2.26%	2.24%

A-3. Additional Discussion

For absorbance and fluorescence spectra, there can be multiple chemical groups within a DOM sample (e.g., quinones, phenols, aromatic rings) contributing to the measured optical

signals.(McKay, 2020b) The exact DOM chemical structures leading to a given absorbance or fluorescence spectrum are mostly unknown for any given sample. However, several structural classes of chromophores in DOM have been inferred and identified using advanced analytical methods.(McKay, 2020b) A large proportion of chromophores and fluorophores in DOM are thought to arise from lignin degradation as well as from microbial degradation of lignin-like chemical species in environments without higher plant inputs (e.g., Pony Lake, Antarctica). Under this hypothesis, DOM is mostly composed and/or derived from lignin, so their chromophores are sp^3 isolated aromatic rings that have varying degrees of oxidation or reduction.(McKay, 2020b) This results in reduced hydroxylated or alkoxylated aromatics, and oxidized quinone aromatics or ketone and aldehyde functionalities. Hydroxylated or alkoxylated aromatics may be expected to fluoresce with high quantum yield (Φ_f) and potentially large Stokes shifts (e.g., $\lambda > 150$ nm for 5-aminosalicylate) but has low absorbance beyond 400 nm. Aromatic ketones and aldehydes similarly do not absorb beyond 400 nm depending on functional group substitution.(Pozdnyakov et al., 2009) Conversely, some quinones and their corresponding hydroquinones have the potential to absorb significantly at visible wavelengths; for example, 4- *tert*-butyl-5-methoxy-1,2-benzoquinone has an extinction coefficient of 910 M^{-1} cm^{-1} at 472 nm. 1,4-Napthoquinone absorbs even more in the visible spectrum, with a peak at 514 nm of 2330 M^{-1} cm^{-1}.(Leresche et al., 2022)

Considering fluorescence, chemical moieties with a carbonyl group (C=O) are prone to rapid intermolecular intersystem crossing (producing excited triplet states), and so will exhibit low fluorescence (e.g., aromatic ketones, aldehydes, and quinones). On the other hand, hydroquinones, phenols, hydroxy benzoic acids and other related compounds will fluoresce to a significant extent. A similar analysis targeting the fluorescence of individual compounds was carried out by Wünsch et al., and concluded that it was reasonable to assume that individual compounds may be

contributing to the overall DOM fluorescence signature based on similar signal intensities and expected concentrations.(Wünsch et al., 2015) For more information on the fundamental basis of DOM absorbance and fluorescence, including recent work on the calculation of absorbance spectra for DOM, please refer to work done by the following authors: D'Andrilli et. al. 2013, Wünsch et. al. 2015, Hawkes et. al. 2019, Wünsch and Hawkes 2020, McKay 2020, Leresche et. al. 2022, and D'Andrilli et. al. 2022 (D'Andrilli et al., 2022, 2013b; Hawkes et al., 2019b; Leresche et al., 2022; McKay, 2020b; Wünsch et al., 2015; Wünsch and Hawkes, 2020).

Appendix B

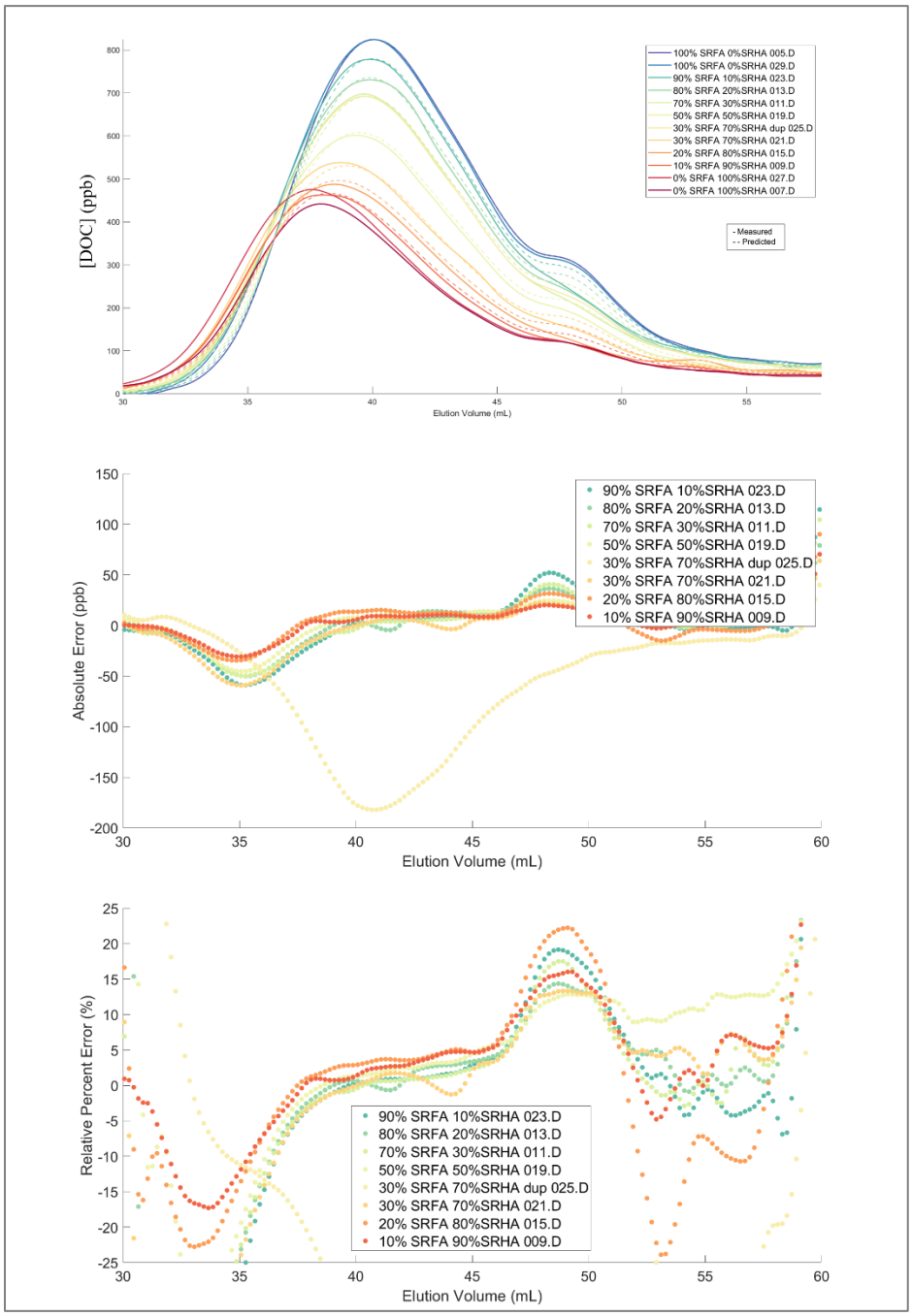

Figure B.1 SRFA/SRHA Blend at Constant UV: DOC Chromatograms and Error. **Top to bottom:** DOC chromatograms (ppb); Absolute error of DOC chromatograms (ppb); relative error (%).

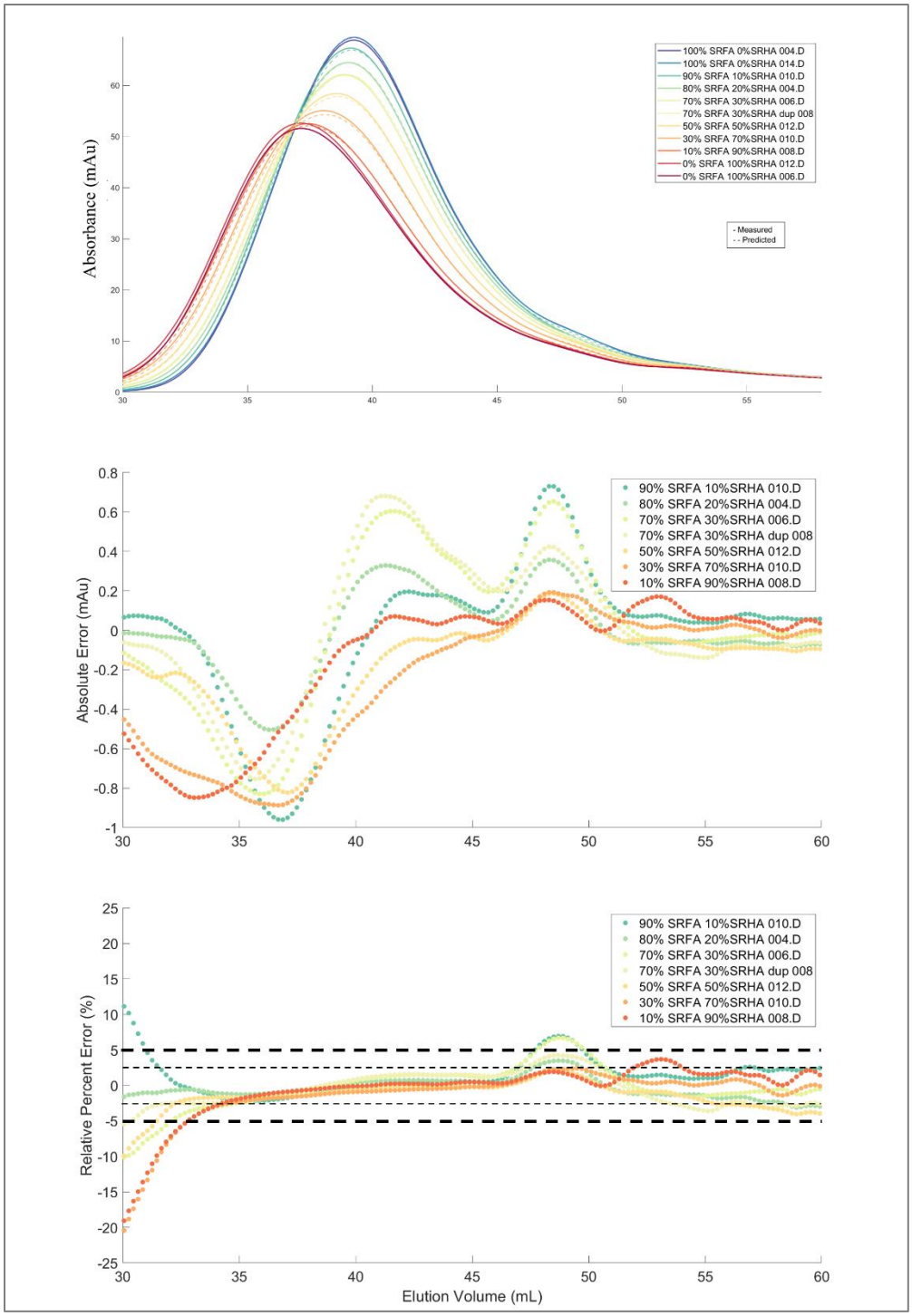

Figure B.2 SRFA/SRHA Blend at Constant UV: Absorbance 275 nm Chromatograms and Error. **Top to bottom:** Absorbance 275 nm chromatograms (mAu); Absolute error of chromatograms (mAu); relative error of chromatograms (%).

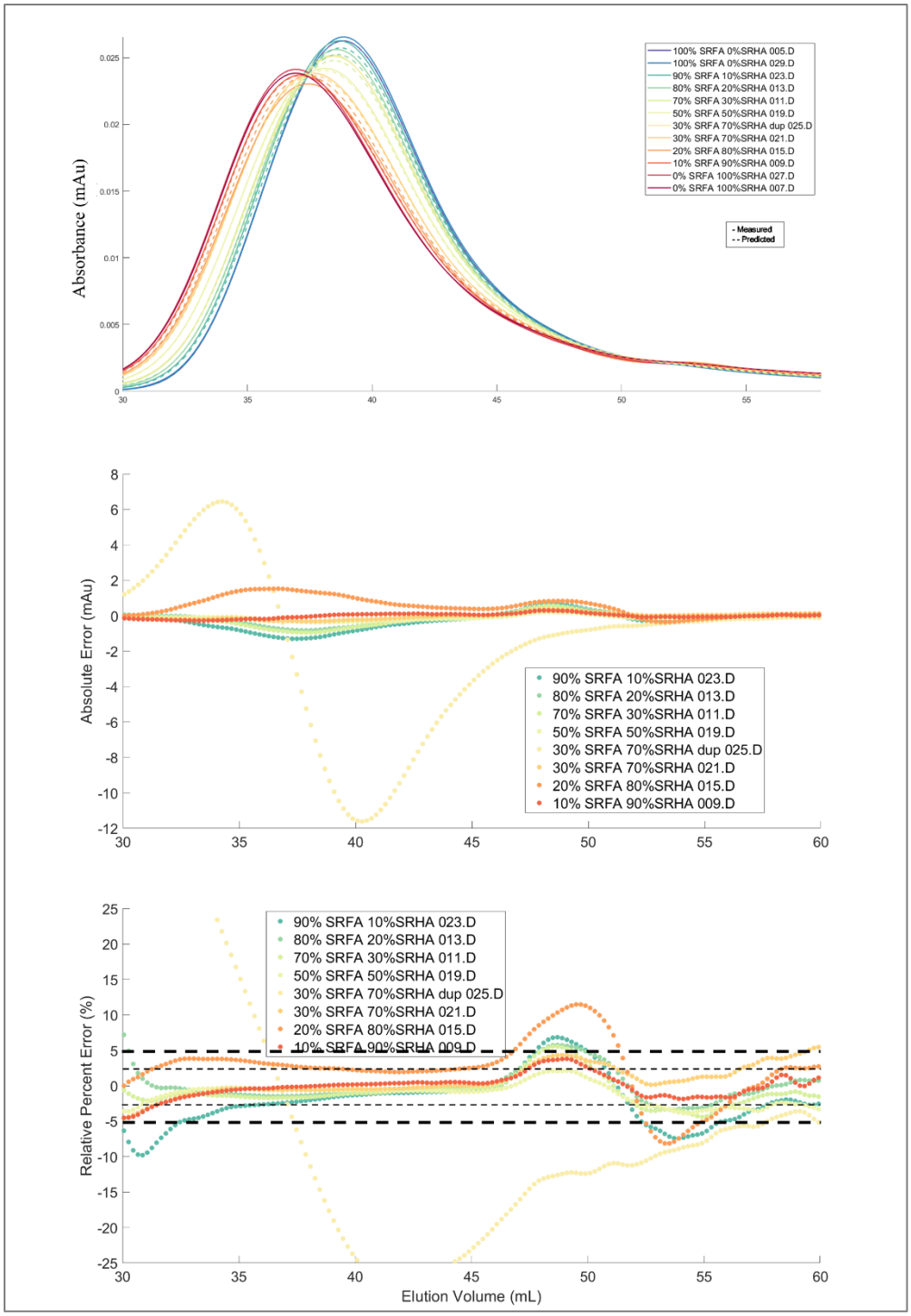

Figure B.3 SRFA/SRHA Blend at Constant UV: Absorbance 350 nm Chromatograms and Error. **Top to bottom** Absorbance 350 nm chromatograms (mAu); Absorbance chromatograms (mAu); relative error (%).

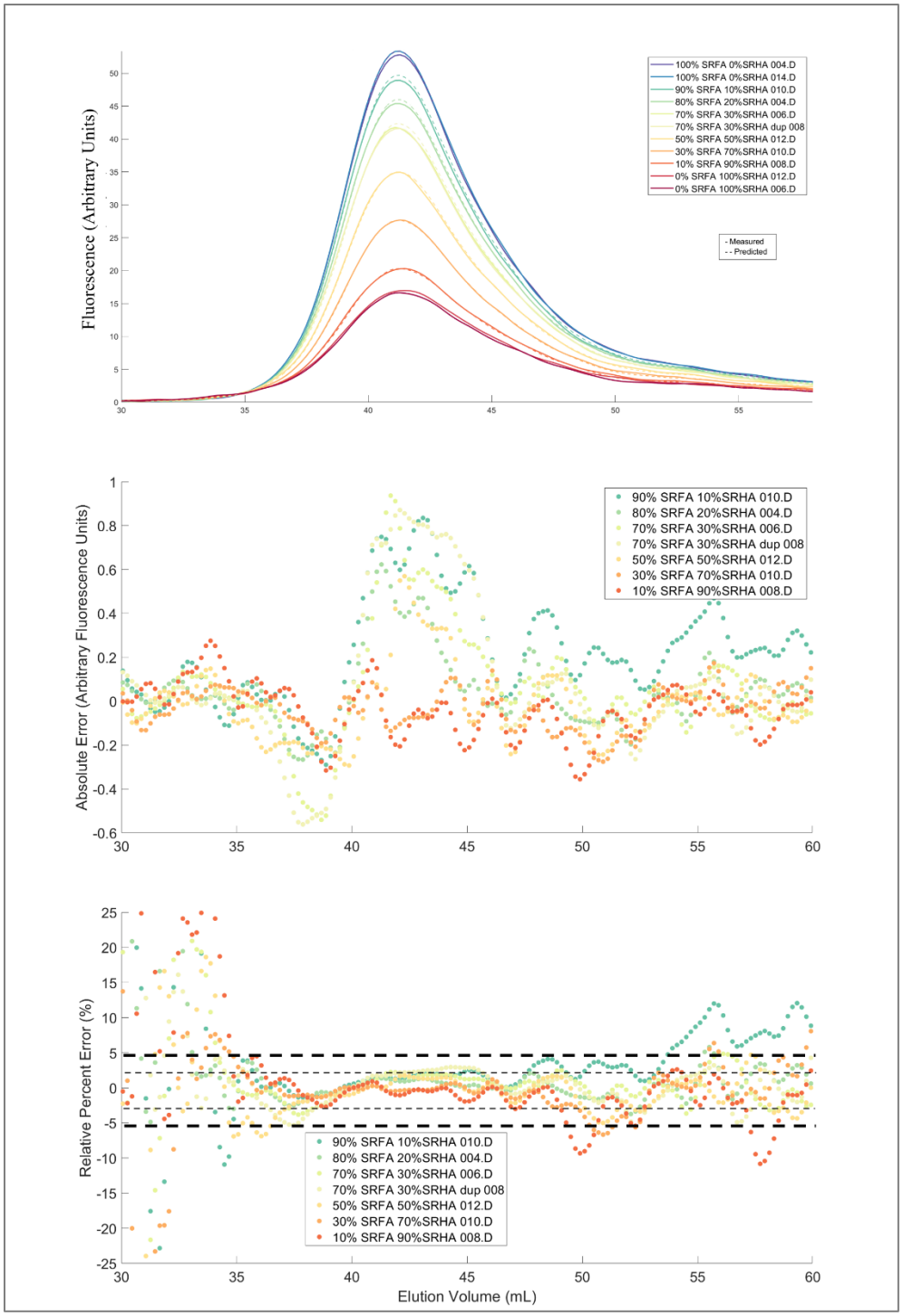

Figure B.4 SRFA/SRHA Blend at Constant UV: λ_{Fex} 275 nm Fluorescence Chromatograms and Error. **Top to bottom** Fluorescence at excitation 275 nm chromatograms (mAu); Absorbance chromatograms (mAu); relative error (%).

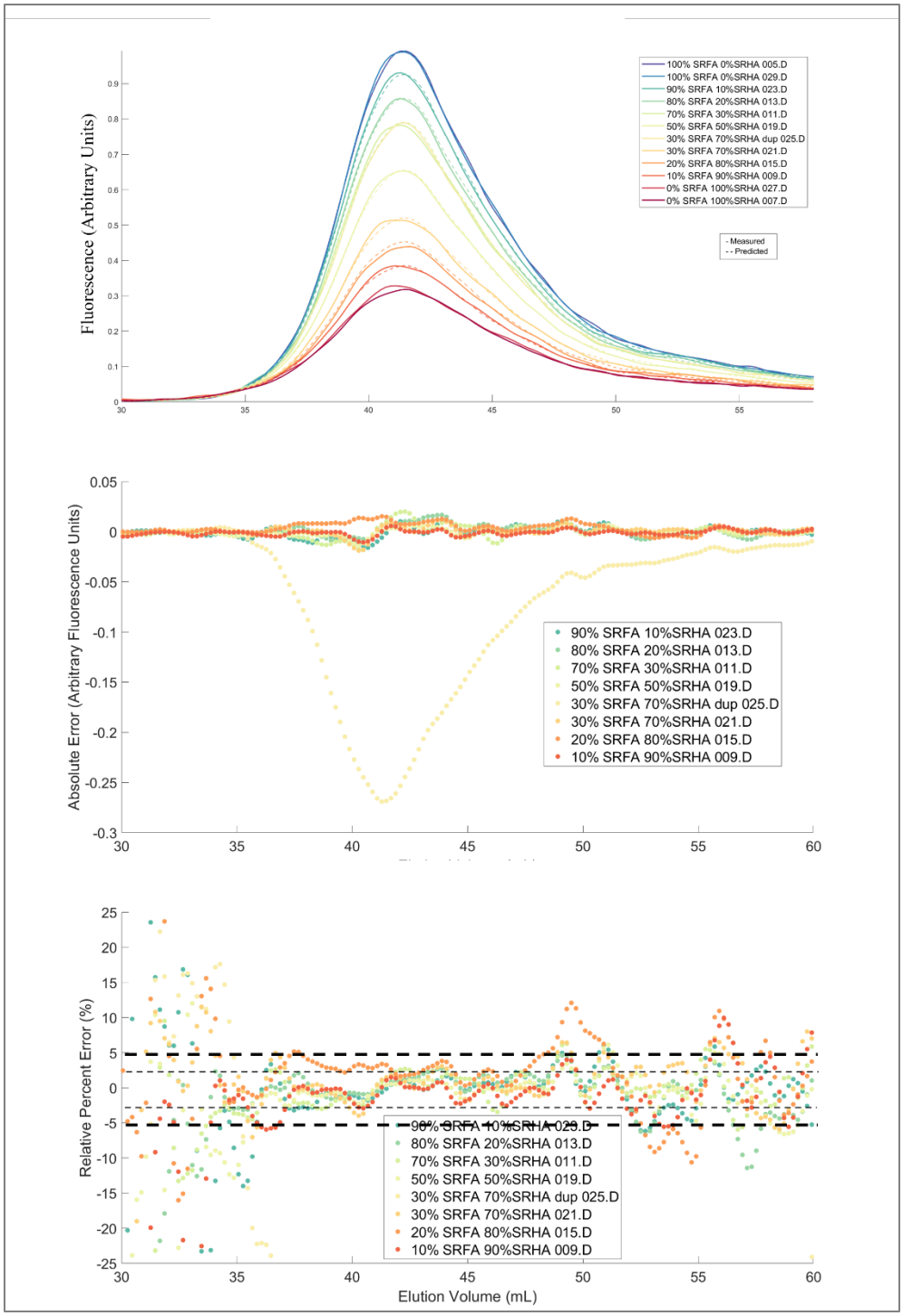

Figure B.5 SRFA/SRHA Blend at Constant UV: λ_{Fex} 350 nm Fluorescence Chromatograms and Error. Top to bottom: Fluorescence at excitation 350 nm chromatograms (mAu); Absorbance chromatograms (mAu); relative error (%).

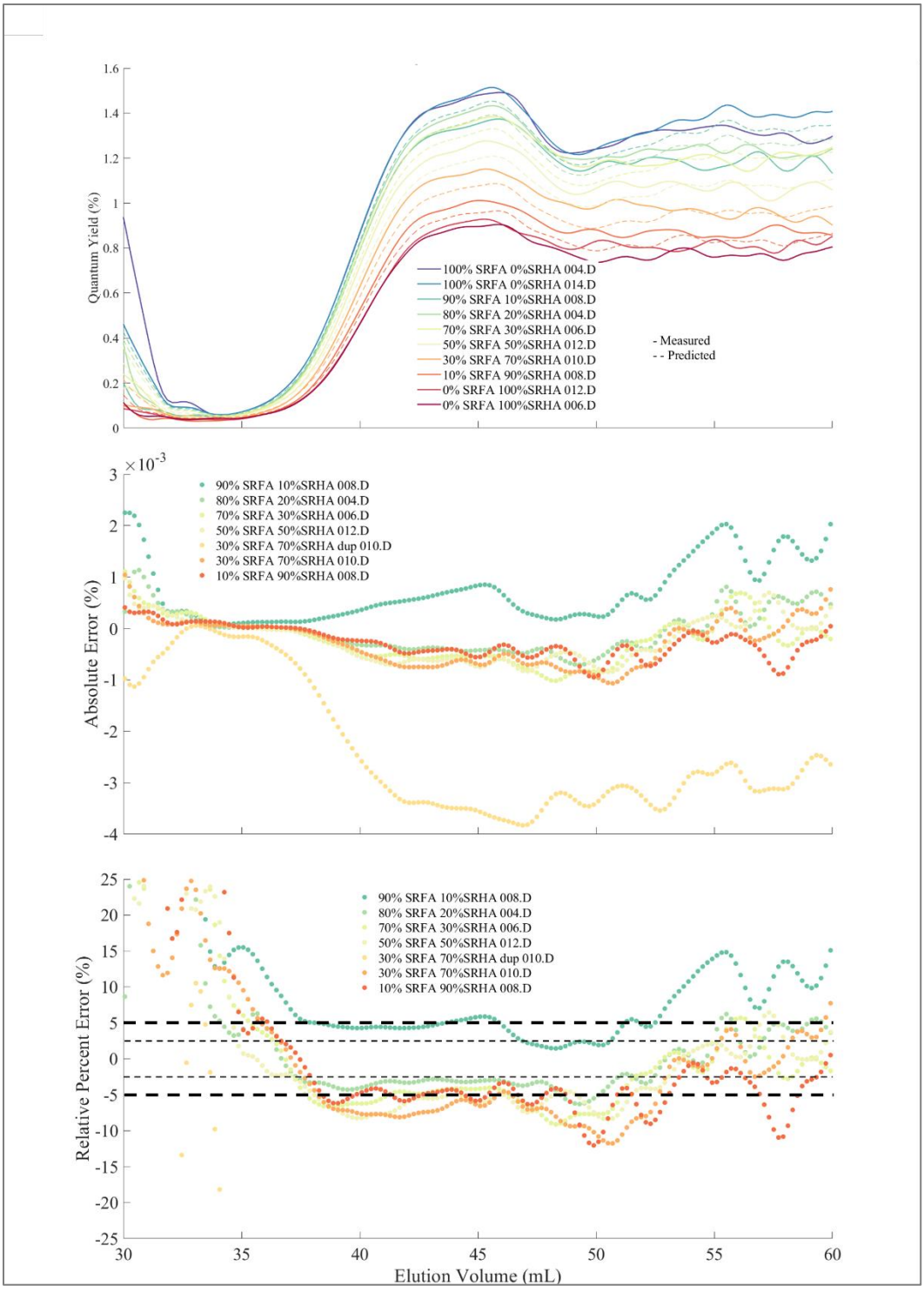

Figure B.6 SRFA/SRHA Blend at Constant DOC: λ_{Fex} 275 nm Φ_F Chromatograms and Error. **Top to bottom:** Fluorescence at excitation 275 nm chromatograms (mAu); Absorbance chromatograms (mAu); relative error (%).

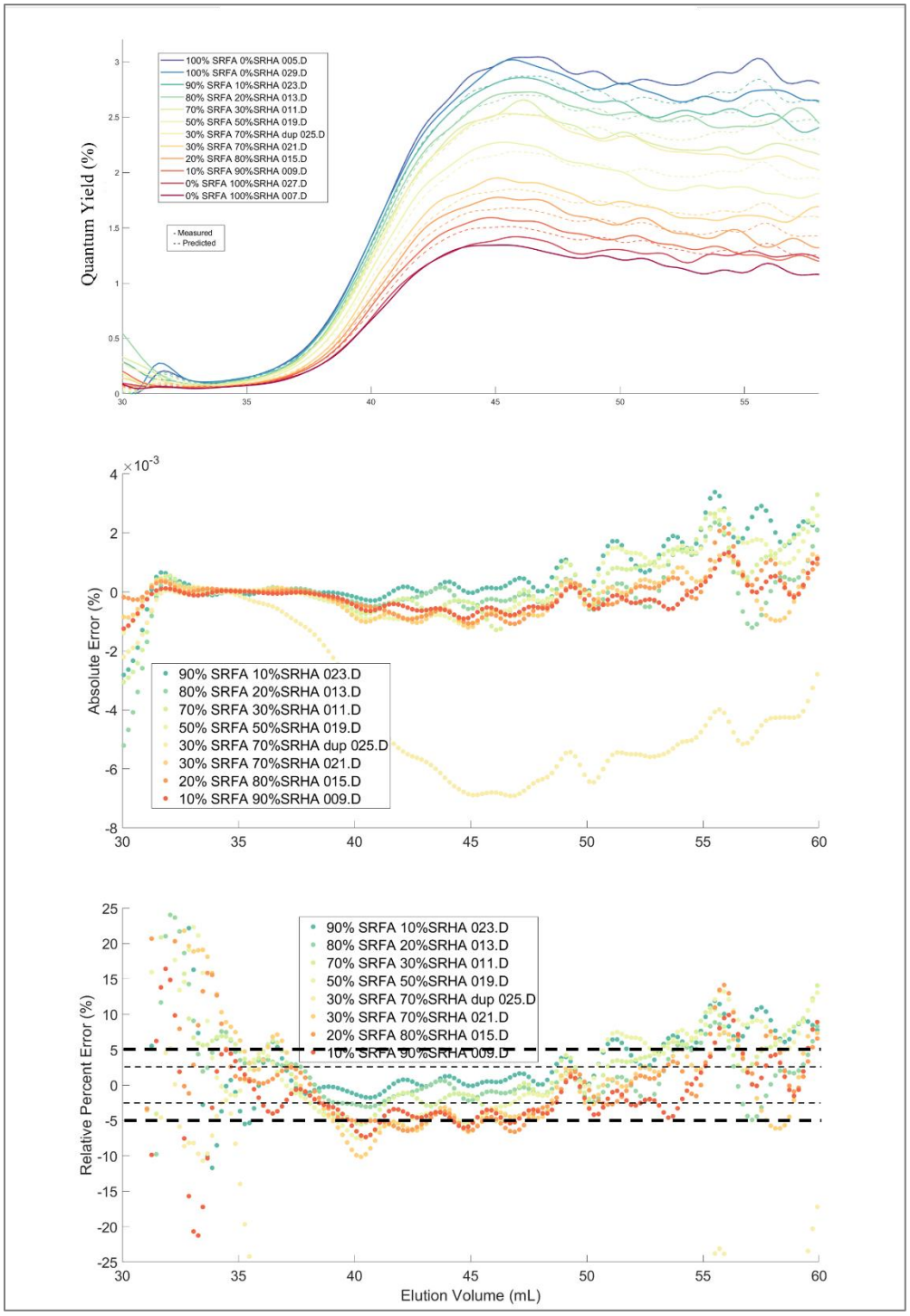

Figure B.7 SRFA/SRHA Blend at Constant DOC: λ_{Fex} 350 nm Φ_F Chromatograms and Error. **Top to bottom:** Fluorescence at excitation 350 nm chromatograms (mAu); Absorbance chromatograms (mAu); relative error (%).

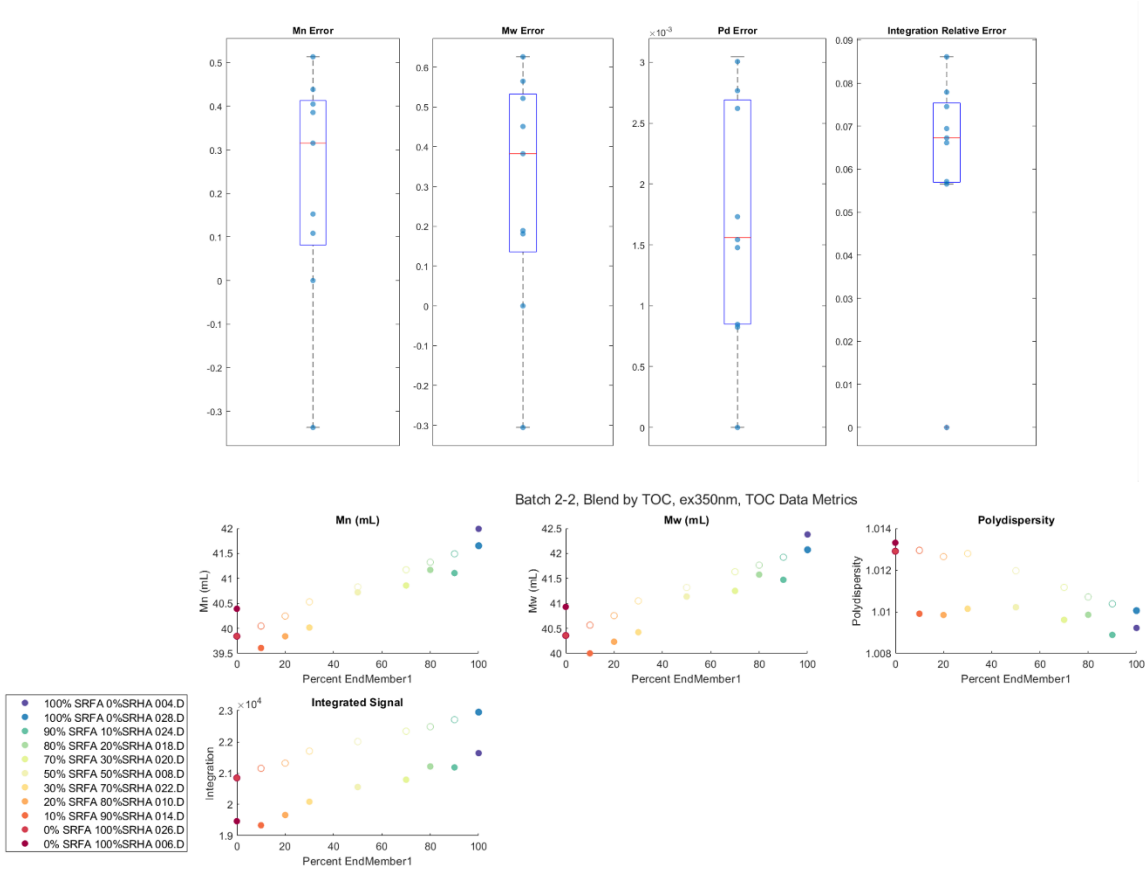

Figure B.8 SRFA/SRHA blend at Constant DOC: DOC Metrics and Metric Error. **Top (left to right):** Error boxplots of M_n, M_w, P_d, and integration value respectively. M_n, M_w, and P_d were calculated as absolute error and integration is calculated as relative error. **Bottom (left to right):** Metric plots of M_n, M_w, P_d and integration values from left to right respectively.

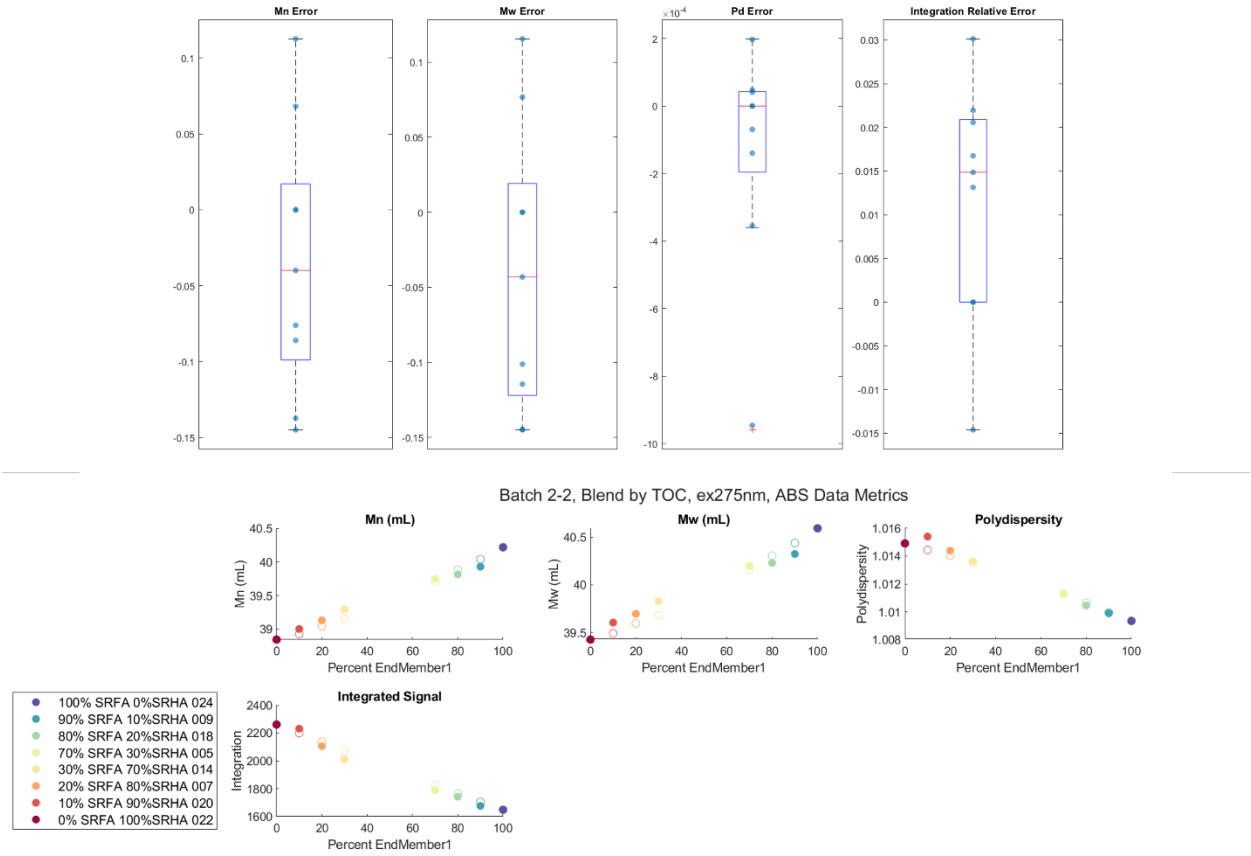

Figure B.9 SRFA/SRHA blend at Constant DOC: Absorbance 275 nm Metrics and Metric Error. **Top (left to right):** Error boxplots of M_n, M_w, P_d, and integration value respectively. M_n, M_w, and P_d were calculated as absolute error and integration is calculated as relative error. **Bottom (left to right):** Metric plots of M_n, M_w, P_d and integration values from left to right respectively.

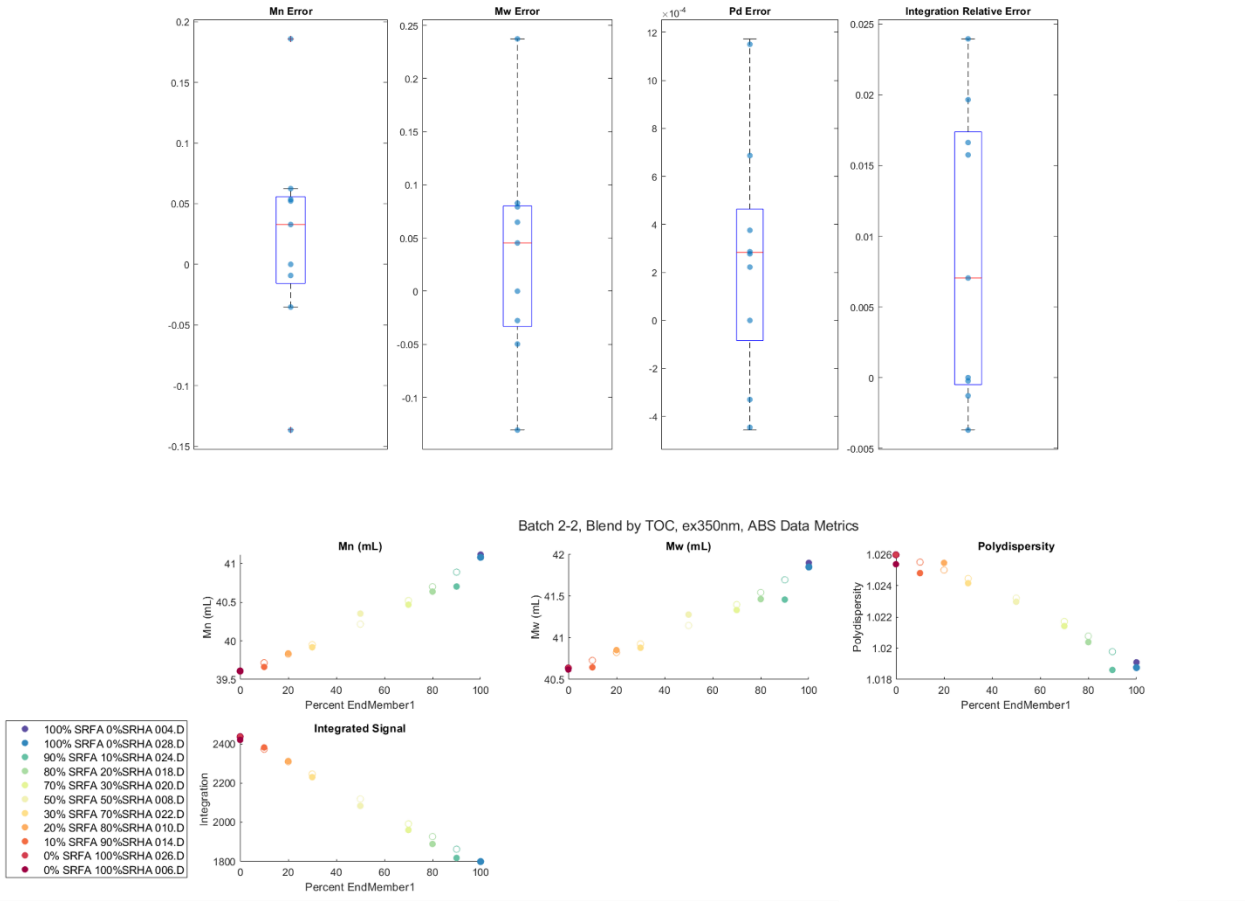

Figure B.10 SRFA/SRHA blend at Constant DOC: Absorbance 350 nm Metrics and Metric Error. **Top (left to right):** Error boxplots of M_n, M_w, P_d, and integration value respectively. M_n, M_w, and P_d were calculated as absolute error and integration is calculated as relative error. **Bottom (left to right):** Metric plots of M_n, M_w, P_d and integration values from left to right respectively.

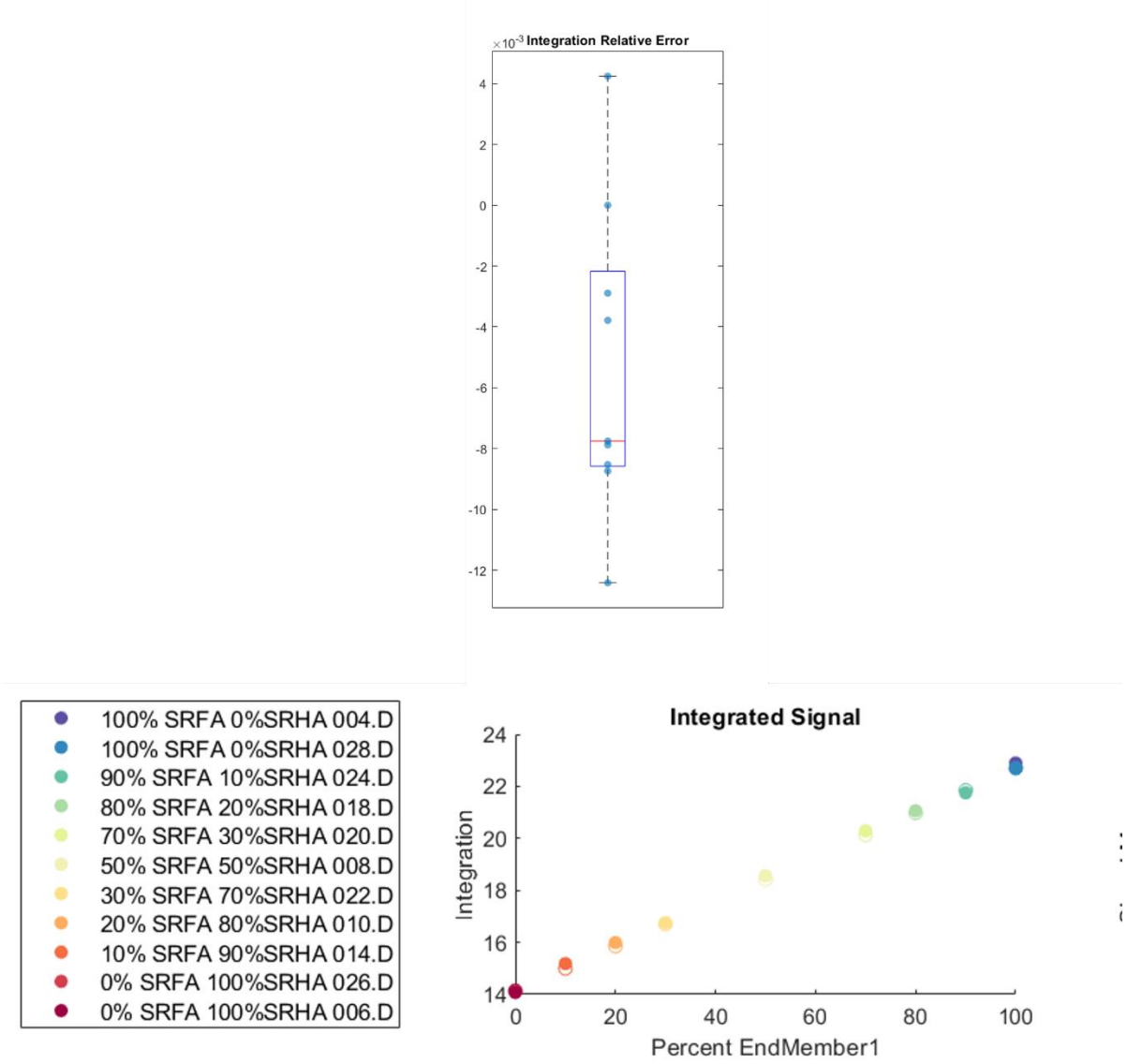

Figure B.11 SRFA/SRHA Blend at Constant DOC: λ_{Fex} 275 nm Fluorescence Metrics and Metric Error. **Top:** Error boxplots of integration value calculated as relative error. **Bottom:** Integration values from left to right respectively.

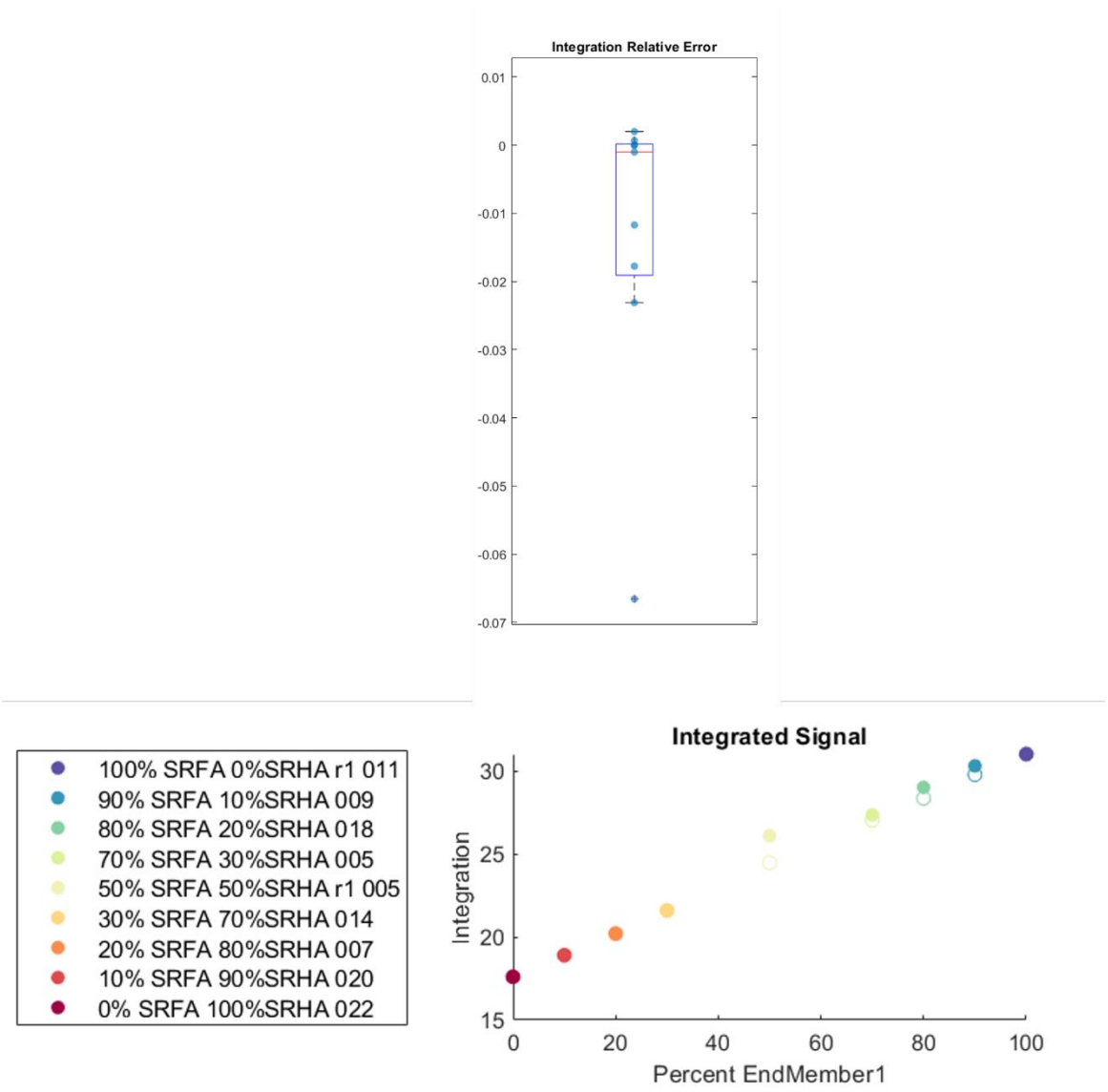

Figure B.12 SRFA/SRHA blend at Constant DOC: λ_{Fex} 350 nm Fluorescence Metrics and Metric error. **Top:** Error boxplots of integration value calculated as relative error. **Bottom:** Integration values from left to right respectively.

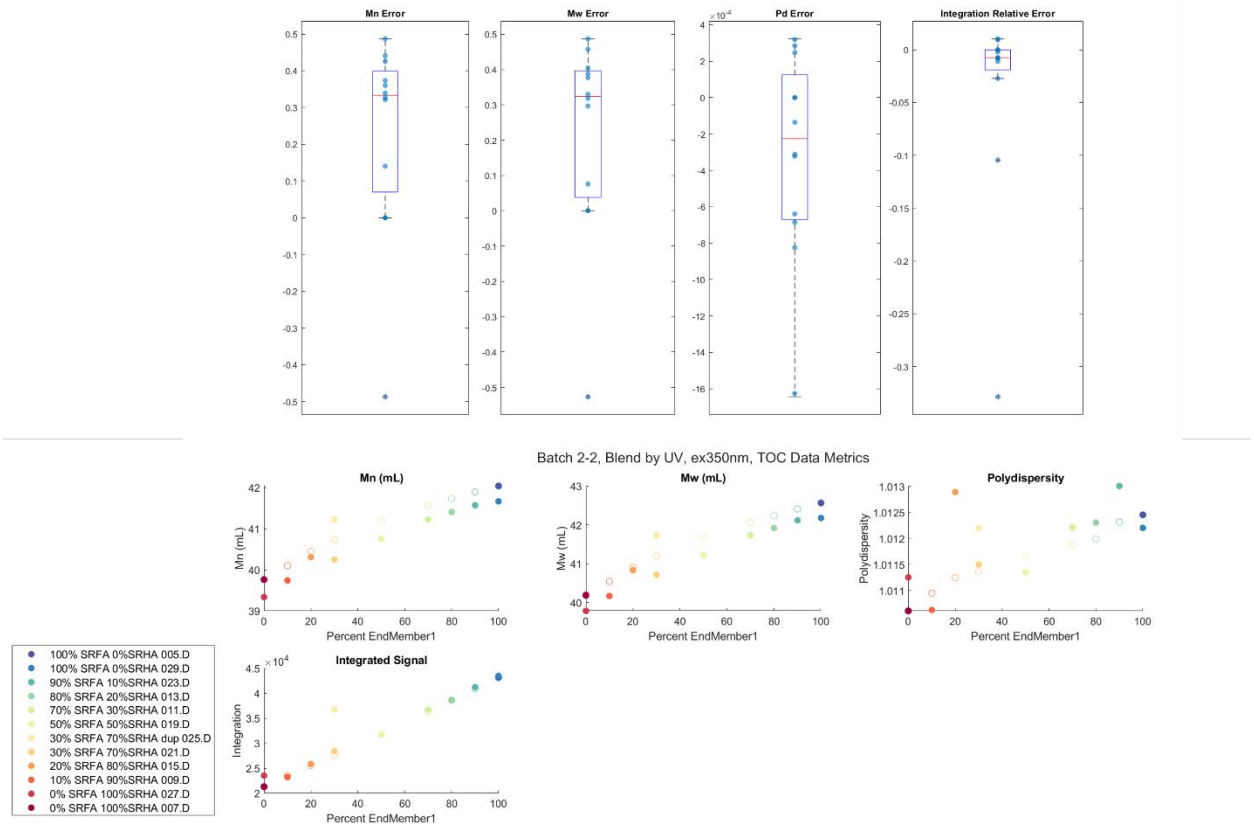

Figure B.13 SRFA/SRHA blend at Constant UV: DOC Metrics and Metric error. **Top (left to right):** Error boxplots of M_n, M_w, P_d, and integration value respectively. M_n, M_w, and P_d were calculated as absolute error and integration is calculated as relative error. **Bottom (left to right):** Metric plots of M_n, M_w, P_d and integration values from left to right respectively.

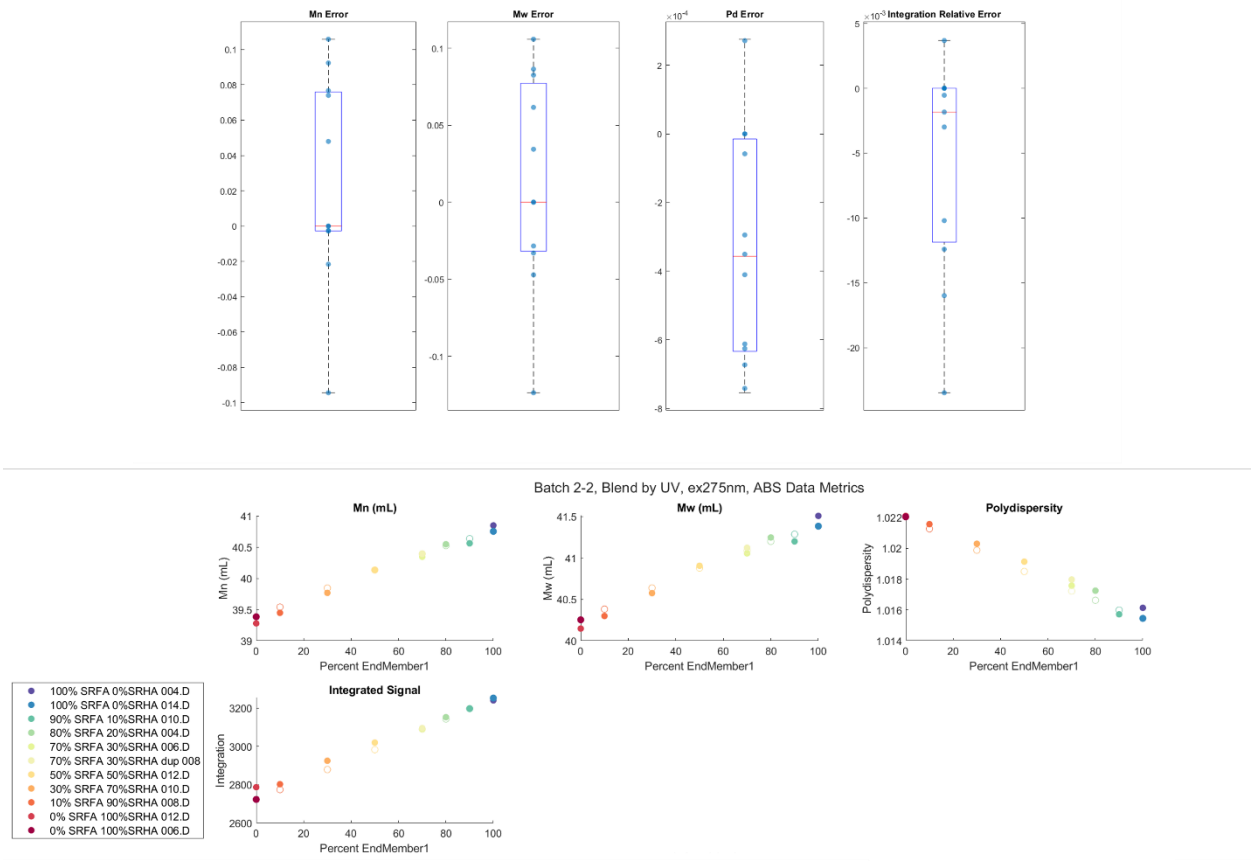

Figure B.14 SRFA/SRHA blend at Constant UV: Absorbance 275 nm Metrics and Metric Error. **Top (left to right):** Error boxplots of M_n, M_w, P_d, and integration value respectively. M_n, M_w, and P_d were calculated as absolute error and integration is calculated as relative error. **Bottom (left to right):** Metric plots of M_n, M_w, P_d and integration values from left to right respectively.

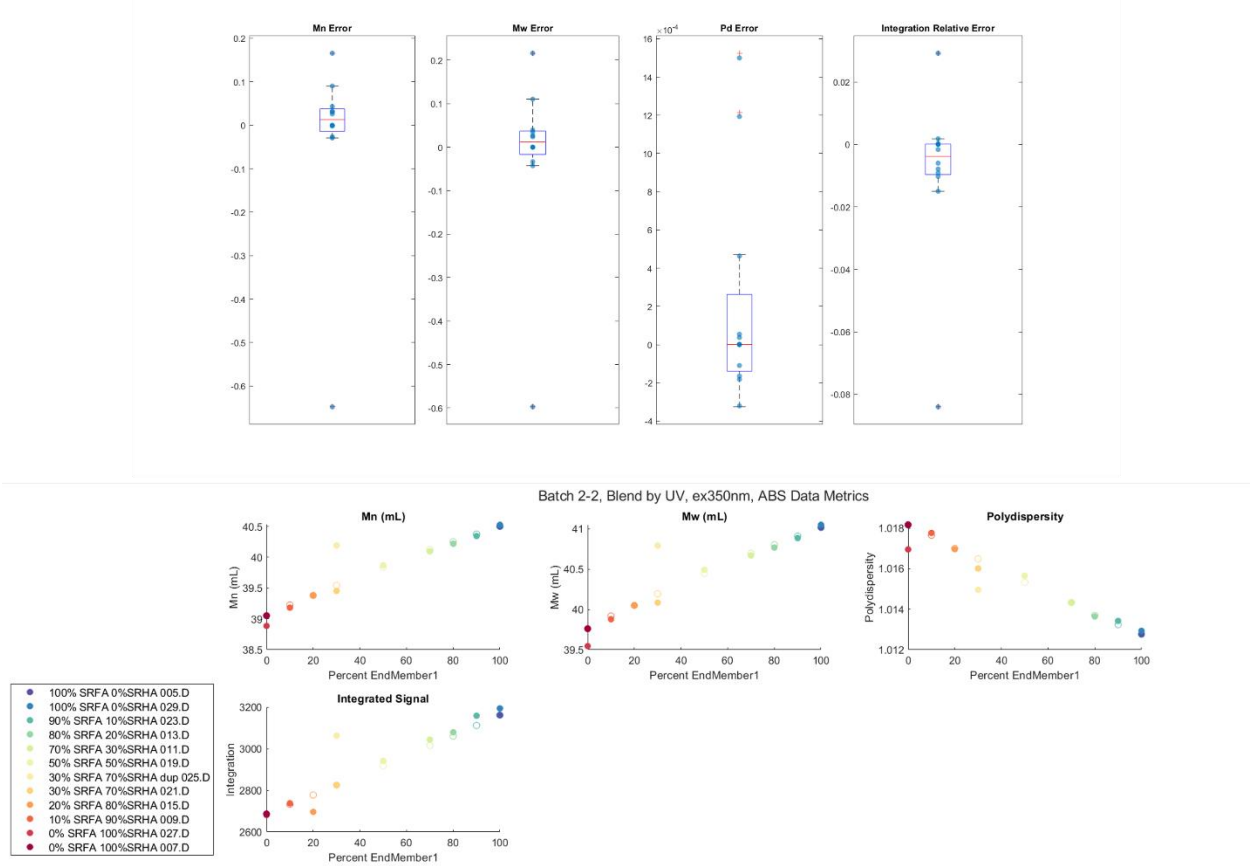

Figure B.15 SRFA/SRHA blend at Constant UV: Absorbance 350 nm Metrics and Metric Error. **Top (left to right):** Error boxplots of M_n, M_w, P_d, and integration value respectively. M_n, M_w, and P_d were calculated as absolute error and integration is calculated as relative error. **Bottom (left to right):** Metric plots of M_n, M_w, P_d and integration values from left to right respectively.

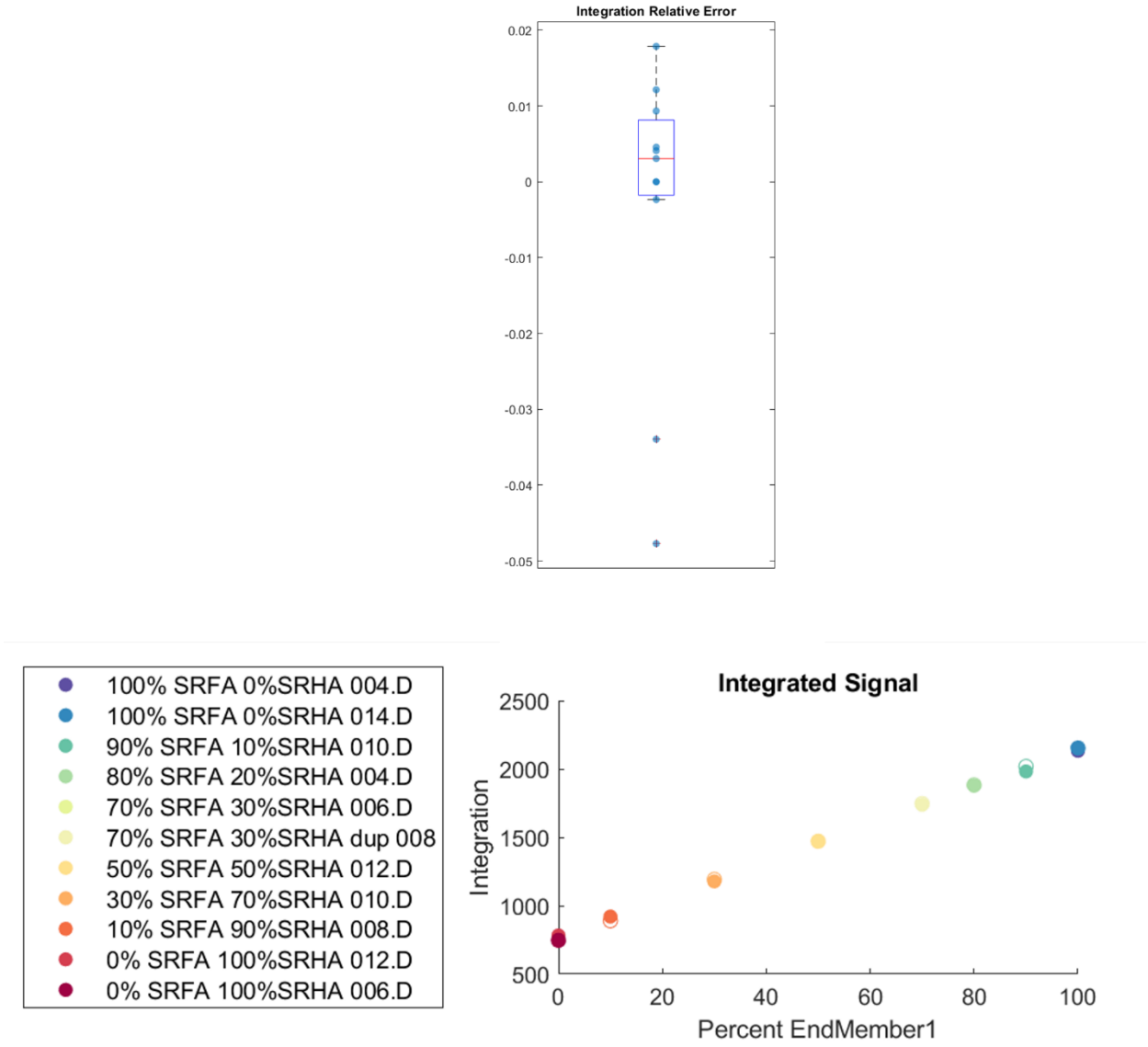

Figure B.16 SRFA/SRHA blend at Constant UV: λ_{Fex} 275 nm Fluorescence Metrics and Metric Error. **Top:** Error boxplots of integration value calculated as relative error. **Bottom:** Integration values from left to right respectively.

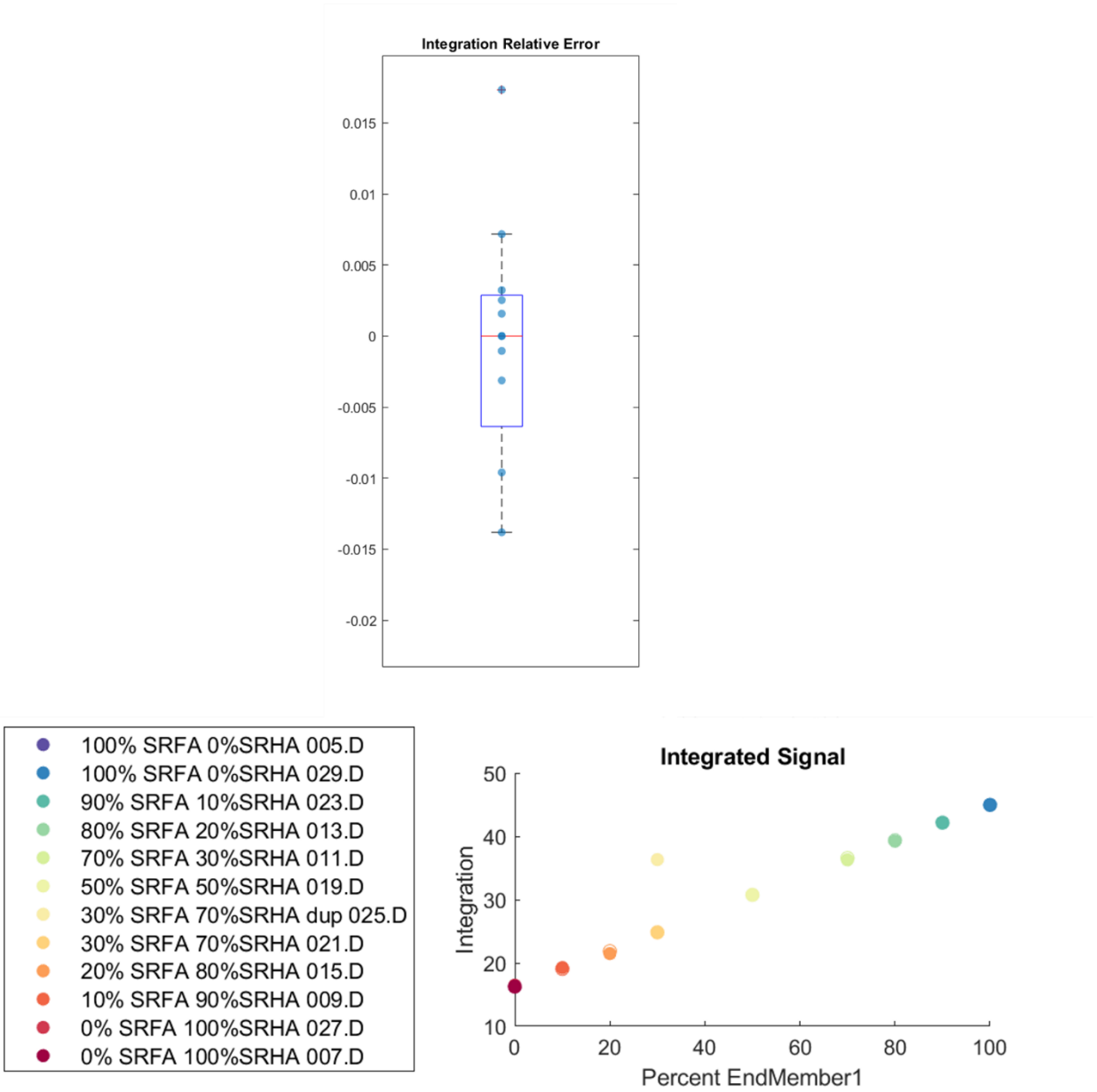

Figure B.17 SRFA/SRHA blend at Constant UV: λ_{Fex} 350 nm Fluorescence Metrics and Metric Error. **Top:** Error boxplots of integration value calculated as relative error. **Bottom:** Integration values from left to right respectively.